STRATEGIES FOR THE PHOTOCHEMICAL OXIDATION OF PHENOL CONTAMINATED WASTE WATER USING TITANIUM(IV) OXIDE-BASED CATALYST

By

MOSES TITUS YILLENG

DEPARTMENT OF CHEMISTRY,

AHMADU BELLO UNIVERSITY, ZARIA

NIGERIA

APRIL, 2014

STRATEGIES FOR THE PHOTOCHEMICAL OXIDATION OF PHENOL CONTAMINATED WASTE WATER USING TITANIUM(IV) OXIDE-BASED CATALYST

By

Moses Titus YILLENG

B.Sc., (2006) M.Sc., (2010) (ABU)
PhD/SCI/6593/2011-2012

A DISSERTATION SUBMITTED TO THE SCHOOL OF POSTGRADUATE STUDIES, AHMADU BELLO UNIVERSITY, ZARIA IN PARTIAL FULFILMENT OF THE REQUIREMENTS FOR THE AWARD OF DOCTOR OF PHILOSOPHY IN ANALYTICAL CHEMISTRY

DEPARTMENT OF CHEMISTRY,

FACULTY OF SCIENCE

AHMADU BELLO UNIVERSITY, ZARIA

NIGERIA

APRIL, 2014

DECLARATION

I declare that the work in this dissertation entitled “Strategies for the Photochemical Oxidation of Phenol Contaminated Waste water Using Titanium(IV) oxide-based Catalyst” has been performed by me in the Department of Chemistry, Ahmadu Bello University, Zaria, under the Supervision of Prof. C.E Gimba, Prof. I.G Ndukwe and Prof. David Rooney. The information derived from the literatures has been duly acknowledged in the text and a list of references provided. No part of this dissertation was previously presented for another degree or diploma at this or any other Institution.

YILLENG Moses Titus _____ _____

Signature Date

CERTIFICATION

This dissertation entitled “STRATEGIES FOR THE PHOTOCHEMICAL OXIDATION OF PHENOL CONTAMINATED WASTE WATER USING TITANIUM(IV) OXIDE- BASED CATALYST” by Moses Titus YILLENG meets the regulations governing the award of the degree of Ph.D. ANALYTICAL CHEMISTRY of Ahmadu Bello University, Zaria and is approved for its contribution to knowledge and literary presentation.

Prof. C.E Gimba Chairman, Supervisory Committee	Signature	Date
Prof. David Rooney Member, Supervisory Committee	Signature	Date
Prof. I. G Ndukwe Member, Supervisory Committee	Signature	Date
Prof. V. O Ajibola Head of Chemistry Department	Signature	Date
Prof. A.A Joshua Dean, School of postgraduate Studies	Signature	Date

DEDICATION

Family!!!

Family means nobody gets left behind, or forgotten.

— YILLENG Family—

Dedicated to **Janet,** my lovely wife and my children, **Joshua**, **Caleb** and **Christabel**

ACKNOWLEDGMENTS

I wish to express my profound gratitude to the Lord God Almighty, the Father of all mercies, grace and favor for the strength rendered unto me each day to acquire knowledge to this level. May His name be glorified through Jesus Christ, His only begotten Son

I would like to express my profound appreciation and sincere thank you to my supervisors, Prof. David Rooney, for giving me the privilege of going to Center for the Theory and Application of Catalysis, Queens University, Belfast, to carried out the research and Prof C.E. Gimba for always believing in my research capability from my M.sc to this point, and for the valuable guidance, positive and constructive criticisms and advises that have been given to me besides sharing knowledge and information. Also many thank you to Prof. I. G Ndukwe and Dr. Haresh Manyar for their cooperation and advice.

My lovely wife, the Beautiful Queen of my Kingdom, Janet, I am short of words to express my appreciation for the support, encouragement and prayer you always rendered to God on my behalf. Thank you very much.

Many thank you to Prof. I.M Bugaje, the Director General/ Chief Executive Officer of the National Research Institute for Chemical Technology, Zaria for funding this research through the STEP-B and for granting the permission to proceed with my studies even were things are rough.

Thank you to Rev. J. Dominion and his wife, Mrs. C. J Dominion, my beloved father and mother in law, for the persistent prayer and support in every ramification. I grateful for the inspiration and the spiritual cover you gave me, May the Almighty God continue to keep you.

To my beloved mothers, Mrs Sarah and Mrs Ruth, I am very grateful for your support morally. I will keep praying to God for long life that you will eat the fruits of your labour, also thank you to my siblings for the immense support to me. I love you all.

I am grateful to all academic staffs and technicians of the Department of Chemistry and Chemical Engineering, Queens University, Belfast, for their helping hands in finishing my research work and the Staffs of Chemistry Department, Ahmadu Bello University, Zaria.

Special thank you to all the brethren of the Belfast Church of Christ, the Doyle's, McElroy's, Melin's, Hanna's, Dinning's Jonathan McEleese's, Gareeth, Anna, Mei, Jessica, for the wise counsel given to me and for the spiritual encouragement, discipleship and financial support.

Thank you to Trevor, Billy, Thomas Sheppard, Richard Morgan, Phillip Macron, Peter Goodrich, Linsey Findley, Cristina Stere, Nati Camacho, Hamill Connor, Helen Daly, Lars, Imran, Yu Wang and Amin and all the staff and Postgraduate students of CenTACat, for the privilege granted me to carry out the research in the Lab and share knowledge with them.

My appreciation also goes to Prof. Andrew Mills and Dr Alexandre Goguete of CenTACat for the professional advice. Mr. Stephen McFarland of Physics Department, Queens University, Belfast for the TEM analysis and Mrs. Jackie O'Connor for the first BET analysis and the safety guidance.

I also wish to thank my dearest friend, Abel Yusuf for always being there for me and my family, and Victor Joseph for his unrelenting effort to pick us to and from the airport anytime we demand. May God bless you.

Furthermore, thanks are due to my colleagues Kenneth (alias Jujal), Emeka Thompson, Edwin Ogwuchi, Valentine Ekwueme, Anwar Auwal, Lamis Madaki, Ahvor Jacob, Dr. Ocholi and Abubakar Yusuf you are a blessing to me.

Finally thanks to my friends, relatives and well-wishers Pon Durfa, Wale, Sunny, Dan Bauchi, Mr Okereke, Musa Latayo, Dr. Ladan, Chris Nnaji and too numerous to mention. May the grace of God keep you all.

ABSTRACT

The photocatalyts are prepared using the sol immobilization and micro emulsion methods and are characterized by the use of SEM/EDX, TEM, XRD, ICP-OES, BET techniques, TGA, DRS UV-Vis, DRIFTS and TPO/TPR. The results obtained from the characterization show that the optical properties of the catalyst has been shifted toward the visible region and the XRD shows that anatase phase is the predominant phase in the TiO_2 used. The photocatalytic degradation of phenol was done by varying the type of oxidant i.e. compressed air, oxygen and hydrogen peroxide, with the different types of photoreactor. The reaction rate was monitored using HPLC and GC-MS. The quantum efficiency of the reaction was calculated using the radiant flux and the rate of reaction determined using the Langmuir-Hinshelwood model with a pseudo-first order kinetics. Using the suspension/slurry photoreactor in oxygen, 86.4% conversion of phenol to CO_2 and H_2O after 120 min was achieved in the case of 1%Pd-TiO_2 and 1%Au-TiO_2 gives 73.4% conversion. For 1%Fe-TiO_2, 1%Cu-TiO_2, P25 (Degussa) and hydrothermal treated TiO_2 the degradation was 64.4, 54.8, 64.5 and 77.8% respectively. In order to achieve the main aim of the research in developing a pilot waste water treatment plant which worked in a continuous mode, the experiment was conducted using the 0.5%Pd-TiO_2 catalyst using the trickle bed system in continuous mode. The results showed that the Phenol conversion efficiency of the 0.5%Pd-TiO_2 was 70.3% and remained stable for 48h. Similar result was obtained in the trickle bed system when P25 was used with oxygen, 71.9% conversion was obtained in 48h. When P25 was used on the trickle bed reactor in the presence of hydrogen peroxide as the oxidant, 99.5% conversion was obtained in 24h. Comparing the amount of phenol converted using visible light and the UV light, it was concluded that the bimetallic photo catalyst i.e., the

0.5%Pd 0.5%Au-TiO_2 are more stable to leaching and have an enhanced activity in the visible region compared to the other catalysts used. To further improve the efficiency of the process, a Taylor flow system was designed and developed to obtain complete mineralization, the complete mineralization were achieved because the surface of the catalyst was not deactivated by poisoning from the hydrocarbons which increased the reactivity life-time of the catalyst to 26h in case of the P25 in the continuous mode: it was 34h for 0.5wt%Pd-TiO_2 and for the 1wt%Au-TiO_2 the reaction rate was slow but consistent for 52h. Using the 2.0%Pd@TiO_2 with the batch mode in oxygen as oxidant, there was a 24% conversion of phenol, 85% conversion was achieved with the trickle bed system and 97% conversion with the Taylor flow system, the increase in the photodegradation rate of phenol was due to the micro emulsion methods used in catalyst synthesis and the Taylor flow photoreactor. This work produced a novel continuous flow micro photoreactor which employed Taylor flow system designed to reduce the mass transfer limitation between oxygen gas and phenol solution. The reactor has the inherent advantages of a fixed-bed catalyst designed to increase the reaction efficiencies over the slurry batch reactor when used with the prepared catalyst in oxygen.

TABLE OF CONTENTS

Title Page iii

Declaration iv

Certification v

Dedication vi

Acknowledgments vii

Abstract ix

Table of Contents xi

List of Figures xix

List of Tables xxv

CHAPTER ONE 1

1.1 Introduction 1

1.2 Photocatalysis 1

1.3 Theory of Photocatalysis 2

1.3.1 Basic principles 4

1.3.2 Photon absorption 5

1.3.3 Charge transfer and trapping 5

1.3.4 Electron –hole recombination 6

1.3.5 Photocatalytic quantum efficiency 8

1.3.6 Reduction and oxidation of molecules at the surface 10

1.3.7 Incident light intensity and wavelength 11

1.3.8 Concentration of reactants 14

1.3.9 Temperature 17

1.3.10 Mass of catalyst 18

1.3.11 Solution pH 19

1.3.12 Dissolved oxygen 21

1.4 Methods for Improving Photocatalytic Efficiency 21

1.4.1 Metal-deposited TiO_2 photocatalyst: 22

1.4.2 Doped TiO_2 and visible light photocatalytic activity 25

1.4.3 Composite semiconductor photocatalyst 25

1.4.4 Dye sensitization 25

1.4.5 Hybrids with Nano materials 26

1.4.6 Role of inorganic adsorbates 26

1.5 Phenol 26

1.5.1 Uses of phenol 27

1.5.2 Properties of phenol 27

1.6 Aim and Objectives 28

1.7 Justification of the Research 30

CHAPTER TWO 31

2.1 Literature Review 31

2.2 Types of photoreactor 33

2.2.1 Slurry/suspension liquid photoreactors systems 33

2.2.2 Immobilized/Packed catalysts photoreactor systems 35

2.3 Conversational waste water treatment 36

2.3.1 Photocatalysis of organic pollutant using transition metal doped TiO_2 37

2.4 Analytical Instrument for Catalyst Characterization 41

2.4.1 Diffuse Reflectance UV-Vis Spectroscopy (DRS) 41

2.4.2 Diffuse Reflectance Infrared Fourier Transform Spectroscopy (DRIFTS) 46

2.4.3 Powder X-Ray diffraction measurements 49

2.4.4 Thermogravimetric Analysis (TGA) 52

2.4.5 Inductively coupled plasma optical emission spectrometer (ICP-OES) 52

2.4.6 Scanning electron microscopy 54

2.4.7 Energy-Dispersive X-Ray (EDX) 56

2.4.8 Transmission Electron Microscope (TEM) 57

2.4.9 The Brunauer–Emett–Teller (BET) 62

2.4.10 Temperature Programmed Reduction (TPR) and Chemisorption 66

2.4.11 Temperature Programmed Oxidation (TPO) 66

2.4.12 High Performance Liquid Chromatography (HPLC) 67

CHAPTER THREE 71

3.1 Experimental 71

3.2 Materials and Reagent 71

3.2.1 Reagents 71

3.3 Methods 71

3.3.1 Preparation of catalyst 71

3.3.2 Sol Immobilization Method 71

3.3.3 Hydrothermal synthesis of TiO_2 nanotubes 72

3.3.4 Micro-emulsion preparation 73

3.4 Preparation of Stock Solution 74

3.4.1 Preparation of phenol stock solution 74

3.4.2 Preparation of resorcinol stock solution 74

3.4.3 Preparation of catechol stock solution 74

3.4.4 Preparation of pyrogallol stock solution 74

3.4.5 Preparation of hydroquinone stock solution 74

3.5 Characterization of Catalyst 75

3.5.1 Diffuse Reflectance UV-Vis Spectroscopy (DRS) 75

3.5.2 Diffuse Reflectance Infrared Fourier Transform Spectroscopy (DRIFTS) 75

3.5.3 Powder X-Ray Diffraction measurements 76

3.5.4 Thermogravimetric Analysis (TGA) 76

3.5.5 Inductively Coupled Plasma Optical Emission Spectrometer (ICP-OES) 77

3.5.6 Scanning Electron Microscopy 79

3.5.7 Transmission Electron Microscope (TEM) 79

3.5.8 The Brunauer–Emett–Teller (BET) 79

3.5.9 Temperature Programmed Reduction (TPR) and Chemisorption 83

3.5.10 Temperature Programmed Oxidation (TPO) 85

3.6 Photocatalysis Experiment 86

3.6.1 Photocatalysis using slurry batch process 86

3.6.2 Ultraviolet emission spectra 88

3.6.3 UV Irradiance Measurement 88

3.6.4 Quantum Yield/Efficiency calculation of the UV Light 88

3.6.5 Quantum Yield/Efficiency calculation of the visible light: 91

3.7 Photocatalysis Process using Trickle Bed in Continuous mode 93

3.7.1 Photocatalysis process using Taylor flow system in continuous mode 95

3.7.2 The reactor flow systems 95

3.8 Analysis 98

3.8.1 High Performance Liquid Chromatography (HPLC) 98

3.8.2 The Gas Chromatography-Mass Spectroscopy 99

CHAPTER FOUR 100

4.1 Results and Discussion 100

4.2 Characterization of Catalysts 100

4.2.1 Diffuse reflectance UV-Vis of Au-Pd/TiO_2 100

4.2.2 Diffuse reflectance UV-Vis of 2%Pd@TiO_2 103

4.2.3 XRD of transition metal doped-TiO_2 106

4.2.4 XRD of Au-Pd/TiO_2 108

4.2.5 XRD of 2%Pd@TiO_2 110

4.2.6 Thermogravimetric Analysis (TGA) of Au-Pd/TiO_2 110

4.2.7 Thermogravimetric Analysis (TGA) of *2*%Pd@TiO_2 114

4.2.8 Estimation of gold and palladium content on Au-Pd/TiO_2 114

4.2.9 Estimation of palladium content in *2*%Pd@TiO_2 115

4.2.10 Scanning electron microscopy of transition metal doped TiO_2 115

4.2.11 Scanning electron microscopy of hydrothermally treated TiO_2 119

4.2.12 Scanning Electron Microscopy (SEM) of Au-Pd/TiO_2 119

4.2.13 Scanning Electron Microscopy (SEM) of 2%Pd@TiO_2 123

4.2.14 Transmission electron microscopy of Au-Pd/TiO_2 123

4.2.15 EDX of 0.5wt%Pd-TiO2 123

4.2.16 Transmission electron microscopy of hydrothermally treated P25 127

4.2.17 Transmission electron microscopy of 2%Pd@TiO_2 127

4.2.18 The Brunauer–Emett–Teller (BET) 130

4.2.19 CO chemisorption - pulse method 131

4.3 Photo Catalysis Experiment 134

4.3.1 Photocatalysis of phenol using transition metals doped TiO_2 134

4.3.2 Effect of H_2O_2, O_2 and N_2 on the photolysis of phenol in UV light 143

4.3.3 Effect of catalyst loading on photocatalytic degradation of phenol 146

4.3.4 Photocatalysis of phenol in air using the batch mode 150

4.3.5 Reusability of 0.5wt%Pd-TiO_2 with air using batch mode 154

4.3.6 Photocatalysis of phenol in O_2 using the batch mode 156

4.3.7 Phenol photocatalysis in O_2 with the batch mode in visible light 159

4.3.8 Reusability of 0.5wt%Pd-TiO_2 with O_2 using batch mode 162

4.3.9 Photocatalysis of phenol in H_2O_2 with the batch mode 164

4.4 Quantum Efficiency of the Catalysts 167

4.4.1 Quantum efficiency of Au-Pd/TiO_2 in air 168

4.4.2 Quantum efficiency of Au-Pd/TiO_2 in oxygen 171

4.4.3 Quantum efficiency of Au-Pd/TiO_2 in hydrogen peroxide 171

4.5 Product Analysis and Reaction Mechanism 176

4.5.1 Photocatalysis with P25 and 0.5%Pd-TiO_2 using trickle bed mode 179

4.5.2 TPO of the used catalyst after using on trickle bed system 182

4.5.3 DRIFTS of the used and fresh P25 Degussa 185

4.5.4 DRIFTS of the used and fresh 0.5%Pd-TiO_2 189

4.5.5 Photocatalysis using 2%Pd@TiO_2 on Batch, Trickle bed and Taylor flow 193

4.5.6 Reusability of 2%Pd@TiO_2 in O_2 and H_2O_2 with batch mode 199

4.5.7 Thermocatalytic oxidation of phenol with P25 on the Taylor flow 202

CHAPTER FIVE 204

5.1 Summary, Conclusion and Recommendation 204

5.2 Summary and Conclusion 204

5.3 Recommendation for Future Work 207

References 209

LIST OF FIGURES

1.1:	Schematic of photocatalytic degradation of organic contaminants	3
1.2:	Influence of some physical parameters on the rate, r, of photocatalytic reactions: (a) radiant flux φ; (b) initial concentration, Co of reactant; (c) temperature, T; (d) mass of catalyst, m	13
1.3:	Method for improving the activity and photo-response of TiO_2	23
1.4:	Fermi level equilibration via charge distribution between UV-irradiated TiO_2 and metal nanoparticles with redox couple	24
2.1:	Specular and diffuse reflection	43
2.2:	Bragg condition	51
2.3:	Mettler-toledo TGA/DSC I STAR^e	53
2.4:	The interaction of electron beam with samples in SEM	55
2.5:	Scanning electron microscopy with EDX	58
2.6:	Schematic outline of TEM	60
2.7:	Transmission electron microscope (TEM) FEI™ Tecnai G2 F20	61
2.8:	Different types of adsorption isotherms	63
2.9:	An Agilent 1100 high performance liquid chromatography (HPLC)	69
3.1:	The schematic diagram of TGA	78

3.2:	Micromeritrics Tristar II	81
3.3:	Example of a BET isotherm	82
3.4:	The picture of Micrometrics AutoChem 2910 system	84
3.5:	Photocatalytic experiment in Slurry batch process	87
3.6:	Spectral distribution of irradiance density for the UV lamp	89
3.7:	Schematic of the Trickle/Taylor flow System in continuous process	94
3.8:	The picture of the Taylor Flow system in continuous mode	96
3.9:	The calibration chart of the mass flow-meter	97
4.1:	The UV-visible diffuse reflectance spectra Au-Pd/TiO_2 with P25	101
4.2:	Diffuse reflectance UV-Vis spectra of Au-Pd/TiO_2 in % reflection	102
4.3:	The diffuse reflectance UV-Vis spectra of the 2%Pd@TiO_2 and the amorphous TiO_2	105
4.4:	X-ray diffraction patterns of the prepared catalyst deposited with transition metals	107
4.5:	The XRD pattern of Au-Pd/TiO_2 prepared by sol immobilization	109
4.6:	The XRD pattern of the 2%Pd@TiO_2 showing the presence of palladium	111
4.7:	TGA result of (a) 2%Pd@TiO_2,(b) 0.25%Au0.75%Pd-TiO_2, (c) 0.5%Au0.5%Pd-TiO_2 (d) 0.25%Pd0.75Au-TiO_2	112

4.8: The TGA result of (e) 0.5%Pd-TiO_2, (f) 1%Au-TiO_2 113

4.9: The SEM of (a) 1%Cu-TiO_2, (b) 1%Fe-TiO_2 117

4.10: The SEM of (c) 1%Au-TiO_2 and (d) 1%Pd-TiO_2 118

4.11: The SEM of the hydrothermal treated TiO_2 120

4.12: SEM images of 0.5wt%Pd-TiO_2 (a, b) and 1wt%Au-TiO_2 (c, d) 121

4.13: The mapping of 0.5%Pd-TiO_2 122

4.14: The SEM images of 2%Pd@TiO_2 124

4.15: The energy dispersive X-ray (EDX) of a single particle of 0.5 wt%Pd-TiO_2 using TEM 125

4.16: The TEM images of 0.5wt%Pd-TiO_2 (a, b) and 0.5wt%Pd0.5wtAu-TiO_2 (b, c) 126

4.17: TEM images of hydrothermal treated P25 Degussa 128

4.18: TEM images of 2%Pd@TiO_2 129

4.19: Pulse data showing TCD response versus pulse number for CO chemisorption chemisorption on the 2%Pd@TiO_2 photocatalyst at -46°C 133

4.20: Pulse data showing TCD response versus pulse number for CO chemisorption on the 0.5%Pd-TiO_2 photocatalyst at -46°C 135

4.21: Photocatalytic degradation of phenol with different transition metals

doped TiO_2 catalysts in oxygen 137

4.22: Photocatalytic degradation of phenol over transition metals doped TiO_2 In oxygen. The linear fit to the data represent pseudo-first-order degradation kinetics 141

4.23: Effect of photolysis on phenol photodegradation using hydrogen peroxide, oxygen and nitrogen in UV light. 145

4.24: Effect of catalyst loading using 0.5wt%Pd-TiO_2 in oxygen 148

4.25: Picture of the Slurry/suspension photoreactor: (a) with sparger and (b) without sparger 151

4.26: Photocatalytic degradation of phenol with air as oxidant over Au-Pd/TiO_2 using the Slurry/suspension photoreactor with UV light 153

4.27: Reusability of 0.5%Pd-TiO_2 in phenol photocatalysis using air as oxidant 155

4.28: Photocatalytic degradation of phenol with oxygen as oxidant over P25 and Au-Pd/TiO_2 using the Slurry/suspension photoreactor with UV light 157

4.29: Photocatalytic conversion of phenol to CO_2 and H_2O using the Slurry batch reactor with oxygen in the visible light of 555nm wavelength 160

4.30: Comparison of phenol converted using the visible and ultra violet light source in oxygen with the slurry Batch reactor 161

4.31: Reusability of 0.5wt%Pd-TiO_2 in phenol photocatalysis with oxygen using the Slurry/suspension batch mode 163

4.32: Photocatalytic degradation of phenol with hydrogen peroxide as oxidant over P25 and Au-Pd/TiO_2 166

4.33: Photocatalytic degradation of phenol over Au-Pd/TiO_2 in Air. The linear fit to the data represent first-order degradation kinetics 169

4.34: Photocatalytic degradation of phenol over Au-Pd/TiO_2 in oxygen. The linear fit to the data represent first-order degradation kinetics 172

4.35: Photocatalytic degradation of phenol over Au-Pd/TiO_2 in H_2O_2 The linear fit to the data represent first-order degradation kinetics 174

4.36: Simplified mechanism for phenol photocatalytic degradation. 177

4.37: Phenol photocatalysis in oxygen and hydrogen peroxide with 0.5wt%Pd-TiO_2 and P25 using the Trickle bed mode 181

4.38: The plot of CO_2 evolved during the TPO using P25 and 0.5wt%Pd-TiO_2 183

4.39: Picture of catalyst bed: (A 1) fresh P25. (B1) P25 in H_2O_2 with Trickle bed (C1) P25 in oxygen with Taylor flow (D1) P25 in oxygen and less UV light with Trickle bed (E1) P25 in oxygen and sufficient UV light with Trickle bed (F1) 0.5%Pd-TiO_2 in oxygen with Taylor flow.

The Picture tags (2) are the same sample dried at 120°C overnight after the experiment 184

4.40: DRIFT of used P25 (Degussa) 188

4.41: DRIFT of 0.5%Pd-TiO_2 190

4.42: Phenol photocatalysis in oxygen with 0.5wt%Pd-TiO_2, 0.5wt%Pd 0.5wt%Au-TiO_2 and P25 using the Taylor flow mode 192

4.43: Photocatalytic degradation of phenol using 2%Pd@TiO_2 with the Slurry/suspension System in oxygen 194

4.44: Phenol photocatalysis using 2%Pd@TiO_2 in oxygen using Trickle bed and Taylor flow system 196

4.45: Effect of hydrogen peroxide concentration on phenol degradation using 198

4.46: Reusability of 2%Pd@TiO_2 in photocatalysis of phenol in oxygen with Slurry/suspension batch mode 200

4.47: Reusability of 2%Pd@TiO_2 in photocatalysis of phenol in hydrogen peroxide with Slurry/suspension batch mode 201

4.48: Thermocatalytic oxidation of phenol in the presence of P25 using the Taylor flow system 203

LIST OF TABLES

1.1: Physical properties and chemical Identity of phenol 29

4.1: The physico-chemical properties of Au-Pd/TiO_2 and P25 with the surface area, pore volume, crystallite size and band gap 104

4.2: The ICP-OES results of Au/Pd-TiO_2 and 2.0wt%Pd@TiO_2 116

4.3: Influence of transition metals doped on TiO_2 on the photocatalytic degradation of phenol in oxygen using the Slurry/suspension mode 139

4.4: Comparison of the photocatalytic rate of phenol degradation in air over Au- Pd/TiO_2 catalysts assuming first order kinetics and the corresponding quantum efficiency 170

4.5: Comparison of the photocatalytic rate of phenol degradation in oxygen over Au-Pd/TiO_2 catalysts assuming first order kinetics and the corresponding quantum efficiency 173

4.6: Comparison of the photocatalytic rate of phenol degradation in hydrogen peroxide 175

4.7: The amount of carbons on the surface of the catalyst and the temperature at which the carbons are evolved as CO_2 186

CHAPTER ONE

1.1 Introduction

1.2 Photocatalysis

Clean water as a basic resource for the survival of man is being threatened by the activities of industries through the discharge of chemicals in rivers and aquifer, agriculture practices that involved the use of pesticides and natural processes like volcanic eruption, and urban activities (Malato *et al*., 2009). Polluted water has been the cause of water borne diseases; and it makes water unfit for human consumption and industrial use. As a result several legislations and initiatives have been introduced by both governments and private organizations in a bit to salvage the rapid deterioration of clean water globally (Wintgens *et al*., 2008; Richardson, 2008; Suarez *et al*., 2008).

Presently, there are several techniques that are being used in reclaiming wastewater into a portable standard, fit for human use. The use of activated carbon in the treatment of wastewater has been one of the most widely acceptable technique (Bradley *et al*., 2002; Lapena *et al.,* 1995). Reclaiming the wastewater involved the removal of suspended solids, bacteria, coliforms, recalcitrant organic compound that are not easily removed by the use of activated carbon technique (Viessman Jr. and Hammer, 1998), due to these an alternative to the use of activated carbon (sludge) has been introduced in many wastewater treatment plants, which involved chemical process also known as Advanced Oxidation Processes (AOPs). The AOP is a technique that is well known for the complete oxidizing and mineralizing of most recalcitrant organic contaminant (Comninellis *et al*., 2008). Nevertheless, advance oxidation process has some technical drawbacks that is negating its industrial or large scale

applications. Diverse modification into the AOP has been proposed by several researchers, which include the integration of photocatalysis in wastewater treatment.

Heterogeneous photocatalytic purification of wastewater constitute the use of light source (electromagnetic radiation) of the required wavelength which are used with photoresponse semiconductor, to generate oxidizing species due to the photogenerated holes used to attack organic pollutant, virus, bacteria etc. through oxidation process to form carbon dioxide, water and dilute inorganic acid.

The photocatalytic decontamination of wastewater has the following features: It is a process that occurs at ambient temperature and normal atmospheric pressure. The detoxification of the organic species to CO_2 occur via oxidation or reduction, the oxidant required can be obtained from the dissolved oxygen in the aqueous solution or atmospheric air. The catalyst used is normally inexpensive, stable and nontoxic. The catalyst can be modified to be used under solar energy

1.3 Theory of Photocatalysis

The diagram in Figure 1 shows the schematic of titanium(IV) oxide semiconductor in a photocatalytic reaction. TiO_2 has a valence band (VB) and Conduction band (CB) separated by Band gap energy of $3.2eV$ in the case of an anatase phase. Figure 1 illustrates seven key steps (1 to 7), which are fundamental steps in the metal-doped TiO_2 photocatalysis. Step 1 is the absorption of photon emitted with the required wavelength to be able to excite electrons from the valence band to conduction band leaving a hole (h^+) in the valence band (VB).

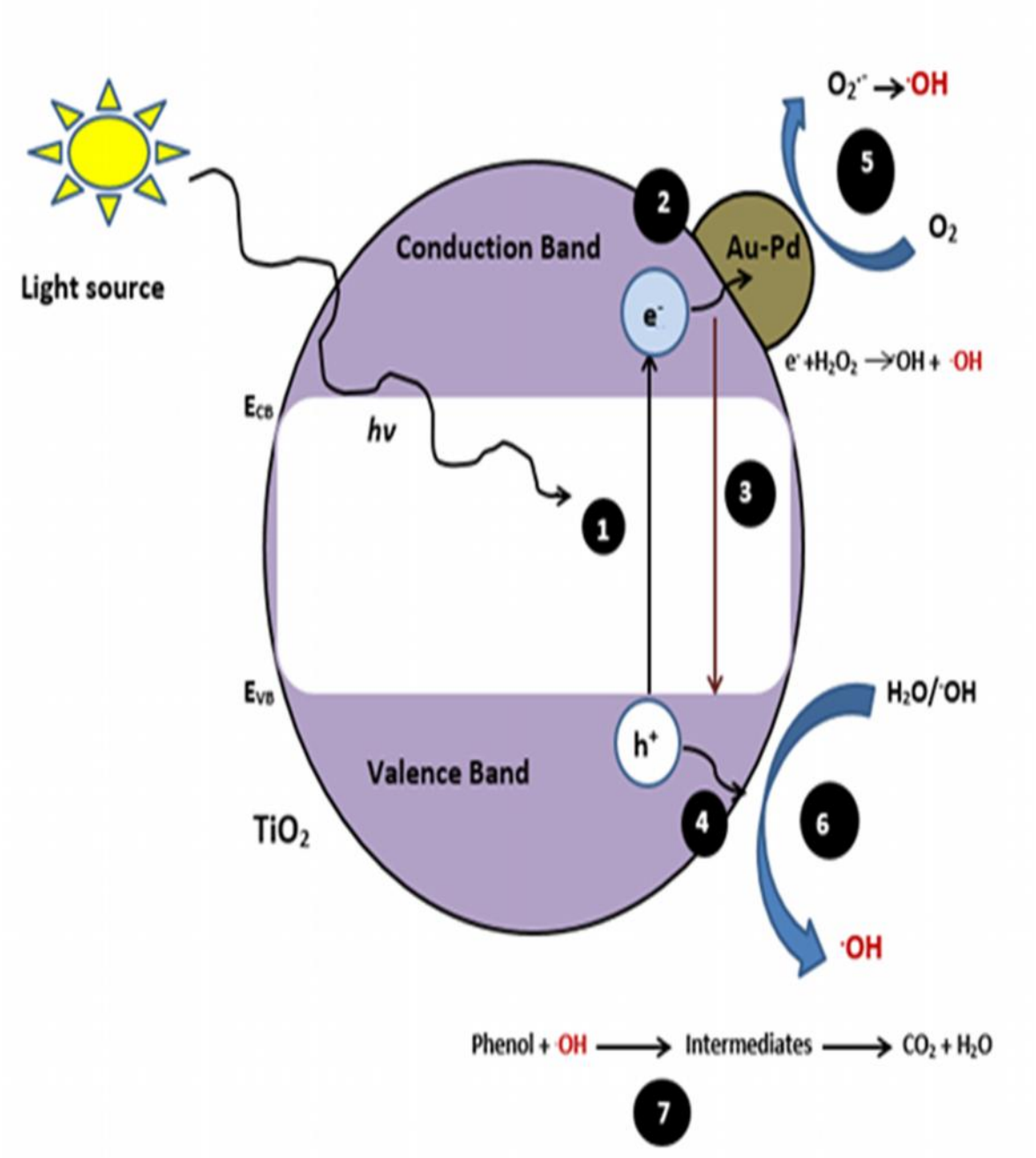


Figure 1.1: Schematic of photocatalytic degradation of organic contaminants

The second step involves the behaviors of charge carriers and electron transfer processes at TiO_2 surface after their creation and stabilization of an electron on the surface to form a trapped electron by the aid of the metal deposited. The essential characteristic of TiO_2 photocatalysis is the electron transfer event, the third step is dedicated to reviewing various electron hole recombination processes at TiO_2 surfaces, with the focus on the dynamics of single electron-hole recombination. The fourth step involves the holes transfer to the surface of the TiO_2 and stabilization of the hole on the surface to form a trapped hole. The fifth process involves the reduction of oxygen molecules; the electron must approach the TiO_2 surface, and in many cases, become chemisorbed by the metal deposited on the surface. The sixth process involves the reduction of water molecule by the positive hole to create reactive hydroxyl species. So the seventh step will review how these additives affect i.e. the electron transfer and catalytic aspects of TiO_2 photocatalyst to mineralize organic pollutant into CO_2 and H_2O.

1.3.1 Basic principles

A photocatalysis process essentially is similar to the conventional catalysis except that the catalyst is activated by photons instead of thermal energy. A simplified diagram of a semiconductor photocatalytic process is presented in Figure 1.1. When electron-hole pairs are formed, the photo-excited electrons can reduce molecular oxygen to give superoxide ion. The positive holes attract hydroxide ions or water molecules adsorbed on the external surface, and form hydroxyl radicals, which are the main species responsible for oxidation of organic chemicals. In liquid phase, a complete oxidation of the organic chemicals can be usually achieved, which leads to the formation of CO_2 and water as benign final products

1.3.2 **Photon absorption**

Photocatalytic oxidation reaction involves the mineralization of organic pollutants into harmless molecules like CO_2 and H_2O in the presence of semiconductors. The process involves the use of light source and oxidizing agent like hydrogen peroxide, oxygen, air etc. The diagram in Figure 1.1 illustrates the mechanism of titanium(IV) Oxide photocatalyst in photoxidation process, only photon with the required energy equal to the band gap energy can promote the excitation of the valence band electron to the conduction band. Photons with energies lower or greater than the band gap energies of the TiO_2 are dissipated in the form of heat. The irradiation of the photocatalyst surface with sufficient required energy leads to the formation of a positive hole (hv^+) in the valence band and an electron (e^-) in the conduction band (CB) which are relevant for the generation of the radical species (Ahmed *et al.,* 2010). The activation of TiO_2 by UV light can be represented by the following steps:

$$TiO_2 + hv \rightarrow e^- + h^+ \qquad 1.1$$

$$e^- + O_2 \rightarrow O_2^- \qquad 1.2$$

1.3.3 **Charge transfer and trapping**

In order for photon absorptivity in a semiconducting photocatalyst to translate into surface photoactivity, generated charge carriers must reach the surface with high probability and be stabilized at the surface for electron/hole transfer processes (and not for recombination events) (Henderson, 2011). Photogenerated charge carriers of opposite sign can be separated efficiently by the electric field, which is formed spontaneously in the space charge region of semiconductor interfaces. Separated electrons and holes can then migrate and reach the surface, where they can get trapped in subsurface and surface states of the semiconductor particle.

$$e_{CB}^{-} \rightarrow e_{trap}^{-} \quad 1.3$$

$$h_{VB}^{+} \rightarrow h_{trap}^{+} \quad 1.4$$

It is believed that Ti (IV) at the surface or in the bulk of the semiconductor particle are reduced by photogenerated electrons forming Ti (III) (Kondarides, 2010), which can be considered to be intrinsic surface states localized below the conduction band edge:

$$e_{CB}^{-} + Ti^{IV}OH \rightarrow Ti^{III}OH \quad 1.5$$

$$e_{CB}^{-} + Ti^{IV} \rightarrow Ti^{III} \quad 1.6$$

1.3.4 **Electron –hole recombination**

When the generated electrons and holes are not involve in the oxidation of organic pollutant and the reduction of the oxidant into reactive species, there will be accumulation of electrons on the conduction band, which will result to rapid recombination of the electrons and holes that are produced initially. The prevention of recombination of the electrons and holes in photocatalysis is a vital issue because the rate of recombination is a rate limiting step in the photocatalysis process. The recombination can result to two major outcomes; (1) Radiative and (2) Non-radiative. There are several attempts by researchers to address the problem of electrons and holes recombination, which involve the use of metals and non-metals dopants on the semiconductor. The radiative decay involves the dissipation of the light absorbed by TiO_2 in the form of heat during the light irradiation, but it was reported by Leytner and Hupp (2000), that in a recombination process 150kJ/mol of energy was released as heat while in non-radiative quenching 310kJ/mol of heat is dissipated. These implies that in TiO_2 recombination process, it mostly take the non-radiative pathway due to the fact that most radiative processes do not release significant amount of energy.

In order to understand the reaction mechanism of photocatalysis process, a simple kinetic model is shown below as reported by Malato *et al*., (2009).

$$TiO_2 + hv \xrightarrow{g} e^- + h^+ \quad (1.7)$$

$$e^- + A \xrightarrow{k_e} A^- \rightarrow (reduction - products) \quad (1.8)$$

$$h^+ + D \xrightarrow{k_h} D^+ \rightarrow (Oxidation - Products) \quad (1.9)$$

$$e^- + h^+ \xrightarrow{k_r} TiO_2 \quad (1.10)$$

$$A^- + D^+ \xrightarrow{k_r'} A + D \quad (1.11)$$

where e^- and h^+ are conduction band electrons and valence band holes, respectively. A and D represent molecules which are reduced and oxidized, respectively. The intermediates species, A^- and D^+, precede the reaction toward reduction and oxidation products. The Photoinduced electron and hole recombine with each other and diminish in the solid (Eq. (1.10)). Indirect recombination or a net recombination may occur between the primary reductant and oxidant, as indicated by Eq. (1.11). According to the reaction scheme of Eqs (1.7)-(1.10), the reaction rates for e^- and h^+ can be expressed respectively as follows:

$$\frac{\delta[e^-]}{\delta t} = -k_e[e^-] - k_r[e^-][h^+] + g \quad (1.12)$$

$$\frac{\delta[h^+]}{\delta t} = -k_h[h^+] - k_r[e^-][h^+] + g \quad (1.13)$$

where, $[e^-]$ and $[h^+]$ are densities (cm^{-3}) of conduction band electrons and valence band holes in the semiconductor particle, respectively, g represents the generation of photoinduced e^- h^+ pairs ($cm^{-3}s^{-1}$), which can be calculated with the flux of the incident light, absorption

coefficient of the system, and the density of the semiconductor material. k_e and k_h are the rates of electron and hole transfers (s^{-1}), respectively. Both of the decay rates must be affected by the molecules, A and D, adsorbed on the particles surface, respectively.

The differential equations can be solved by employing a steady state approximation for $[e^-]$ and $[h^+]$:

$$g - k_e[e^-] = k_r e^- h^+ \quad 1.14$$

$$k_h[h^+] = k_e[e^-] \quad 1.15$$

which lead to the following relationship;

$$\frac{1-\Phi_e}{\Phi_e^2} = \frac{k_r}{k_e k_h} g \quad 1.16$$

where Φ_e, defined by $\Phi_e = k_e[e^-]/g$, is the quantum yield of the electron transfer. The dependence of quantum yield on the incident light intensity is supported by the experimental evidence of the electron transfer to methylviologen induced by laser (Nosaka and Fox, 1988).

When the quantum yield is so low that the recombination reaction becomes relatively dominant, Eq. (1.16) is simplified to $\Phi_e = (k_e k_h / k_r g)^{\frac{1}{2}}$ or $[e^-] = (k_h g / k_r k_e)^{\frac{1}{2}}$. This relationship indicates that the steady amount of photoinduced electron is proportional to the square root of the light intensity. A similar relationship can be also obtained for the case of the photoinduced holes, and an equation similar to Eq. (1.16) is used to calculate the hole transfer yield, Φ_h, (Kaneko and Okura, 2002).

1.3.5 **Photocatalytic quantum efficiency**

The quantum efficiency of a photocatalytic process is a vital way to compare the activity of different photocatalyst involved in a photocatalytic process. Quantum yield is defined as the

number of defined events (reactant consumed or product formed) which occur per photon absorbed by the system at a given wave length. Quantum efficiency is defined as the number of defined events (reactant consumed or product formed) which occur per photon absorbed by the system at broadband radiation (Serpone and Salinaro, 1999).

Based on the proposed photocatalysis mechanism described above, the electron-hole pairs generated upon light irradiation do not necessarily lead to the degradation of organic chemicals. Therefore, the light use efficiency is usually less than 100%. This efficiency may vary from one photocatalyst to another, which is generally attributed to the difference in the chemical, structural, electronic, and optical properties of photocatalyst materials. In heterogeneous photocatalysis, quantum efficiency has commonly been taken to quantify the photocatalytic activity. It is defined as the number of reactants consumed or product formed relative to the number of photons at wavelength λ absorbed by the photocatalyst:

$$\Phi_A = \frac{n}{n_{ph}} \qquad 1.17$$

where Φ_A= quantum yield at wavelength λ; n = number of molecules reacted or molecules formed; n_{ph} = number of absorbed photons at wavelength λ.

The number of absorbed photons is experimentally difficult to determine owing to the reflection, scattering, transmission, and absorption of the photocatalyst particles in aqueous suspension. It has been suggested that light losses due to scattering or reflection can be significant, accounting for up to 70% of the incident light (Serpone and Salinaro, 1999) and (Panayotov and Yates Jr, 2003). To circumvent the problem of quantifying the exact number of photons absorbed by photocatalyst particles, researchers often use the term apparent quantum efficiency reference to incident photons to quantify the photocatalytic activity.

Apparent quantum efficiency is defined as the number of reactant molecules converted divided by the number of photons of the incident light supplied: Φ is number of reactant molecules per number of photons supplied. This apparent quantum efficiency, Φ can be also expressed as the initial reaction rate divided by the incident photon flux:

$$\Phi = \left(\frac{N_a V_i dC_a/dt}{dN_{ph}/dt}\right) \quad 1.18$$

where: V_i = volume of the reaction solution (L); t = reaction time (s); C_a = concentration of the reactant A (mol L^{-1}); N_{ph} = number of photons supplied in time t; N_a = Avogadro's number, 6.022×10^{23} (number of molecules mol^{-1}). The apparent quantum efficiency for liquid photocatalysis is usually very low, typically around a few percent. This is the main obstacle that has prevented this technology from being widely commercialized. Currently, extensive research has been conducted to design a more effective photocatalysis system. Photocatalyst materials were engineered to achieve lower bandgap energy and thus stronger light absorption in both UV and visible ranges. In the meantime, more efficient photocatalytic reactors were designed to achieve high illuminated surface area per unit volume of liquid.

1.3.6 **Reduction and oxidation of molecules at the surface**

In this reaction, h^+ and e^- are powerful oxidizing and reductive agents respectively. The oxidative and reductive reaction steps are expressed as:

Oxidative reaction:

$$h^+ + Pollutants \rightarrow CO_2 \quad 1.19$$

$$h^+ + H_2O \rightarrow OH\cdot + H^+ \quad 1.20$$

Reductive reaction:

$$OH^{\cdot} + Pollutants \rightarrow CO_2 \quad 1.21$$

Hydroxyl radical generation by the photocatalytic oxidation process is shown in the above steps. In the degradation of organic pollutants, the hydroxyl radical, which is generated from the oxidation of adsorbed water where it is adsorbed as OH^-, is the primary oxidant; and the presence of oxygen prevents the recombination of an electron–hole pair. The desired process consists in the reaction of the activated electron with an oxidant (O_2), yielding a reduced product(O_2^-), and the reaction of the photogenerated hole with a reductant to produce an oxidized product, as indicated in Figure 1.1 (Kondarides, 2010)

In aerated conditions, molecular oxygen adsorbed on the surface of the semiconductor acts as electron acceptor, while adsorbed water molecules and hydroxyl anions act as electron donors, leading to the formation of very powerful oxidizing $OH^{\cdot}$ radical. In the presence of an organic molecule (Pollutants) adsorbed in the catalyst surface, hydroxyl radical is the primary oxidizing entity, reacting by adduct formation, followed by structural breakdown into several intermediates till, eventually, total mineralization. (Serpone and Salinaro, 1999)

1.3.7 Incident light intensity and wavelength

Light intensity determines the extent of light absorption by the semiconductor catalyst at a given wavelength. The rate of initiation of photocatalysis, electron-hole formation in the photochemical reaction is strongly dependent on the light intensity (Cassano and Alfano, 2000). The light-induced nature of activation of photocatalytic processes implies that the reaction rate should increase with increasing the number of incident photons and, thus, light intensity, I. This is true for very small values of I, typically of the order of a few mW/cm^2, where the rate increases linearly with increasing light intensity, above a certain value of I, the reaction rate becomes proportional to the square root of light intensity as shown on Figure

1.2(a). With increasing light intensity, the extent of band bending tends to decrease and the surface reactions strongly compete with processes involving electron-hole recombination. Under these conditions, the rate becomes half order with respect to I. At even higher light intensities, the rate may become independent of I and the rate becomes mass transfer limited. While in some cases the rate of reaction exhibited a square root dependency on the light intensity, others observed a linear relationship between the two variables (Herrmann, 1999; Ollis *et al*., 1991; Al-Sayyed *et al.*, 1991). The effect of light intensity on the organic pollutant degradation rate was reviewed, and it has been reported that the rate is proportional to the radiant flux φ for $\varphi \geq 25\text{mW/cm}^2$, and above 25mW/cm^2 the rate has been shown to be varied as $\varphi^{\frac{1}{2}}$, indicating a too high value of the flux and an increase of the electron-hole recombination rate. At high intensity, the reaction rate was independent of light intensity. This is likely because, at low intensity, reactions involving electron-hole formation are predominant and electron-hole recombination is insignificant (Ollis *et al.*, 1991). Besides, energy loss due to light reflection, transmission and energy loss as heat is inevitable in the photocatalytic process (Yang and Liu, 2007).

The rate dependence of a photocatalytic process on light intensity can be introduced in a global rate equation in a power form (Hermann, 2005)

$$r \propto I^{a} \qquad 1.22$$

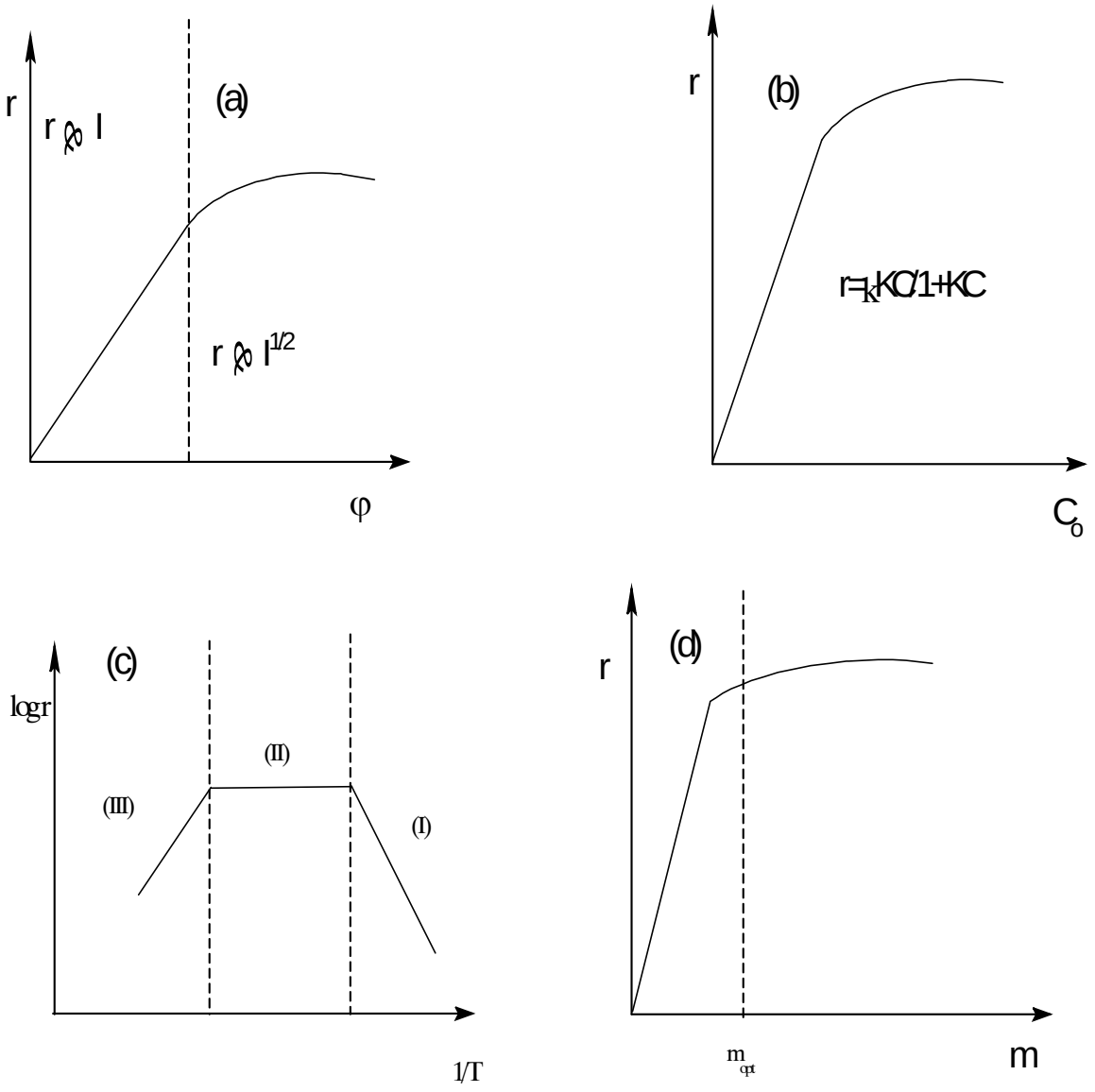


Figure 1.2: Influence of some physical parameters on the rate, r, of photocatalytic reactions: (a) radiant flux φ; (b) initial concentration, C_o of reactant; (c) temperature, T; (d) mass of catalyst, m redrawn from (Hermann, 2005).

With $0 \leq a \leq 1$. Clearly, in any photocatalytic system, the optimal light power utilization corresponds to the domain where r is proportional to I, i.e., when a = 1.

Different light sources with varying wavelength will produce different photochemical result when used with semiconductors, titanium(IV) Oxide exists in three different forms i.e. the rutile, anatase and brookite phases. P25 Degussa which is the most commonly used titanium(IV) Oxide standard in photochemical reactions has a crystalline ratio of anatase to rutile (70/80:30/20). Light source of >>380nm is sufficient for photonic activation due to the bandgap energy of the rutile phase of 3.12eV and the anatase phase of 3.20eV (Gaya and Abdullah, 2008; Chong *et al*., 2010). Due to the bandgap of the rutile phase 3.12eV it implies that the rutile titanium(IV) oxide will be photo active with light source of 400nm wavelength. The electromagnetic spectrum can be classified as: The UVA ranges from 315 to 400nm (3.10 to 3.94ev), the UV-B ranges from 280 to 315nm (3.94 to 4.43ev) and the UV-C ranges from 100 to 280nm (4.43 to 12.4ev) (Rincon and Pulgarin, 2005). Most of the photocatalytic experiment were conducted using the UV-A light source due to the bandgap energy of the titanium(IV) Oxide it can undergo photonic activation at the wavelength ranges within the UV-A (Chin *et al.,* 2006; Ochuma *et al*., 2007)

1.3.8 **Concentration of reactants**

One of the prerequisite for a photocatalytic reaction to proceed is adsorption of at least one reactant on the photocatalyst surface, because interfacial electron transfer has to compete with the very fast electron-hole recombination process. The adsorption of a substance *i* on the photocatalyst surface can be described by the Langmuir isotherm:

$$\theta_i = \frac{K_i C_i}{1+K_i C_i} \qquad 1.23$$

where θ_i is the surface coverage, K_i the adsorption equilibrium constant, and C_i the initial concentration of species *i* in the aqueous solution. It should be noted here that the surface

coverage of an adsorbed species in the dark may be significantly different than that under illumination conditions. The electromagnetic radiation can change the equilibrium position of a chemisorption process by affecting the bond strength between the adsorbed molecule and the semiconductor surface, this is due to the change that occurs both on the Fermi level of the semiconductor and the population of the surface electrons and holes upon irradiation.

The rate of a photocatalytic reaction is related to the surface coverage of reactants and products by equations which are similar to those developed for thermal catalytic reactions. In most cases, the kinetics of a photocatalytic process can be described adequately with the use of *Langmuir-Hinshelwood* (LH) or *Eley-Rideal* (ER) pathways (Kondarides, 2010). The LH mechanism has been found to apply in a great number of photocatalytic reactions occurring in the liquid or in the gas phase. According to this model, the primary redox intermediates undergoes subsequent thermal surface reaction before desorbing from the surface. Using a simple unimolecular reaction occurring in the liquid phase where reactant A yield product P and the reactant is significantly more strongly adsorbed than the product (Kondarides, 2010), the LH rate equation is of the form:

$$r_{LH} = k_{LH}\theta_A = \frac{k_{LH}K_AC_A}{1+K_AC_A+K_SC_S} \qquad 1.24$$

where r_{LH} is the reaction rate, k_{LH} is the rate constant, and subscript "A" and "S" refer to the reactant and solvent, respectively. Similarly, the rate of a bimolecular surface reaction $A + B \rightarrow P$ between two surface species adsorbed independently on the surface is of the form:

$$r_{LH} = k_{LH}\theta_A\theta_B = \frac{k_{LH}K_AC_AK_BC_B}{(1+K_AC_A+K_SC_S)(1+K_BC_B+K_SC_S)} \qquad 1.25$$

when Eq. (1.25) reduces to a form similar to Eq. (1.24), under such condition the concentration of one of these surface species at the photostationary state is considered constant, where $C_s >> C_A$ and that C_s stays essentially constant, the part of the semiconductor surface covered by the solvent is approximately unchanged (Kondarides, 2010). Under these conditions Eq. (1.23) can be written as:

$$r_{LH} = \frac{k_{LH}K'C_A}{1+K'C_A} \qquad 1.26$$

where $K' = K_A/(1 + K_sC_s)$. For dilute solutions, where $K_AC_A << 1$, the reaction is of the apparent first order, whereas for high reactant concentrations, where $K_AC_A >> 1$, the reaction rate is maximum and is of the apparent zero order as shown on Figure 1.2(b). The *Eley-Rideal* kinetic treatment implies that reactions occur between a surface species and a reactant molecule diffusing simultaneously from the fluid. The rate of the reaction is as follows

$$r_{ER} = K_{ER}C_A \qquad 1.27$$

where k_{ER} is the reaction rate constant. Eq. (1.27) is a pseudo-first-order rate equation. If both LH and ER pathways are operating simultaneously, then mixed behavior for the reaction rate versus concentration of the reactant is to be expected (Kondarides, 2010), keeping the experimental condition constant while varying the initial concentration of organic molecule in aqueous solution will result to different irradiation time for complete degradation of the organic molecules, due to the fact that as the concentration of the organic molecules increases it concurrently saturates the surface of the photocatalyst thereby reducing the photoresponse of the catalyst which leads to rapid deactivation of the photocatalyst (Saquib and Muneer, 2003; Arana *et al*., 2004).

Hong *et al.,* (2001) studied the effect of initial concentration of phenol on the photocatalytic efficiency of titanium(IV) oxide mixed with water; it was observed that the rate of phenol decomposition is high with the minimum concentration of phenol, also Parida and Parija also reported that the rate of phenol degradation decreases when the concentration was increased under both solar radiation and visible light (Hong *et al*., 2001; Parida and Parija, 2006)

1.3.9 **Temperature**

The bandgap energy of semiconductor photocatalysts is too high for thermal excitation to become significant at ambient temperature. Therefore, photo driven reaction steps are in principle, not sensitive to minor changes in temperature and the true activation energy, E_t, is theoretically zero. When temperature is varied in such a range that thermal transformation of reactant does not occur, then the rate may vary with temperature as shown in Figure 1.2(c). This behavior can be explained within the frame of the *Lagmuir-Henshelwood* mechanism described in section 1.3.8, by considering that adsorption and desorption are thermally activated processes. For the simple case of a unimolecular reaction ($A \rightarrow P$) where product P adsorbs on the same sites as reactant A, Eq. (1.24) can be written as:

$$r_{LH} = k_{LH}\theta_A = \frac{k_{LH}K_A C_A}{1+K_A C_A+K_p C_P} \qquad 1.28$$

If the surface coverage of P is high, desorption of P can be the rate-limiting step and the apparent activation energy of the reaction, E_a, is given by:

$$E_a = E_t - Q_A + Q_P \qquad 1.29$$

where Q_A and Q_P are the (positive) heats of adsorption of reactant A and P, respectively. At intermediate temperatures, P may be weakly adsorbed and the rate is, practically, independent of temperature, i.e. $E_a = E_t \approx 0$ (Figure 1.2(c), region II). At low temperatures, adsorption

of the inhibition product P is favored ($Q_P >> Q_A$) and E_a tends asymptotically to Q_p (region). Finally, at high temperatures the adsorption of reactant A, may become rate-limiting and E_a tends to Q_A, i.e., it takes negative values region (region III). The above considerations often apply in photocatalytic reactions occurring in aqueous solutions, such as degradation of organic pollutants present in water and wastewater. An increase in reaction temperature generally results in increased photocatalytic activity however reaction temperature >>80^0C promotes the recombination of charge carriers and disfavors the adsorption of organic compounds on the titania surface. A reaction temperature below 80^0C favors the adsorption whereas further reduction of reaction temperature to 0^0C results in an increase in the apparent activation energy (Chong *et al.,* 2010). In this case, the apparent activation energy is usually very small at ambient conditions (a few kJ/mol) and, as a consequence, the optimum reaction temperature is generally in the range of 20-80^0C (Hermann, 2005). Generally, the increase in temperature enhances recombination of charge carriers and desorption process of adsorbed reactant species, resulting in decrease of photocatalytic activity. This is in conformity with Arrhenius equation, for which the apparent first order rate constant K_{app} should increase linearly with exp(-1/T) (Gaya and Abdullah, 2008).

1.3.10 **Mass of catalyst**

The rate of photocatalytic reactions is generally proportional to the catalyst loading due to the higher surface area of the photocatalyst that is available for adsorption of the reactants. For reactions occurring in photocatalyst suspensions, the initial rate increases linearly with increasing mass, m, of photocatalyst up to a certain limit and then gradually levels off as shown on Figure 1.2(d). The linear region corresponds to the true heterogeneous catalytic regime and its limit represents the maximum amount of photocatalyst in which the surface of

all particles is totally illuminated. Above this limit, the solution opacity increases and screening effect of excess particles occurs, which masks part of the photosensitive surface. For even higher photocatalyst contents, a decrease in reaction rate is often observed, which is due to a reduction of light penetration in solution and the contribution of "terminal" reactions between the photogenerated species. A number of studies have reported the effect of TiO_2 loadings on the treatment efficiency of the photocatalytic reactor (Daneshvar *et al*., 2006; Gaya and Abdullah, 2008; Chin *et al.,* 2006; Chong *et al*., 2009; Kondarides, 2010). Although a direct comparison between these studies is difficult to be made due to the differences in the working geometry, radiation fluxes and wavelengths used, it was evident that the optimum dosages of photocatalyst loading were dependent on the dimension of the reactor. With these, the photoreactor of choice should be used under an optimized condition to avoid the use of excess amount of catalyst which can reduce the photons efficiency. Therefore, the optical path length of a photoreactor is a function of the light scattering and amount of catalyst used

1.3.11 **Solution pH**

The photocatalytic process involves the formation of hydroxyl radical ($^{\cdot}OH$) and reactive oxygen species; these also mean that the process is pH dependent. The aqueous solution pH affect the surface charge of semiconductors, which also affect the rate of adsorption of the organic pollutant unto the surface of the catalyst, the rate of adsorption and rate of mineralization are shown to be at maximum near the zero point charge of the semiconductor in solution (Subramanian *et al.,* 2000).

Semiconductors can act like diprotic acid in aqueous solution, due to their amphoteric properties, in the case of TiO_2 it reacts with water in the following manner:

$$TiOH_2^+ \overset{pK_{a1}}{\longleftrightarrow} TiOH + H^+ \quad 1.30$$

$$TiOH \overset{pK_{a2}}{\longleftrightarrow} TiO^- + H^+ \quad 1.31$$

For P25 Degussa, pK_{a1} = 4.5 and pK_{a2} = 8.0, which yield a pH of zero point of charge (pH_{zpc}) equal to 6.25. Thus, the rate of adsorption of organic pollutant unto the surface of titanium(IV) Oxide is a function of the electrical charge on the organic pollutant in solution and the titanium(IV) oxide surface. From the pK_a values above it is evident that at low pH more of the negatively charged organic molecules will be adsorbed due to the interaction with the positively charged TiO_2 surface, and repulsive force will be experienced in the same solution with positively charged organic molecules, thereby decreasing the amount of pollutant adsorbed on the catalyst surface. At higher pH the exact opposite will occur. According to Nernst's law; varying the pH of the solution, will shift the energies of the valence and conduction band edges by 0.059 V per pH unit (at ambient temperature) (Nozik *et al.*, 1996; Matsumoto, 1996; Kormann *et al.*, 1988). According to the Nernst law the solution pH affect the energies of the valence and conduction band edges which in turn affect the rate of the $OH^{\cdot}$ radical formation, therefore, the holes at the valence band are considered as a major step in the oxidation at low pH and the hydroxyl radicals are the predominant species produced at both neutral and high (Shifu and Gengyu, 2005; Matthews, 1990). Generally, it is expected that the rate of decomposition of organic pollutants on the surface of TiO_2 to be higher in the presence of excess hydroxyl species, but it was discovered by researchers that titanium(IV) oxide have high oxidizing activity at low pH due to the presence of excess H^+ and thus it decreases the rate of the photocatalytic degradation (Sun *et al*., 2006). Several investigations had being done to logically look at the effect of pH on the photocatalytic degradation and adsorption of organic pollutant in aqueous solution using

titanium(IV) oxide catalyst. (Singh *et al.*, 2007; Rahman and Muneer, 2005; Wen-Yu and Ku, 2007; Mrowetz *et al.*, 2006). To obtain a complete mineralization of organic pollutant in photocatalysis it involves optimizing the whole process which include obtaining the right pH for the solution and the semiconductor photocatalyst to be use.

1.3.12 Dissolved oxygen

There are several controversial reports concerning the role of O_2 in photocatalytic reaction (Henderson, 2011), oxygen acts as an electron scavenger during photocatalytic reactions were for several reactive species like O_2^{-}, HO_2 and dissolved oxygen are form (Ilisz and La, 1999). It has been reported that all the reactive species are generated through the reaction of the conduction band electron with O_2, therefore oxygen is indispensable in the generation of singlet oxygen, hydrogen peroxide, superoxide radical and hydroxyl radical (Chatterjee and Mahata, 2001). Due to the importance of these reactive species formed in the presence of oxygen and the ability of oxygen to reduce recombination rate, oxygen is very vital in photocatalytic degradation of organic pollutants (Zhang *et al*., 2009; Dijkstra *et al*., 2001; Chong *et al*., 2009). More also, the reactive species aid the stabilization of the intermediates formed during the process. The amount of oxygen needed in liquid phase photocatalysis need to be optimized due to the ability of oxygen to act as an electron sink and provides a weightless form for the titanium(IV) Oxide particles in solution (Habibi *et al.*, 2005)

1.4 Methods for Improving Photocatalytic Efficiency

Titanium (IV) dioxide as a photocatalyst has some limitation, which tend to affect its activity in photocatalysis. The bandgap of titanium (IV) dioxide is 3.2eV for the anatase phase which is the most used phase of TiO_2 in photocatalysis, implying that anatase can be photo-excited with UV light source above 350nm. The solar spectrum contains about 4% UV radiation

reaching the surface of the earth, this implies that if the solar radiation will be used for photocatalysis, the process is already limited due to the small amount of the total UV radiation from the solar radiation. Also the rapid rate of electron-hole recombination in TiO_2 is energy wasting, due to these several methods are already in use in order to improve the photoresponse, suppressed the recombination rate and thus improve the activity of titanium(IV) Oxide in the photocatalytic degradation of organic pollutant (Kamat and Meisel, 2002), these include; the use of dye sensitizers (Vinodgopal *et al.,* 1996), metallic ion deposition (Ni *et al.,* 2007), transition metals doping (Litter, 1999), incorporation of carbon (Yu *et al.,* 2005), and doping with non-metals (Fujishima *et al.,* 2008) as depicted on Figure 1.3. The introduced species can act as trap centers for the photogenerated electrons and holes and thus enhance electron-hole separation.

1.4.1 **Metal-deposited TiO_2 photocatalyst:**

Metal deposited onto titanium(IV) Oxide is use to improve it photoresponse and also to reduce the rate of electrons-holes recombination. This is one of the prominent and frequent ways of improving TiO_2 activity in photocatalysis (Dobosz and Sobczy'nski, 2003; Hu *et al*., 2003; Jang *et al*., 2008). Metals like Cu, Fe, Pd, Au, Ag etc. have been deposited onto TiO_2, these metals have the ability of altering the optical properties of the TiO_2 semiconductor so as it can be photoexcited in the visible light region (known as bathochromic shift). The metals also act as trap centers, in which they trap the electrons generated from the valence band thus promoting charge separation which further decrease the recombination of the electron and hole. When a UV light is irradiated on a metal deposited TiO_2 (e.g. Au-TiO_2) a Fermi level equilibration due to charge distribution is established between the metal and titanium(IV) oxide,

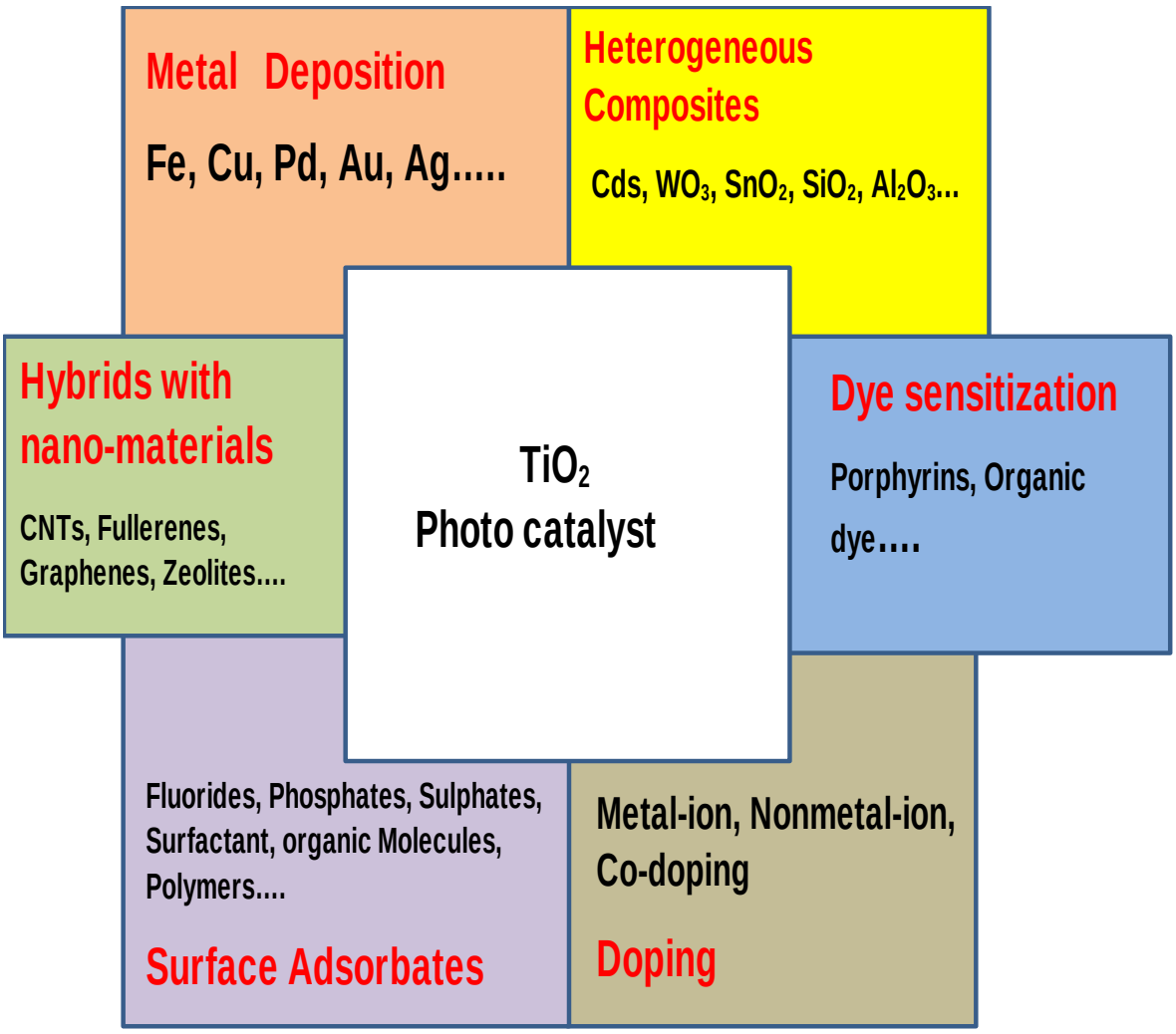


Figure 1.3: Method for improving the activity and photo-response of TiO_2 (Park et al., 2013)

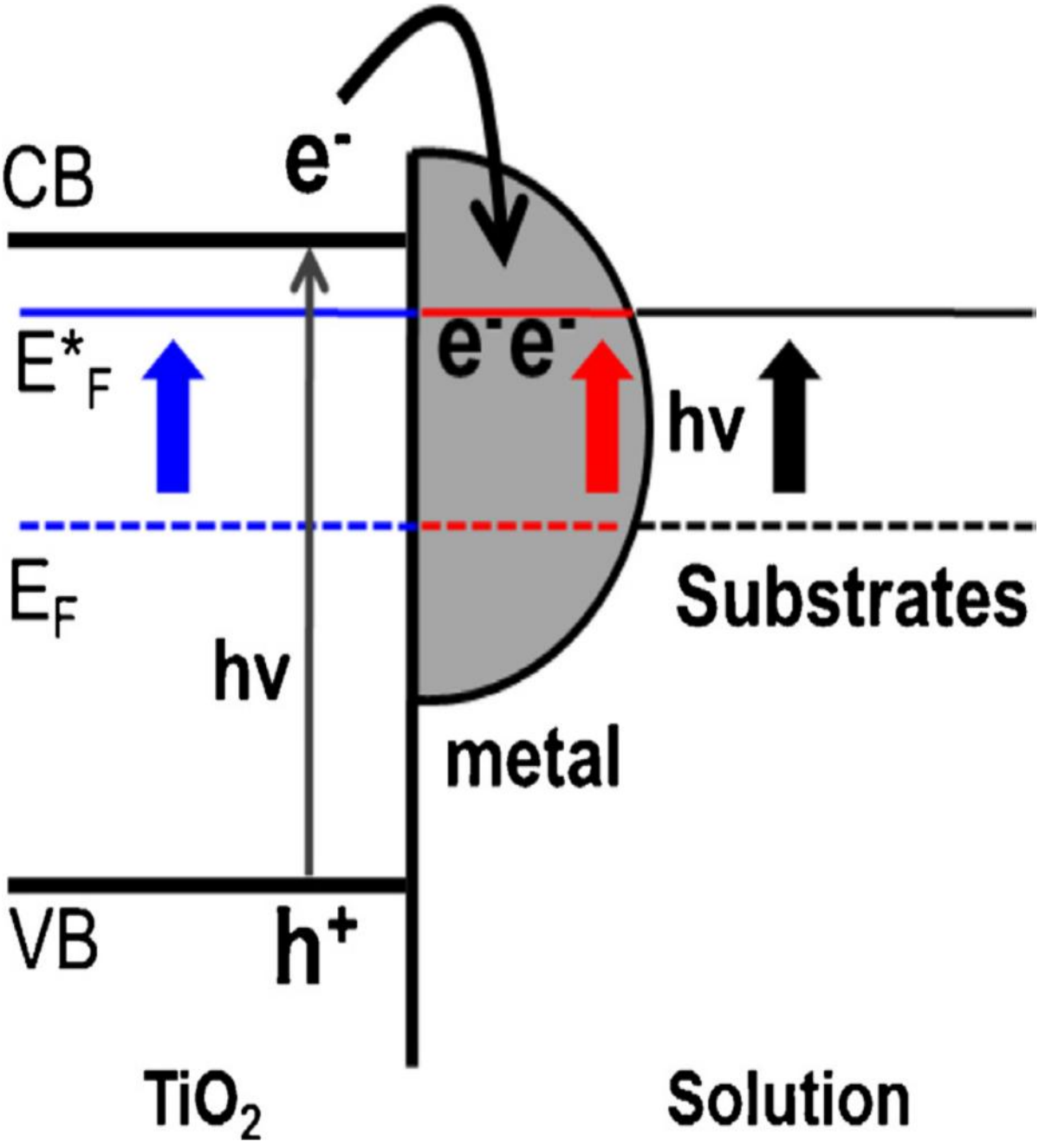


Figure 1.4: Fermi level equilibration via charge distribution between UV-irradiated TiO_2 and metal nanoparticles with redox couple (Park et al., 2013).

which enhance the photocatalytic activity of the photocatalyst (Chandrasekharan and Kamat, 2000; Subramanian *et al.,* 2004) as shown on Figure 1.4. The valence electrons of gold and silver oscillate in their nanoparticles. These feature is called localized surface plasmon resonance (LSPR) (Rycenga *et al.,* 2011), and happens when the metals are deposited onto TiO_2 semiconductor used in photo-reaction (Maicu *et al*., 2011; Ismail *et al.,* 2009). These free oscillations of the free electrons of gold and silver are known to make titanium(IV) oxide reactive in visible light when used in photocatalysis (Kowalska *et al*., 2010; Yu *et al*., 2013).

1.4.2 Doped TiO_2 and visible light photocatalytic activity

Another way to retard the rate of recombination and enhance the visible light response of titanium(IV) Oxide semiconductor is by using dopants. Dopants are usually classified into metal ions (transition metals and noble metals) and nonmetal ions, and the selection of dopant is very crucial in determining overall photocatalytic activities of semiconductors (Park *et al.,* 2013). There has been a large number of studies that tried various doping combinations of metal/metal e.g., Au/Pd, (Hamill *et al*., 2014; Su *et al*., 2012), non-metal like Nitrogen (Asahi *et al.,* 2001).

1.4.3 Composite semiconductor photocatalyst

Composite semiconductors can improve photocatalytic activity due to their ability to increase charge separation and extension of the catalyst to be visible light responsive (Beydoun *et al*., 1999). Coupled semiconductor system with promising photocatalytic performance include CdS-TiO_2, Bi_2S_3-TiO_2, CdS-ZnO, CdS-Ag_2S, ZnO-ZnS, ZnO-ZnSe etc.

1.4.4 Dye sensitization

Dye sensitization is another way to expand the range of wavelength at which semiconductor responds to visible light. This is achieved by attaching a sensitizer (S), onto the surface of a

semiconductor particle. Irradiation of the dye sensitized semiconductor by visible light results in excitation of an electron to either the singlet or triplet excited state (S*) of the molecule (Kondarides, 2010).

1.4.5 Hybrids with Nano materials

Nanocomposites containing carbon nanotubes (CNTs) have attracted great attention because of the unique electrical and structural characteristics of CNTs. Since CNTs can show excellent electron conduction, high surface areas and strong adsorption capacities, they are also used as effective dopants and also supports for TiO_2 based photocatalytic materials. The ability of carbon nanotubes to conduct both electricity and heat foster their role to support the separation of the photogenerated electron-hole pairs through the formation of heterojuctions at the titanium(IV) Oxide/carbon nanotubes interface (Yu *et al*., 2007).

1.4.6 Role of inorganic adsorbates

The presence of electron donors or acceptors in photocatalytic reaction can decrease the rate of recombination of electrons-holes pair, with these the electrons and holes are made readily available for the generation of the reactive species needed in the reaction (Park and Choi, 2004) inorganic anions such as sulphate (Samantaray *et al.*, 2003), fluoride (Kim *et al.*, 2010) and phosphate (Raj *et al.*, 2009; Korosi *et al*., 2007), have been used in such photocatalysis to enhance the rate of the reaction.

1.5 Phenol

Phenol is a mono-substituted aromatic hydrocarbon. In its pure state, it exists as a colorless or white solid. This pure compound is mixed with water and commercially sold as a liquid product, it gives off a sweet, acrid smell detectable to most people at 40 ppb in air and at

about 1–8 ppm in water (Toxicological Profile, 1998). It evaporates more slowly than water, and it is also combustible. Phenol is one of the most widely used organic compounds in existence, due to its used as one of the basic starting material in the pharmaceutical, agricultural (pesticides), petrochemical industries.

1.5.1 Uses of phenol

Phenol is one of the basic feeds stock in most petrochemicals, agro-allied chemicals and Pharmaceuticals Company, which make it to be used in a broad spectrum. More also, phenolic resins are used in paints and polymer materials, also phenol is used in the production of epoxy resins which is a precursor to other chemicals. Phenol has an antiseptic effect which makes it useful in the production of bactericides, fungicides, insecticides, pesticides and acaricide etc. The cosmetic industries are also known to be a major users of phenol in the production of ointments, antiseptic soaps and lotions etc.

1.5.2 Properties of phenol

Phenol is categorized as one of the aromatic compounds, in which an $^{-}$OH group is attached directly to a benzene ring as illustrated in Table 1.1. The crystals are often rather wet and discolored. Phenol has a limited solubility in water. It is slightly acidic. Its molecule has weak tendencies to lose the H^+ ion from the hydroxyl group, resulting in the highly water-soluble phenoxide anion $C_6HO_5^-$. High concentration of phenol and its derivatives is found in nature. They are contaminates found in waste water derived from different chemical industries such as resin manufacturing, petrochemical, oil-refineries, paper making as well as iron smelting. However, phenol is highly corrosive and moderately toxic. It causes many effects on humans by burning the skin and other tissues that it comes into contact with. This gives severe skin burning and if inhaled serious it is harmful to the body.

1.6 Aim and Objectives

The aim of this work is to develop a pilot wastewater treatment plant which work with the principle of photocatalysis with the use of light source of UV-visible (solar light) wavelength, using phenol in solution as a probe molecule. The optimizations of the process for efficient wastewater treatment will be done so that the plant can run continuously for longer time duration: To achieve the above aim the following objectives will focus on: The development of photocatalyst using an established methods but with few modifications: To deposit copper, iron, gold and palladium unto titanium(IV) Oxide (P25 Degussa) and also produce bimetallic Au-Pd on P25, so as to reduce the recombination rate of electron-ho pair during photocatalysis and also shift the band-gap of the modified P25 into visible light region.

To study the effect of mono and bimetallic catalyst system namely gold palladium on the photocatalytic oxidation of phenol and observe the effect of metallic ratio on the reactions activity and selectivity.

To study the effect of the preparation of catalyst using (sol immobilization, microemulsion and hydrothermal treatment method) on the photocatalytic degradation of phenol and other substituted phenol compounds with oxygen, air and hydrogen peroxide as oxidant

Table 1.1: Physical properties and chemical identity of phenol (Lide, 1993)

Properties	Value
Melting point, ^{0}C	14
Boiling point, ^{0}C	181.8
Water solubility, g/L at 25^{0}C	87
Molecular weight g/mol	94.11
Density, at 20^{0}C	1.0576
Log K_{OW} (1-Octanol-water coefficient)	1.46

To investigate the effect of different oxidant in the photocatalytic degradation of phenol using compressed air, oxygen and hydrogen peroxide as oxidant. Due to economic consideration of the cost of H_2O_2, oxygen will be used to optimize the batch reactor.

To transfer the photocatalytic experiment which begin with the continuous stir tank reactor (CSTR batch process) to the use of trickle bed system and the Taylor flow system in continuous mode.

To make use of the modified catalyst of the M-doped TiO_2 (where M = Cu, Fe, Pd and Au) in photocatalytic degradation of phenol. Also, the photocatalytic activities and rate constants of each M-doped TiO_2 and P25 TiO_2 were studied.

Finally, the thermo-catalysis efficiency of P25 will be tested using the Taylor flow system, to try the viability of the system running 24h both in the presence of UV light and in the dark.

1.7 Justification of the Research

The conventional wastewater treatment process is costly in terms of the chemicals used in the process. In this research, the natural resources that were bestowed on nature like sunlight and air can be harnessed and used in the photocatalytic treatment of organic waste in water by these a sustainable green chemistry pathway was achieved. More also, in line with the Nigeria's economic objective of self-reliance, this work will motivate local industries to embark on the production of titanium(IV) Oxide from the rutile ore deposited in Middle Belt region of Nigeria: conserve foreign exchange used for the importation of material hither to bridge the gap between demand and supply of titanium(IV) Oxide, there by checking the present high cost.

CHAPTER TWO

2.1 Literature Review

Toxic chemicals found in water supplies and aquifers can be trace to human activities from chemical industries, pharmaceuticals, agricultural pesticides etc. Due to the carcinogenic effect of these chemicals and their support to some pathogens in water, there are several wastewater treatment techniques in use to restore the quality of water from these toxic organic pollutant found in water. These techniques include the use of activated carbon and sludge, filtration, biological treatment, chemical treatment involving the use of hydrogen peroxide, ozone and the use of UV light (Legrini *et al.,* 1993; Mills *et al.,* 1993; Ollis, 1989; Robert and Malato, 2002). These techniques used in wastewater treatment has some limitation which ranges from technical issues to the overall efficiency of the methods and the economic cost of maintaining the treatment plant. One of the basic limitations of the use of activated carbons/sludge is the issue of phase transfer of organic pollutant, which is not a total decomposition of the pollutant. The use of biological treatment is cost effective but the organic pollutant can be toxic to the microorganism used which can reduce the overall efficiency of the process. The use of strong oxidizing chemicals in the treatment process is effective but the oxidants used are of hazardous nature coupled with the requirement of high-energy artificial UV light source required (Mills *et al.,* 1993; Robert and Malato, 2002). Also the formation of stable intermediates contributes to the surge in the overall treatment cost when total mineralization are to be achieved in the wastewater. Due to the problems associated with the use of the techniques listed above, research interest are being focused no the use of TiO_2 for the complete mineralization of organic pollutant and some pathogenic microorganisms in water in the presence of light, non-toxicity, low cost and its non-

selectivity toward a wide range of organic pollutant in aqueous solution (Ollis, 1989; Matthews, 1990). The use of metal semiconductors have been shown to be very effective in the treatment of wastewater when compared with fenton oxidation process (Kar *et al*., 2013; Hoffmann *et al*., 1995; Herrmann, 1999) due to the following merits of Photocatalysis: the use of solar radiation and low energy UV light which leads to total mineralization of pollutant to CO_2 and water. The non-selectivity of the photocatalyst allows it to mineralize a broad spectrum of organic pollutant. The process can take place at ambient temperature and normal atmospheric pressure. The industrial application of photocatalysis in wastewater treatment can be enhanced through reactor design which will further increase the efficiency of the process. The problems associated with the reactor design are as follows: (i) Light exposure has to sufficiently reach the catalyst surface (ii) Substantial portion of the photocatalyst has to be illuminated with the light (iii) The issue of mass transfer in the reaction mixture has to be minimized, and (iv) the photocatalyst has to be stable towards leaching of the active metals and corrosion.

This research examined the mineralization of aqueous phenol solution in a designed and fabricated new type of continuous Taylor flow photo reactor using modified TiO_2 as catalyst. Chemical, pharmaceutical, petrochemical as well as petroleum refinery use phenols to a great extent. Due to toxicity of phenols and their derivatives, their disposal in water bodies causes severe problem to human and animal health. Over the past ten years solar activated photocatalytic purification of water has received significant attention with research focus moving from laboratory studies to pilot experimentation (Malato *et al.,* 2009).

2.2 Types of photoreactor

The design of highly efficient photoreactor is paramount in the application of photocatalysis in wastewater remediation. The major aim of reactor design in photocatalysis is to pave a pathway for the scale up of the bench scale photoreator to industrial treatment plant using the techniques. To achieved this goal several factors need to be addressed which include the distribution coefficient between the organic pollutant and the photocatalys, mass transfer, kinetics and thermodynamic of the reaction, flow rate of the effluent and oxygen, and the light source (Mccullagh, 2011). In designing the Photoreactor the state of the photocatalyst need to be critically examined i.e. whether the catalyst will be used as suspension or supported (immobilized) or it will be packed on a bed, these will also determine the cost of the treatment plant in such a way that if the suspension mode is to be used the issue of catalyst filtration from the treated waste water need to be put to account which entails the type of filtrate to be used etc.

2.2.1 Slurry/suspension liquid photoreactors systems

Titanium(IV) oxide semiconductor has been widely investigated as a photocatalyst in both slurry/suspension and immobilized systems. The main advantage of using photocatalyst slurries is the larger surface area compared with the immobilized system and limited mass transfer effect. The separation of the photocatalyst is, however, economic extensive and is a major drawback in the commercialization of the system. It was also reported that it was difficult to effect irradiation of all the photocatalyst particles in the slurry in the unit due to shielding from the light source of particles in the body of the unit by particles closer to the reactor walls (Mccullagh, 2011). Therefore depth of light penetration into the slurry reactor was restricted. A wide range of photocatalytic reactors have been developed and reported:

i. Photocatalytic Taylor vortex reactor (Dutta and Ray, 2004; Sczechowski *et al.*, 1995)

ii. The rotating disk photocatalytic reactor (Dionysiou *et al*., 2000)

iii. Slurry reactor Immersed membrane (Erdei *et al.*, 2008).

The effect of light wavelength on the complete decomposition of phenol solution was investigated in the presence of TiO_2 and oxygen using the suspension/slurry system (Chun *et al.*, 2000). This study was further supported by Saravanan *et al.*, (2009), who demonstrated the complete mineralization of phenol at low concentration (50mg/l) in water, under solar irradiation for 5h using P25, Rahmani *et al.*, (2008), illustrate the complete mineralization of phenol using the suspension system and effect of medium pH on the reaction. In a bit to obtain complete degradation of phenol in a short time, Laoufi *et al.*, (2008), reported 99% conversion of phenol to CO_2 and water in 4h. The reaction conditions investigated involved the use of helical photoreactor with TiO_2 suspension and UV radiation sources of 15W and 400W low-pressure mercury vapor quartz lamps. The lamps emissive lengths were 254 nm and 365 nm respectively. Dagan and Tomkiewicz (1993), reported the photodecomposition of salicylic acid with TiO_2 aerogels using a suspension mode system. The reaction was performed in a Pyrex cell with a quartz window for illumination and under constant stirring. The cell was irradiated by 85W Hg lamp. Irradiation intensity was between 300 and 400 nm and oxygen was not added to the reaction vessel. Thus, oxygen used in the reaction is merely atmospheric oxygen dissolved in the solution. The experiment shows a much higher photocatalytic activity under the conditions used.

San *et al*., (2001) investigated the photodegradation of 3-aminophenol (3-AP) in a TiO_2 batch suspension photoreactor. They reported that this process followed pseudo-first-order kinetics, with the apparent rate constant depending on the initial 3-AP concentration.

Furthermore, the addition of electron acceptors enhanced the reaction rate significantly. Mass transfer within slurry reactors has not received a great deal of attention primarily because such problems have not been recognized as being major impediments to the application of a slurry reactor.

2.2.2 Immobilized/Packed catalysts photoreactor systems

Photoreactor operating with immobilized catalysts eliminate the need for catalyst separation step and almost eliminate the problem due to light penetration. The major drawback with the immobilized catalysts system is the mass transfer limitation, which can easily occur, coupled with the limited surface area available for the reactants. A variety of support materials have been used for the photocatalytic applications including silica based materials (Silica gel, glass/quartz wool, and beads), lamp casings, glass tubes, hollow beads, membranes, optical fibers, zeolites, activated carbon, pellets, stainless steel, etc. A wide range of photocatalytic reactors have been developed and used as Immobilized systems such as:

i. Annular photoreactor (Mohseni 2005; Vincent *et al.*, 2008)
ii. Packed bed photoreactor (Mehrvar *et al.*, 2002)
iii. The monolith photoreactor (Hossain *et al*., 1999)
iv. Coated fibre optic cable reactor (Peill and Hoffmann, 1995)

Al-Ekabi and Serpone (1988) investigated TiO_2 supported on a glass matrix for the photo-decomposition of phenol, 4-chloropheol, 2,4-dichlorophenol, and 2,4,5-trichlorophenol. The degradation followed first-order kinetics with the reaction occurring on the surface of the semiconductor. The irradiation source was an AM-1 filter simulating solar irradiation. A fixed bed reactor system employing a fiber-optic cable (OFR) was reported by Peill and Hoffmann (1995), the system was conceived to allow for remote light distribution to

photocatalysts, to effectively determine quantum yields through effective light flux measurement. Furthermore OFR allowed for reactor reuse to assess different coatings and light input angles, and to minimize potential heating and photocatalyst delamination. They anchored TiO_2 particles onto quartz fibres and light was transmitted to the TiO_2 particles via radial refraction of light out of the fibre. This study was followed with an investigation into the application of the OFR system to the photocatalytic degradation of pentachlorophenol, oxalate and dichloroacetate. The OFR configuration enhanced not only the distribution but also the uniformity of activated photocatalyst within a particular reaction volume compared to standard fixed-bed designs. These characteristics reduced mass transport limitations for photochemical conversion efficiency and allowed higher processing capacities. Furthermore, potential light loss via absorption or scattering by the reaction medium was minimized. The OFR system could be used in batch or continuous flow operation for both liquid and or gas phase reactions. The transmission cable also allowed for remote light delivery to the photocatalyst.

2.3 Conversational waste water treatment

Some methods were used in the treatment of wastewaters containing resistant organic matters such as phenol. Degradation of phenol usually takes place by physicochemical methods including adsorption using activated carbon (Ozkaya, 2006), biological treatment (Wang *et al.*, 1999), emulsion liquid membrane (Wan *et al.*, 1997), ion exchanges, advanced oxidation processes (AOPs) (including cavitation, Fenton, and photocatalyst) (Wang *et al*., 1999; Petrovic *et al.*, 2011), chemical oxidation (methods in which ozone and water are used), photochemical and electrochemical, and ultrasound waves such as sonochemical, photochemical, photo-sonochemical (Lifka *et al.*, 2003), and hybrid of mentioned methods.

However, advanced oxidation processes (AOPs) are among the most effective processes in degradation of resistant compounds. UV/TiO_2 process is one of the latest and most effective methods for the treatment of these pollutants. Advanced oxidation process those not involved the transfer of pollutant from one form to another as the case with activated carbon but it involved the complete mineralization of these recalcitrant waste into harmless compound like water and carbon dioxide.

It is estimated that more than 1500 chemical pesticides have been produced and as many as 8,000 individual formulations are available for specific application (Becker and Wilson, 1978). This has caused many undesirable effects, such as disturbing the ecosystem and resulting in environmental contamination. These harmful and hazardous materials are leached into surface and ground waters.

The potable water thus has to be made free of these materials, because they may accumulate in the food chain and many have short- and long-term effects on human and animal life. (Bansal and Goyal, 2010).

2.3.1 Photocatalysis of organic pollutant using transition metal doped TiO_2

The photocatalytic decomposition of organic pollutant in aqueous solution using modified titanium(IV) Oxide with transition metals has been demonstrated by several researchers by varying the conditions of the reaction or the reactor design as the case may be. The basic aim of the structural modification of TiO_2 for photocatalysis is to enhance the photoresponse of the catalyst and also improve the photocatalytic activity. Sonawane and Dongare (2006), investigated the photocatalytic degradation of phenol in sunlight with Au/TiO_2 thin films prepared using Sol–gel synthesis. The investigation showed that doped catalyst promoted the photoresponse of TiO_2 and increased photocatalytic decomposition of aqueous solution of

phenol in sunlight. Doping 1–2% Au into TiO_2 also improved the photocatalytic activity by 2–2.3 times than undoped, also the catalyst was very stable and it can be used for a number of times with no much change in efficiency for long term use. Also Maicu *et al.,* (2011), comparatively studied the photodeposition of Pt, Au and Pd on pre-sulphated TiO_2 prepared by sol gel method for the photocatalytic decomposition of phenol performed by using a UV-transparent plexiglas top window (threshold absorption at 250 nm) with a sun-like radiation spectrum for 2h and a main emission line in the UVA range at 365 nm. The study showed that the photoactivity of the catalysts with respect to the doped metal species was in the following order Pt >>Pd >>Au. Non-sulphated Pt-doped TiO_2 showed a significant enhancement in photoefficiency after metal deposition, as illustrated by an enhancement factors (Ef) of 2.37. Pd deposition resulted in modest improvements in the photoactivity (Ef = 1.17), while photodeposited Au actually resulted in a lowered catalytic activity in comparison to unmodified TiO_2, with a calculated Ef of 0.63. In the same way Loganathan *et al.,* (2011), reported the photocatalytic degradation of 4-chlorophenol with TiO_2 nanoparticles doped with silver, platinum, and gold synthesized by acetic acid hydrolyzed sol-gel method, according to the results obtained, the photocatalytic mineralization of 4-chlorophenol over the catalysts established the activity order as: Au doped nano TiO_2 >> Pt doped nano TiO_2 >> Ag doped nano TiO_2 >> pure nano TiO_2, and established the cathodic influence of metals in suppressing electron-hole recombination during the reaction. The reactivity order followed the electro-negativity and electron affinity order of the dopant metal atom. From this study, it was concluded that Ag, Pt and Au doped nano TiO_2 catalysts could be better materials than bulk commercial TiO_2 for the mineralization of organic pollutants. The study of the effect of deposition of silver on structural characteristics and photoactivity of TiO_2-based photocatalysts in phenol decomposition was also studied using light emission

at 365 nm in suspension mode, the experiment showed that the optimum metal loading was 0.3wt% Ag and the photocatalyst also showed greater efficiency in photocatalysis than bare TiO_2 and P25 for different pollutants (Meli'an *et al*., 2012).

Rengaraj and Li (2006), enhanced the photocatalytic activity of TiO_2 by doping with Ag, these were used for the degradation of 2, 4, 6-trichlorophenol (TCP) in aqueous suspension with a UV-A light source with a main emission at 365 nm. It was found that with a suitable amount (0.5 wt %), the Ag dopant effectively increased the photocatalytic activity of the TiO_2 by reducing the recombination rate between the electron-hole pairs. Also the experiments demonstrated that TCP was effectively degraded in aqueous Ag-TiO_2 suspension by more than 95% within 120 min, while total organic carbon (TOC) was also converted into CO_2 by a high proportion of up to 80%. Furthermore, a nano-catalyst Fe on TiO_2 was prepared and tested for efficient total organic carbon (TOC) removal during the photocatalytic oxidation of chlorophenols in aqueous solution with 254nm light irradiation. The study showed that the 2,4-dichlorophenol photo-degradation efficiency catalyzed by Fe/TiO_2 increased with increasing iron concentration, reaching a maximum at 1.0 wt% Fe, matched with the highest TOC removals (often 70–80%) and highest conversion (almost 100%), at 18 Fe atom to every 20 nm TiO_2 crystal (though 0.5 or 0.8 wt% Fe had also high activity), and then decreased with a further increase in iron content, also for 2,4-dichlorophenol degradation, acidic conditions (preferably pH 4) were more favorable than alkaline conditions (Liu *et al*., 2012).

Yu *et al.,* (2010), investigated the photocatalytic degradation of malathion in aqueous solution using an Au–Pd/TiO_2 nanotube film with a rectangular quartz reactor (40mm×50mm×60mm) under the UV light irradiation i.e. 450W high-pressure mercury lamp (principal wavelength 365 nm). The photocatalytic experiments revealed that, compared with

a naked TiO_2 film, Malathion could be more efficiently degraded by using Au–Pd/TiO_2 as a photocatalyst. Su *et al.,* (2012), reported the synergetic effect of noble metal nanoparticles (Au, Pd, Au-Pd alloys) with a narrow size distribution supported on nanocrystalline TiO_2 (M/TiO_2) which have been synthesized via a sol-immobilization route on the photodecomposition of phenol with continuous irradiation by light-emitting diode (LED) UV light source at 365 nm. The effect of metal identity (Au, Pd, Au-Pd alloys) and size on the photocatalytic performance of M/TiO_2 has been systematically investigated using phenol as a probe molecule. A different phenol degradation pathway was observed when using M/TiO_2 catalysts as compared to pristine TiO_2. It was discovered that the metal nanoparticles directly participate in the photocatalytic reactions and play a significant role in suppressing the benzoquinone-to-hydroquinone conversion process. The results suggest that the metal nanoparticles can mediate undesired redox reactions that ineffectively consume photogenerated radicals, thus improving the photo-oxidation efficiency of phenol. Pd supported on TiO_2 tends to yield a higher conversion to CO_2 and exhibits better long-term photoactivity than the corresponding Au/TiO_2 materials. Photocatalytic degradation of phenol using titanium dioxide has already been studied through experiments in mini-Batch reactor (Nickheslat *et al*., 2013; Hadj-Salah and Boultif, 2004; Saravanan *et al.,* 2009; Chun *et al.,* 2000; Su *et al*., 2012), unfortunately, most of the experiment make used of batch reactor and the experimental conditions used by each of them appear to be so different that it is impossible to compare the results or to get global view of photocatalytic performance of the system for the studied substances.

2.4 Analytical Instrument for Catalyst Characterization

2.4.1 Diffuse Reflectance UV-Vis Spectroscopy (DRS)

Background

Spectroscopy in the ultraviolet (UV), visible (Vis) and near infrared (NIR) region of the electromagnetic spectrum are often called electronic spectroscopy because electrons are transferred from low-energy to high-energy atomic or molecular orbitals when the material is irradiated with light (Weckhuysen *et al*., 2000). Such electron transfer processes may take place in transition metal ions (d-d transitions and ligand-to-metal or metal-to ligand charge transfer transitions), and inorganic and organic molecules (mainly $n \rightarrow \pi^*$ and $\pi \rightarrow \pi^*$ transitions). They are responsible for the color of matter. Spectroscopic investigations of solutions, gas phase and individual crystals usually take place in transmission, but it is very difficult to obtain transparent films of powders and solids (e.g., heterogeneous catalysts), making transmission experiments almost impossible. Alternatively, diffuse reflected light can be collected and this technique has been named diffuse reflectance spectroscopy (DRS) (Weckhuysen *et al.,* 1999). One of the advantages of DRS is that the obtained information is directly chemical in nature since outer shell electrons of the transition metal ions are probed. This provides information about the oxidation state and coordination environment of transition metal ions in catalytic solids. Diffuse reflectance is an excellent sampling technique as it eliminates the time-consuming process of pressing pellets for transmission measurements. Diffuse reflectance can also be used to study the effects of temperature and catalysis by configuring the accessory with a heating chamber.

Principles of Diffuse Reflectance Spectroscopy in the UV-Vis Region

The interaction of light of the UV-Vis-NIR region with catalytic solids is considered to be a complex process due to absorption and scattering phenomena. These phenomena are largely overcome by the application of techniques such as DRS spectroscopy. Although transmission mode certainly has advantages, almost all UV-Vis-NIR investigations in the catalysis field have been conducted in diffuse reflection mode due to the high absorption and scattering of the materials. DRS is based on the reflection of light by a powdered sample, and the dimensions of the individual particles in such powdered sample are comparable to the wavelength; i.e., 0.2-3 μm (Weckhuysen *et al.*, 2000). This makes it impossible to distinguish the phenomena of reflection, refraction and diffraction; the light is scattered. There are two extreme situations of reflection: specular and diffuse reflection are shown in Figure 2.1 In the case of specular reflection from a smooth and non-absorbing medium, the light beam is reflected under the same angle by the surface as that of the incoming light beam. On the other hand, diffuse reflected light from a non-absorbing medium involves photons, which are scattered in all directions. Three different regimes can be distinguished: (1) single scattering; (2) multiple scattering; and, (3) dependent scattering. The first type arises when scattering centers are sufficiently apart that each is illuminated only by light particles not previously scattered, and on the average, there is no phase relationship between the photons scattered from neighboring particles. In the case of multiple scattering, the scattering centers are still far enough apart that they may be treated as independent, but each center is now illuminated by photons scattered from adjacent particles. Dependent scattering arises when, in addition to multiple scattering, phase coherence exists between scattered photons from adjacent centers (Weckhuysen, 2004).

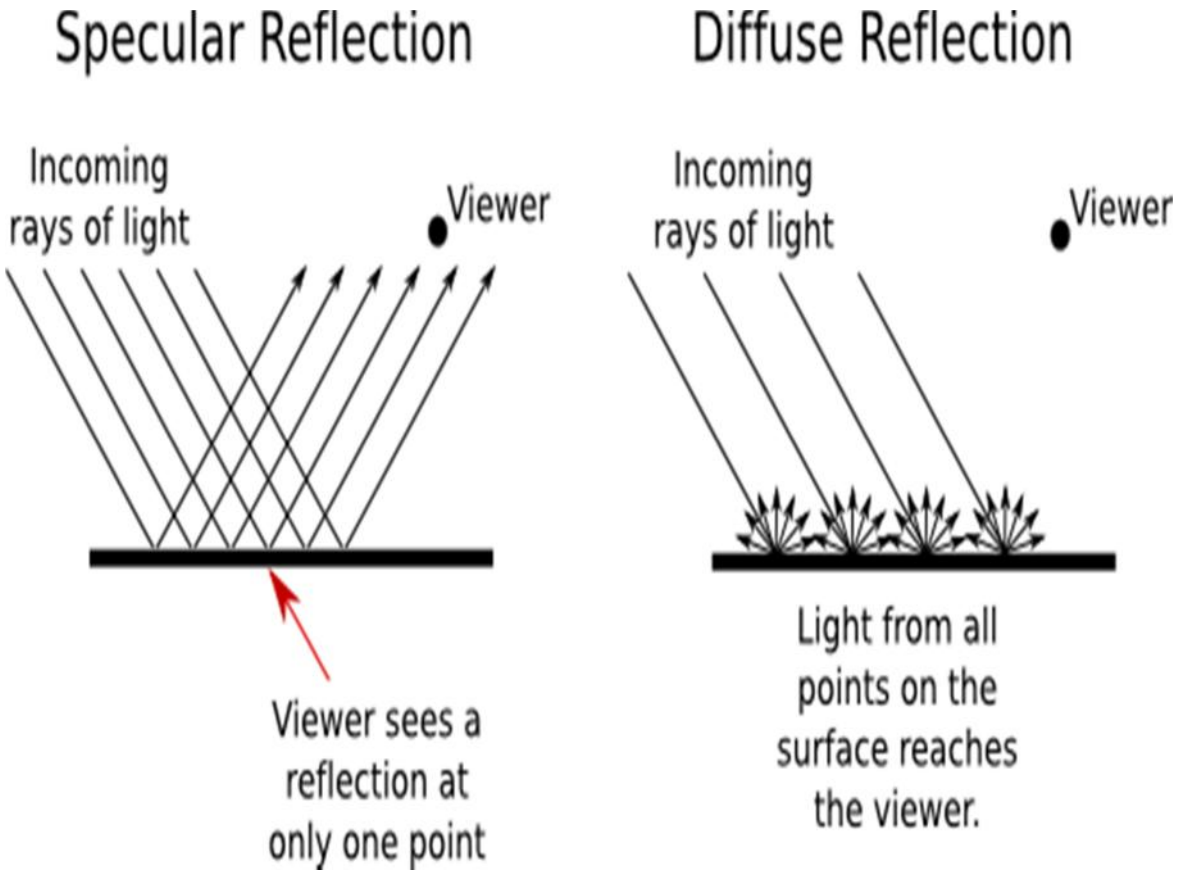


Figure 2.1: Specular and diffuse reflection

Absorption measurements based on electromagnetic radiation in Ultraviolet and visible region 200-800nm have been widely used for quantitative and qualitative measurements of liquid and solid samples (Higson, 2004; Skoog et al., 1998). The absorbance of the sample is calculated by using the ratio between the incident and transmitted beam intensities.

The Beer-Lambert law which relates the absorbance to sample concentration is given below

$$A = \log \frac{I_o}{I} \qquad 2.1$$

where A = Absorbance; I_o = Incident beam intensity; I = Transmitted beam intensity. When photoabsorption is measured in a reflection mode, I can be an intensity of reflection, but, different from the measurement in a transmission mode, it is impossible to measure intensity of incident light by removing a sample because of the lack of reflection, and thereby an integration sphere, the inner wall of which is covered with a "standard reflection material" such as barium sulfate, should be used based on the assumption that a such standard material reflects all incident light, i.e., 100% reflection. Even if this reflection problem is solved, measured optical density cannot be absorbance, since absorbance can be defined for the case where extinction of light intensity is assumed to be induced only by photoabsorption, not by scattering. When such an effect of light scattering is neglected, absorbance is proportional to the concentration of a given material dispersed in a homogeneous medium but not to the number of photons absorbed by a solid sample. This is easily understood by the fact that absorbance 1 and 2 correspond to 90 and 99% absorption of incident light. In order to calculate the extent of photoabsorption of a solid sample, it is necessary to measure absorption $\frac{I}{I_o}$ not absorbance (Ohtani *et al.,* 1997). It is possible to obtain the corresponding

absorption spectrum from the reflected light by transforming the reflectance data into Kubelka-munk (K-M) function (Weckhuysen *et al.*, 1999; Jentoft, 2009). K-M function or remission function f (R) links the reflectance at infinite sample thickness with absorption coefficient (k) and scattering coefficient (s).

The Kubelka–Munk (K–M) function is defined as

$$f(R) = \frac{(1-R)^2}{2R} = \frac{k}{s} \qquad 2.2$$

where R, k and s are diffuse reflectance$\left(= \frac{I}{I_o}\right)$, absorption coefficient and scattering coefficient, respectively. The K-M theory has some limitations and can be applied only when the following conditions are fulfilled. (Weckhuysen *et al.*, 1999; Jackson and Hargreaves, 2009)

i. The layer of the sample is of infinite thickness (generally thicker than a couple millimeter for typical materials

ii. The Incident radiation is monochromatic and completely diffused

a) For samples diluted with a medium of less photoabsorption, K–M function can be a measure of sample concentration. The information obtained from the application of UV-Vis spectroscopy is detailed below oxidation states and coordination environments of metals from charge transfer transition.

b) Particle sizes and shapes of dispersed metals from surface plasmon resonance

c) Band gaps of semiconductors from analysis of absorption edge

d) Nature of surface adsorbate or functional groups (Jentoft, 2009)

2.4.2 **Diffuse Reflectance Infrared Fourier Transform Spectroscopy (DRIFTS)**

Background

In diffuse reflectance spectroscopy, the electromagnetic radiation reflected by roughened surfaces is collected and analyzed. When this technique is applied in FTIR region, it is termed as diffuse reflectance infrared Fourier transform spectroscopy (DRIFTS). It is also known as "Kubelka–Munk "reflection, because they developed a theory on the radiation transport in scattering media (Kubelka and Munk, 1931).

Light incident onto a solid sample may be partly reflected regularly (specular reflection) by the sample surface, partly scattered diffusely, and partly penetrates into the sample. The latter part may be absorbed within the particles or be diffracted at grain boundaries, giving rise to diffusely scattered light in all directions. Diffuse reflectance spectroscopy associated with the reflected lights which are produced by diffuse scattering as shown on Figure 2.1. Since regular reflection distorts the DRS spectra, thus, the regular reflection component should be eliminated in diffuse reflectance measurement. The DRIFTS accessory is designed to eliminate the specularly reflected radiation. In diffuse reflectance spectroscopy, there is no linear relation between the reflected light intensity (band intensity) and concentration, in contrast to traditional transmission spectroscopy in which the band intensity is directly proportional to concentration. Therefore, quantitative analyzes by DRIFTS are rather complicated. The empirical Kubelka–Munk equation relates the intensity of the reflected radiation to the concentration that can be used for quantitative evaluation. The Kubelka-Munk equation is defined as:

$$f(R_\infty) = \frac{(1-R)^2_\infty}{2R_\infty} = \frac{c}{k} = \frac{K}{s} \qquad 2.3$$

where $f(R_\infty)$ = Kubelka–Munk function,

R_∞ = the absolute reflectance of layer (the ratio of the sample diffuse reflectance spectrum and a non-absorbing reference (normally KBr or KCl)), both measured at indefinite depth.

K is the absorption coefficient; s = the diffusion (scattering) coefficient which is proportional to the fraction of diffused light; k is molar absorption coefficient (proportional to the fractional of transmitted light) and c is sample concentration.

The reflectance R_∞, indicates the sample is thick enough that no radiation reaches the back surface (indefinite thickness). In the case of $R_\infty < 0.01$, the simpler function log $1/R_\infty$ is often used for measuring the diffuse reflectance. Since such small R_∞ value is usually found in the near-IR region, therefore, an alternative relationship between concentration and reflected intensity in near–IR is defined as:

$$\log\left(\frac{1}{R_\infty} = k'c\right) \qquad 2.4$$

where k´ is a constant.

In Kubelka-Munk equation it is assumed that s is independent of wavelength and the sample is weakly absorbing. The former condition is achieved by proper sample preparation and the latter by dilution of strong absorbing samples with non-absorbing substrate powder (such as KBr or KCl). Therefore, to obtain reproducible results, particle size, sample packing and dilution should be carefully controlled, especially for quantitative analysis.

Infrared spectroscopy is one of the most widely used tool to study the catalyst surfaces. This technique can provide information about the adsorbed species or reaction intermediates and their structures on catalytic surfaces under reaction conditions. The energy of IR radiation is

not energetic enough to cause electronic transition in molecules like in the case of UV-Vis. However, it is strong enough to cause molecular vibrational and rotational transitions.

In the diffuse reflectance mode, samples can be measured as loose powders, with the advantages that not only is the tedious preparation of discs unnecessary but also diffusion limitations associated with tightly pressed samples are avoided. The DRIFT make use of reflected radiant energy that has been partially absorbed, transmitted and partially scattered by a surface, with no defined angle of reflection. In diffuse reflectance spectroscopy, diffusely scattered light can be directly, collected from material in a sampling cup or, alternatively, collected by using an abrasive sampling pad. In mid-IR, the diffusely reflected light from sample is generally collected by large ellipsoidal mirrors, which cover as much area above the sample as possible and focused on the detector. (Niemantsverdriet, 2007; Khoshhesab, 2012).

Normally, the IR radiation in the middle range (4000-400cm^{-1}) is used for the analysis. If the energy of the radiation matches with the energy of molecular vibration of the molecule, the absorption will occur. Absorption of IR only occurs if the molecule has a change in dipole moment during vibration or rotation and species with polar bonds will absorb IR strongly whereas the molecules with covalent bonds exhibit weak IR band. In the case of rotational transitions, the energy needed to cause the change in rotational states is very low (Skoog *et al.*, 1998) corresponding to far-IR region (200-10cm^{-1}).

Fourier transform infrared (FTIR) spectroscopy is a measurement technique operating under the principle of Michelson interferometer which the data are collected and converted from an interference pattern (interferograms) to spectrum (Farrauto and Bartholomew, 1997). The

FTIR has many advantage over the dispersive type because it gives better signal-to-noise ratio, precise measurement and also the ability to increase the scan speed.

DRIFTS is a versatile technique for analyzing nontransparent samples, powders, roughened surfaces and coating. It offers the advantages of easy sample preparation and applicability to analyze samples at elevated temperature and pressure (Armaroli *et al.,* 2004). By using diffuse reflectance, it eliminates the need for sample preparation i.e. (Pelletization) as needed in traditional transmission methods. Moreover, this techniques give the avenue to study the surface species on the catalyst under reaction conditions.

2.4.3 Powder X-Ray diffraction measurements

Background

X-ray diffraction is a non-destructive technique widely used for determining the structure of crystalline solids. X-rays are electromagnetic radiation with photon energies in the range of 100eV-100keV. Only the short wavelength X-rays a few angstroms to 0.1Å (1keV-120keV) are used for diffraction applications (Cullity, 1978). Since the X-ray wavelength is comparable to the size of atoms, it is suitable for probing the structural arrangement of atoms and molecules in a wide range of materials. By heating the tungsten filament, the electrons are emitted and accelerated by a potential difference in the X-ray tube towards a metal target. Once the electrons hit the metal target or anode, usually copper or molybdenum, the anode emits X-ray continuous spectrum superimposed with intense X-ray peaks (Kα and Kβ). The radiation is monochromated and the Kα radiation, in this case, is used for X-ray diffraction. With X-ray diffraction the reflection only occurs when the conditions for constructive interference are fulfilled which is demonstrated in term of Bragg's law. The Bragg condition for the reflection of X-rays is shown in Figure 2.2. The parallel X-ray light (rays 1, 2) falls

on a crystal with a lattice plane distance d and is scattered below the angle Θ (rays 1', 2'). The proportion of the beam that is scattered on the first and second plane has a phase difference of ACB. The X-ray data are recorded in term of intensity of the diffracted peaks, while varying the diffraction angle Θ. The XRD pattern is obtained by plotting the value of 2Θ versus intensities of each diffraction angle. ACB = 2d sin *q*. The condition is fulfilled when the phase difference is a whole multiple of the wavelength λ shown in the equation $n\lambda = 2d \sin \Theta$, where n is reflection order (1, 2, 3 ...) and λ *is* X-ray wavelength.

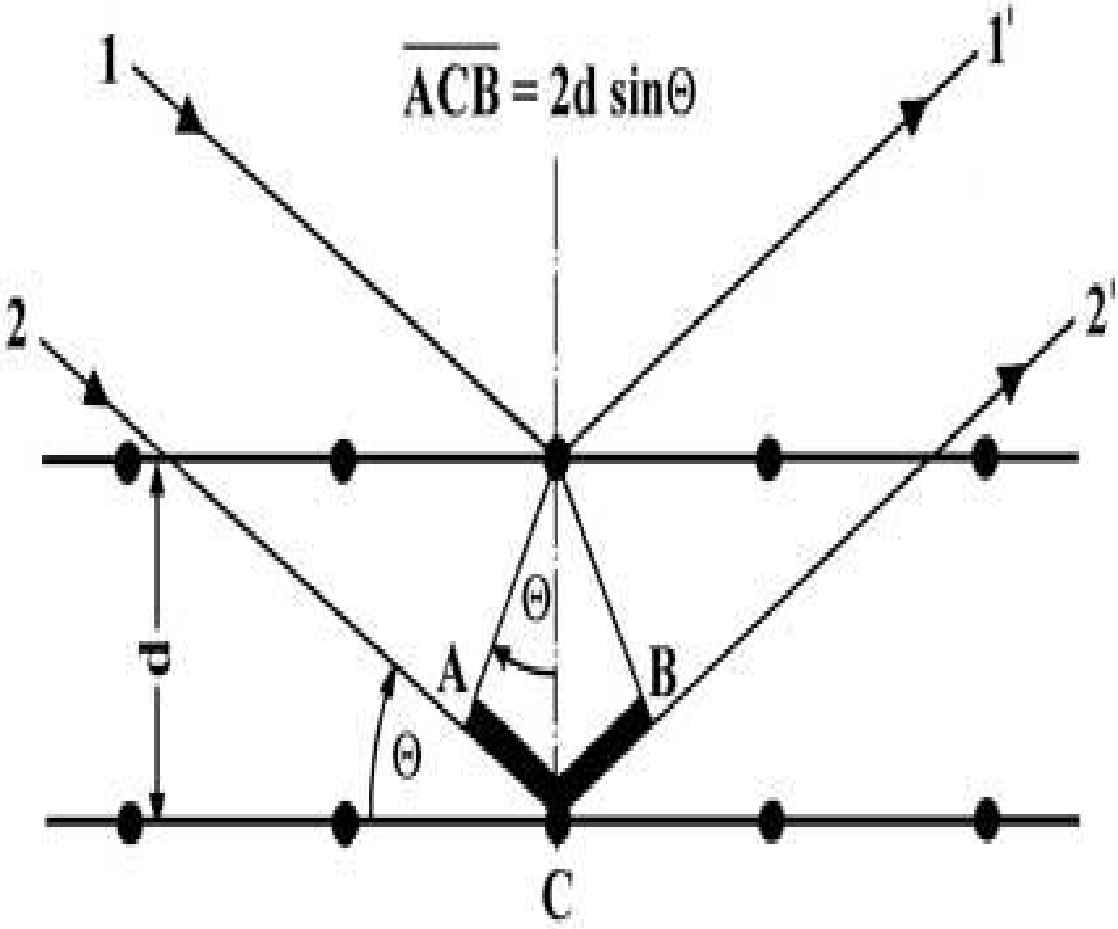


Figure 2.2: Bragg condition

2.4.4 Thermogravimetric Analysis (TGA)

Background

Thermogravimetric analysis (TGA) measures the mass change of a material as a function of temperature and time, in a controlled atmosphere. It is ideally used to assess volatile content, thermal stability, degradation characteristics, aging/ lifetime breakdown, sintering behavior and reaction kinetics. Differential scanning calorimetry (DSC) measures the heat flow associated with phase transitions or reactions, such as melting, crystallization, solid phase transition, glass transition, curing, sorption, etc. It is ideally used to determine melting point, glass transition temperature, crystallinity, degree of curing, heat capacity, crystalline impurities, etc.

2.4.5 Inductively coupled plasma optical emission spectrometer (ICP-OES)

Background

ICP is an argon plasma maintained by the interaction of an RF field and ionized argon gas. The plasma can reach temperatures as high as 9726.85ºC, allowing the complete atomization of the elements in a sample and minimizing potential chemical interferences. Inductively coupled plasma optical emission spectroscopy (ICP-OES) is the measurement of the light emitted by the elements in a sample introduced into an ICP source. ICP-OES measures the light emitted at element-specific characteristic wavelengths from thermally excited analyte ions. This light emitted is separated and measured in a spectrometer, yielding an intensity measurement that can be converted to an elemental concentration by comparison with calibration standards. The measured emission intensities are then compared to the intensities of standards of known concentration to obtain the elemental concentrations in the unknown sample.



Figure 2.3: Mettler-toledo TGA/DSC I STAR^{e} (Schematic of TGA/DSCI, 2012)

2.4.6 **Scanning electron microscopy**

Background

The Scanning Electron Microscope (SEM) uses a focused beam of high-energy electrons to generate a variety of signals at the surface of solid specimens. The signals that derive from electron-sample interactions reveal information about the sample including external morphology (texture), chemical composition, and crystalline structure and orientation of materials making up the sample. In most applications, data are collected over a selected area of the surface of the sample, and a 2-dimensional image is generated that displays spatial variations in these properties. Areas ranging from approximately 1 cm to 5 microns in width can be imaged in a scanning mode using conventional SEM techniques (magnification ranging from 20X to approximately 30,000X, spatial resolution of 50 to 100 nm). The SEM is also capable of performing analyses of selected point locations on the sample; this approach is especially useful in qualitatively or semi-quantitatively determining chemical compositions (using EDX) (Egerton, 2005). Scanning electron microscopy (SEM) involves rastering a narrow electron beam over the surface and detecting the yield of either secondary or backscattered electrons as a function of the position of the primary beam. Contrast is caused by the orientation: Parts of the surface facing the detector appear brighter than parts of the surface with their surface normal, pointing away, from the detector. The secondary electrons have mostly low energies ($\approx 5 - 50\ eV$) and originate from the surface region of the sample. Backscattered electrons come from deeper and carry information on the composition of the sample, because heavy elements are more efficient scatterers and appear brighter in the image (Chorkendorff and Niemantsverdriet, 2006).

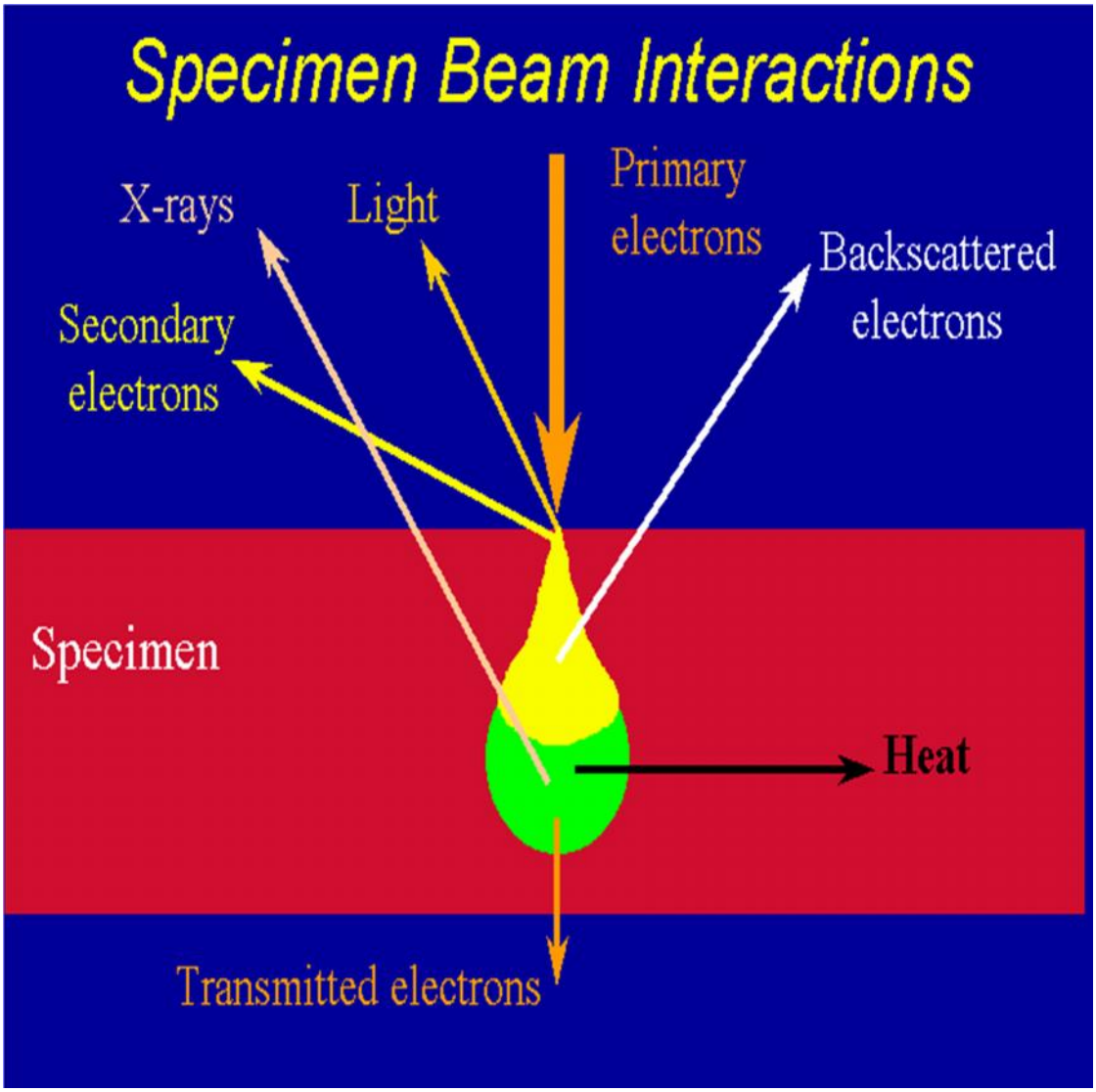


Figure 2.4: The interaction of electron beam with samples in SEM

SEM analysis is considered to be "non-destructive"; that is, x-rays generated by electron interactions do not lead to volume loss of the sample, so it is possible to analyze the same materials repeatedly. The Diagrammatic illustration of the Interaction of electrons with a sample using the Scanning Electron Microscope is shown on *Figure* 2.4. The SEM is routinely used to generate high-resolution images of shapes of objects and to show spatial variations in chemical compositions by: acquiring elemental maps or spot chemical analyses using EDX, discrimination of phases based on mean atomic number (commonly related to relative density) using BSE, compositional maps based on differences in trace element "activators" (typically transition metal and Rare Earth elements). The SEM is also widely used to identify phases based on qualitative chemical analysis or crystalline structure also The SEM is critical in all fields that require characterization of solid materials. The main difference between SEM and TEM is that SEM sees contrast due to the topology and composition of a surface, whereas the electron beam in TEM projects all information on the mass it encounters in a two-dimensional image, which, however, is of sub nanometer resolution.

2.4.7 **Energy-Dispersive X-Ray (EDX)**

Interaction of an electron beam with a sample target produces a variety of emissions, including x-rays. An energy-dispersive (EDX) detector is used to separate system software is used to analyze the energy spectrum in order to determine the abundance of specific elements. EDX can be used to find the chemical composition of materials down to a spot size of a few microns, and to create element composition maps over a much broader raster area. Together, these capabilities provide fundamental compositional information for a wide variety of materials. (Goldstein *et al.*, 2003) EDX systems are typically integrated into either

an SEM instrument. EDX systems include a sensitive x-ray detector, a liquid nitrogen Dewar for cooling, and software to collect and analyze energy spectra. The detector is mounted in the sample chamber of the main instrument at the end of a long arm, which is itself cooled by liquid nitrogen. The most common detectors are made of Si(Li) crystals that operate at low voltages to improve sensitivity, but recent advances in detector technology make available so-called "silicon drift detectors" that operate at higher count rates without liquid nitrogen cooling. An EDX detector contains a crystal that absorbs the energy of incoming x-rays by ionization, yielding free electrons in the crystal that become conductive and produce an electrical charge bias. The x-ray absorption thus converts the energy of individual x-rays into electrical voltages of proportional size; the electrical pulses correspond to the characteristic x-rays of the element. (Clarke and Eberhardt, 2002; Reimer, 1998), the picture of Scanning electron microscopy with EDX from FEI^{TM} is shown on *Figure* 2.5.

2.4.8 **Transmission Electron Microscope (TEM)**

Background

It was discovered in the 1920s that the accelerated electrons behave in a vacuum just like light. Electrons travel in straight lines and have a wavelength much smaller than that of light. In addition, the electric and magnetic field also have the same effect on electrons as lenses and mirrors have on visible light. By replacing light with electrons a resolving power of 0.1nm at magnification of 1 million times is achieved in TEM. Thus, it is a very powerful tool for investigation of surface texture, morphology, crystallite size and size distribution of catalysts (Satterfield, 1980; Farrauto and Bartholomew, 1997). The transmission electron microscope uses a high energy electron beam transmitted through a very thin sample to image and analyze the microstructure of materials with atomic scale resolution.



Figure 2.5: Scanning electron microscopy with EDX (Quanta Scanning electron microscope, 2013)

The electrons are focused with electromagnetic lenses and the image is observed on a fluorescent screen, or recorded on film or digital camera. The electrons are accelerated at several hundred kV, giving wavelengths much smaller than that of light: 200kV electrons have a wavelength of 0.025Å. The schematic outline of TEM is presented in *Figure* 2.6. In TEM, a primary electron beam of high energy and high intensity passes through a condenser to produce parallel rays that impinge on the sample. As the attenuation of the beam depends on the density and the thickness of the sample, the transmitted electrons form a two-dimensional projection of the sample mass, which is subsequently magnified by the electron optics to produce a so-called bright field image. The dark field image is obtained from the diffracted electron beams, which are slightly off-angle from the transmitted beam. Typical operating conditions of a TEM instrument are 100–200 keV electrons, 10^{-6} mbar vacuum, 0.5 nm resolution and a magnification of 3 x10^5 to 10^6 (Chorkendorff and Niemantsverdriet, 2006). If the sample is not thin enough, electrons will simply be stopped and no image would be shown. Normally, the thickness of specimens for TEM is around 0.5μm or less. An alternative way of studying a thicker sample is to use a higher speed electrons (Higher accelerating voltage).

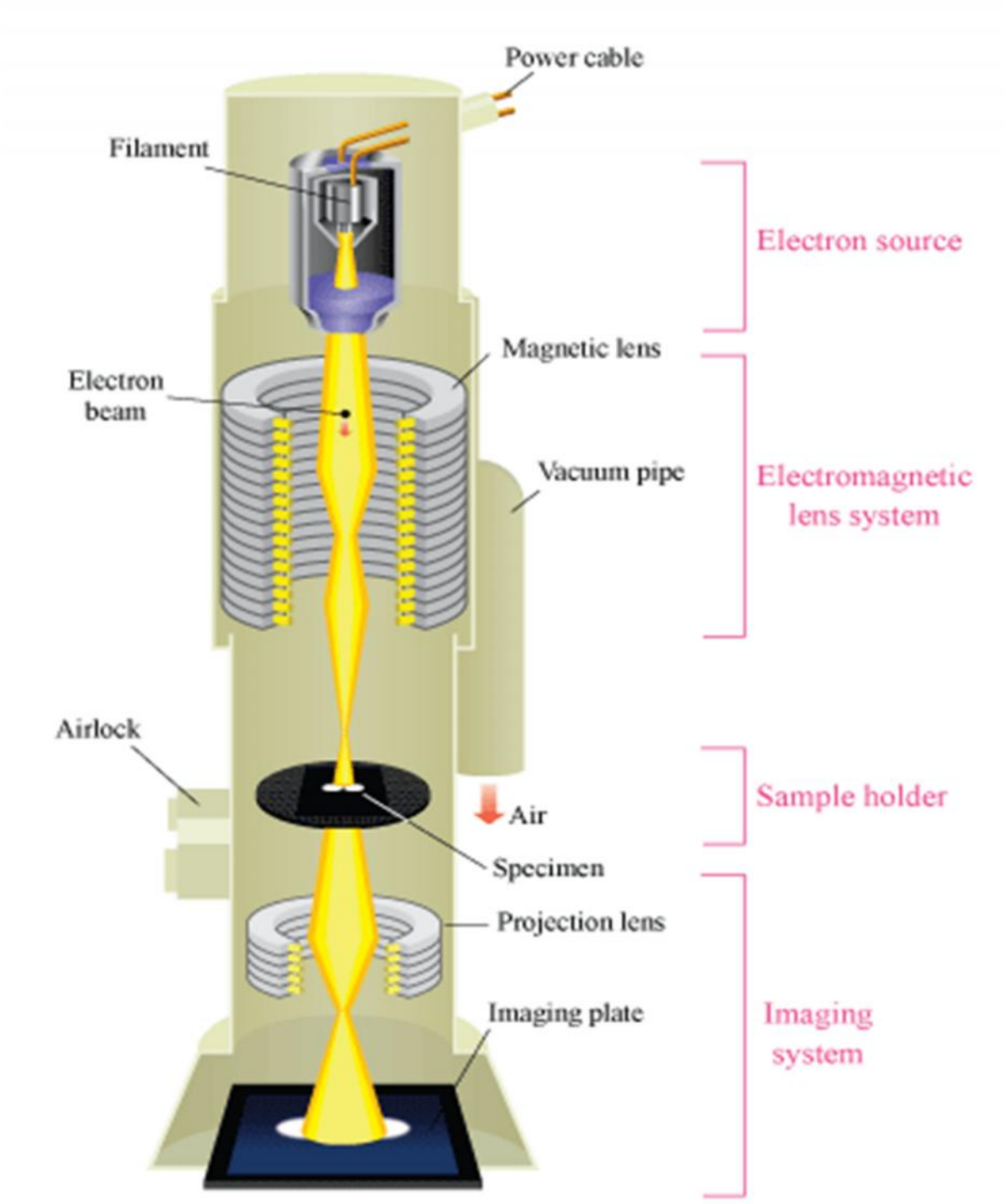


Figure 2.6: Schematic outline of TEM (Basic principle of TEM, 2013)



Figure 2.7: Transmission electron microscope (TEM) FEI™ Tecnai G2 F20 (FEI Technai, 2013)

2.4.9 The Brunauer–Emett–Teller (BET)

Background

The importance of surface area, pore size and pore volume is obvious since they determine the accessibility to active sites and also the ability of products to be transported from the catalyst surface (Wijngaarden *et al.,* 1998). To measure the total surface area the principle of physical adsorption by van der Waals forces has been applied. By measuring the amount of gas adsorbed, the surface area is determined. Any inert gas such as krypton, argon and nitrogen can be used for this measurement. However, nitrogen is a preferable choice because it is cheaper and readily available. General physical adsorption isotherm are shown in *Figure* 2.8.

Classification of Adsorption Isotherms

Adsorption isotherms should conventionally be plotted on the basis of relative pressure, p/p^o (x-axis) versus amount adsorbed expressed as a molar quantity (y-axis) in $mmolg^{-1}$, to allow comparisons to be made. The experimental procedure involves the use of partial pressure, where the actual pressure is expressed with respect to the saturation vapor pressure at a constant temperature of adsorption, hence the process is isothermal. Adsorption data may alternatively be expressed in terms of an isobar, the variation in uptake with temperature at constant pressure, or an isostere, the change in temperature with pressure at a constant surface coverage. Isotherms provide a significant amount of information about the adsorbent used and the interaction with the adsorbate in the system, including: assessment of the surface chemistry and fundamentals involved in the adsorption process; estimates of the surface area,

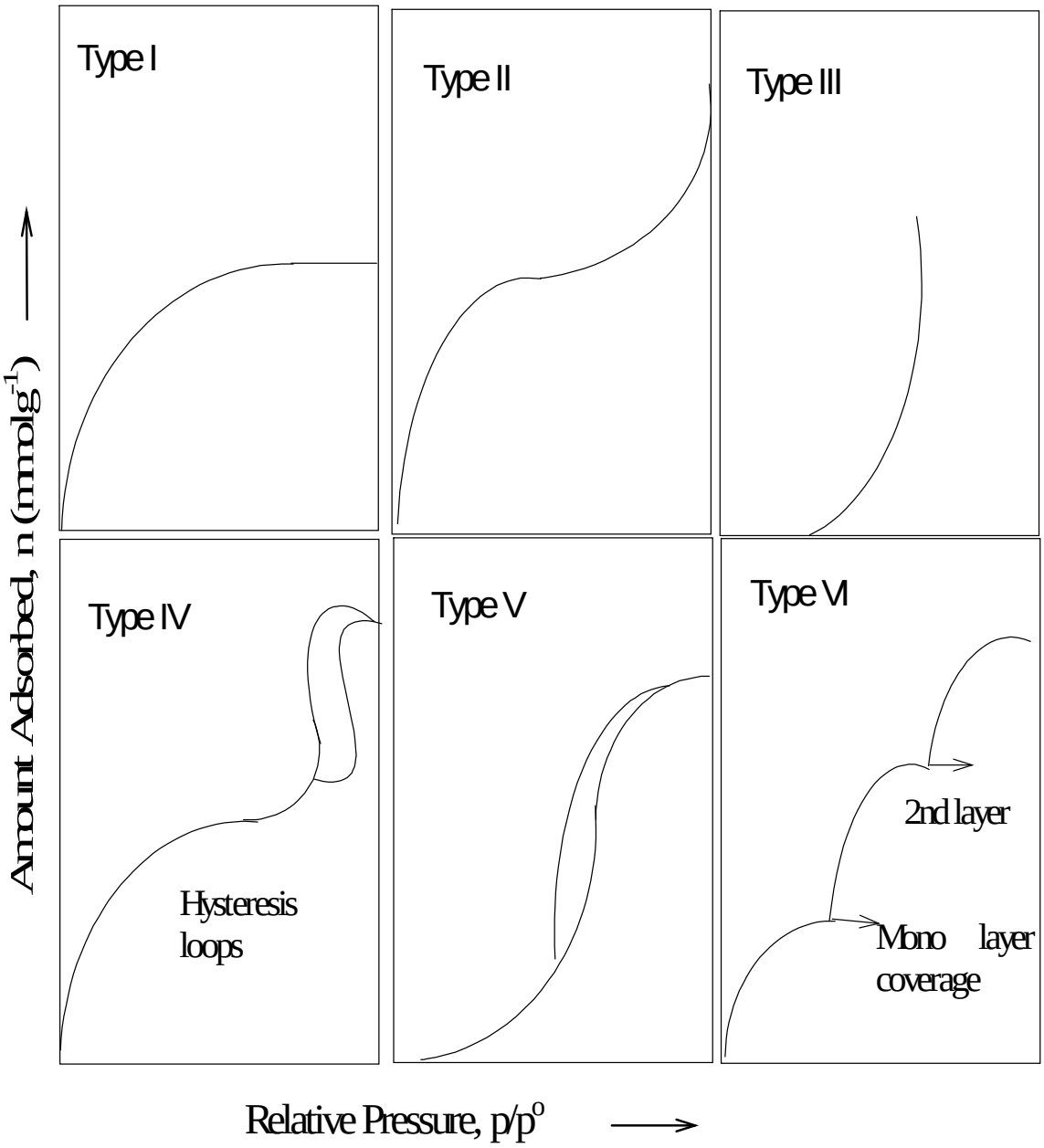


Figure 2.8: Different types of adsorption Isotherms

pore volume and pore size distribution; efficiency profiles for catalysts used in industrial processes. The interpretation of adsorption isotherms can yield a large amount of information about the processes involved, as outlined above. The extent of adsorption on a surface, usually denoted n, is generally a function of the temperature, pressure and nature of the adsorbent and adsorbate: n = f (P, T, adsorbate, adsorbent).

For isothermal adsorption of a particular system this simplifies to n = f (P) T, adsorbent, adsorbate, by working within the limits of vacuum and the saturation vapor pressure, the pressure may be expressed in terms of relative vapor pressures, i.e. p/p^o: n = f (p/p^o)T, adsorbent, adsorbate. This gives a universal basis upon which all isotherms may be displayed in order to make the comparison of results easier. The above relationship may be used to graphically represent uptake profiles in the form of an 'adsorption isotherm'. All adsorption isotherms should fit at least one, or at least a combination of two or more, of the six recognized types classified by Brunauer, Deming, Deming and Teller (B.D.D.T. system) (Brunauer *et al.,* 1940).

Type I Isotherm - these are typical of adsorbents with a predominantly microporous structure, as the majority of micropore filling will occur at relative pressures below 0.1. The adsorption process is usually complete at a partial pressure of ~0.5. Examples include the adsorption of nitrogen on carbon at 77K and ammonia on charcoal at 273K.

Type II Isotherm - physical adsorption of gases by non-porous solids is typified by this class of isotherm. Monolayer coverage is followed by multi-layering at high relative pressures. Carbons with mixed micro- and meso-porosity produce type II isotherm. Type III Isotherm -

the plot obtained is convex to the relative pressure axis. This class of isotherm is characteristic of weak adsorbate-adsorbent interactions (Kiselev, 1968), and is most commonly associated with both non-porous and microporous adsorbents. The weak interactions between the adsorbate and the adsorbent lead to low uptakes at low relative pressures. However, once a molecule has become adsorbed at a primary adsorption site, the adsorbate-adsorbate interaction,which is much stronger, becomes the driving force of the adsorption process, resulting in accelerated uptakes at higher relative pressure. This cooperative type of adsorption at high partial pressures is known as cluster theory and examples include the adsorption of water molecules on carbon where the primary adsorption sites are oxygen based.

Type IV Isotherm - A hysteresis loop, which is commonly associated with the presence of mesoporosity, is a common feature of Type IV isotherms, the shape of which is unique to each adsorption system. Capillary condensation gives rise to a hysteresis loop (Sing *et al.*, 1985) and these isotherms also exhibit a limited uptake at high relative pressures.

Type V Isotherm - these isotherms are convex to the relative pressure axis and are characteristic of weak adsorbate-adsorbent interactions (Kiselev, 1968)**.**. These isotherms are indicative of microporous or mesoporous solids. The reasons behind the shape of this class of isotherm are the same as those for type III and again water adsorption on carbon may exhibit a type V isotherm.

Type VI Isotherm - introduced primarily as a hypothetical isotherm, the shape is due to the complete formation of monomolecular layers before progression to a subsequent layer. It has been proposed, by Halsey (1948), that the isotherms arise from adsorption on extremely homogeneous, non-porous surfaces where the monolayer capacity corresponds to the step

height. One example known to exist is the adsorption of krypton on carbon black (graphitized at 3000 K) (Kratschmer *et al.*, 1999).

2.4.10 Temperature Programmed Reduction (TPR) and Chemisorption

Temperature programmed reduction (TPR) is the method used to determine the number of reducible species on the surface of the catalyst and the reduction temperature of each reduced species, the method is involving the effect of temperature on surface reactions. The results are obtained by monitoring the reaction products or the pre-adsorbed species which desorb from the catalyst surface as a function of temperature. Normally, analysis data are plotted as quantities desorbed versus temperature or time. Temperature programmed desorption is commonly used to determine the number, type and strength of active sites available on the surface (Farrauto and Bartholomew, 1997; Micromeritics Autochem2910, 1999). Pre-reducing the catalyst at 300ºC, temperature at which the support surface is fully reduced and carrying out the pulse chemisorption experiment at low temperature prevent the Hydrogen spill over from taking place (Fornasiero, *et al.*, 1997; Salasc, *et al.*, 2002; Perrichon, *et al.*, 2004; Bernal, *et al*., 1993).

2.4.11 Temperature Programmed Oxidation (TPO)

Temperature programmed oxidation (TPO) is sometimes used to investigate the quantity of reduced species but widely used to determine different forms of carbonaceous deposits on catalyst surface (which is applied to this study), temperature Programmed Oxidation system is typically used to quantify coke deposits in heterogeneous catalysts. Carbons and carbides are amenable to evaluation by careful oxidation while being heated. A stream of diluted oxygen (e.g. 2-10% O_2 in He) directed over the sample during a linear heating ramp generates a signal due to the loss of O_2 from the gas stream. The products of oxidation, CO and CO_2

need not be trapped. Different forms of carbon such as amorphous, nanotube, filament and graphitic, oxidize at different temperatures due to varying availability of reactive carbon-carbon bonds. In this way, fullerenes, soot's, cokes on catalysts etc., can be quickly characterized and differentiated. Oxidation catalysts, e.g. those incorporating chromium, cobalt, copper and manganese, and redox supports like ceria can also be characterized by using the Temperature Programmed Oxidation (ChemBET Overview, 2013)

2.4.12 High Performance Liquid Chromatography (HPLC)

Chromatography is a technique by which a mixture sample is separated into components. Although originally intended to separate and recover (isolate and purify) the components of a sample, today, complete chromatography systems are often used to both separate and quantify sample components. The term, "chromatography" was coined by the Russian botanist, Tswett, who demonstrated that, when a plant extract was carried by petroleum ether through a column consisting of a glass tube packed with calcium carbonate powder, a number of dyes were separated. He named this analysis method "Chromatographie" after "chroma" and "graphos", which are Greek words meaning "color" and "to draw," respectively. "Chromatography" represents a separation technique; whereas a "chromatograph" is a system for performing chromatography. The chart displaying the time-dependent change in signal intensity as a result of the separation is called a "chromatogram".

HPLC is a separation technique that involves: The injection of a small volume of liquid sample into a tube packed with tiny particles (3 to 5 micron (μm) in diameter called the stationary phase) where individual components of the sample are moved down the packed tube (column) with a liquid (mobile phase) forced through the column by high pressure delivered by a pump. These components are separated from one another by the column

packing that involves various chemical and/or physical interactions between their molecules and the packing particles. These separated components are detected at the exit of this tube (column) by a flow -through device (detector) that measures their amount. An output from this detector is called a “liquid chromatogram” from the HPLC picture in *Figure* 2.9 the following component function thus:

Pump

The role of the pump is to force a liquid (called the mobile phase) through the liquid chromatograph at a specific flow rate, expressed in milliliters per min (mL/min).

During the chromatographic experiment, a pump can deliver a constant mobile phase composition (isocratic) or an increasing mobile phase composition (gradient).

Column

Considered the “heart of the chromatograph” the column’s stationary phase separates the sample components of interest using various physical and chemical parameters.

Injector

The injector serves to introduce the liquid sample into the flow stream of the mobile phase.

Typical sample volumes are 5 to 20 microliters (μL).

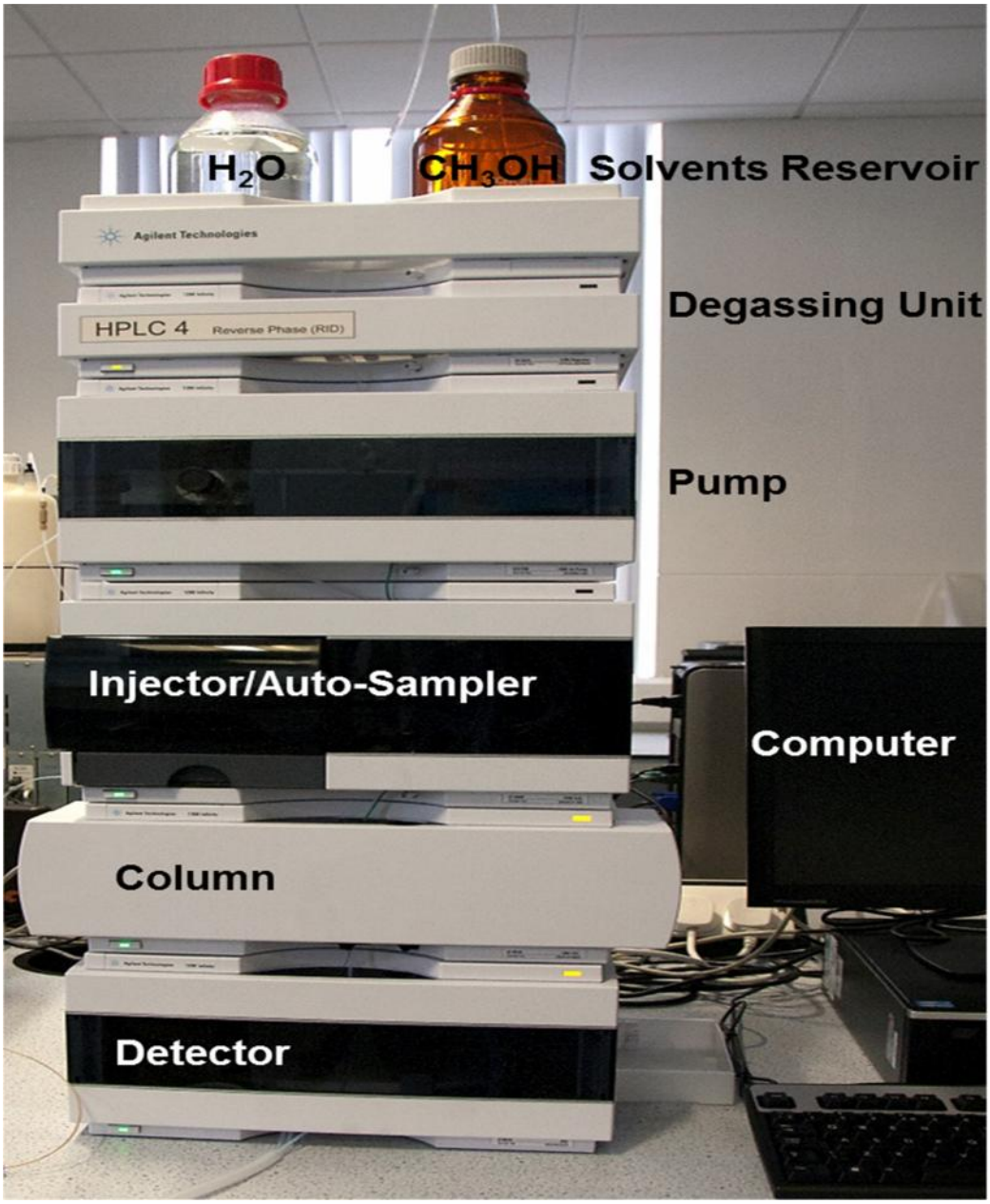


Figure 2.9: An Agilent 1100 high performance liquid chromatography (HPLC)

The injector must also be able to withstand the high pressures of the liquid system.

An autosampler is the automatic version for when the user has many samples to analyze or when manual injection is not practical

Detector

The detector can see (detect) the individual molecules that come out (elute) from the column.

A detector serves to measure the amount of those molecules so that the sample can be analyze quantitatively.

The detector provides an output to a recorder or computer that results in the liquid chromatogram (i.e., the graph of the detector response).

Computer

Frequently called the data system, the computer not only controls all the modules of the HPLC instrument but it takes the signal from the detector and uses it to determine the time of elution (retention time) of the sample components (qualitative analysis) and the amount of sample (quantitative analysis).

CHAPTER THREE

3.1 Experimental

3.2 Materials and Reagent

3.2.1 Reagents

All the reagents used for experimental studies were of analytical reagent grade, phenol, palladium (II) chloride, hydrogen tetrachloroaurate (III), copper (II) Sulphate, Iron (II) chloride, Poly (VinylAlcohol), Hydrogen tetraoxosulphate (VI), Sodium Hydrogen trioxocarbonate (IV), dichloromethane, and methanol (HPLC grade) where obtained from Sigma Aldrich, UK, titanium(IV) Oxide (P25) was obtained Degussa AG, sodium borohydride powder was obtained from Lancaster Synthesis UK and oxygen gas (99.5% Purity) was obtained from BOC, UK.

3.3 Methods

3.3.1 Preparation of catalyst

3.3.2 Sol Immobilization Method

Preparation of Au/TiO2 and Pd/TiO2 Catalyst

The catalysts were prepared using sol immobilization method as reported elsewhere (Su *et al.,* 2012; Essam *et al.,* 2007), except for some few modifications. A standard sol-immobilization method was utilized to prepare the metal nanoparticles (i.e., Au, Pd, Au-Pd) supported on TiO_2, for the preparation of supported gold and gold and palladium colloids using PVA as a protective ligand, aqueous solutions of $PdCl_2$ and $HAuCl_4.3H_2O$ of the desired concentration were prepared. A poly vinyl alcohol (PVA) (1 wt% aqueous solution, Aldrich, MW = 10 000, 80% hydrolyzed) solution was freshly prepared just prior to synthesis

of the metal colloid. A representative protocol for preparing a catalyst comprising Au-Pd nanoparticles with 1 wt% total metal loading on a TiO_2 support is as follows.

To an aqueous $PdCl_2$ and $HAuCl_4$ solution of the desired concentration, the required amount of a PVA solution (1 wt %) was added (PVA/ (Au & Pd) (w/w) = 1.2); a freshly prepared solution of $NaBH_4$ (0.1 M, $NaBH_4$/ (Au&Pd) (mol/mol) = 5) was then added to form a dark brown sol. After 30 min of sol generation, the colloid was immobilized by adding TiO_2 (acidified to pH 1-2 by using hydrogen tetraoxosulphate (VI)) under vigorous stirring conditions. The amount of support material required was calculated to have a total final metal loading of 1 wt %. After 2 h, the slurry was filtered and the catalyst was washed thoroughly with distilled water (neutral mother liquors) and dried at 120ºC overnight. Sol immobilized mono-metallic gold and palladium catalysts were prepared using a similar methodology.

3.3.3 Hydrothermal synthesis of TiO_2 nanotubes

Titanium(IV) Oxide nanotube was produced using hydrothermal method similar to that described by Kolen'ko *et al.*, (2006), with a few modification of using methanol than water in typical nanotube preparation, 3 g of the TiO_2 (P25 Degussa) powder was mixed with 200 cm^3 of 5M NaOH in methanol and stirred for 4h on a magnetic stirrer followed by hydrothermal treatment in a Teflon-lined autoclave high-pressure stainless steel reactor at 90 °C for 8h. After hydrothermal treatment the obtained TiO_2-nanotubes were centrifuged and washed with deionized water until pH is neutral, then 0.1M HNO_3 solution was dispersed by ultra-sonication for 30min. The acid treated TiO_2 nanotubes were washed continually with deionized water to pH 7. The resulting sample was dried in oven at 120 °C overnight after which it was calcined at 300^0C for 4h to get titanium(IV) Oxide nanotubes.

3.3.4 **Micro-emulsion preparation**

To 108.8cm^3 of n-hexane in 250cm^3 round bottom flask, 0.6cm3 of deionized water was added and stir at 500rpm with magnetic stirrer, ensuring the flask is closed, 5.821g of CTAB was added to the solution, after which 43.92cm^3 of 1-butanol was slowly added and the stirring continue for 1h. The flask was closed by stopper to avoid evaporation or loss of any solvent which will destabilize the microemulsion, gradually, the mixture will result in a clear transparent microemulsion (if it does not dissolve all the CTAB 0.5cm^3 of deionized water was added to increase the molar ratio between water and surfactant), allow the solution to achieve equilibrium for 2 to 24h by stopping the magnetic stirrer.

Preparation of 2%Pd-TiO_2

Split the microemulsion into two different 100cm^3 round bottom flask containing 60cm^3 each. To the first flask 1.56cm^3 of $PdCl_2$ (1g of $PdCl_2$ in 100cm^3 of deionized water), 1.56cm^3 of $NaBH_4$ (0.4677g to 5cm^3 of deionized water) was added to the second flask, stir the both flask for 30 min, after which the microemulsion were mixed in a 250cm^3 round bottom flask and it was stirred for another 30min solution turning black. To the mixed microemulsion 2.0cm^3 of titanium-n-butoxide was added and stirred for 4h, to the mixed microemulsion 60cm^3 of methanol was added to break the microemulsion and centrifuged at 600rpm for 5 min. The microemulsion was washed with methanol and the nanoparticles separated into glass vial then dried in the oven for 24h at 120°C, lastly the prepared nanoparticles was calcined at 300°C for 4h in air. (Sanchez-Dominguez *et al.*, 2009; Zhang *et al.*, 2007)

3.4 Preparation of Stock Solution

3.4.1 Preparation of phenol stock solution

To prepare 1000 cm^3 of a 0.001M solution of phenol, 94.112mg of phenol was dissolved in deionized water, and then dilute the solution to a final volume of 1000 cm^3 with deionized water.

3.4.2 Preparation of resorcinol stock solution

To prepare 1000 cm^3 of a 0.00lM solution of resorcinol, 110.111mg of resorcinol was dissolved in deionized water, and then dilute the solution to a final volume of 1000 cm^3 with deionized water.

3.4.3 Preparation of catechol stock solution

To prepare 1000 cm^3 of a 0.001M solution of catechol, 110.111mg of catechol was dissolved in deionized water, and then dilute the solution to a final volume of 1000 cm^3 with deionized water.

3.4.4 Preparation of pyrogallol stock solution

To prepare 1000 cm^3 of a 0.001M solution of pyrogallol, 126.11mg of pyrogallol was dissolved in deionized water, and then dilute the solution to a final volume of 1000 cm^3 with deionized water.

3.4.5 Preparation of hydroquinone stock solution

To prepare 1000 cm^3 of a 0.001M solution of hydroquinone, 110.111mg of hydroquinone was dissolved in deionized water, and then dilute the solution to a final volume of 1000 cm^3 with deionized water.

3.5 Characterization of Catalyst

3.5.1 Diffuse Reflectance UV-Vis Spectroscopy (DRS)

Procedure

The optical characterization of the photocatalyst was carried out using Diffuse Reflectance UV–vis spectrophotometer equipped with a Harrick Praying Mantis™ diffuse reflection accessory used for solid samples (Perkin Elmer Lambda 6505) in the wavelength range from 250 to 800 nm with scanning speed of 300nm/min. Before recording any spectrum, the signal was maximized by adjusting the height of the sample holder using a micrometer. Firstly, the spectrum of reference material (MgO) was recorded and saved as an auto-zero (background spectrum). Then the analysed sample was replaced into the microsampling cup by using the provided sample funnel. To obtain a flat surface, a flat blade is needed to level off the surface. After that, the sample holder with the sampling cup was placed into the praying mantis. In cases where the sample was a very strong absorber, dilution of the sample with a non-absorbent matrix is needed. In those studies, the sample was normally diluted with MgO.

3.5.2 Diffuse Reflectance Infrared Fourier Transform Spectroscopy (DRIFTS)

Procedure

The diffuse reflectance cell (Sampling chamber) used in these experiments was provided by Spectra Tech™. The cell is located in a VERTEX 70 FTIR (Bruker), operating at a resolution of $4cm^{-1}$. The cell contains a dome with ZnSe window. The dome is sealed with the base plate by using O-ring and screws to provide an airtight connection. The system is operated by OPUS software, version 5.5. The fresh and used sample were place on the sample holder

located in the dome and then the spectra is taken and analyzed, to obtain a flat surface, a flat blade is needed to level off the sample surface.

3.5.3 Powder X-Ray Diffraction measurements

Procedure

X-ray diffraction patterns of the samples were collected at room temperature using Cu-Kα radiation (wavelength l = 1.5406Å), by a Philips X'Pert3 Analytical diffractometer. The diffraction intensity was measured in the 2Θ range between 20° to 90° with a step size of 0.017°and time per step is ca 10.2s. The scan speed used for the analysis was $0.21°s^{-1}$. The obtained result was then matched with diffraction patterns (JCPDS files) from software library. The sample was replaced into the microsampling holder by using spatula, to obtain a flat surface, a flat blade is needed to level off the surface. The average crystallite sizes were determined using the Scherer formula

$$D = \frac{0.9\lambda}{\beta \cos\theta} \qquad 3.1$$

where λ is the wavelength characteristic of the Cu-Kα radiation, β is the full width at half maximum (in radians) and Θ is the angle at which the 100% intensity peak appears.

3.5.4 Thermogravimetric Analysis (TGA)

Thermal characterization of the catalyst samples was performed using Mettler-Toledo TGA/DSC I STAR^e instrument with heating rate of 20ºC/min in nitrogen (N_2) atmosphere. Thermal Analysis (TGA and DSC) detects the interatomic and inter-/intra- molecular interactions as related to an imposed external change in temperature.

*Test Procedure***:** The Nitrogen gas was set as the inert gas and the oxidative (O_2), the required flow rates was adjusted to provide the appropriate environments for the test. Then the catalyst

was placed in the specimen holder and the temperature of the furnace was raise to 500°C, the initial weight was set to read 100%, then heating program was initiated. The gas environment is preselected for thermal decomposition (inert - nitrogen gas) and an oxidative decomposition (air or oxygen). The schematic diagram of TGA used is presented in Figure 3.1.

3.5.5 Inductively Coupled Plasma Optical Emission Spectrometer (ICP-OES)

Procedure

The active metal content of the catalysts used for the photoctalytic degradation reactions which include both the fresh and used catalyst were analyzed using Inductively Coupled Plasma-Optical Emission Spectrometer (ICP-OES, P-1000, Perkin- Elmer). Inductively Coupled Plasma (ICP) analytical techniques can quantitatively measure the elemental content of a material from the ppt to the wt% range. The only elements which cannot be measured by ICP methods are C, H, O, N and the halogens. The catalyst samples are digested in an acidic aqueous solution (mixture of nitric acid and sulfuric acid). The sample solution is then sprayed into the core of the inductively coupled argon plasma, were the temperature was raise to approximately 9726.85°C. At such high temperature, all analyte species are atomized, ionized and thermally excited, and they were detected and quantified with an emission spectrometer (OES).

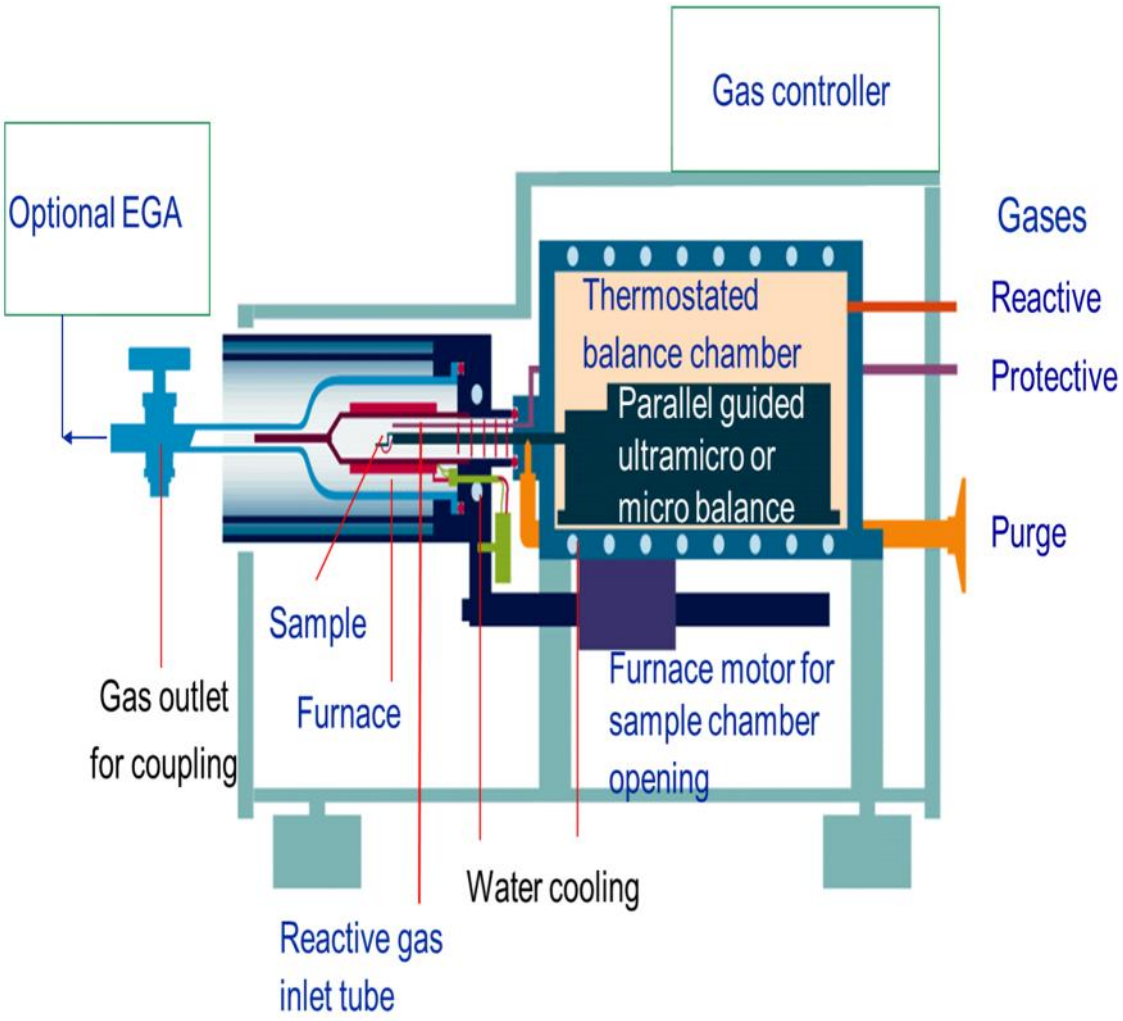


Figure 3.1: The schematic of TGA (Schematic of TGA/DSCI, 2012)

3.5.6 Scanning Electron Microscopy

Procedure

Minimal preparation includes acquisition of a sample and placing it on a Clean Carbon strap that will be attached on the sample holder, which fit into the SEM chamber and some accommodation to prevent charge build-up and the sample from making a contact with the Detector. The Crystalline structure and External morphology of the catalyst was viewed using Quanta Scanning Electron Microscope FEI Quanta 250 of the School of chemistry and Chemical engineering Queens University, Belfast.

3.5.7 Transmission Electron Microscope (TEM)

Procedure

The TEM samples are prepared by weighing 5mg of the Catalyst sample in 50cm^3 methanol after which the sample is Sonicate for 20min to ensure a complete dispersion of the particles. A TEM sample must be approximately 1000Å or less in thickness in the area of interest. The entire sample must fit into a 3mm diameter cup and be less than about 100 microns in thickness. A thin, disc shaped sample with a hole in the middle, the edges of the hole being thin enough for TEM viewing. The Samples were analyzed and recorded using The FEI Tecnai™ F20 Transmission electron microscopes (TEMs) at 200kV at the Nanostructured Media School of Physics and Science, Queens University, Belfast.

3.5.8 The Brunauer–Emett–Teller (BET)

Procedure

The Brunauer–Emett–Teller (BET) surface area of the synthesized transition metals doped TiO_2 catalysts were measured from N_2 sorption isotherm at 77K using a Micromeritrics

Tristar II surface area and porosity as shown on *Figure* 3.2, the samples were degassed under flowing nitrogen at 250°C for 4h using the Smart Prep™ 065. The degassing unit removes adsorbed contaminants from the surface and pores of a sample in preparation for analysis. The sample tube in the analysis port was again degassed before the Dewar containing liquid nitrogen was automatically elevated upwards to submerge the sample tube. A predetermined pressure of nitrogen was bled into the manifold above the analysis port. The sample analysis port valve was then opened, exposing the sample to nitrogen. The quantity of adsorbed nitrogen was determined by the difference in the recorded pressure. The sample analysis port was then closed and the manifold filled with a slightly higher pressure of nitrogen before re-exposure to the sample followed by calculation of the next value. Repeating this process led to the generation of an isotherm of the type shown in Figure 3.3 the surface area of the sample was then calculated from the isotherm using the Brunauer–Emett–Teller (BET) equation and N_2 cross-sectional area of 0.162nm^2.

$$\frac{P_e}{(P_o - P_e)V_{ads}} = \frac{1}{CV_m} + \frac{(C-1)}{CV_n} * \frac{P_e}{P_o} \qquad 3.2$$

where P_e is the equilibrium pressure (i.e after sample is exposed to N_2 in manifold), P_o the saturation pressure, V_{ads} the volume of nitrogen adsorbed, V_m the volume of nitrogen monolayer and C is constant.

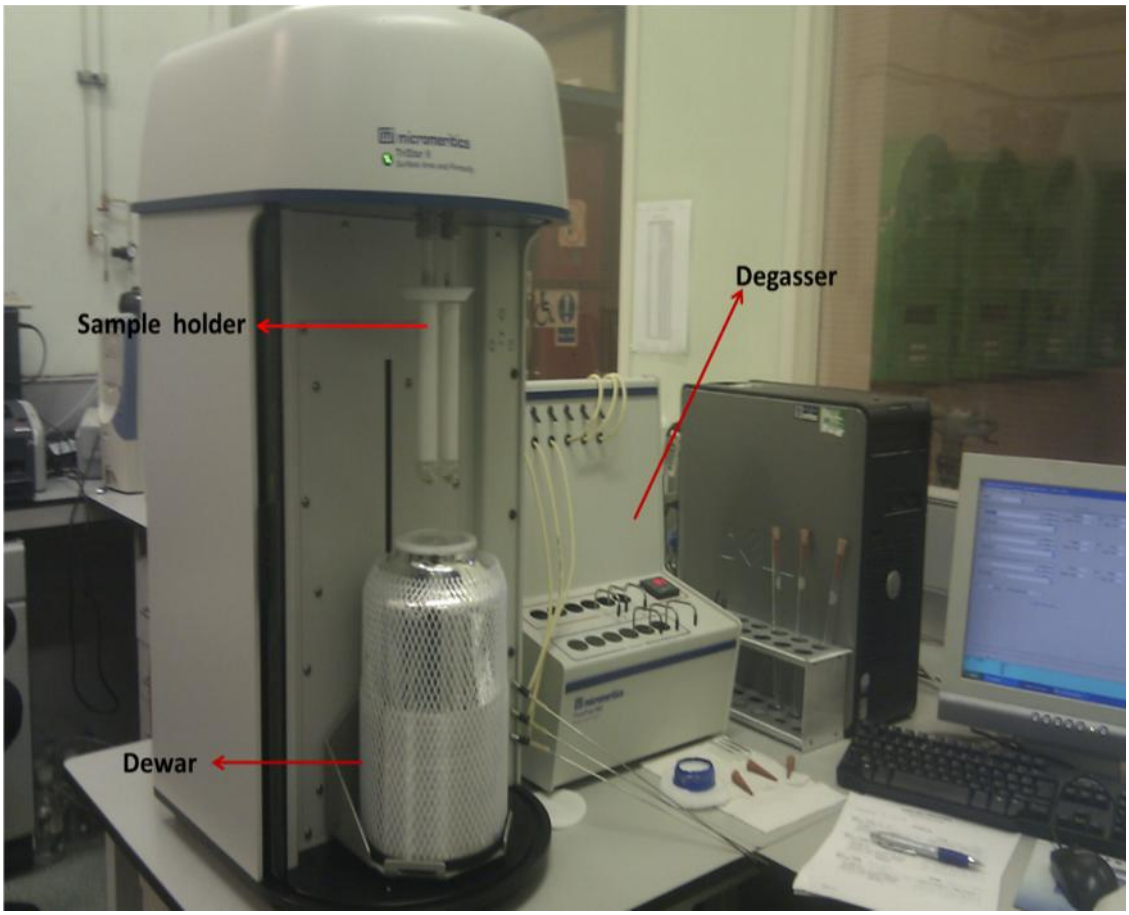


Figure 3.2: Micromeritrics Tristar II

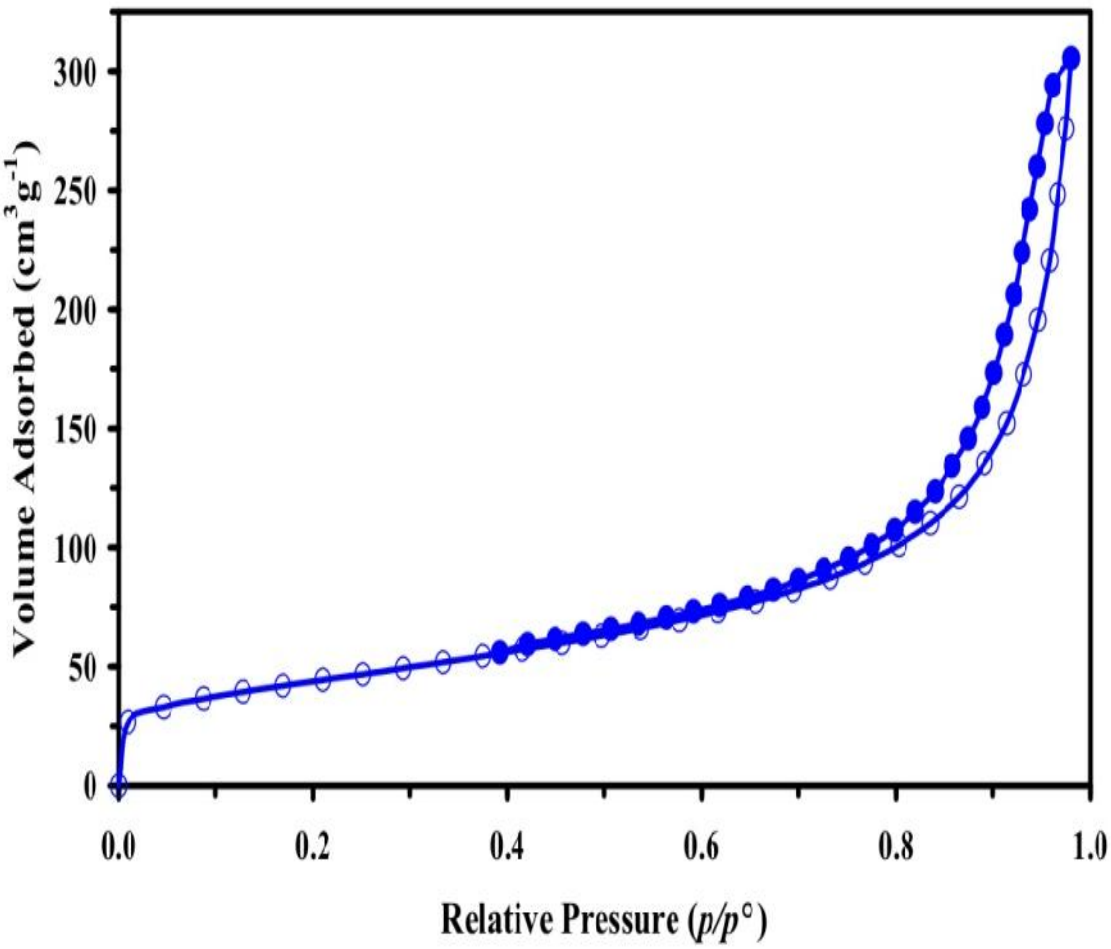


Figure 3.3: Example of a BET Isotherm

3.5.9 Temperature Programmed Reduction (TPR) and Chemisorption

Procedure

The metal dispersion was determined using the Temperature Programmed Reduction (TPR) and CO-chemisorption using Micrometrics Auto-Chems 2910. The gases (i.e H_2 and Ar) were supplied by BOC (>99.9% Purity) and used without further purification, 0.1 g of the sample was loaded into a quartz U tube and held in place by a quartz wool plug. The U tube was then positioned in the furnace. The catalyst was pre-treated at 300ºC (Temperature Ramp at 5ºC/min) in 5%H_2/Ar mixture for 1 hour. After purging in argon at the same temperature for 2 hours, the sample was cooled to -80ºC, and the H_2 pulse chemisorption experiment was performed. In order to carried out hydrogen pulse chemisorption experiment under Isothermal conditions (at -80ºC), the reactor was submerged in a cold bath, obtained by mixing liquid nitrogen and isopropyl alcohol. The chemisorption of hydrogen was performed by pulsing a known volume of H_2/Ar mixture over the catalyst (Argon was used as the carrier gas), an on line thermal conductivity detector (TCD) measured any H_2 not chemisorbed by the sample. Hydrogen was pulsed over the catalyst sample once every ten minutes until the response peaks were of consistent area. The amount of hydrogen chemisorbed per pulsed was calculated by difference in peak area (The area for a pulse of no H_2 chemisorption had been predetermined). The difference in was converted into a concentration using a calibration equation. Finally, by calculating the number of hydrogen atoms that had been chemisorbed, the number of surface palladium atoms in the sample was determined (assuming a Pd/H_2 ratio of 1).



Figure 3.4: The Picture of micrometrics AutoChem 2910 System

The metal dispersion (D_m) of the catalyst was calculated from

$$D_m(\%) = \frac{no.Pd_{surface}}{no.Pd_{sample}} x100 \qquad 3.3$$

and the surface area of Palladium was calculated by

$$Pd.S.A\left(m^2/g_{cat}\right) = \frac{no.Pd_{surface}Pd_{aa}}{SW} \qquad 3.4$$

where $no.Pd_{surface}$ is the number of palladium atoms on the sample surface, $no.Pd_{sample}$ the total number of palladium atoms in sample, Pd_{aa} the atomic area of a palladium atom ($1.27x10^{15}$atoms/cm^2) and SW the sample weight (g)

3.5.10 **Temperature Programmed Oxidation (TPO)**

Procedure

The Temperature Programmed Oxidation experiment was done using the following condition, 0.10 g of catalyst sample was packed in a quartz micro-reactor under 10% O_2/He at 45ml/min and 1%Kr/Ar at 5ml/min using temperature ramp of 10ºC/min reaching a maximum temperature of 900ºC, before the temperature ramp begin the quartz micro-reactor used with the sample was stabilized by heating the electric furnace at 50ºC for 30min, this is done so that the mass spectrometer detector will also be stabilized. The importance of the TPO techniques is to find the most viable and efficient way of reduction condition for the optimum regeneration of the spent/deactivated catalysts. The amount of CO_2 and eventually CO produced during the TPO step were measured by mass spectrometer.

3.6 Photocatalysis Experiment

3.6.1 Photocatalysis using slurry batch process

Photocatalytic activity was evaluated using phenol degradation experiments. The reactors used were closed Pyrex reactors with an outer diameter of 42.0 mm and a height of 210 mm and thickness of 4mm, to 100 cm^3 of a solution containing 0.001M of phenol in deionized water from Barnstead Nanopure diamond machine and 0.2 g of the catalyst was added to the reactor. The pH of the aqueous phenol solution was monitored during the reaction using the Jenway 3010 pH meter. The suspension was stirred magnetically using yellow line MST basic magnetic stirrer at 650 rpm at ambient temperature for 2h in the dark, and a small amount of the suspension was withdrawn to analyze equilibrium concentration of phenol in the solution. The mixture was then exposed to UV light using a Rayonet RMR-600 reactor. The RMR-600 consists of 279.4mm in square and 266.7mm high (external measurements) chamber manufactured from Alzak aluminum. The reactor has 6 (8 watts) UV lamps (350nm wavelength), with an arc length of 76.2mm each (48 lamp watts total) and for the visible light a florescence lamp of (555nm was used with 315, 00 lux). The distance between the UV lamp and the surface of the solute was set at 63.5mm. An oxygen balloon was connected to the reactor in order to assure a high oxygen saturation of the solution without the need for a sparger and condenser. At selected time intervals of approximately 20 min over a typical 2h reaction, 2.5 mL of the suspension was withdrawn and filtered using Acrodisc CR 13mm syringe filter with 0.45μm PTFE membrane for HPLC analysis, the diagram is presented on Figure 3.5

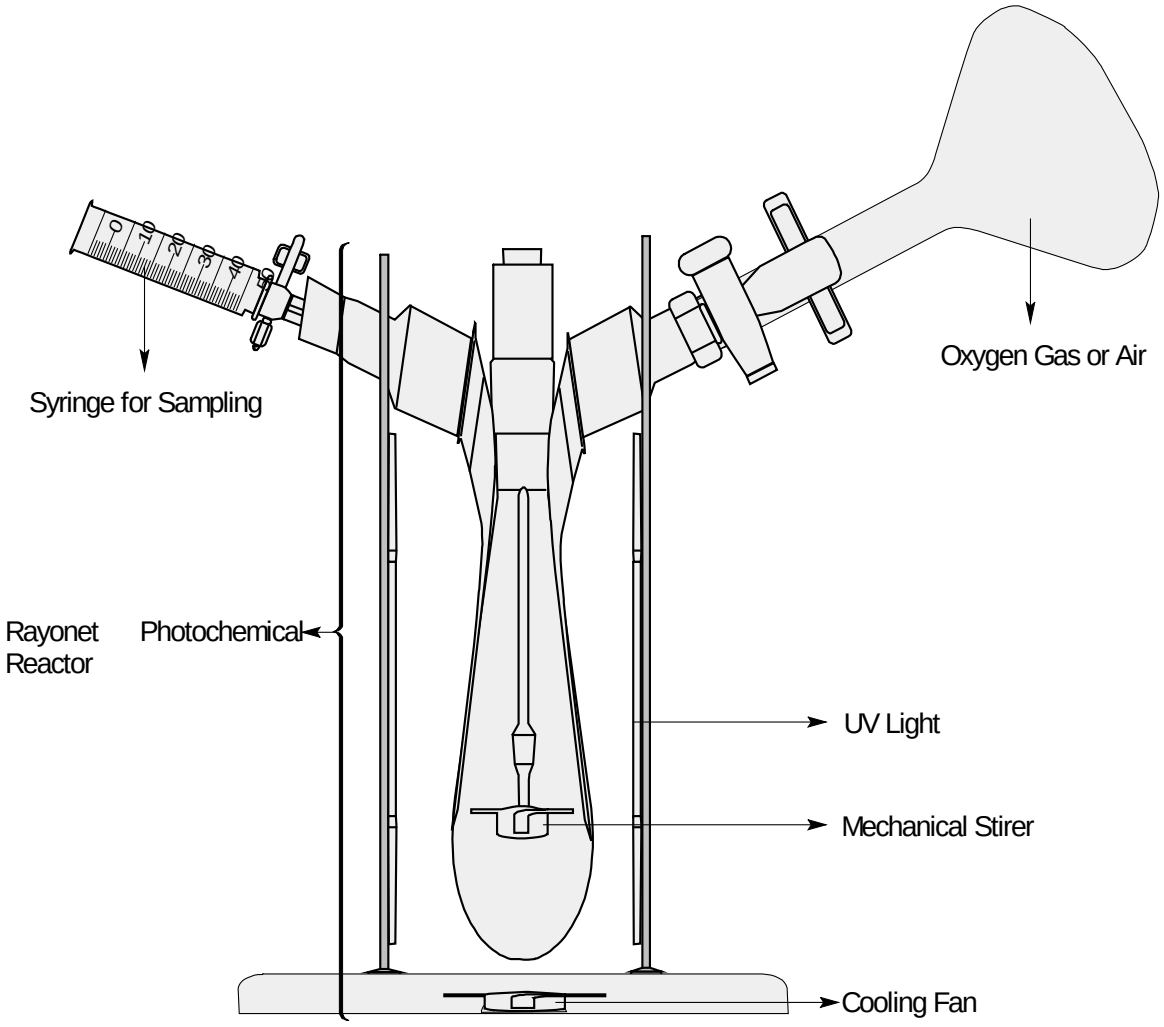


Figure 3.5: Photocatalytic experiment in Slurry batch process

3.6.2 Ultraviolet emission spectra

The ultraviolet light used for the experiment is classified as UV-A. This UV category has a wavelength range between 320 to 400nm. The light source is a UV lamp that comes with a UV-A cut off filter, resulting to a transmission wavelength of between 300 to 400 nm and a peak at 350nm.

The UV lamp: The emission spectra of the bulb installed in the UV lamp is shown in Figure 3.6, for this work, a RPR-3500A lamp equipped with 8watt bulb (Southern New England Ultraviolet Company) is used as a UV light source. The bulb has an emission spectra ranging from 300 to 400nm with a distinct peak at 350nm.

3.6.3 UV Irradiance Measurement

UV radiation reaching the reactor inside the Rayonet compartment is measured using UVX Radiometer (UVP Inc., Upland CA) equipped with a UVX-36 long wave sensor. It is calibrated at 365nm but can be used also for 335 to 380nm applications.

3.6.4 Quantum Yield/Efficiency calculation of the UV Light

Energy of a single photon at 350 nm (wavelength of lamp) $= \frac{hC}{\lambda}$

$= (6.626 \times 10^{-34} \times 2.998 \times 10^{8}) / 350 \times 10^{-9} = 5.6756 \times 10^{-19}$ J

The Average value of measured irradiance of the UV lamp within 1.5cm from the reactor

$I = 0.19 mW/cm^2 = 0.00019 J/cm^2/s$

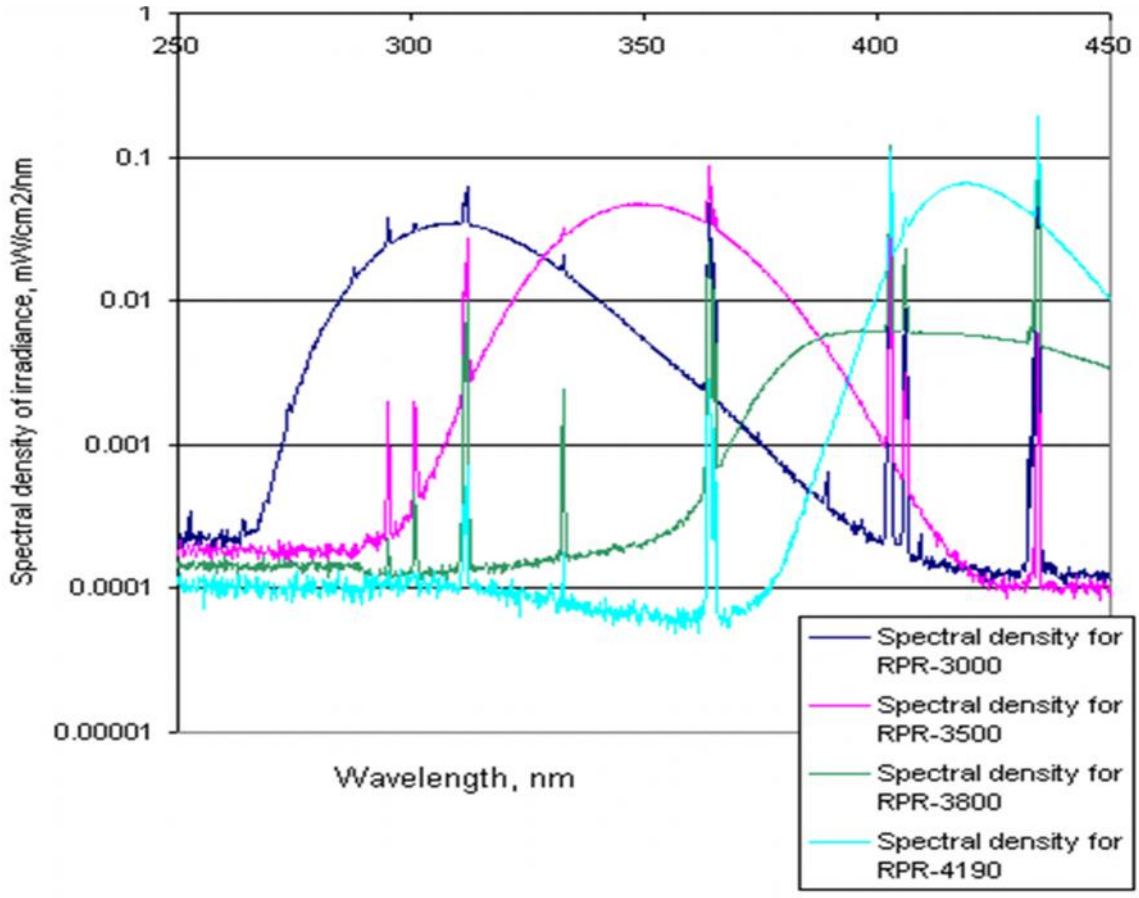


Figure 3.6: Spectral distribution of Irradiance density for the UV lamp

$N_{photons}$= 0.00019 / 5.6756x10^{-19} = 3.3477x10^{14} photons/cm^2/s.

Area of reactor = Area of Cylinder

area of reactor $= 2\pi r_{in} l$

l = length of cylinder

r_{in}= r_{out} - thickness

r_{in} = internal radius

r_{out} = outer radius = 2.0cm

reactor thickness = 0.4cm

r_{in} = 2.0-0.4 = 1.6cm

where length of reactor = 11cm.

Area of reactor = (2xπx1.6x11) =110.58cm^2

Number of Photons Incident on the reactor surface area =

3.3477x10^{14}photons/cm^2/s x area of reactor

$N_{photons}$ = 3.3477x10^{14} photons/cm^2/s x 110.58cm^2

$N_{photons}$ = 3.7020x10^{16}photons/sec.

Quantum yield ϕ describes the number of reactant molecules transformed or product molecules formed divided by the number of photons at a given wavelength (Serpone and Salinaro, 1999).

$$\Phi = \frac{N_{molecules}}{N_{photons}} \qquad 3.5$$

$N_{molecules}$ =Number of Phenol molecules converted to CO_2 i.e. the Initial rate of reaction

$N_{photons}$= Number of Photons per second incident inside reactor

where $N_{molecules}$= Initial rate per second x Na x Volume

Volume = 0.1liter

Na= Avogadro number ($6.022x10^{23}$)

Initial rate of reaction from the data is in millimoles per minutes this is converted to Moles per second

Quantum Yield =Initial rate of reaction/ Amount of photons absorbed by the photocatalyst at wavelength

Quantum efficiency = Initial rate of reaction/ Amount of photons absorbed by the photocatalyst at wavelength x 100

Measuring luminous flux per unit area of Visible Light

A florescence lamp at 555nm was as a visible light source to trigger the photocatalytic reaction and was positioned at 1.5cm away from the reactor within the Rayonet compartment, the focused intensity on the reactor was (31500 lux) that is 0.004612 W/cm^2, which was measured using "LIGHT METER Model : LX-101A".

3.6.5 **Quantum Yield/Efficiency calculation of the visible light:**

Energy of a single photon at 555 nm (wavelength of lamp) $E = hc/\lambda$

= $(6.626 \times 10^{-34} \times 2.998 \times 10^{8}) / 555 \times 10^{-9} = 3.57923 \times 10^{-19}$ J

The Average value of the measured luminous flux per unit area of the florescence lamp within 1.5cm from the reactor

$N_{phtons} = 0.004612 / 3.57923 \times 10^{-19} = 1.2885 \times 10^{16}$ photons/cm^2/s.

Area of reactor = Area of Cylinder

area of reactor = $= 2\pi r_{in} l$

l = length of cylinder

$r_{in} = r_{out}$ - thickness

r_{in} = internal radius

r_{out} = outer radius = 2.0cm

reactor thickness = 0.4cm

r_{in} = 2.0-0.4 = 1.6cm

where length of reactor = 11cm

Area of reactor = $(2 \times \pi \times 1.6 \times 11) = 110.58$cm^2

Number of Photons Incident on the reactor surface area =

1.2885×10^{16}photons/cm^2/s x Area of reactor

$N_{photons} = 1.2885 \times 10^{16}$ photons/cm^2/s x 110.58cm^2

$N_{photons} = 1.42487 \times 10^{17}$photons/sec

3.7 Photocatalysis Process using Trickle Bed in Continuous mode

Photocatalytic activity of the prepared catalysts were also evaluated using phenol degradation experiments. The reactor used in the case of the continuous flow system was a tubular trickle bed column made with quartz glass with external diameter of 9.89mm and internal diameter of 9.56mm. The reactor was attached to three neck 100 cm^3 round-bottomed flask, the flask was connected to Polytetrafluoroethylene (PTFE) Tube, and the complete set up was connected to Masterflex L/S Digital Drive, 600 RPM, 115/230 VAC, HV-07523-80 pump, for the circulation of the phenol solution. A 100 cm^3 portion of 0.001M phenol aqueous solution and 1.0 g of a Pd, Au, and Pd/Au-TiO_2 pelletized with 456-600μm size were added to the reactor. The pH of the aqueous phenol solution was adjusted from 3.5 to 6.4 using Jenway 3010 pH meter. Then the complete set-up was exposed to UV light under a Rayonet RMR-600 reactor. The RMR-600 is 279.4mm in square and 266.7mm in high. The chamber is manufactured from Alzak aluminum and is 228.6mm deep x 177.8mm diameter. The reactor has Six (8 watts) UV lamps with 350 nm, with an arc length of 76.2mm each (42 lamp watts total). The top opening is 127mm diameter. The main emission of the lamp was 350 nm. The distance between the UV lamp and the surface of the tubular Trickle bed column with the catalyst was position at 15 cm, the schematic of the Trickle/Taylor flow system is presented on Figure 3.7

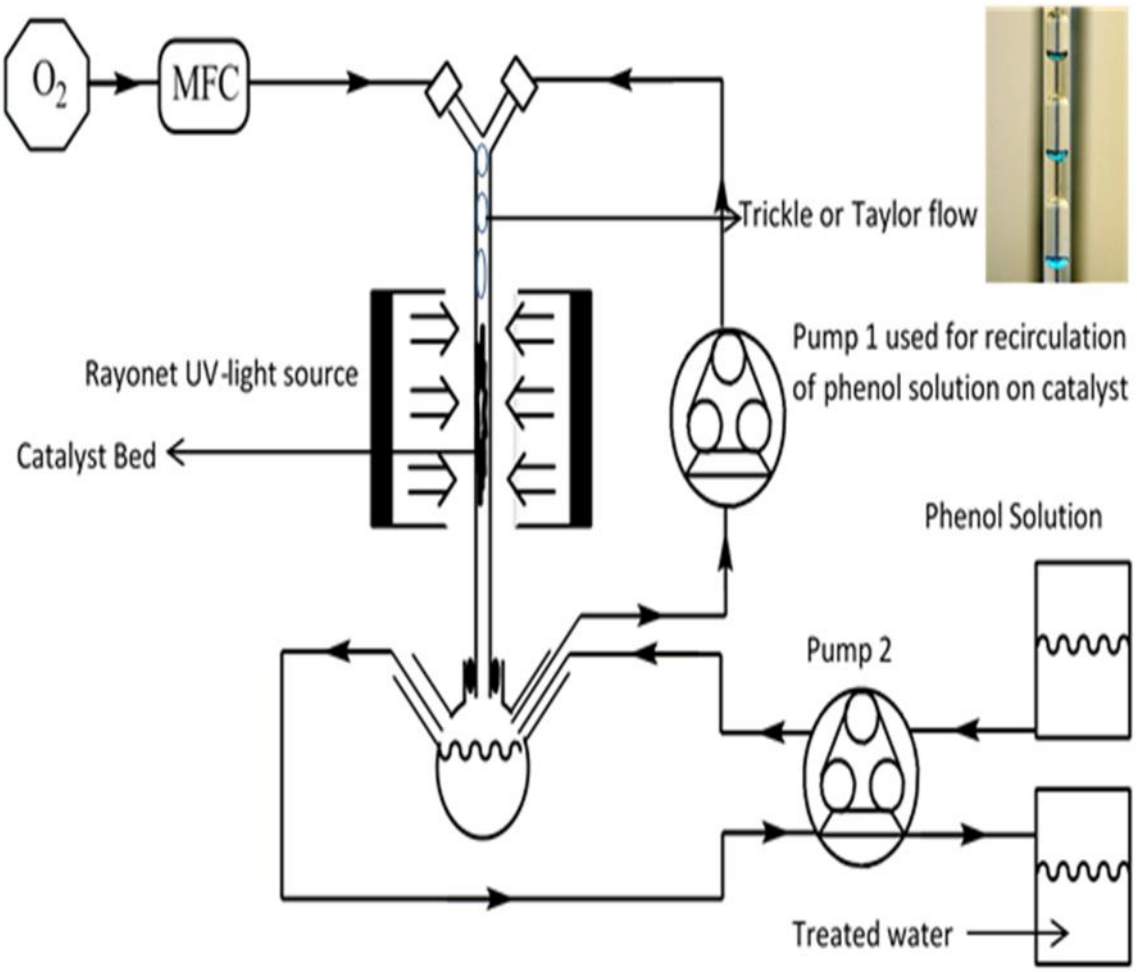


Figure 3.7: Schematic of the Trickle/Taylor flow system in continuous process

3.7.1 Photocatalysis process using Taylor flow system in continuous mode

The photocatalysis of phenol was also evaluated using the catalyst prepared on the Taylor flow system. The experimental setup for the Taylor flow system is similar with the trickle bed process except for the difference in the tubular quartz column that contains the catalyst. This contains a special type of connection using the 1.588mm size tube to form a constriction within the Swagelok valve so as to produce the alternating flow between the oxygen and the phenol solution. The picture of the Taylor flow system is shown on Figure 3.8, and the Picture of the Photo-reactor i.e the quartz column is inserted on the Taylor flow as shown on Figure 3.7.

3.7.2 The reactor flow systems

Oxygen Delivery System. The schematic of the experimental set-up is shown in Figure 3.7, using the Taylor flow system oxygen is carried from the Cylinder into the reactor using Teflon and stainless steel tubing. System piping is made from 6.35mm sized and 316 stainless-steel tubing and inter-connected by Swagelok tube fittings. An On/Off valve controls the main supply of oxygen going into the system. Through a mass flow controller unit (Aera FC-7700C), oxygen flowrate is adjusted to the value of 15 sccm (standard cubic centimeter per minute). The calibration chart of the mass flow-meter used in the experiment is shown in Figure 21. Oxygen flowrate is monitored using a mass flow meter (ROD 4 Aera) which is operated with the mass controller unit. Flowmeter digital readout is calibrated by setting various flowrates between 0 to 100% i.e. flowrates in percentage.

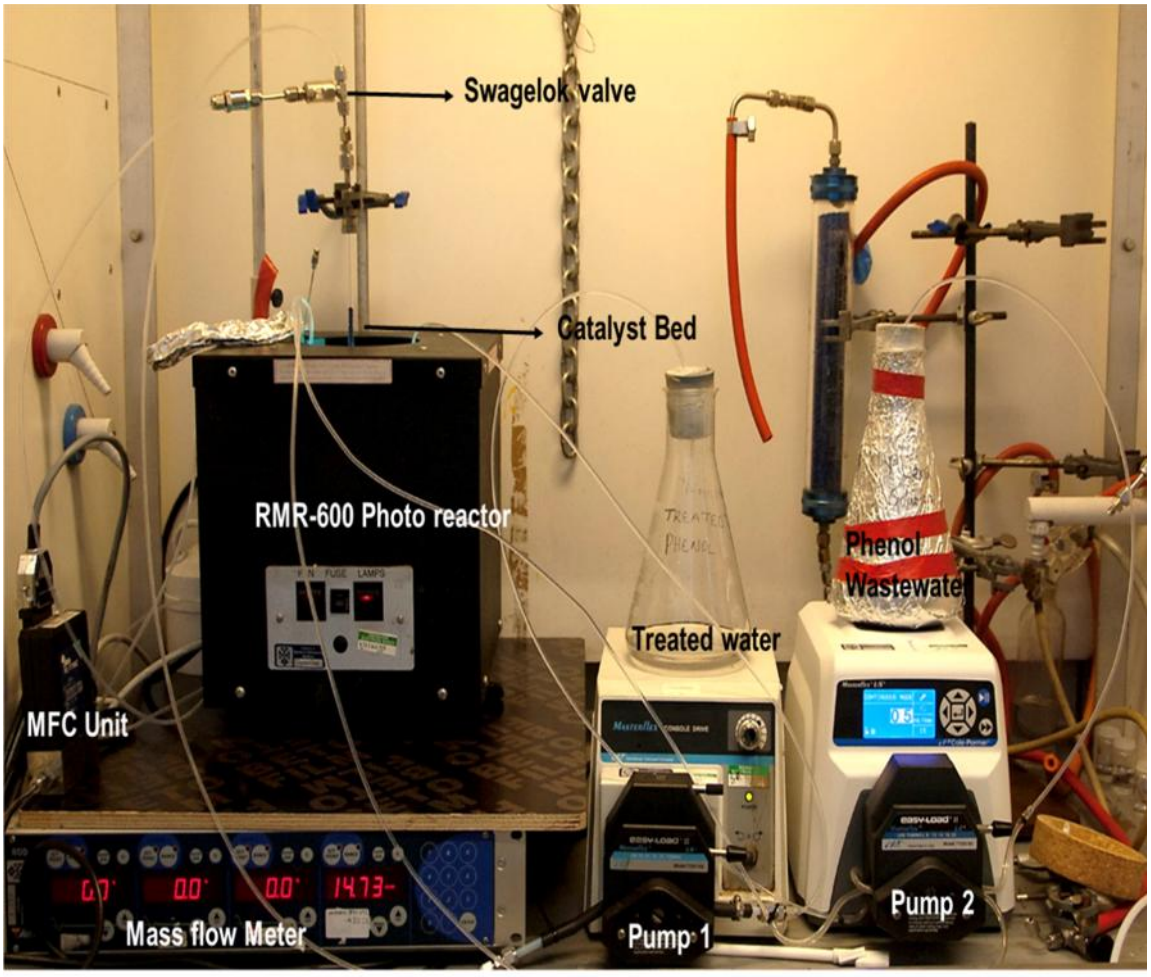


Figure 3.8: Picture of Taylor flow system in continuous mode

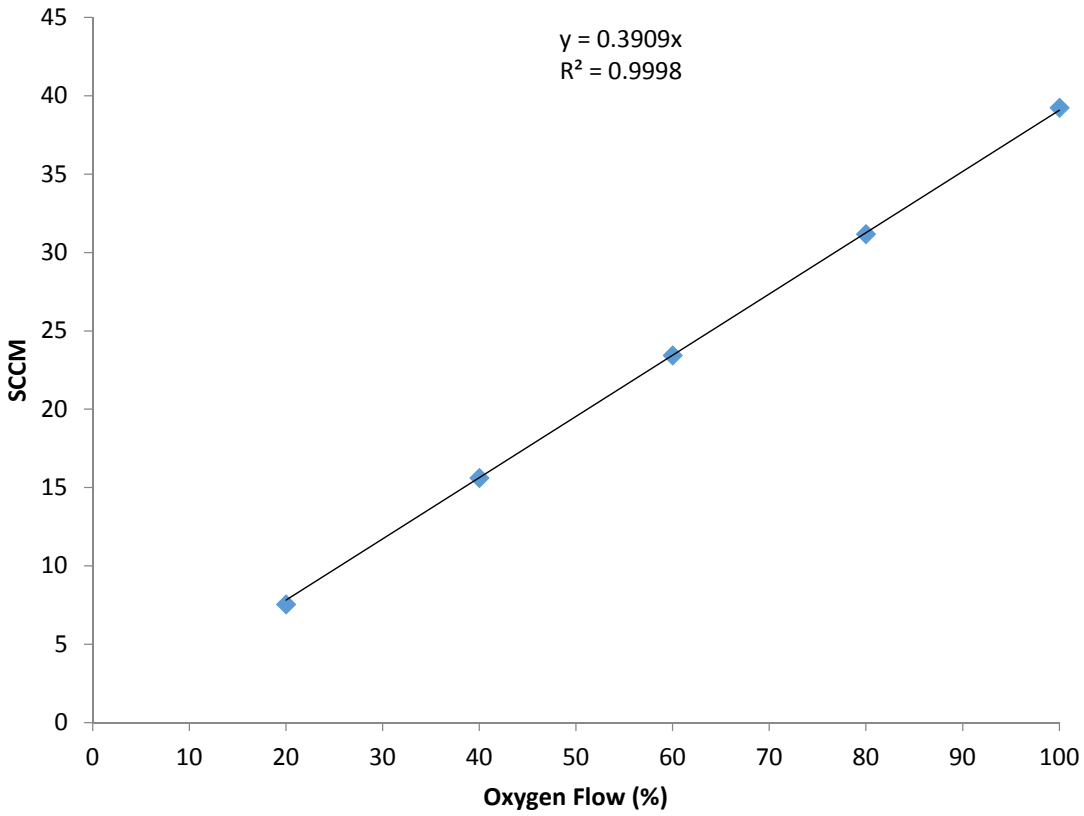


Figure 3.9: The calibration chart of the mass flow-meter

The calibration is done by using a bubble lo-meter. Oxygen coming out of the mass flowmeter is monitored using the bubble lo-meter, which then displaces the liquid water inside the burette to 15cm interval, using a stopwatch, to measure the time it takes to for each flow in percentage to reach the 15cm interval. Actual flowrate is computed by dividing the displaced volume of water with average time in seconds. This gives the flowrate in standard cubic centimeter per minute (sccm) the process is repeated to come up with five measurement points

3.8 **Analysis**

3.8.1 **High Performance Liquid Chromatography (HPLC)**

Procedure

The HPLC technique was mainly used to monitor the formation of any intermediates during the photocatalytic reaction of phenol mineralization. In the quantitative analysis, an Agilent 1100 was used which was equipped with Eclipse XDB C18 reverse phase column (3.5µm, 4.6*150mm) and Diode Array Detector (DAD) at wavelength of 254nm at flow rate of 1.0µ/min, Column temperature of 300°C with 50% methanol and 50% water was used as mobile phase. The prominent peak of phenol was obtained at around 2.99–3.04 min retention time. At selected time intervals of 60 min for 24h in the case of the slurry/suspension mode reactor and interval of 1h for 52h in the case of the Trickle bed/ Taylor flow system. About 1.5 ml of the solution was withdrawn for HPLC analysis to monitor the rate of the mineralization of the phenol.

3.8.2 The Gas Chromatography-Mass Spectroscopy

The GC-MS techniques was used to identify the intermediates formed during the reaction and to ascertain the completion of the photodegradation of phenol in the reaction. The phenol solution was treated with dilute sulphuric acid and sodium hydrogen carbonate after the photodegradation then the phenol was extracted with dichloromethane. The extract was analyzed using Perkin Elmer Clarus 500 GC-MS with auto-sampler at injection temperature at 250°C. Amount of sample injected was 1.0µL, the carrier gas used is helium at a flow rate of 1ml/min and split flow of 50:1 was used. The oven temperature was programmed with initial temperature of 50°C for 5 min; it was ramp at 100°C/min to 300°C hold for 10 min.

CHAPTER FOUR

4.1 Results and Discussion

4.2 Characterization of Catalysts

4.2.1 Diffuse reflectance UV-Vis of Au-Pd/TiO_2

The determination of band gap energies is essential for identification of changes in the electronic structure of the titanium(IV) Oxide (P25) after deposition with gold and palladium. From the DRS UV-Vis spectra obtained in Figure 4.1 and Figure4.2, an absorption peak, with a center at 580 nm was observed for 1wt%Au-TiO_2 at a high intensity. This was due to the surface plasmon resonance of spatially confined electrons in 1.0wt% Au-TiO_2 catalyst. There are band gap excitations at a region near 400 nm in all the spectra. The transmittance edge of Au-Pd/TiO_2 samples varies as the content of Au metals in TiO_2 (Yang L 2000); with these they exhibit a slight red shift (the band gap excitation was slightly shifted to longer wavelengths) in the band transition from the normal value with adding the metal at various ratios. This red shift was attributed to the charge-transfer transition between the d electrons of the dopant and the Conduction Band (CB) or Valance Band (VB) of TiO_2 (Chen and Mao, 2007). Thus, the high level of dispersion and interaction between the dopant metal atom and TiO_2 particles would be expected to enhance the catalytic activity of metal doped TiO_2 (Loganathan *et al.*, 2011). Based on the origin of excitation, the band gap values of TiO_2 (P25 Degussa) and 0.5%Au.0.5%Pd, 1.0%Au, 0.5%Pd, 0.25%Au.0.75%Pd, 0.75%Au.0.25%Pd were calculated, and the values found to be 3.2, 2.99, 3.01, 2.97, 2.97 and 2.97eV respectively as presented on Table 4.1.

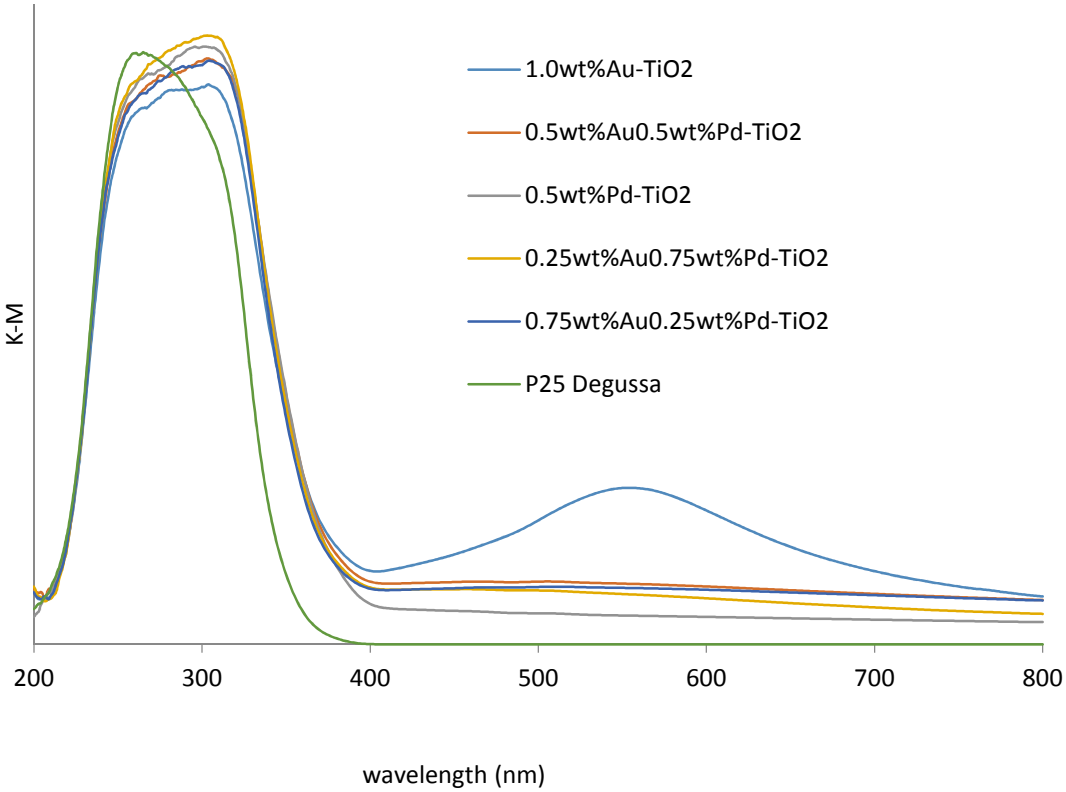


Figure 4.1: The UV-visible diffuse reflectance spectra of Au-Pd/TiO_2 and P25

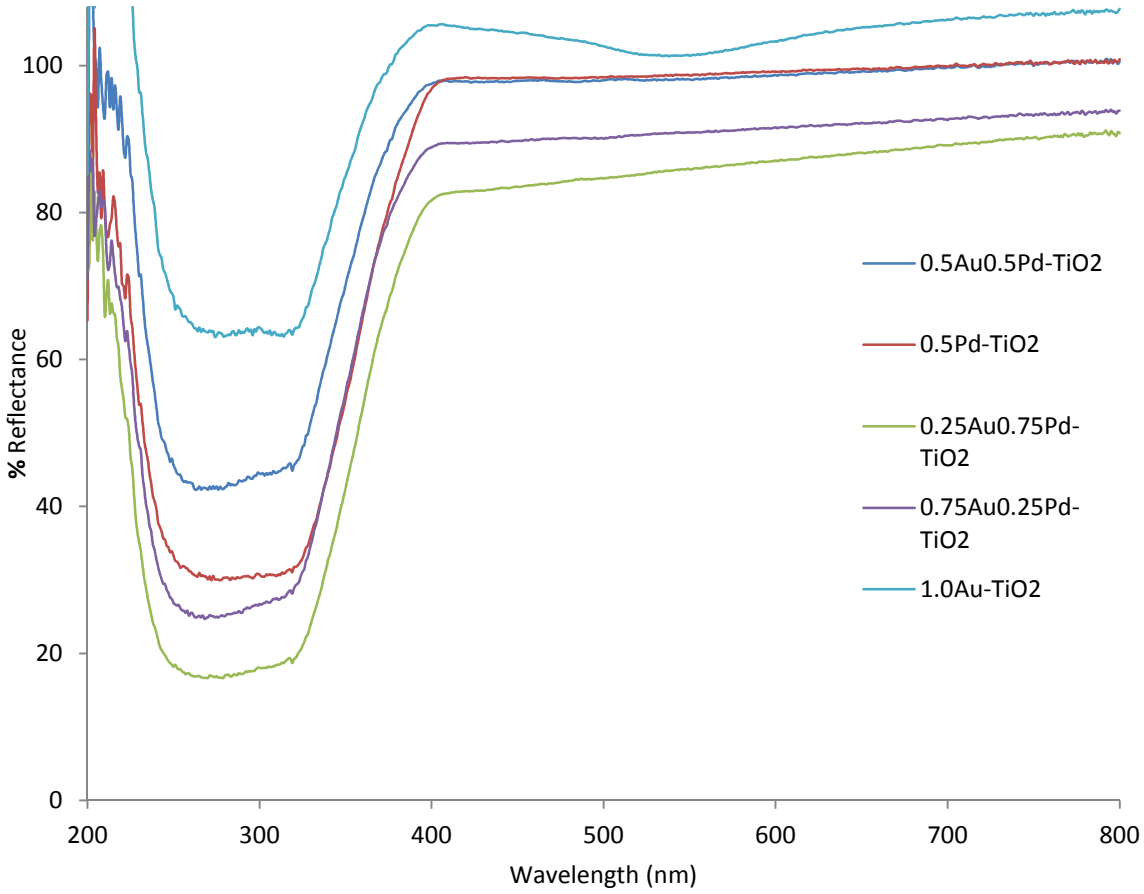


Figure 4.2: Diffuse reflectance UV-Vis spectra of Au-Pd/TiO_2

Relying on the similar appearance of all the spectra, it can be concluded that varying the Au and Pd content during the synthesis may not influence the crystallization of TiO_2 which was confirmed on the XRD result. Comparing the optical absorption spectra shown in Figure 4.1, it deduced that the Au-Pd/TiO_2 catalyst with significant bandwidth show stronger visible light absorption, suggesting great potentials of these catalysts in photocatalysis with applications in the visible light range.

4.2.2 Diffuse reflectance UV-Vis of 2%Pd@TiO_2

From the result of the DRS UV-Vis spectra of the catalyst prepared using the microemulsion, shown in *Figure* 4.3 the amorphous titanium(IV) Oxide displayed absorption bands in the UV region at 325 and 415 nm also the 2%Pd@TiO_2 also exhibits bands at the same positions, but there exists absorption bands in the far UV region at 270 nm on the 2%Pd@TiO_2 which can be attributed to the effect of the palladium nanoparticles on the catalyst. The absorption of the 2%Pd@TiO_2 in the visible region confirm the reports by Ohde *et al.*, (2002), that the palladium nanoparticles are known to absorb in the UV-vis region. The ability of the catalyst to absorb UV light explains the reasons the 2%Pd@TiO_2 support the photocatalytic oxidation of phenol.

Table 4.1: The physico-chemical properties of Au-Pd/TiO_2 and P25 with the Surface area, pore Volume, crystallite size and Band gap

CATALYST	$A_{BET}(m^2g^{-1})$	Vp (cm^3g^{-1})	P (nm)	Crystallite Size (nm)		Band Gap (eV)
				Anatase	Rutile	
1%Au-TiO_2	43.63	0.10	10.66	22.3	31.6	3.01
0.75%Au.0.25%Pd-TiO_2	44.80	0.12	10.00	22.2	34.2	2.97
0.5%Au.0.5%Pd-TiO_2	45.76	0.14	10.57	22.4	35.3	2.99
0.25Au%.0.75Pd-TiO_2	48.83	0.15	11.90	21.9	34.7	2.97
0.5%Pd-TiO_2	47.05	0.13	12.60	22.9	34.6	2.97
2%@Pd-TiO_2	190.09	0.19	3.91	32.7		-
P25 Degussa	55.00	0.19	-	15.6	19.9	3.12

Crystallite size calculated using Scherrer formula $\mathbf{D = K\lambda/\beta Cos\theta}$. Band gap energies were calculated using the formula $\boldsymbol{E = (h*c)/\lambda}$, where; h = Planck constant (6.63×10^{-34} J s^{-1}), λ = cut off wavelength from the % reflectance graph, c= speed of light in a vacuum ($\approx3\times10^{8}$ m s^{-1}) and 1eV = 1.6×10^{-19} J (Conversion factor)

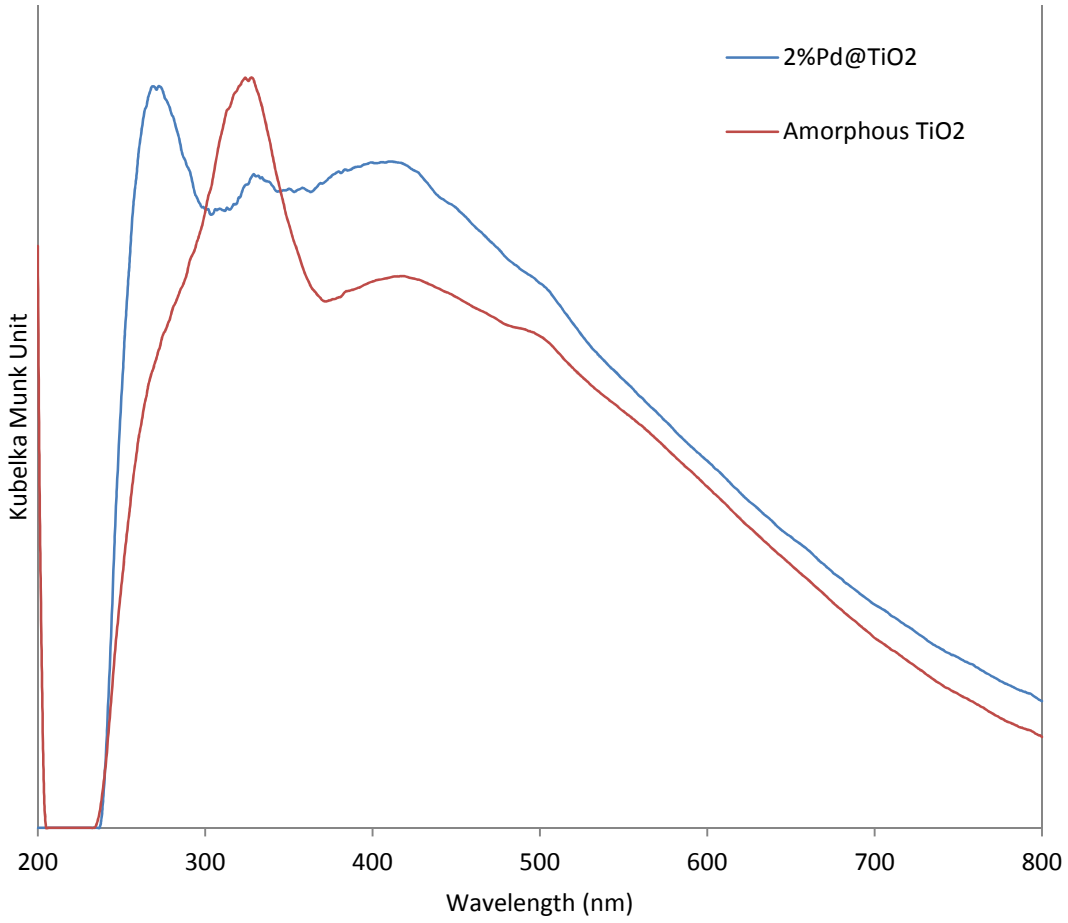


Figure 4.3: The Diffuse reflectance UV-Vis spectra of the 2%Pd@TiO_2 and the amorphous TiO_2

4.2.3 **XRD of transition metal doped-TiO_2**

X-ray diffraction (XRD) patterns of the catalyst deposited with transition metals shows anatase peaks for all studied samples. The XRD patterns of Pd-TiO_2, Au-TiO_2, Fe-TiO_2, Cu-TiO_2 and P25 Degussa, resemble each other as the same preparation conditions are used, the results is shown on *Figure* 4.4. But the pattern for the hydrothermal treated P25 shows a significant transformation of the anatase to rutile phase, while the Hombikat (commercial titanium(IV) Oxide from Hombikat) is mostly anatase with the smallest average crystallite size of 5.4 nm. The crystallite size of the samples were calculated using the prominent anatase peak at 2θ= 25.27°. The Pd-TiO_2, Au-TiO_2, Fe-TiO_2, Cu-TiO_2 and P25 Degussa has a crystallite size of 22.3nm but the average size of the rutile peak of the hydrothermally treated P25 is 33.3nm.

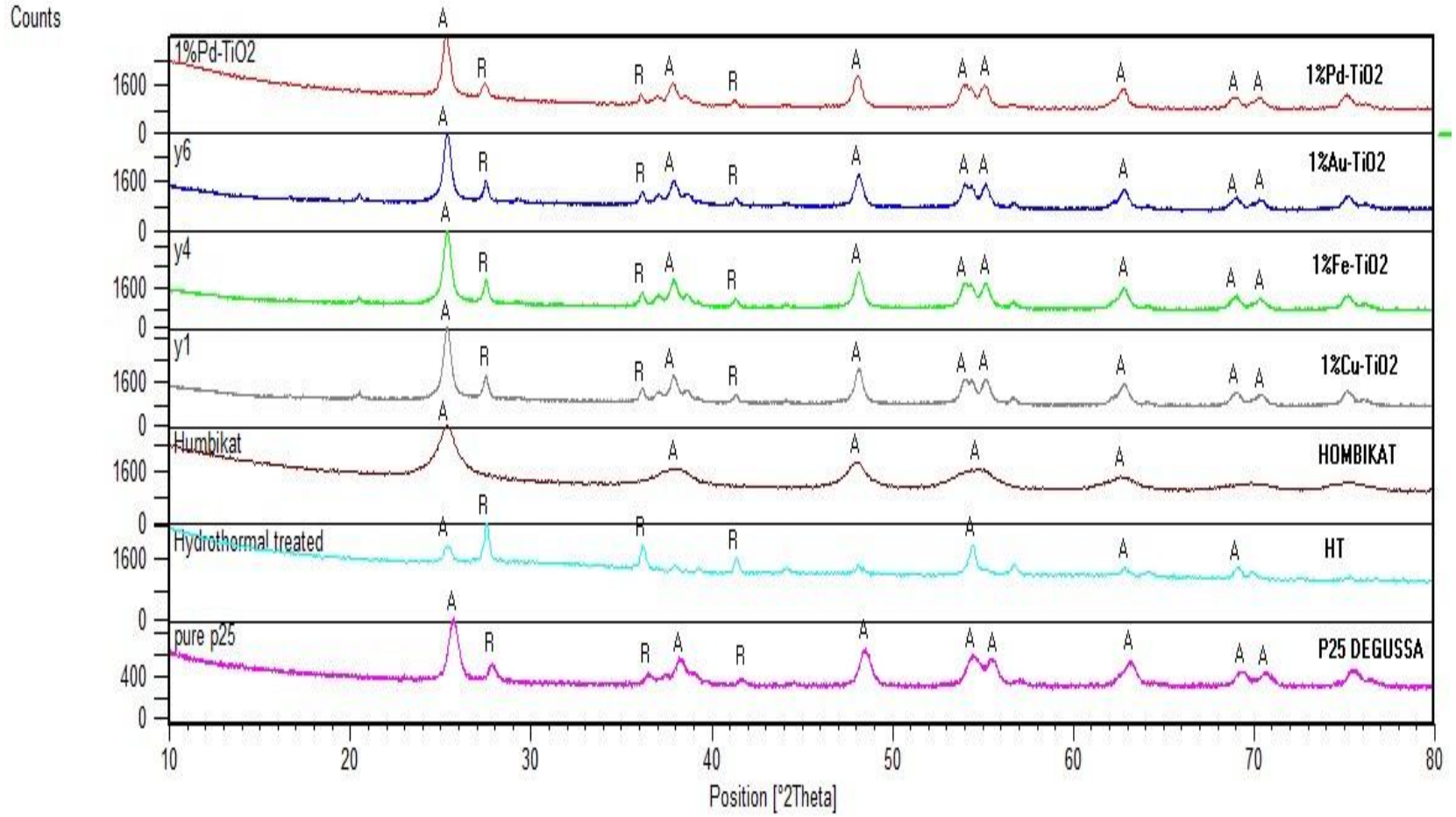


Figure 4.4: X-ray diffraction patterns of the prepared catalyst deposited with transition metals

4.2.4 **XRD of Au-Pd/TiO_2**

The phase structure, crystallite size, and crystallinity of TiO_2 plays an important role in the photocatalytic activity of the catalyst prepared, and many studies have confirmed that anatase phase of titanium(IV) Oxide shows higher photocatalytic activity than brookite or rutile phase (Carp *et al.*, 2004). The XRD patterns of Au-Pd/TiO_2 catalysts calcined at 120°C for 24h were show in *Figure* 4.5. There existed diffraction peaks, which lay at 25.40, 37.90, 48.00 and 53.90°, corresponding to the anatase phase. The large surface area, high crystallinity, low crystallite size, and crystal structure are important properties that influence the photocatalytic activity of TiO_2. The average crystal size of TiO_2 was determined to be 22.3 nm calculated using the characteristic anatase peak at 2θ= 25.30 and 34.1nm for the rutile peak at 2θ= 27.40. The peaks marked x in the prepared catalyst which appear at 20.51° may be due to impurities as a result of catalyst preparation, because the peak does not correspond to any element included in the samples. There were no peaks that indicate the presence of the metal nanoparticles or the metal oxide when compared with JCPDS 88-2335, 88-2434 and 4-0784. This is an indication that the sizes of the metals nanoparticles are between 2 to 4nm. For the characterization of supported metal catalysts XRD technique has limited capacity to detect crystalline particles with a size below 2 to 4 nm (Wanke and Flynn, 1975), this is in line with the results reported by Hamill *et al.*,(2014).

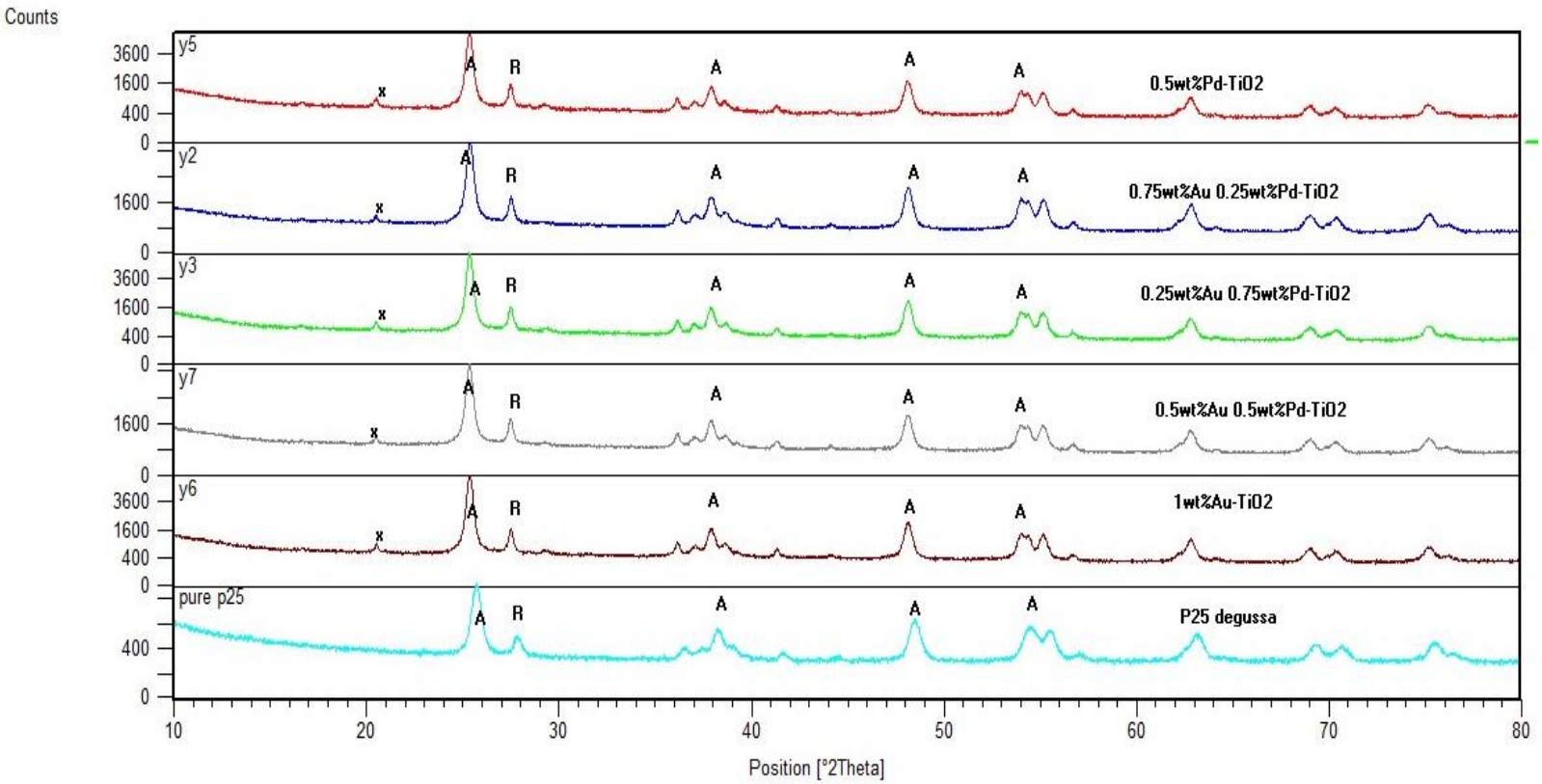


Figure 4.5: The XRD Pattern of Au-Pd/TiO_2 prepared by sol immobilization

4.2.5 XRD of 2%Pd@TiO_2

From the XRD result of 2%Pd@TiO_2 as shown on *Figure* 4.6, the average crystallite size of palladium core-shell in the TiO_2 was determined to be 32.68 nm calculated using the characteristic palladium peaks at 2θ= 38.6, 44.7, 65.1 and 78.5°. The titanium-n-butoxide used in the catalyst preparation produced an amorphous titanium(IV) Oxide which explains the absence of the anatase and rutile peaks on the XRD result. The modification of the titanium(IV) Oxide with palladium gave a characteristic peaks at 2θ= 38.6, 44.7, 65.1 and 78.5° which corresponds to the palladium 111, 200, 220 and 311 respectively when compared with PDF# 84-0300. The pure amorphous titanium(IV) Oxide without palladium nanoparticles did not show any peaks on the XRD.

4.2.6 Thermogravimetric Analysis (TGA) of Au-Pd/TiO_2

Thermogravimetric Analysis (TGA) measures the mass of a sample as it is submitted to a selected temperature program in a defined atmosphere. The TGA curves show three weight loss steps. The first step is between 25 and 180°C corresponding to the removal of volatiles (moistures, solvents) and adsorbed water. The main weight loss occurred between 350 and 550°C that could be assigned to high temperature pyrolysis of carbon species from the PVA used in the catalyst preparation and the third step above 550°C might be assigned to loss probably accompanied with collapse of inter-agglomerate and escape of trace moiety during the phase transformation from anatase to rutile (Yu *et al.*, 2000; Porter *et al.*, 1999; Song and Pratsinis, 2000). This is also in agreement with the results obtained from the XRD analysis, the TGA result of the Catalyst are present in *Figure* 4.7 and 4.8

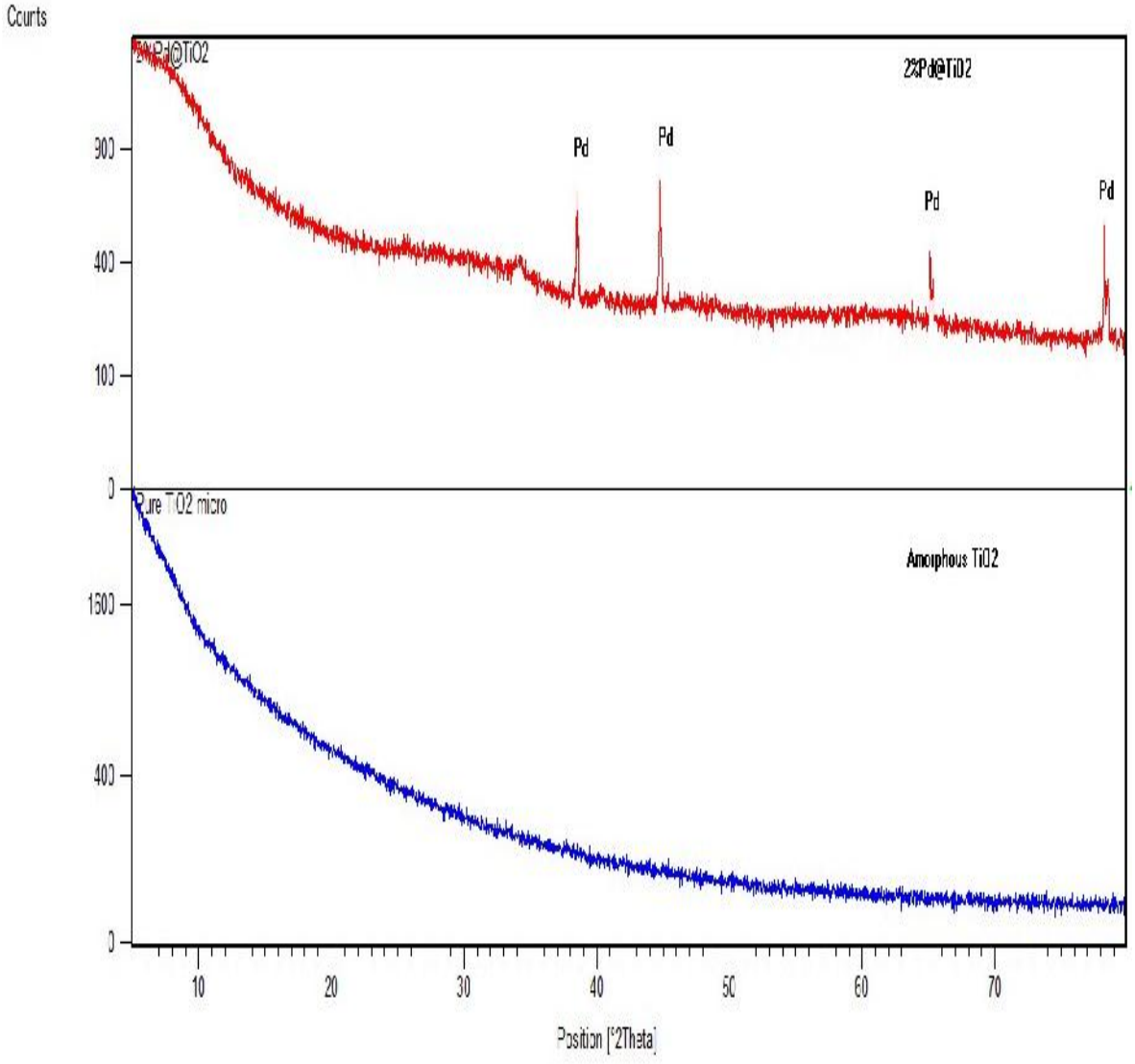


Figure 4.6: The XRD Pattern of the 2%Pd@TiO_2 showing the presence of palladium

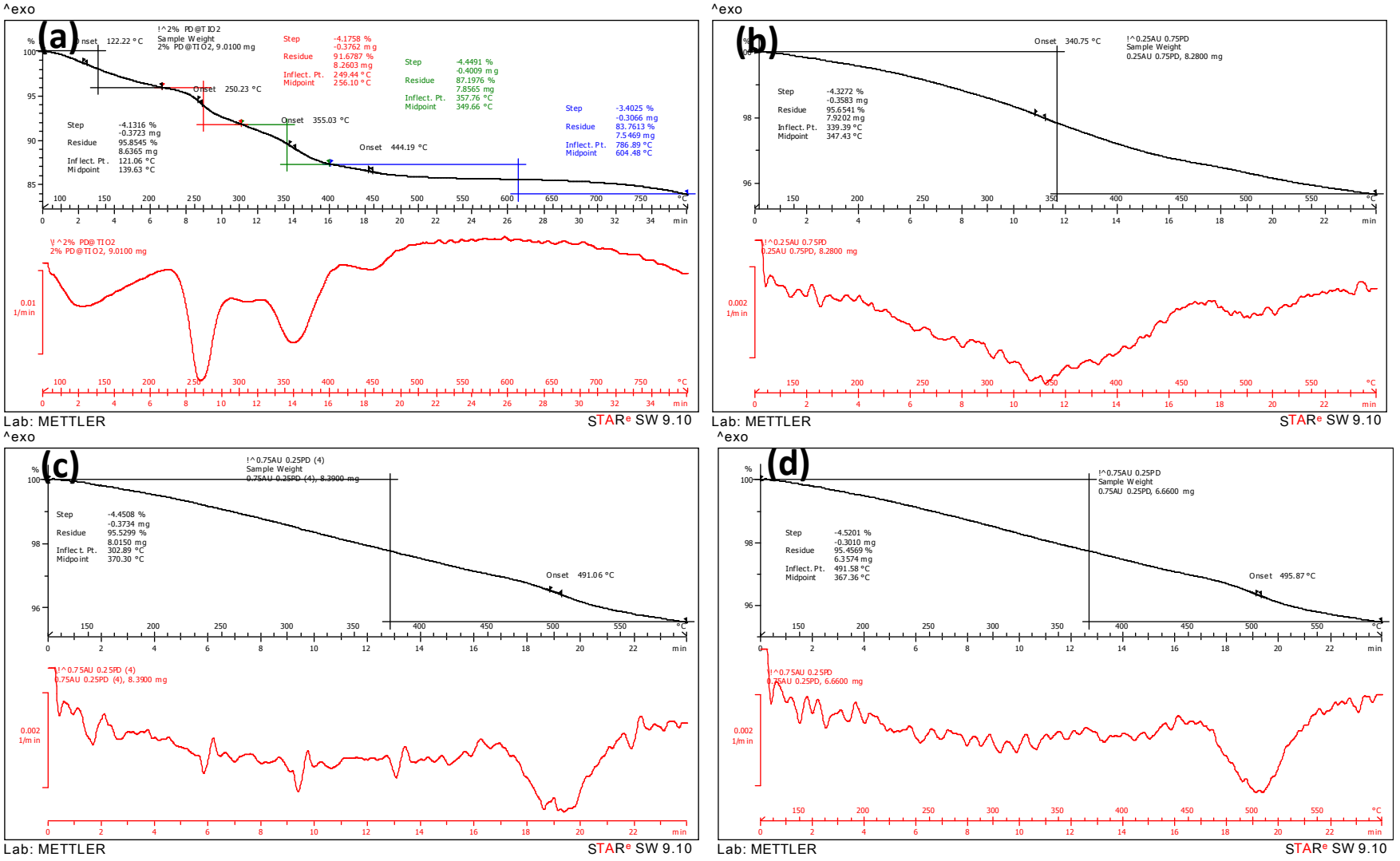


Figure 4.7: TGA result of (a) 2%Pd@TiO_2,(b) 0.25%Au0.75%Pd-TiO_2, (c) 0.5%Au0.5%Pd-TiO_2 (d) 0.25%Pd0.75Au-TiO_2

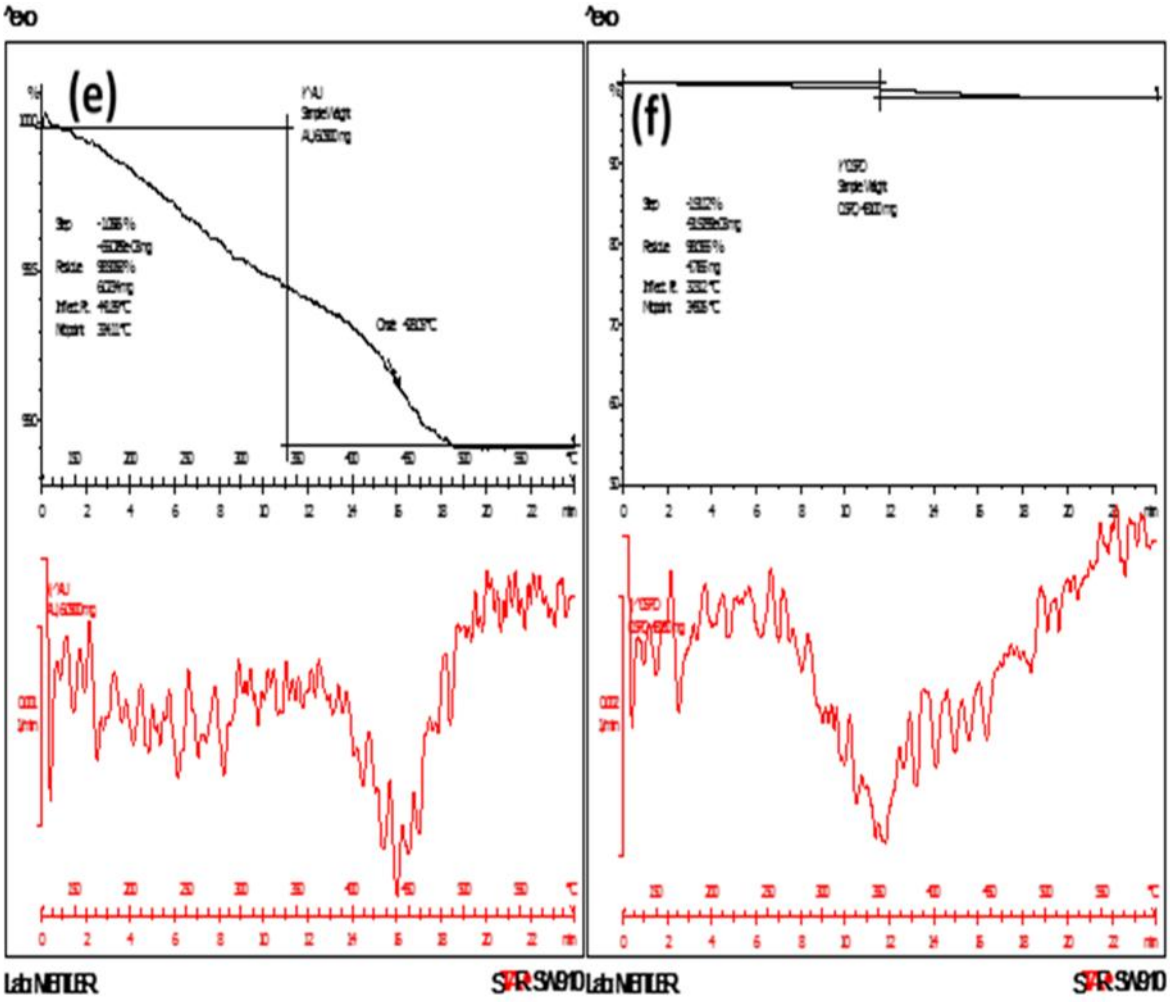


Figure 4.8: The TGA result of (e) 0.5%Pd-TiO_2, (f) 1%Au-TiO_2

4.2.7 Thermogravimetric Analysis (TGA) of *2*%Pd@TiO_2

The TGA result obtained for 2.0wt%Pd@TiO_2 catalyst shown on *Figure* 4.7(a), shows a different pattern from the other samples. The TGA curve shows four weight loss steps. In the first step the main weight loss is between 10 and 122°C which corresponds to the removal of volatiles like n-hexane, methanol and 1-butanol that were used in the preparation of the catalyst. The second step is a weight loss between 122 to 250°C which is due to adsorbed water. The third weight loss occurred between 250 and 355°C that could be assigned to high temperature pyrolysis of carbon species from the CTAB used in the catalyst preparation and the fourth step above 444°C might be assigned to loss probably accompanied with collapse of the core shell moieties.

4.2.8 Estimation of gold and palladium content on Au-Pd/TiO_2

The results of the compositional analysis of the fresh and used Au-Pd/TiO_2 catalysts are conducted using the ICP-OES technique. The results are presented in *Table* 4.2. From the results obtained suggest that the estimated gold and palladium content on titanium(IV) Oxide are in good agreement with the expected theoretical values. Also the results show a small degree of leaching of the gold metals compare to the palladium metals. Although the palladium based catalyst which is the most reactive in mineralization of phenol shows a great level of instability in the suspension mode which is due to leaching and poisoning of the catalyst with hydrocarbons that were formed due to incomplete mineralization of the intermediates' formed in the course of the reaction. These also explain why the catalysts become deactivated after the fourth cycle in the photocatalysis of phenol. It also indicates that the catalyst active surface has been greatly affected which explains why the P25 Degussa shows more reactivity in the conversion of phenols compared to the other samples. There is

a 2–5% deviation in results for gold and palladium content as compared to theoretical values. This may be attributed to the instrumental errors as well as personal (human) errors during the sample preparation and sample analysis. The result obtained by the techniques is comparable to theoretical values.

4.2.9 Estimation of palladium content in *2%*Pd@TiO_2

The compositional analysis of the fresh catalysts was conducted by ICP-OES technique. From *Table* 4.2 the results show that the catalyst prepared contains 1.8% palladium for the 2wt%Pd@TiO_2. The result also shows a small degree of leaching of the palladium metals. This explains why the catalysts reactivity reduces with time as the photoxidation of phenol progresses. The result shows a 2–5% deviation in the amount of palladium from the calculated value. This may be attributed to the instrumental errors as well as personal (human) errors during the sample preparation and sample analysis. However, the results obtained by the techniques are comparable to the theoretical values.

4.2.10 Scanning electron microscopy of transition metal doped TiO_2

The morphology of the transition metals doped photocatalysts was examined by scanning electron microscope (SEM). The micrographs of 1%Cu-TiO_2, 1%Fe-TiO_2, 1%Au-TiO_2 and 1%Pd-TiO_2 are shown in Figure 4.9 (a), (b) and Figure 4.10 (C) and (d) respectively. The figure shows typical surfaces of doped TiO_2 (Degussa P25) with the average crystallite size about 22 nm. When metals were doped on the TiO_2, aggregates could be observed clearly from the micrographs in Figure 4.9, that the morphology of the doped TiO_2 powder was completely different from each other based on the type of metal used. The copper doped TiO_2 powders has a flat smooth and flake-like surface, while the Pd-TiO_2 and Fe-doped TiO_2 formed a lump that composed of some small particles agglomeration on the surfaces.

Table 4.2: The ICP-OES results of Au/Pd-TiO_2 and 2.0wt%Pd@TiO_2

CATALYST	ICP-OES			
	Fresh Samples		Used Samples after four reuses	
	Au (%)	Pd (%)	Au (%)	Pd (%)
1%Au-TiO_2	1.02	-	0.96	-
0.75%Au.0.25%Pd-TiO_2	0.74	0.23	0.60	0.11
0.5%Au.0.5%Pd-TiO_2	0.46	0.40	0.46	0.39
0.25Au%.0.75Pd-TiO_2	0.21	0.72	0.19	0.68
0.5%Pd-TiO_2	-	0.43	-	0.33
2%Pd@TiO_2	1.8	-	1.78	-

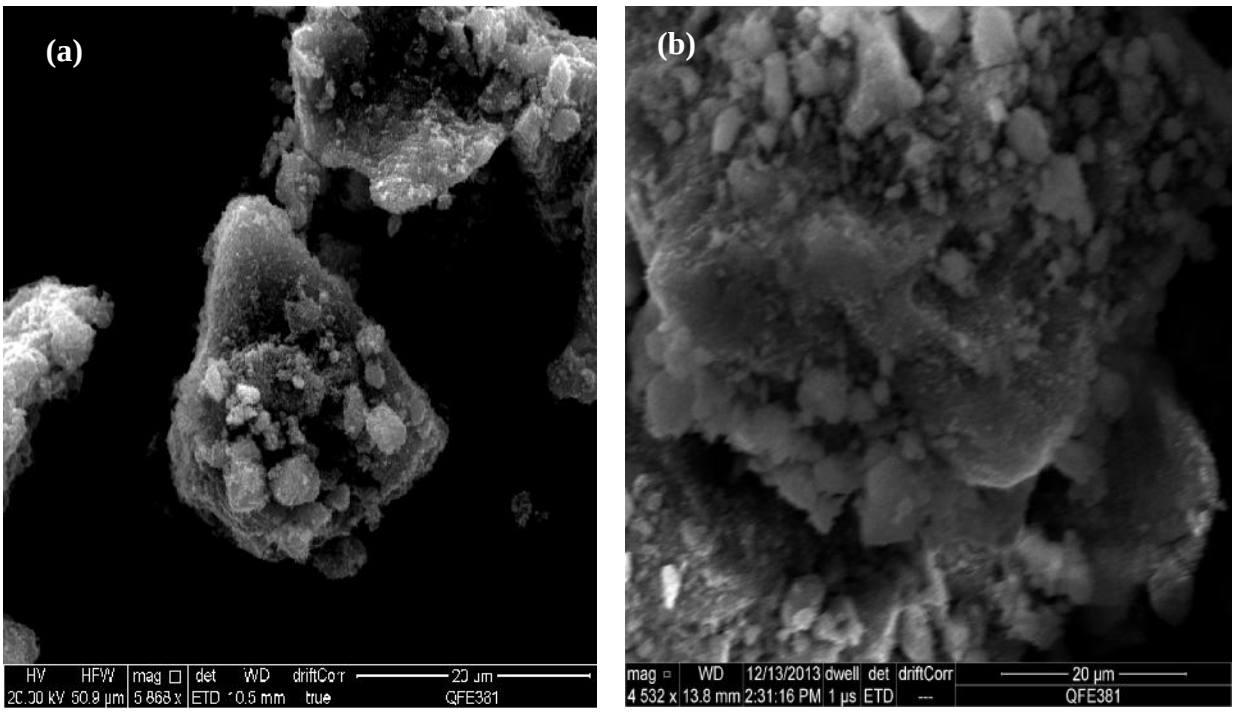


Figure 4.9: The SEM of (a) 1%Cu-TiO_2 and (b) 1%Fe-TiO_2

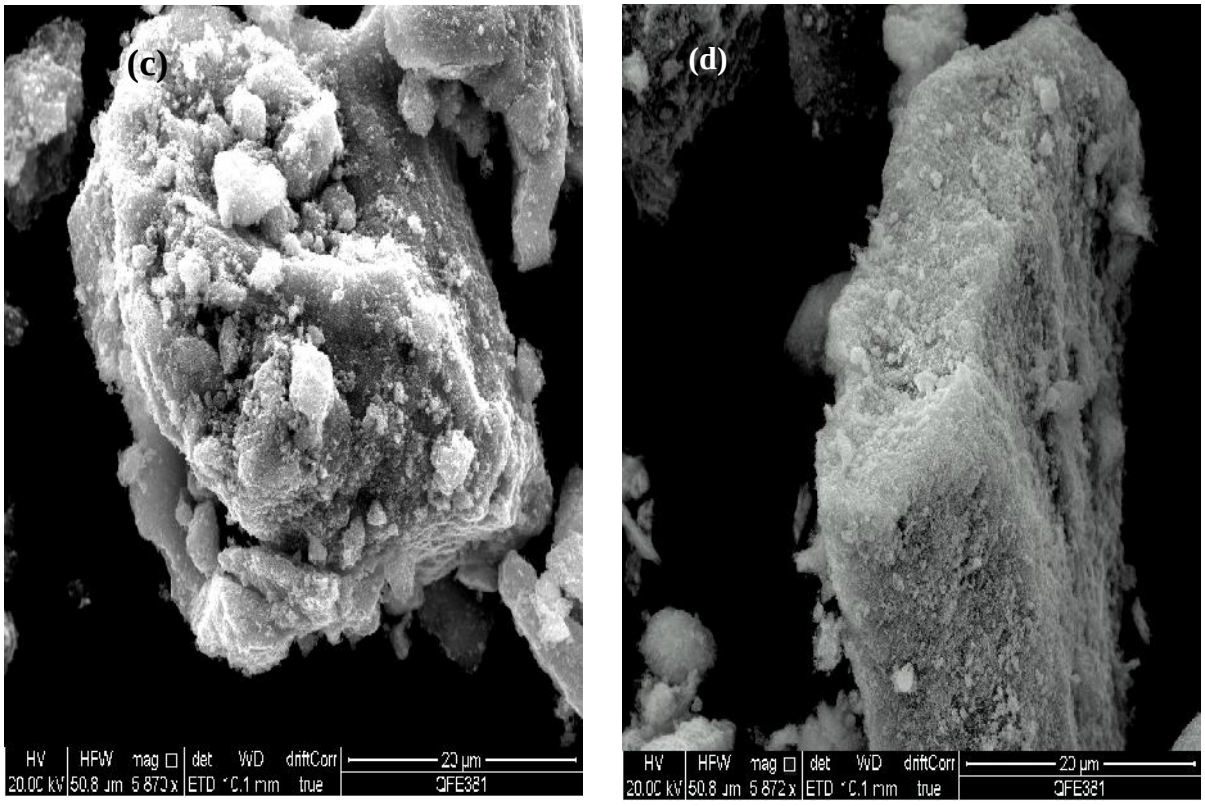


Figure 4.10: The SEM of (c) 1%Au-TiO_2 and (d) 1%Pd-TiO_2

4.2.11 Scanning electron microscopy of hydrothermally treated TiO_2

In general, the hydrothermally treated TiO_2 powders consist of nano-sized primary particles with a spherical shape of agglomerated powder particles, which are packed on layers of cubic flakes as shown on Figure 4.11 (a), also a close look into these powders' micrographs on Figure 4.11 (b) reveals that a degree of rode-like shape are also formed.

4.2.12 Scanning Electron Microscopy (SEM) of Au-Pd/TiO_2

The surfaces of the catalysts were observed to be extremely rough and nanocrystalline hence provide the enhanced high surface area to absorbed incident light. The SEM images of 0.5wt%Pd-TiO_2 and 1wt%Au-TiO_2 are shown in Figure 4.12. The microscopic rough surface could temporarily trap microscopic oxygen gas bubbles on rough surface that may have acted as tiny lens and spherical mirrors that helped to concentrate the incident light (Gleckman *et al.,* 1989). The Au particles were slightly elliptical in appearance. This slightly elliptical appearance of the Au colloid is typical for particles in metal sols which generally exhibit some polydispersity in both metal colloid particle size and shape (Khlebtsov *et al.*, 1996; Bloemer *et al.,* 1990). The EDS and mapping of 0.5wt%Pd-TiO_2 are shown is Figure 4.13, the result confirmed the existence of Pd and revealed that Pd was rich in the catalyst prepared. The deposited Au–Pd alloy was further analyzed using other techniques to verify the presence of gold and palladium

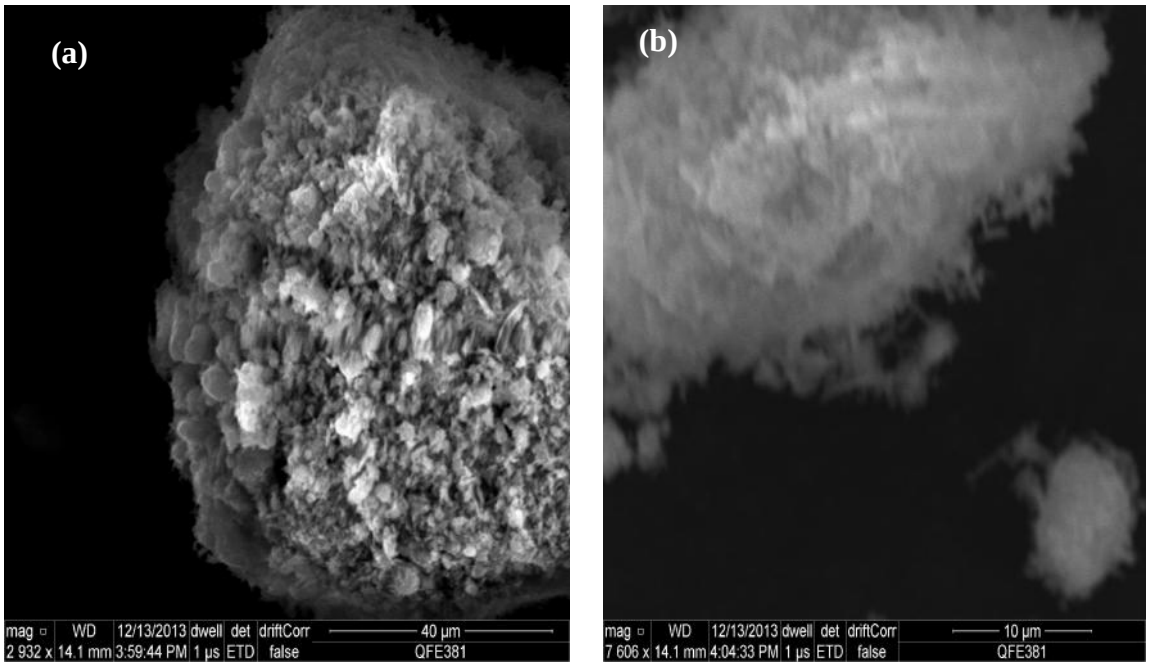


Figure 4.11: The SEM of the hydrothermal treated TiO_2

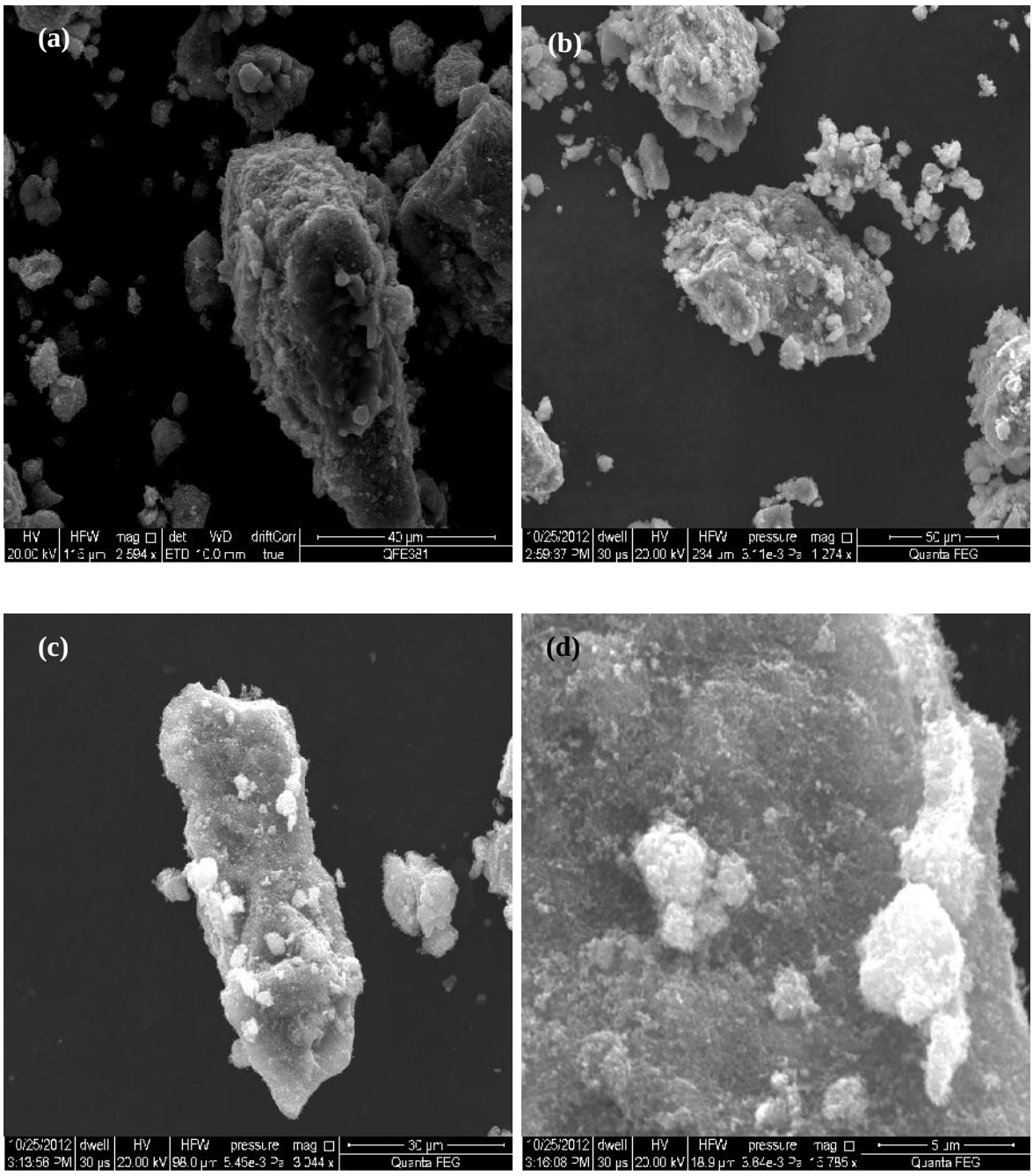
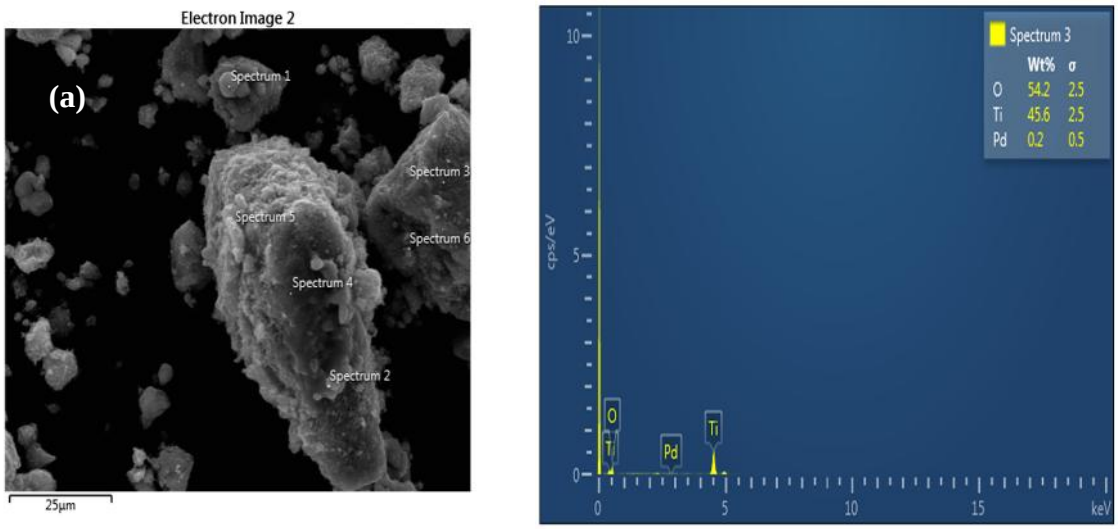


Figure 4.12: SEM images of 0.5wt%Pd-TiO_2 (a, b) and 1wt%Au-TiO_2 (c, d)



The EDX of 0.5%Pd-TiO_2

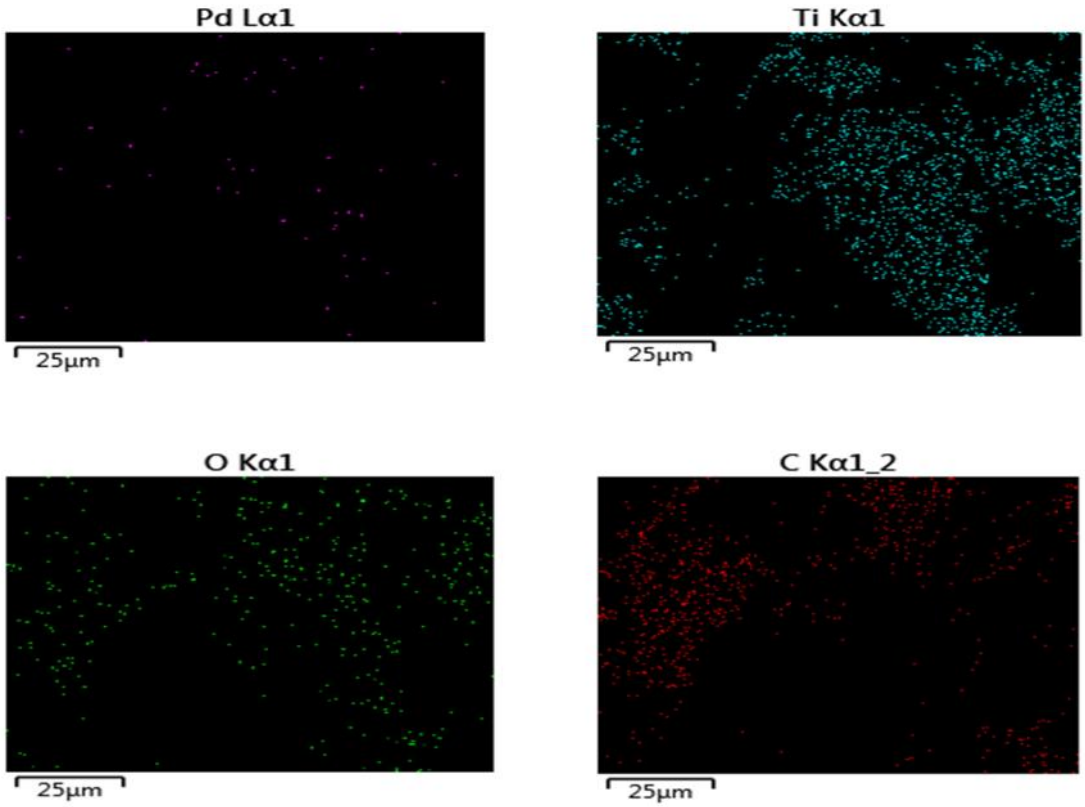


Figure 4.13: The mapping of 0.5%Pd-TiO_2

4.2.13 Scanning Electron Microscopy (SEM) of 2%Pd@TiO_2

The surfaces of the catalysts were observed to be slightly smooth and nanocrystalline hence provide the enhanced high surface area to absorbed incident light. *Figure* 4.14 shows the SEM images of 2%Pd@TiO_2. The microscopic rough surface could temporarily trap microscopic oxygen gas bubbles on rough surface that may have acted as tiny lens and spherical mirrors that helped to concentrate the incident light (Gleckman *et al.*, 1989).

4.2.14 Transmission electron microscopy of Au-Pd/TiO_2

The TEM images obtained show the presence of dispersed metallic particles on the P25 Degussa support. The TEM images support the result obtained from the XRD analysis in Figure 4.5 as no Au or Pd peaks are detected on the XRD result. The TEM images are reported in *Figure* 4.15 which confirm the presence of highly dispersed metal nanoparticles. One particle was selected within the image in Figure 4.15(b) i.e. 0.5wt%Pd-TiO_2 and was subjected to further EDX analysis and this is shown on Figure 4.16 which confirmed the presence of palladium. All the samples showed the presence of the metals used in the modification of the P25 which peaks were not seen on the XRD analysis.

4.2.15 EDX of 0.5wt%Pd-TiO2

The energy dispersive X-ray (EDX) spectra of 0.5 wt %Pd-TiO_2 are shown in Figure 4.16. The peaks corresponding to titanium, oxygen and the palladium metal can be clearly seen in the spectra. In addition to these peaks, the presence of Cu (source) and Si (grid) were also observed which is due to the sample holder that is used for the TEM-EDX analysis. The EDX results also confirmed the ICP-OES result of the elemental analysis done

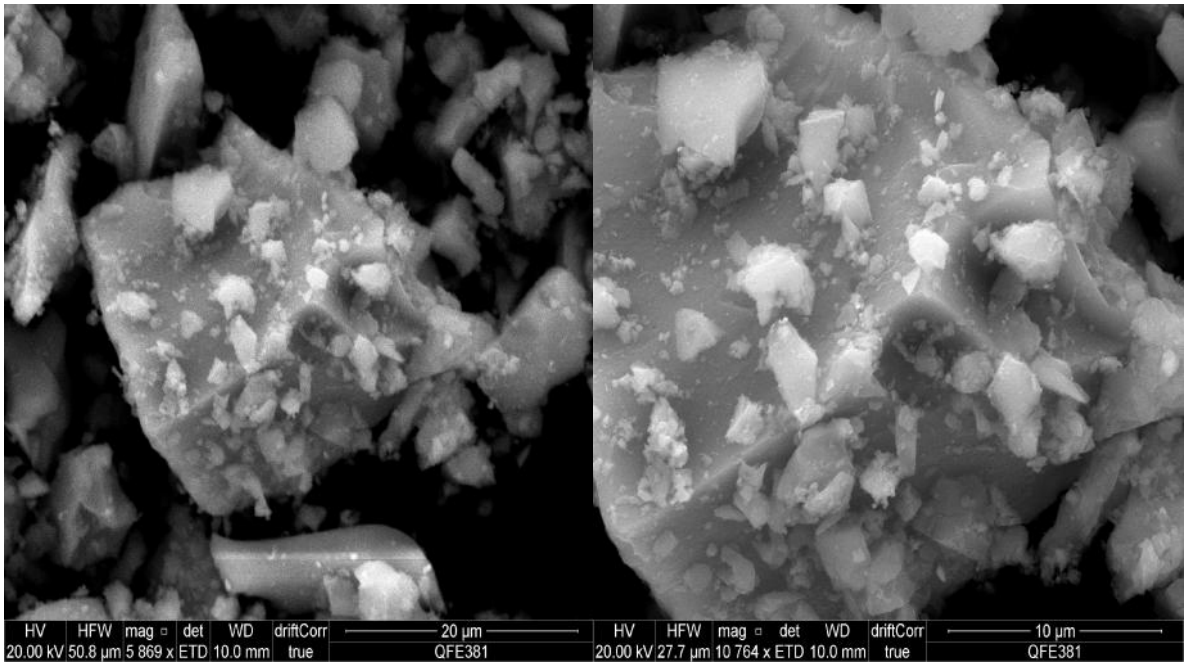


Figure 4.14: The SEM images of 2%Pd@TiO_2

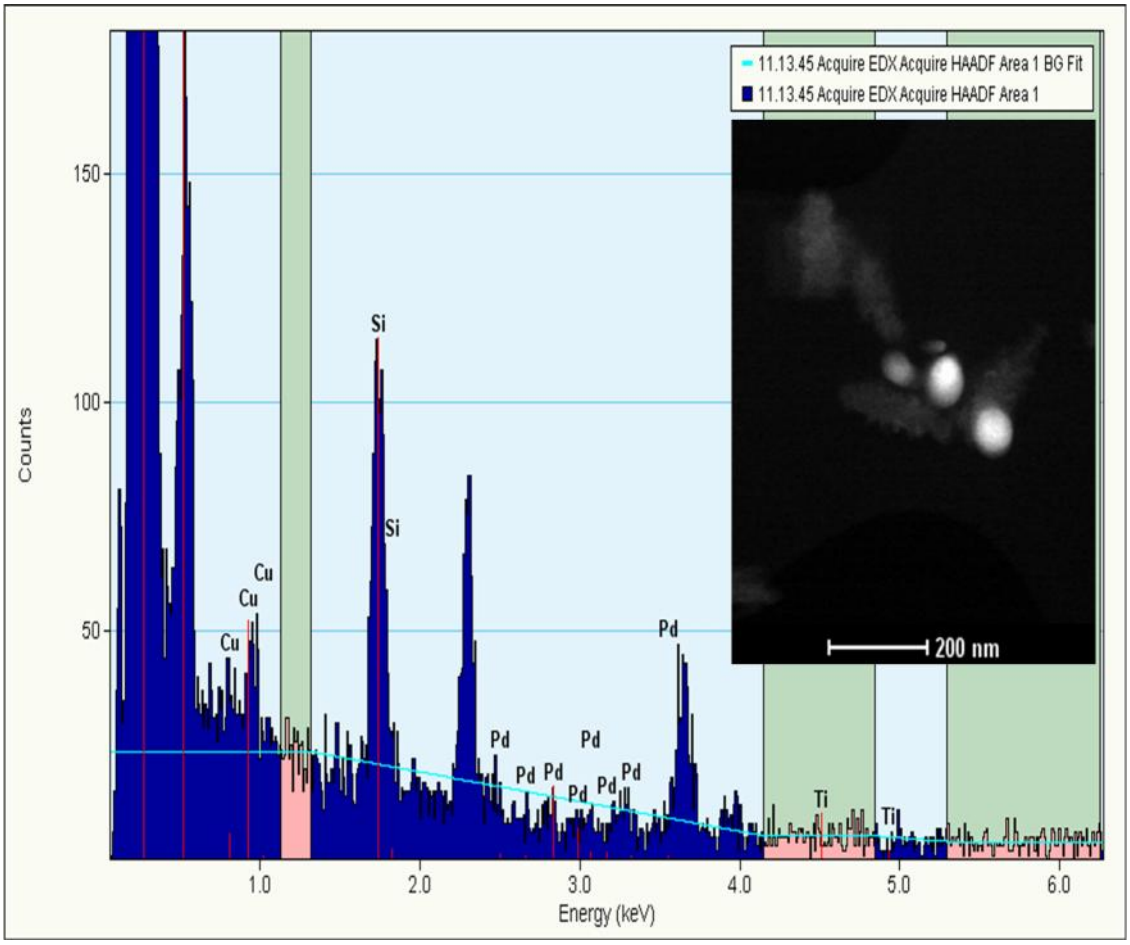


Figure 4.15: The Energy Dispersive X-ray (EDX) of a single particle of 0.5 wt%Pd-TiO_2 using TEM

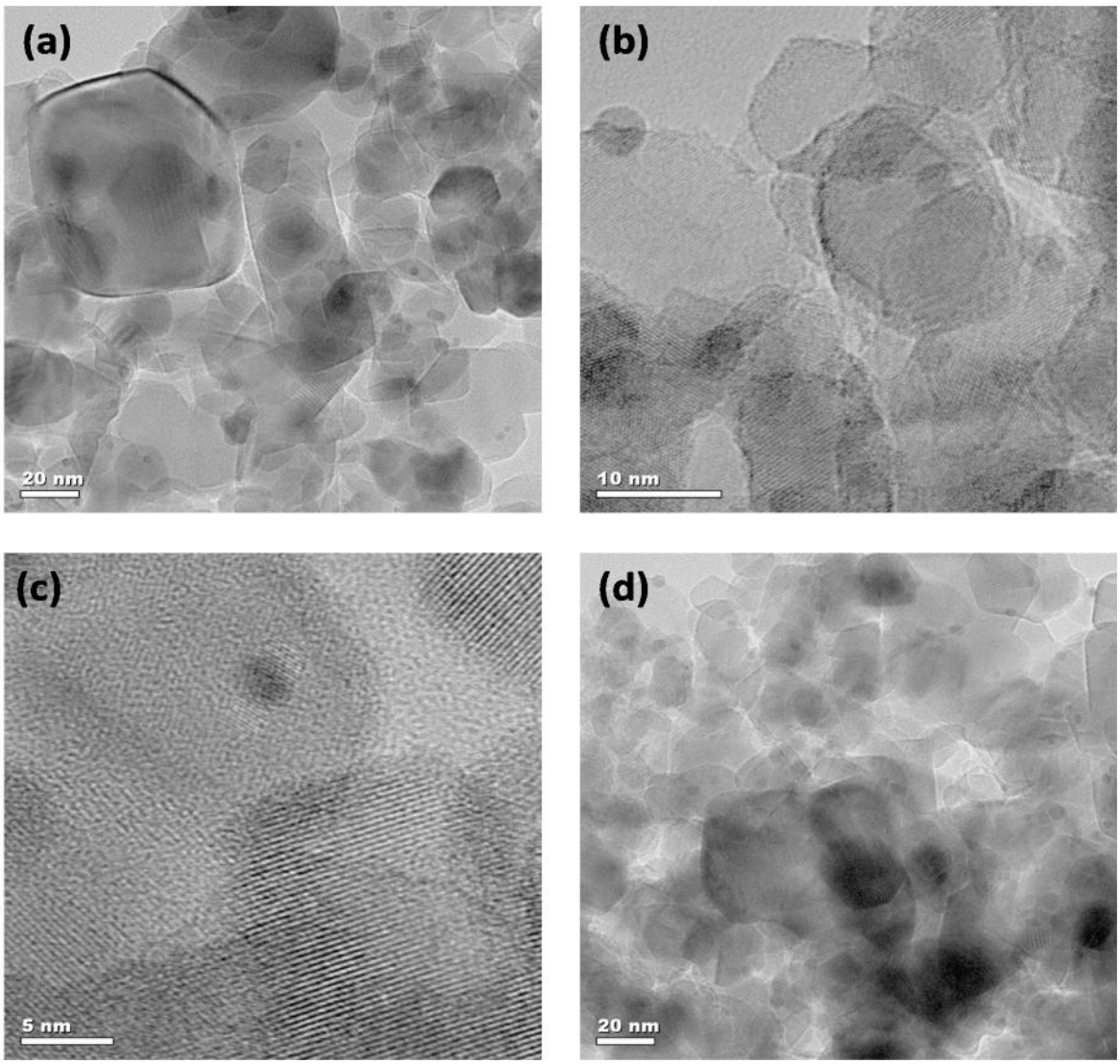


Figure 4.16: TEM images of 0.5wt%Pd-TiO_2 in (a, b) and 0.5wt%Pd0.5wtAu-TiO_2 in (b, c)

4.2.16 Transmission electron microscopy of hydrothermally treated P25

Transmission electron microscopy was applied to investigate the microstructure of titanium (IV) oxide prepared by high temperature hydrothermal treatment of P25 Degussa in aqueous solutions of 5 M sodium hydroxide in methanol at 100°C using an autoclave line with PTFE at process duration of 12h. Figure 4.17 shows a typical TEM image of the prepared catalyst. The sample mostly consists of cubic like particles of different sizes packed in layers, in good agreement with the SEM data.

4.2.17 Transmission electron microscopy of 2%Pd@TiO_2

Transmission electron microscopy measurements were done with a TECNAI FEI instrument which did not reveal the shell clearly. Cores were clearly observable, but there was no sharp contrast for the shell. Subsequent images were collected with the same instrument, and some of the images are shown in Figure 4.18. The figure shows a collection of TiO_2 covered palladium particles with particle size is 35 ± 15 nm along one axis and a range of particle morphologies. Although most of the particles seen in this image are spherical or oval, faceted structures were also observed. The shell is evident and more distinct on each particle, and more TEM studies were done with this material. A closer look at each of these particles reveals that the shells completely covered the particles (*Figure* 4.18 (c)). There appears some non-uniformity in the shell thickness, yet the coverage is complete. The typical palladium particle size is in the range of 4.3 nm as seen on Figure 4.18 (d). Microscopy did not reveal free particles of metals or oxides.

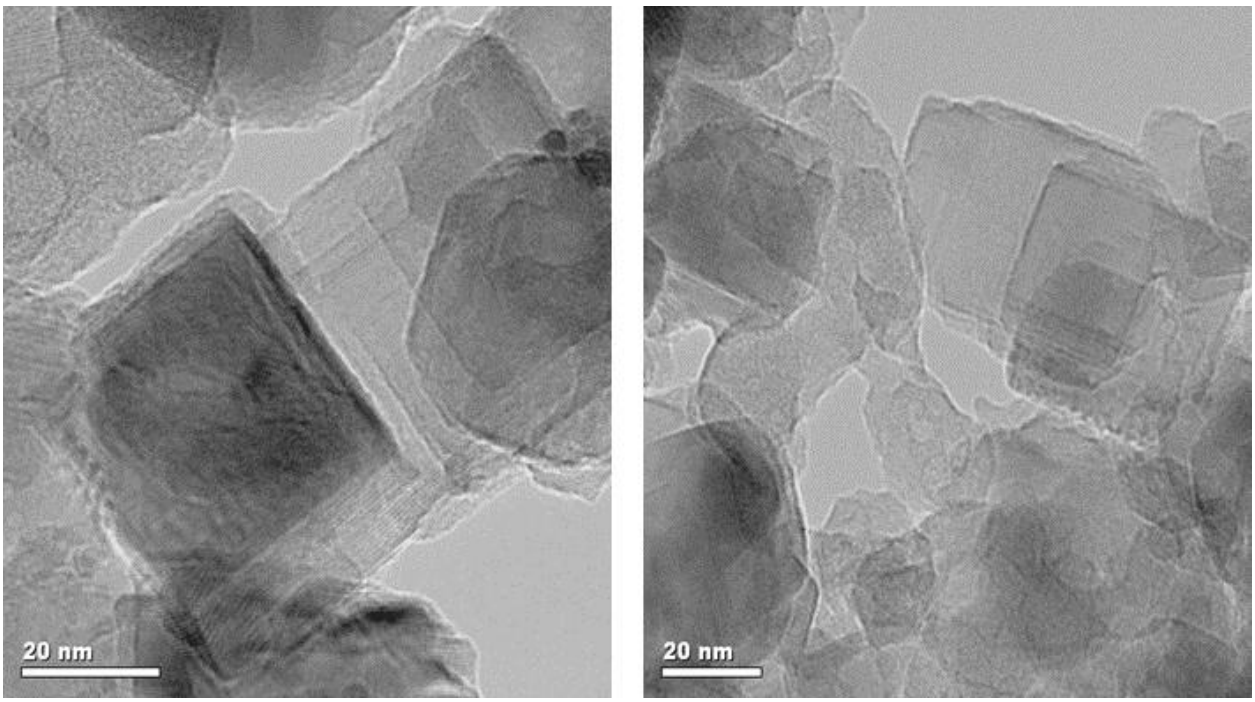


Figure 4.17: TEM images of hydrothermally treated P25 Degussa

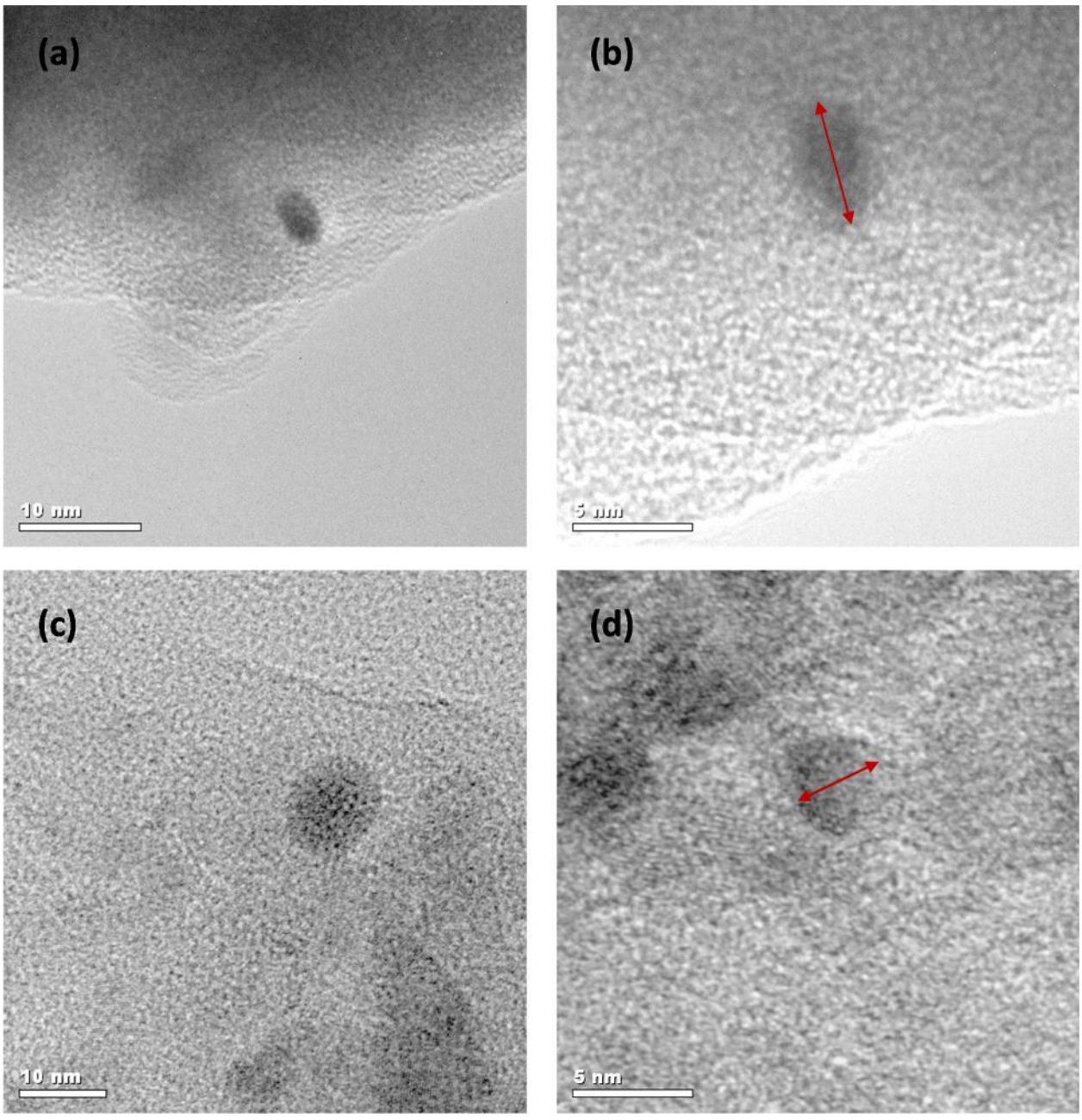


Figure 4.18: TEM images of 2%Pd@TiO_2

4.2.18 The Brunauer–Emett–Teller (BET)

A typical catalyst contains one or more group of pores whose size and volume depend on preparation method. The pores are classified in different classes depending on their size:

i. Micropores (θ < 2 nm),

ii. Mesopores (2 < θ< 50 nm),

iii. Macropores (θ > 50 nm).

The porous structure enables the solid catalyst to have a total surface area much higher than that corresponding to the external one. Most common catalysts have a specific surface area between 1 and 1000m^2g^{-1} while their external specific surface area is in the range 0.01-10 m^2g^{-1}. In fact the catalytic process takes place at the surface. To reach the surface sites the molecules of the reactants must diffuse through the porous system of the Catalyst, while the reaction products follow the opposite path. Mass transfer process inside the granules depends on pore size (bulk diffusion in macropores, Knudsen diffusion in mesopores and molecular diffusion in micropores). Also deactivation phenomena (i.e. organic material deposition) are greatly influenced by pore size; deposition of carbonaceous material with blockage of micropore mouth and coverage of the whole wall in mesopores and macropores are typical examples. The morphological characteristics of interest are the specific surface area, the specific pore volume, and the distribution of the area and of the pore size (Leofanti *et al.*, 1997). The data obtained on the BET analysis are: surface area, pore volume and pore size of the catalyst as presented on Table 4.1. The surface area and pore volume show an increasing order with gold and palladium loading. Deposition on titanium(IV) Oxide nanoparticles with metals resulted in increase in BET surface area and pore volume. Larger

surface area increased adsorption desorption capacity and consequently good photocatalytic activity (Diebold, 2003; Hussain and Siddiqa, 2011). The extensive photocatalytic application of the 0.5wt%Pd-TiO_2 catalyst can be attributed to the anatase particle size of 22.9nm and surface area of 47.05 m^2g^{-1} and the pore volume of 0.13cm^3g^{-1} which also indicate that the sample is a macro pores catalyst. Also it was found that BET surface areas of the titania were slightly decreased after the impregnation with Pd and Au suggesting that the metals particles are deposited in some of the pores of the TiO_2

4.2.19 CO chemisorption - pulse method

Surface area plays an important role in the reactivity of a catalyst. The reactivity of a catalyst is proportional to the number of active sites. Due to the importance of active sites, their dispersion on the support is a vital issue to note. Dispersion is defined as the fraction of total atoms or molecules of the active phase available at the surface for catalysis, i.e. for a specified catalytic phase

$$Dispersion(\%) = \left(\frac{N_{AS}}{N_{TA}}\right) x100 \qquad 4.1$$

N_{AS} is the number of surface atoms or molecules and N_{TA} is the total number of atoms or molecules of the specified catalytic phase. Dispersion is an average property that ranges from 0 to 1 (Farrauto and Bartholomew, 1997). However the dispersion of metals like Pd, Au, Fe, Cu etc., on a support like titanium(IV) Oxide is very vital due to the fact that agglomeration of the metal particles can easily happen. The larger the metal particles due to agglomeration the less reactive the catalyst because it has reduce the amount of the active sites. A high dispersion means that many atoms are at the surface and implies an effective usage of the component. The addition of metals on the catalyst can alter the properties of the active sites

by affecting the reactivity and selectivity. Depending on the effect of the metals on the catalyst it will be called a promoter if it enhance the reactivity or a poison when it lowered the activity (Bowker, 1988).

Theory

Pulse chemisorption is used to determine the amount of adsorbate that adsorbs on the catalyst surface. This study utilized CO as the adsorbate gas. Pulse chemisorption is accomplished by sending pulses of CO from the switching valve to the reactor until all the catalyst sites are saturated. The amount of CO pulsed to the reactor is known through the sample loop size and the CO gas composition in the sample loop. The amount of CO adsorbed from each pulse is calculated by subtracting the molar amount of CO in the sample loop (nCO, loop) from the molar amount of CO detected downstream of the reactor by the TCD (nCO, TCD), defined in the equation below.

$$\text{CO uptake (Per Pulse)} = n_{COloop} - n_{COTCD} \qquad 4.2$$

There are several inconsistencies observed with the CO chemisorption experimental result after running single sample five times. Due to these, it was chosen not to report the particle size diameter using this technique, but the metal surface area and dispersion are reported. At the -46°C, it was found that the adsorption rate of CO unto the catalyst was too slow. From the pulse data of the experiments shown in *Figure* 4.19 for the 2%Pd@TiO_2 the metallic surface area was 0.134m^2/g and dispersion of 1.506%. The same pattern was also observed when 0.5%Pd-TiO_2 was analyzed, the pattern was shown on Figure 4.20, the metal surface area was 0.205m^2/g and the dispersion was 9.023%.

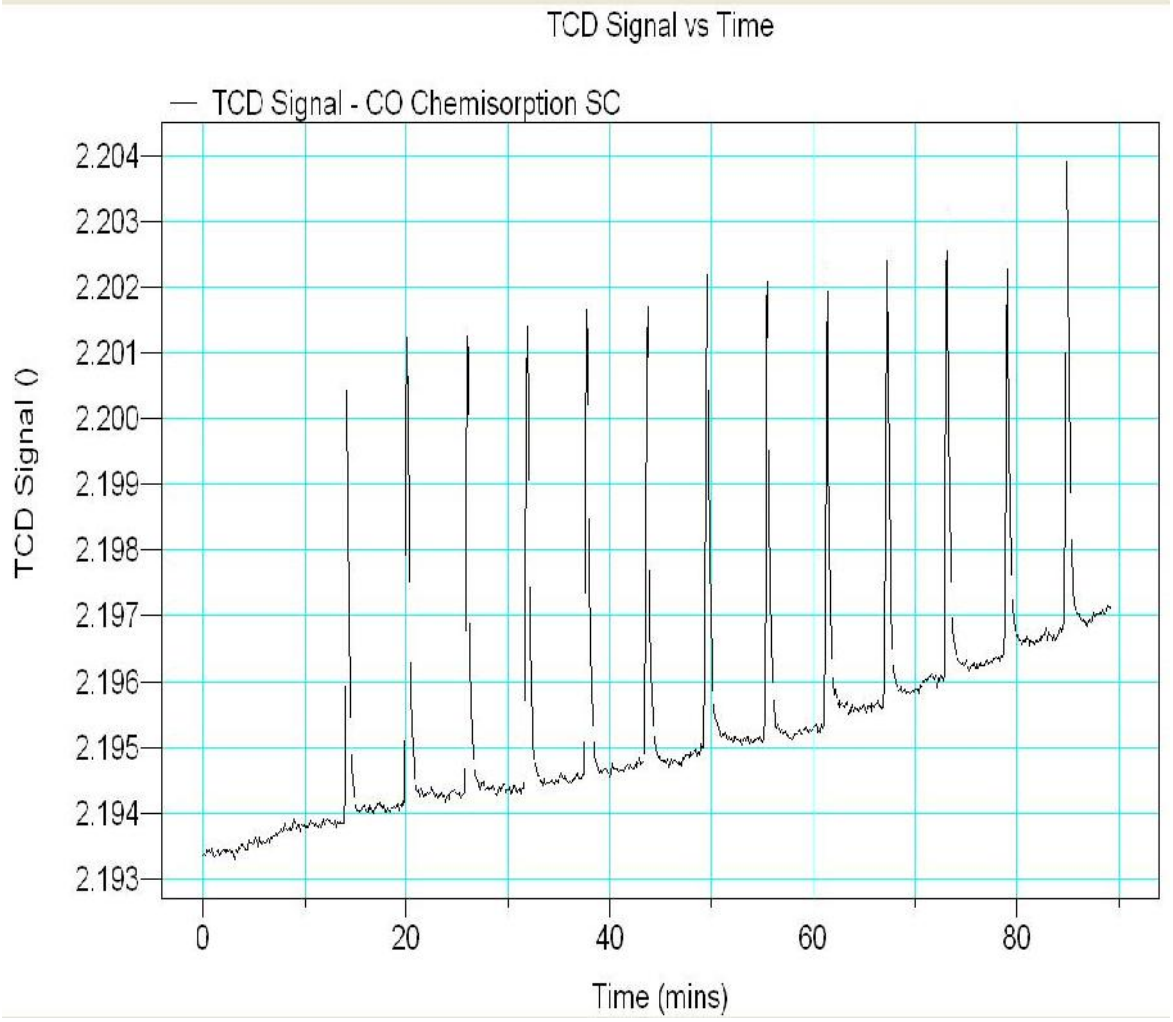


Figure 4.19: Pulse data showing TCD response versus pulse number for CO chemisorption chemisorption on the 2%Pd@TiO_2 photocatalyst at -46°C

The CO chemisorption adsorption unto the photocatalyst was not consistent as when compared to hydrogen adsorption due the fact that the stoichiometry of CO adsorption on metals is highly variable because of the possibility of each CO adsorbing either in the hollows of three or fourfold sites such that the one CO molecule binds to 2-4 metal atoms or, in the other extreme, 2-3 CO molecules adsorbing on a single metal atom; the actual CO-metal species formed depend on the metal and its dispersion/surface structure (Farrauto and Bartholomew, 1997). The low dispersion observed using this technique correspond with the image obtained from the TEM analysis. Another method that could be used to measure dispersion is transmission electron microscopy (TEM). This approach is quite tedious since a lot of pictures must be acquired of different part of the structure before the dispersion of the active phase can be estimated (Lin *et al.*, 2008). A high dispersion also causes problems with the contrast of the pictures.

4.3 Photo Catalysis Experiment

4.3.1 Photocatalysis of phenol using transition metals doped TiO_2

In order to improve the photo-response and to enhance the photocatalytic efficiency of TiO_2 under visible light irradiation, the structural modification of titanium(IV) Oxide was achieved by depositing transition metal on the surface. The Photocatalytic experiment was conducted using 0.2g of catalyst in 100mlcm^3 of 0.001M phenol solution using the slurry/suspension batch reactor as described in experimental section. The recombination of photogenerated electrons and holes is the reason behind the low photoactivity of TiO_2. Structural imperfections in the TiO_2 lattice generate trap sites which may act as recombination centers, leading to a decrease in the levels of electrons and holes.

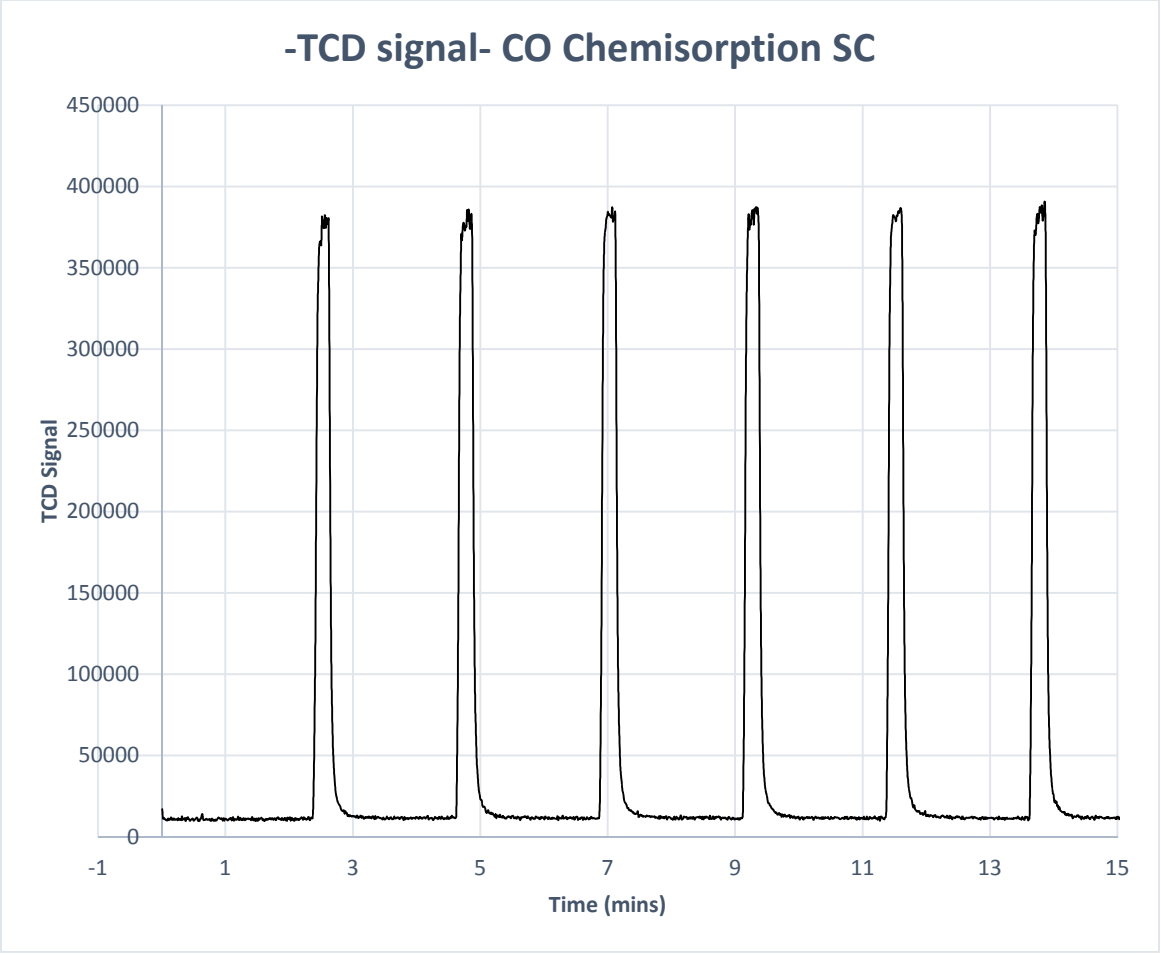


Figure 4.20: Pulse data showing TCD response versus pulse number for CO chemisorption on the 0.5%Pd-TiO_2 photocatalyst at -46°C

In order to enhance the TiO_2 photocatalysis as well as its response into the visible spectrum of solar light, TiO_2 has been deposited with certain transition metals like Au, Pd, Fe and Cu. These metals are to act as charge trapping sites and thus reduce electron-hole recombination. Both positive and negative results have been reported from doping TiO_2 with metal ions. The increase in charge separation efficiency will enhance the formation of both free hydroxyl radicals and active oxygen species (Kato *et al*., 2005). Based on these studies P25 Degussa was deposited with gold, palladium, iron and copper nanoparticles by keeping the optimum metal loading to 1wt%. The metals were deposited using the Sol immobilization method. Table 4.3 shows the influence of transition metals on the photocatalytic degradation of phenol. The efficacy of the modified TiO_2 were tested using the photocatalytic degradation of phenol in slurry/suspension batch made in oxygen. The results represented in *Figure* 4.21 show that 86.4% conversion of phenol to CO_2 and H_2O after 120 min was achieved in the case of 1%Pd-TiO_2 and 1%Au-TiO_2 gave 73.4% conversion. For 1%Fe-TiO_2, 1%Cu-TiO_2, P25 and hydrothermally treated TiO_2 the degradation is 64.4%, 54.8%, 64.5% and 77.8% respectively. These trends can be attributed to the fact that the photocatalytic properties of the catalyst in oxygen is as a result of the monometallic catalyst had higher selectivity and reactivity, due to the fact that the metals deposited on the titanium(IV) Oxide those not block the active site on the support, with these more surface area are involved in adsorption of the phenol onto the surface of the catalyst and the transition metals are acting as a trap centers and participating in the photocatalysis (Karvinen and Lamminmaki, 2003). It has been reported by Karvinen and Lamminmaki (2003), that the catalytic activity of palladium modified TiO_2 is better than that of unmodified TiO_2 in term of reactivity,

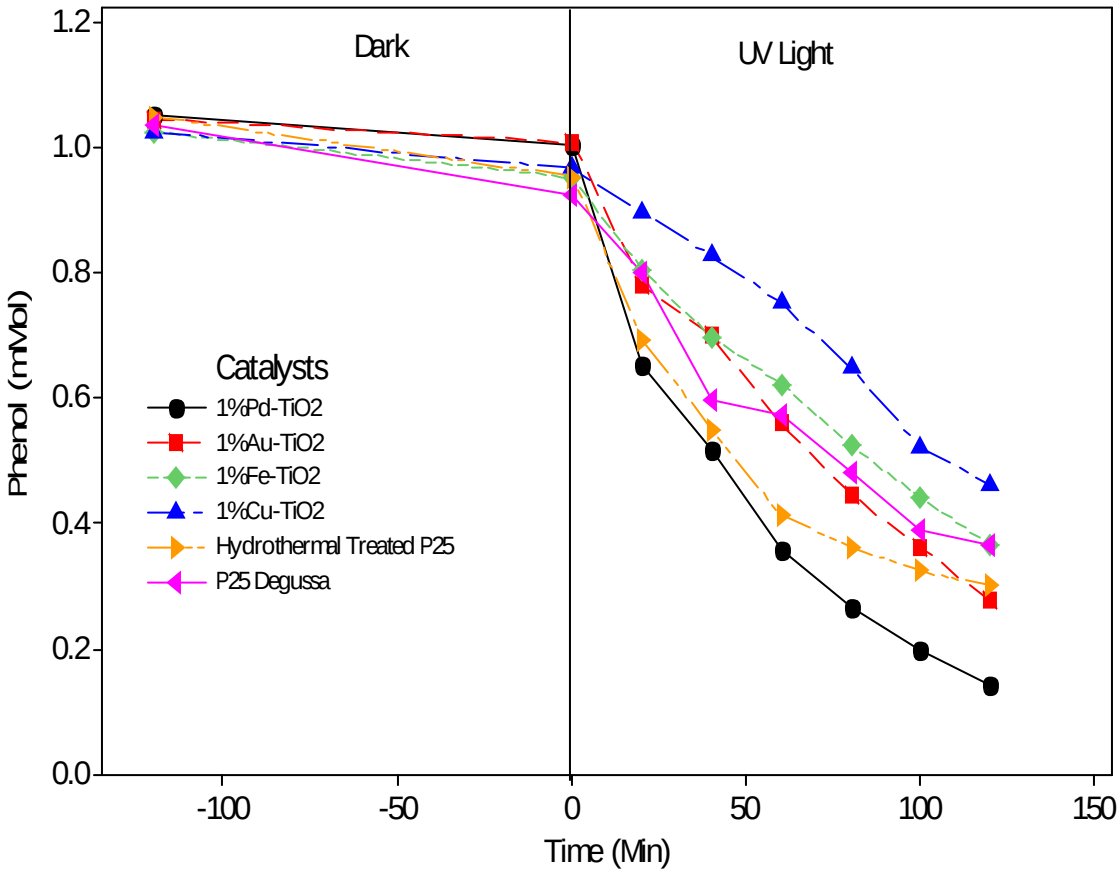


Figure 4.21: Photocatalytic degradation of phenol with different transition metals doped TiO_2 catalysts in oxygen

the iron and copper has an activity lower than the Pd and Au which can be due to the phase transformation aided by Fe and Cu, i.e they enhance the formation of rutile phase during calcination, and the rutile phase is not a good photocatalyt when compare to anatase, this phase transformation was also monitored using XRD analysis as presented on Figure 4.4. In addition, the comparatively low reaction rate experienced with 1%Cu-TiO_2 can be due to the dissolution of copper in aqueous solution when illuminated with UV light (Kaneko and Okura 2002), The effect of addition of Cu^{2+}on TiO_2 in the photocatalytic decomposition of phenol acted positively or negatively, depending on the concentration of Cu on the TiO_2. Less than 0.1 mM Cu^{2+} increased the rate, but a larger amount was detrimental. This shows that for depositing copper metal on TiO_2 there is an optimum amount that needs to be deposited. In addition, the trapping of electrons by Cu^{2+} and the trapping of holes by its reduced form were proposed to explain the decrease of the $e^- - h^+$recombination rate and a higher production of $OH^{\cdot}$ radicals:

$$Cu^{2+} \xrightarrow{e^-} Cu^{+} \xrightarrow{e^-} Cu \qquad 4.3$$

$$Cu \xrightarrow{h^+} Cu^{+} \xrightarrow{h^+} Cu^{2+} \qquad 4.4$$

The negative effect of high Cu^{2+} concentrations was attributed to the short circuiting reactions that create a cyclic process without generating active $HO^{\cdot}$ radicals, and retard the reaction (Cunningham and Sedlak, 1994; Sclafani and Schiavello, 1992). Cu^{2+} at concentrations higher than 1mM hindered phenol degradation and the detrimental effect was attributed to CuO deposition on the TiO_2 surface. Cu^{2+} can also compete with oxygen for the conduction band electrons. Another proposed reason for the decrease in the rate was the formation of

Table 4.3: Influence of transition metals doped on TiO_2 on the photocatalytic degradation of phenol in oxygen using the Slurry/suspension mode

Catalyst	Rate ($X10^{-7}$ S^{-1})	Phenol Converted (%)
1%Pd-TiO_2	2.630	86.4
1%Au-TiO_2	1.741	73.4
1%Fe-TiO_2	1.298	65.4
1%Cu-TiO_2	1.051	54.8
Hydrothermal Treated P25	1.605	77.8
P25 Degussa	1.317	64.5

surface complex structures of Cu^{2+} ions with phenol or its degradation products, which can act as surface poisons (Bideau *et al.*, 1992). The Pd metals deposited on the surface of the TiO_2 increase the selectivity of the photocatalyst, also it enhanced the photocalytic efficiency of the catalyst by the ability of palladium in both oxide (PdO) and reduced formed to be very reactive in phenol photo-oxidation. The hydrothermally treated P25 has an enhanced photocatalytic activity due to the formation of a large surface area and the contribution of the crystallite size. Even though the hydrothermal process increased the phase transformation of anatase to rutile, it cannot be used for further studies due to its instability in the reaction medium. It is noted that even though the deposition of transition metals improved the photo-response of the catalyst but it does not improve the photocatalytic efficiencies. The rate of reaction of the catalyst as in the case of copper *Figure* 4.22 shows that the Linear fit to the data represent Pseudo-first-order degradation kinetics. The kinetics of the photocatalytic degradation of phenol on solid surface has been reported in terms of Langmuir- Hinshelwood (L-H) equation (Su *et al*., 2012). The Langmuir-Hinshelwood expression is widely used in semiconductor photocatalysis to determine the rate and order of the photocatalytic degradation of organic pollutants (Sauer, *et al.*, 2002; Khezrianjoo and Revanasiddappa, 2012).

$$\frac{1}{k_{obs}} = \frac{1}{(k_c K_{LH})} + \frac{[Ph]_o}{k_c} \qquad 4.5$$

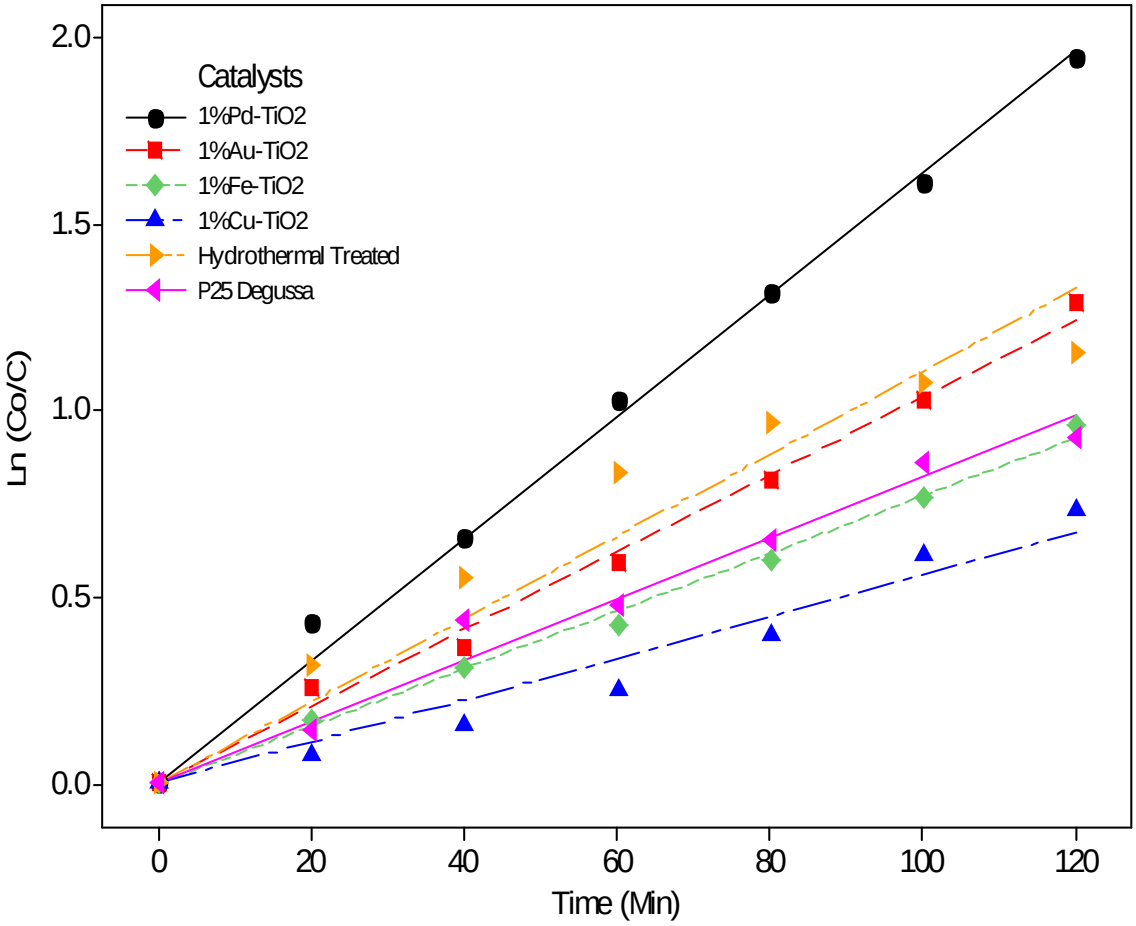


Figure 4.22: Photocatalytic degradation of phenol over transition metals doped TiO_2 in oxygen. The linear fit to the data represent pseudo-first-order degradation kinetics

where $[Ph]_o$ is the initial concentration of phenol (mgL^{-1}), K_{LH} is the Langmuir-Hinshelwood adsorption equilibrium constant (Lmg^{-1}) and k_c is the rate constant of the catalyst surface reaction ($mgL^{-1}min^{-1}$). Fitting of the experimental data into the Langmuir-Hinshelwood model has been shown to work only for organic pollutant of single component. The photocatalytic degradation of phenol follows pseudo-first-order kinetics with respect to the concentration of the bulk solution of phenol.

$$r = \frac{dC}{dt} = k_{obs}C \qquad 4.6$$

Integrating the equation with the following restriction $C = C_o$ at $t = 0$, with C_o being the initial concentration of the phenol solution and t the reaction time. The following expression is obtained:

$$\ln\left(\frac{C_0}{C}\right) = k_{obs}\,C \qquad 4.7$$

from the expression, k_{obs} is the apparent pseudo-first-order rate constant and is affected by the concentration of phenol. The plot of $\ln(C_o/C)$ versus irradiation time for the photocatalysis experiment using the slurry batch reactor in oxygen with the different modified photo catalyst in UV light is presented in *Figure* 4.22. Deposition of gold nanoparticles alters the adsorption of water and diminishes the population of surface the hydroxyl group bonded to the titanium(IV) Oxide (titanol). As mentioned earlier, it is on these surface hydroxyl groups where the deposition step anchors monometallic gold species depending on the solution pH and initiates the nucleation of the gold nanoparticles. Therefore, in this regard, deposition of gold can play a negative effect, decreasing the

photocatalytic activity of titania under UV illumination. This negative effect is expected to occur when gold is not playing any active role in the process and simply masks and covers the surface titanol groups. It has been reported that in photocatalytic reactions, it is considered that the deposition of metals, such as gold, palladium, iron and copper, on TiO_2 increases the charge separation efficiency and inhibits recombination of electron and hole produced by UV absorption (Hoffmann *et al*., 1995; Linsebigler *et al.*, 1995; Subramanian *et al.*, 2001). The increase in charge separation efficiency will enhance the formation of active oxygen species. From these considerations, it is expected that the deposition of metals on TiO_2 enhances the interaction with phenol and the formation of active oxygen species, which result in high degradation rate of phenol. Palladium, gold, iron and the hydrothermally treated TiO_2 has a superior photocatalytic activity than the commercial P25 Degussa under the experimental conditions. It has also been reported that Fe-doped TiO_2 was found to have very high photocatalytic activity under visible light irradiation than Degussa P25, Fe^{3+} cations acted as shallow traps in the TiO_2 lattice, Fe ions trapped not only electrons but also holes, which leads to increase of photoactivity (Litter 1999). From the results obtained the Pd and Au deposited on the TiO_2 increased the visible light response of the catalyst and the photocatalytic efficiency of the system, but the target of the studies is to obtain complete mineralization of phenol in the least contact time. This lead to further experiment into the synergetic effect of gold and palladium deposited onto P25 in Continuous Stir Tank reactor (CSTR) used for the photocatalytic degradation of phenolic wastewater.

4.3.2 Effect of H_2O_2, O_2 and N_2 on the photolysis of phenol in UV light

Individual contributions of UV light at 350nm, H_2O_2, O_2 and N_2 in the absence of any other oxidant on phenol photodegradation was tested using 100 ml of 1mM of phenol solution

using the Slurry/suspension batch mode. The results obtained are shown in Figure 4.23. The rate of phenol photolysis increased in the following order: UV light under nitrogen atmosphere < UV light under O_2 atmosphere < UV light at in 0.17 M of H_2O_2 (1.75 ml) < UV light in 1.39 M H_2O_2 (14.11 ml). There was 8.8% degradation of phenol by nitrogen and UV light, UV light with Oxygen showed 28.5% degradation, while 1.75ml of 0.17 M hydrogen peroxide led to 32.1% phenol degradation which is significant. However, a notably improved degradation was obtained with 14.11ml of 1.39 M hydrogen peroxide with UV light where 42.2% degradation was observed within 120 min irradiation time. However, increasing the amount of hydrogen peroxide showed superior performance of hydrogen peroxide in the photolysis of phenol. It is reported that hydrogen peroxide dissociates in aqueous solutions, forming HO^{2-} anion (Venkatadri and Peters, 1993) and O_2 in a chain reaction, which convert substrates to other oxygenated intermediate compounds. It was observed from these studies that higher concentrations of hydrogen peroxide have to be used in order to achieve higher conversions of phenol to CO_2 and water in the presence of UV light. The combination of UV light and a small amount of H_2O_2 enhanced strongly the efficiency of phenol destruction. In the first step, hydrogen peroxide absorbs UV light and decomposes to highly reactive hydroxyl radicals (·OH), then, hydroxyl radicals, which are non-selective powerful oxidants and reacted with most organic compounds with very high rate constants ($k \approx 10^6 - 10^{10} M^{-1} S^{-1}$) (Safarzadeh-Amiri, 2001; Esplugas *et al*., 2002; Huang and Shu, 1995). The hydroxyl radicals can abstract H-atom from many sites of an organic molecule or add to any C=C bond or accept an electron, producing therefore a wide spectrum of products (Hugul *et al*., 2000). The photolysis of phenol using hydrogen peroxide, oxygen and nitrogen show the necessity of oxidant in the photocatalytic reaction.

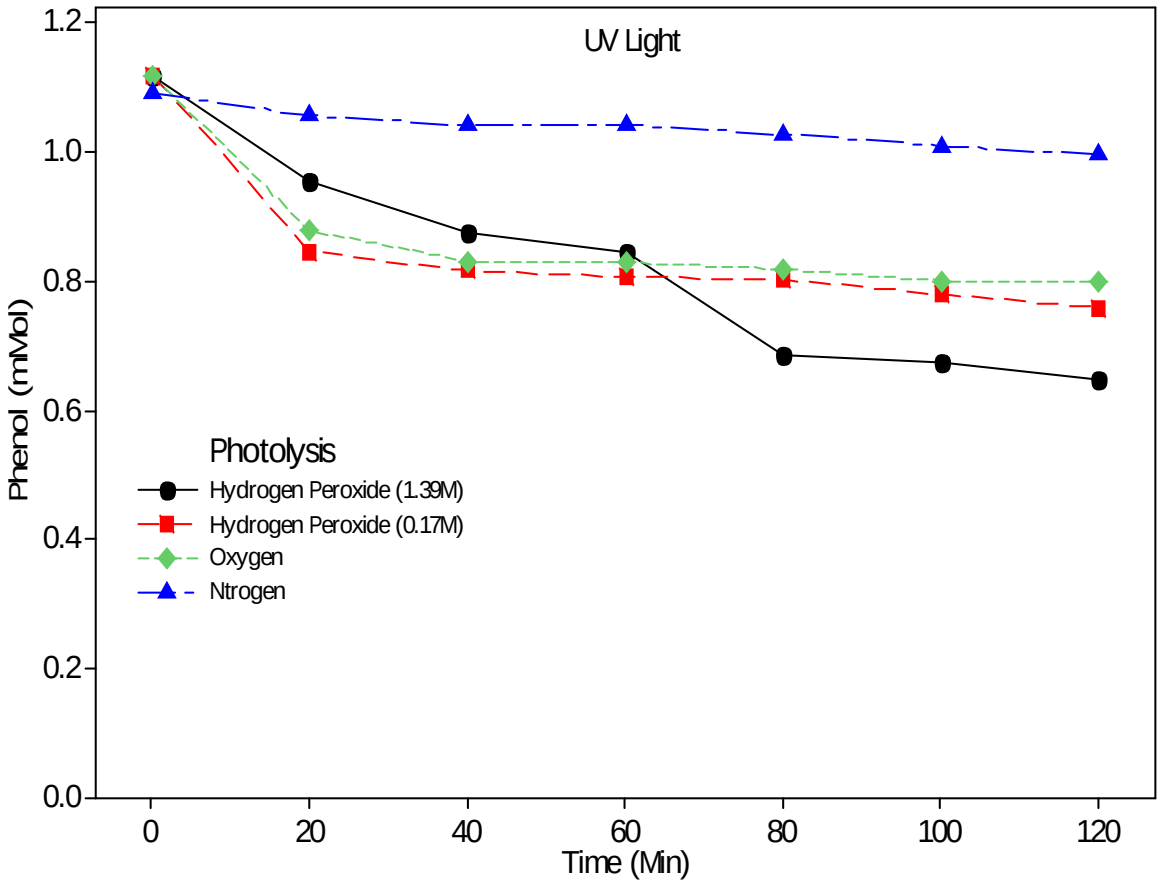


Figure 4.23: Effect of photolysis on phenol photodegradation using hydrogen peroxide, oxygen and nitrogen in UV light.

According to Kondarides (2010), there is an optimum molar ratio between concentrations of hydrogen peroxide and pollutant [H_2O_2/pollutant], for which ·OH radicals' concentration photogenerated becomes enough to oxidize all the organic matter present in the reaction medium. It must be noted that an excess of ·OH radicals formation could be detrimental to the photoactivity as a consequence of hydrogen peroxide disproportioning to water and molecular oxygen. The optimum molar ratio described in literature was around 10–100moles (Adan *et al*., 2006). For this reason, 1.75 ml of hydrogen peroxide solution was used in this study. Thus from economic considerations, combination of photocatalysis with oxygen or air offers an efficient solution for organic pollutant removal from waste water. Further study with phenol using the Au-Pd/TiO_2 were used for the suspension and Trickle/Taylor flow mode to obtain an improved process.

4.3.3 Effect of catalyst loading on photocatalytic degradation of phenol

Either in static, or in slurry or in Continuous flow photoreactors, the initial rates of reaction were found to be directly proportional to the mass *m* of catalyst. This indicates a true heterogeneous catalytic regime. However, above a certain value of *m*, the reaction rate levels off and becomes independent of m. This limit depends on the geometry and on the working conditions of the photoreactor. It was found equal to 1.3mg TiO_2/cm^2 of a fixed bed and to 2.5 mg TiO_2/cm^3 of suspension (Herrmann 1999). These limits correspond to the maximum amount of TiO_2 in which all the particles are totally illuminated. For higher quantities of catalyst, a screening effect of excess particles occurs, which masks part of the photosensitive surface. For applications, this optimum mass of catalyst has to be chosen in order to avoid excess of catalyst and to ensure a total absorption of efficient photons. In these experiments,

using the suspension/slurry batch photoreactor, an optimum amount of Au-Pd/TiO_2 used is 2.0 g/100 ml., whereas for the Continuous flow reactor, which has a recirculation flow rate of 3ml/min and a continuous flow of 0.083 ml/min from the reservoir, the optimum catalyst concentration was only 1 g/ of pelletized catalyst per 300 ml of phenol solution. To determine the optimal dosage of the catalyst to be used in the experiment, 0.5wt%Pd-TiO_2 was used in 100 ml of 1.0 mM phenol solution for 80 min at the pH of 6.4 using the Suspension Batch mode. The result obtained was shown in *Figure* 4.24. Finding the optimum loading capacity avoids an ineffective excess of catalyst within the system. The dosage of catalyst is an important parameter in suspended photocatalytic degradation processes (Kutty and Ahuja, 1995; Mogyorosi *et al.*, 2002). Several studies have indicated that the photocatalytic rate initially increased with catalyst loading and then decreased at higher values because of light scattering and screening effects. The tendency toward agglomeration (particle–particle interaction) also increases at high solids concentration, resulting in a reduction in surface area available for light absorption and hence a drop in photocatalytic degradation rate. Although the number of active sites in solution will increase with catalyst loading, a point appears to be reached where light penetration is compromised because of excessive particle concentration. The trade-off between these two opposing phenomena results in an optimum catalyst loading for the photocatalytic reaction (Adesina, 2004). From the result in *Figure* 4.24 it is shown that increase in catalyst loading beyond the optimum point will result to the shielding of the light from an even distribution of light to the surface of the catalysts. For this experiment, the photo degradation of phenol was found to increase with increase in 0.5wt%Pd-TiO_2 loading up to 0.4g. An increase in the amount of catalyst provides an increased number of active sites for adsorption. However, this also causes simultaneous increase in solution opacity which further causes a decrease in the penetration of UV light.

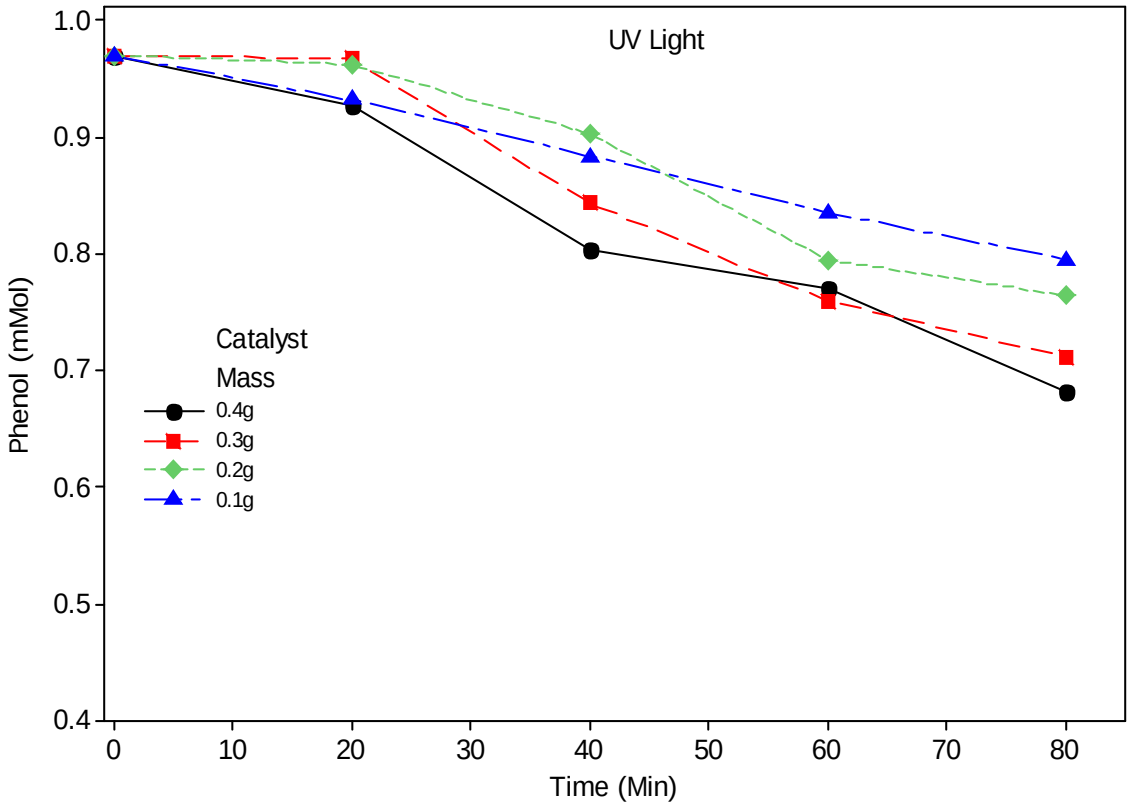


Figure 4.24: Effect of catalyst loading using 0.5wt%Pd-TiO_2 in oxygen

It was believed that as the catalyst loading increased the photo degradation rate should also increase as well, owing to the higher holes and hydroxyl radicals that were generated. This suggests that the amount of photo-catalyst to be used should maintain a balance between these two opposing effects. It can be seen from the result obtained in *Figure* 4.24, that the photocatalytic degradation for phenol increases as the catalyst loading is increased from 0.1g to 0.2g but when the catalyst loading is increased further to 0.3g, the rate of degradation decreases. However, when the amount of catalyst was increased to 0.4g the rate of conversion of phenol to water and CO_2 was also slightly increased which is mainly due to the increase in adsorption of the phenol onto the surface of the catalyst. The decrease in degradation rate with increase in catalyst loading can be attributed to the increased opacity of the solution which hinders the light transmission through the solution. However, an excess dosage of the catalyst decreases the light penetration via shielding effect of the suspended particles (Burns *et al*., 2001; Sobczynski *et al*., 2004). The increase in the amount of catalyst result to decrease in effective light intensity and the photo generation of electrons and positive holes would be reduced leading to reduces rate of photocatalytic degradation (Mangrulkar *et al.*, 2011). From the experiment it can be concluded that the conversion of phenol is influenced by different factors: (a) all of the additional catalyst surface area does not come in contact with a pollutant because of external mass-transfer resistance, (b) the pollutant cannot reach some of the catalyst surface area because of agglomeration of the catalyst particles (internal mass-transfer resistance), (c) light cannot reach some of the catalyst surface area because of absorption and scattering (shielding effect) of light, (d) light cannot penetrate the agglomerates and activate the inner surfaces, and/or (e) a combination of all of the above (Mehrotra *et al.*, 2003). Hong

investigated the effect of catalyst dosage (1.0–4.0 g/l) on the photocatalytic degradation of phenol. Under the conditions tested, optimum degradation was achieved at 2.0 g/l (Hong *et al.,* 2001), which also agreed with the result obtained in our experiments. The optimal dosage was also found to depend on the initial solute concentration (Herrmann, 1999). Based on the experimental results shown in *Figure* 4.24, the dosage of 0.2 g catalysts is selected for further studies because in this case the shielding effect is avoided whatever types of catalysts particles were adopted.

4.3.4 Photocatalysis of phenol in air using the batch mode

The photocatalysis of Phenol in compressed air using the Slurry/Suspension batch mode with Sparger to increase the solubility of the compressed air in the phenol solution were done using the catalyst prepared. The Picture of the Photoreactor with sparger is shown in *Figure* 4.25. Using 1mM of phenol in water and air as oxidant it was identified that the most efficient catalyst for the photocatalytic oxidation of phenol to CO_2 and H_2O was the 0.5%Pd-TiO_2 it converted 49.76% in 120min followed by 1.0%Au-TiO_2, 0.75Pd0.25Au-TiO_2, 0.5Au0.5Pd-TiO_2 and 0.75Au0.25Pd-TiO_2 with 36.86, 27.87, 18.7 and 16.41% respectively. The photocatalytic degradation of phenol in air depicts the reaction with limited oxygen supply, these were performed to compare catalysts photoreactivity under the 'toughest' reaction regime, where the overall reaction rate could be mass transfer limited by the supply of oxidant. In this case, most of the oxidant is from the dissolved oxygen within the liquid and additional oxygen was provided by mass transfer through the surface of the reaction liquid. The rate of the photocatalytic mineralization of phenol is completely suppressed in the absence of electron scavenger such as molecular oxygen which are supplied from the oxidant present (Diebold, 2003). Due to limited supply of the molecular oxygen the rate of

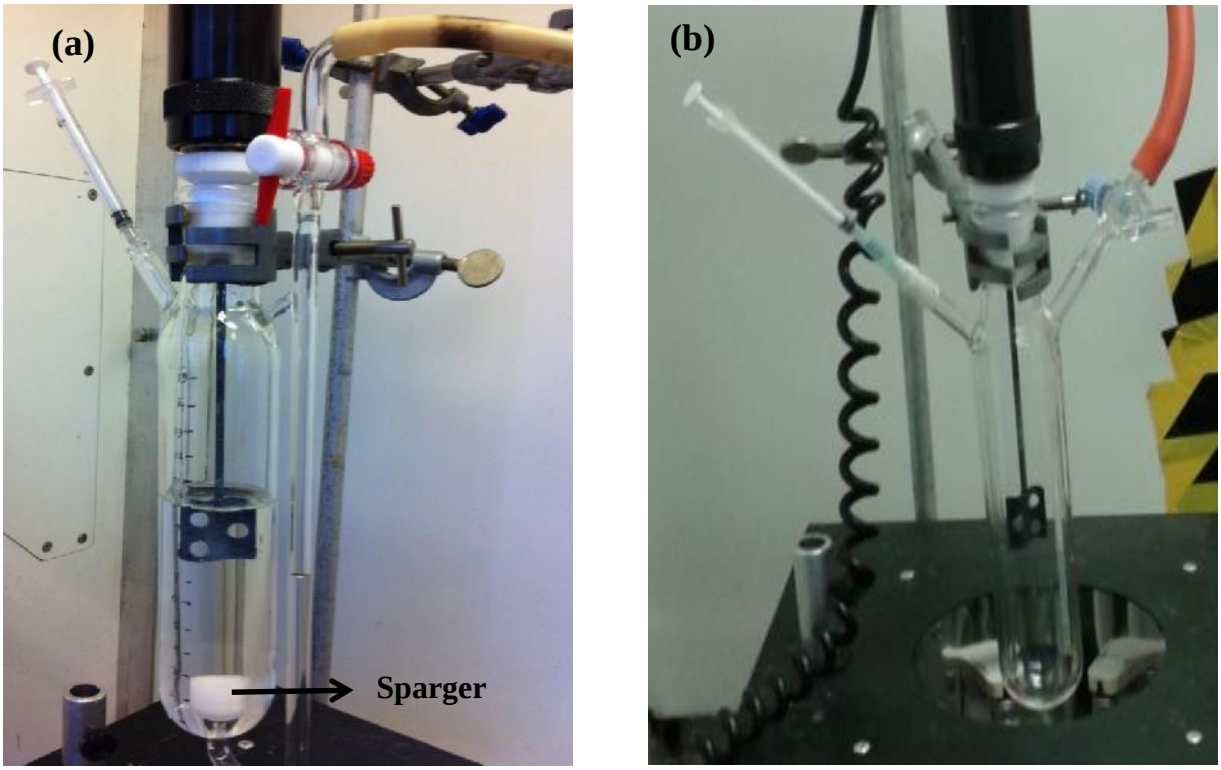


Figure 4.25: Picture of the Slurry/suspension photoreactor: (a) with sparger and (b) without sparger

recombination of electron-hole pair was favorable which explained the limited photodegradation of phenol in the experiment. Several engineering aspects have to be optimized in order to make the catalytic processes economical. These are mainly reactor design and mass-transfer limitations, process energetics, flow rate and types of oxidants. The sources of oxidants may be either air or dioxygen (in most investigations), dissolved hydrogen peroxide or ozone are used. The rate of oxidation by air is limited by the low solubility of oxygen in water and the slow rate of air-to-liquid mass transfer. The enhanced solubility of oxygen at elevated pressures provides a strong driving force for catalytic reactions (Matatov-meytal and Sheintuch, 1998). Due to the high solubility of oxygen at elevated pressures the reactor design in the experiment was modified with a spager so that the compressed air can be used at a high pressure. Under these condition the availability of the dissolved oxygen for the photocatalysis of phenol was enhance due to reduction of the mass transfer limitation. The amount of phenol converted is limited due to the type of oxidant used. From the result on Figure 4.26 it is shown that the 1.0Au%-TiO_2 has the highest ability to adsorb phenol but the rate of the mineralization of phenol is limited in the presence of air. It must be noted that when expensive oxidant such as H_2O_2 or O_3 are used the running costs are higher and therefore such processes need to be optimized. It has been reported by Matatov (1998), that enhanced solubility of oxygen in aqueous solution at elevated pressures provides a strong driving force for catalytic reactions. Oxygen flux can be improved by using soluble and active oxidants like hydrogen peroxide or ozone. Oxygen flux can also be increased by reducing the mass-transfer resistance. The film mass transfers between the air bubble and the liquid bulk and between the fluid and the catalyst can be reduced by improving agitation and by inducing smaller air (or oxygen) bubbles. These suggest that most of the data concerning oxidation of phenol which typically require 10-60 min for significant conversion typically

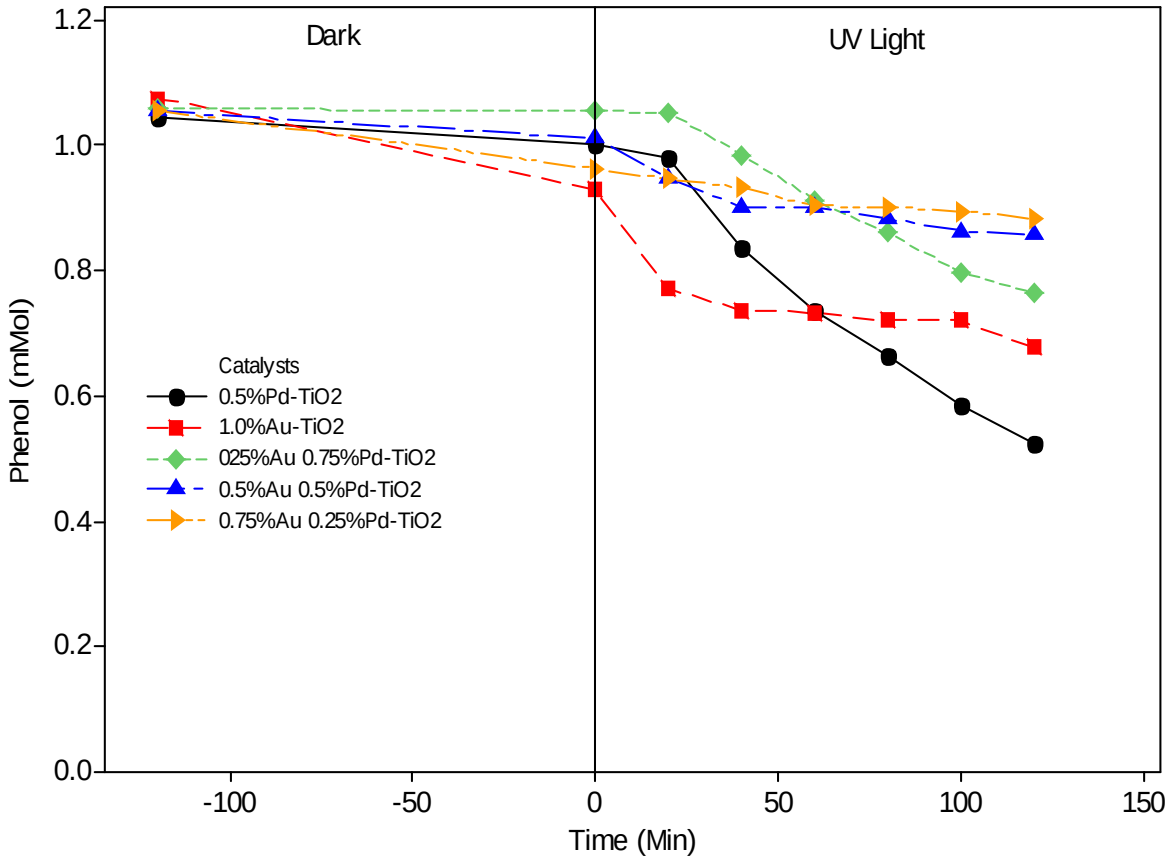


Figure 4.26: Photocatalytic degradation of phenol with air as oxidant over Au-Pd/TiO_2 using Slurry/suspension photoreactor with UV light

using catalysts that are a few millimeters in diameter, are limited by pore diffusion. Indeed, limitations due to intra-particle diffusion have been found to be significant in catalytic systems with particle diameters as low as 20μm. For particles larger than 40µm, it has been proposed that the oxidation of phenol occurs predominantly on the outer surface. Using compressed air as oxidant in this experiment shows that the presence of oxygen is as vital as its availability for the reaction due to the effect of the oxidant on the rate of the reactions.

4.3.5 Reusability of 0.5wt%Pd-TiO_2 with air using batch mode

After establishing that 0.5wt%Pd-TiO_2 has the highest efficiency in the photocatalytic mineralization of phenol in compressed air, the same catalyst was used to determine its reusability in phenol photodegradation. In this experiment the resulting solution from the photocatalytic degradation of phenols were filtered, and the catalyst washed and dried at 120°C overnight, the dried catalyst were subsequently used again under the same experimental conditions with a fresh phenol solution. The results obtained show a loss in activity which is due to deactivation of catalyst by deposition of the intermediates formed and as a result of the active metal leaching hence the filtrate was subjected to ICP-OES analysis to assess the loss of Pd^{2+} ions into the reacting solution as a result of dissolution of PdO. Figure 4.27 and Table 4.2 show that the 0.5wt%Pd-TiO_2 catalyst lost 60.9% activity which is equivalent to 20.2% palladium metal loss after being reused for 4 times while some loss of activity is attributed to the immense amount of intermediates deposited on the surface of the catalyst due to the insufficient oxygen to support the photocatalytic process. The use of air as an oxidant in the photocatalytic degradation of phenol is a viable pathway when considering the economic implication of using H_2O_2, but the major bottleneck is the low amount of oxygen present in air and the availability of the oxygen for the reaction.

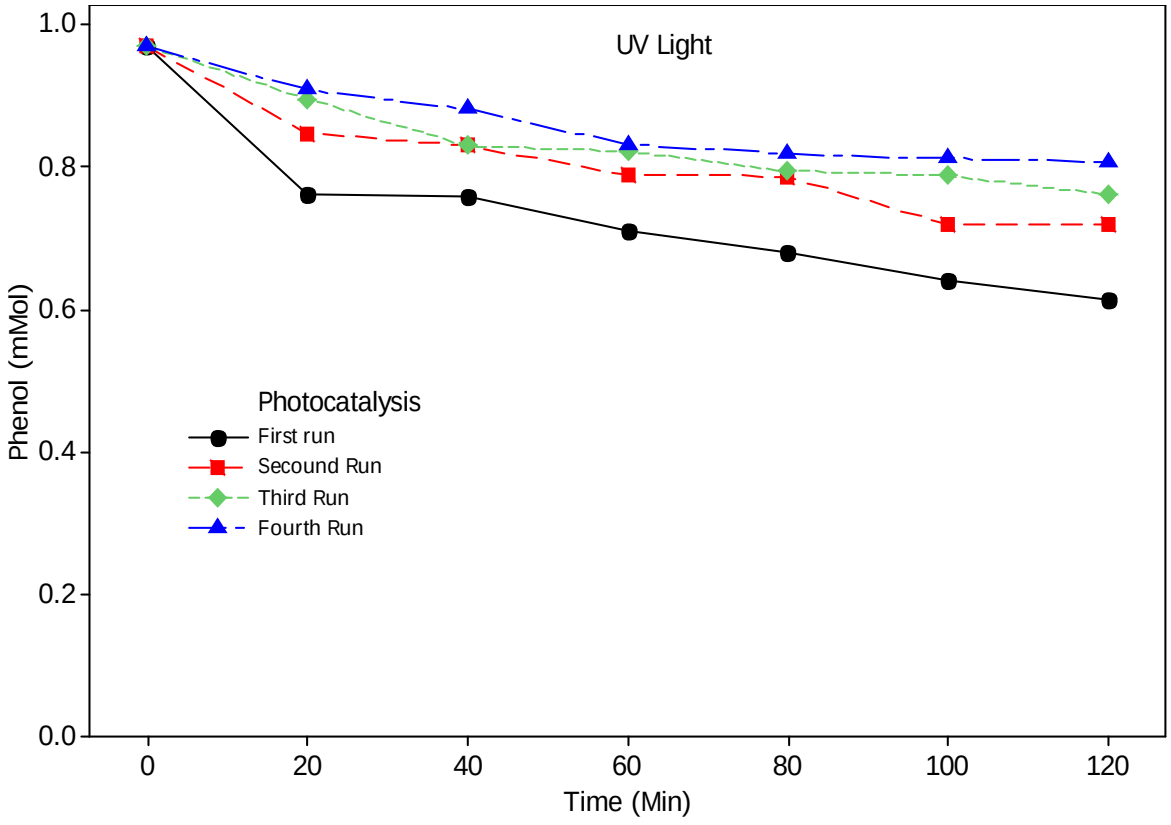


Figure 4.27: Reusability of 0.5%Pd-TiO_2 in phenol photocatalysis using air as oxidant

4.3.6 **Photocatalysis of phenol in O_2 using the batch mode**

The results obtained in the photocatalytic degradation of phenol with oxygen as oxidant at reaction pH 6.4 over P25 and Au-Pd/TiO_2 catalysts show that in all cases, the photocatalytic process was initiated after an initial equilibration period (120 min) during which relatively negligible amounts of phenol was chemisorbed on the catalyst surface, always lower than 3–4%. The result shows that 86.4% conversion of phenol to CO_2 and H_2O after 120 min could be achieved using 1.0% Pd-TiO_2 with Oxygen whereas the 0.5%Pd-TiO_2 gives 79.7% and 1% Au-TiO_2 gives 73.4% conversion. For 0.5%Au0.5%Pd-TiO_2, 0.25%Pd0.75%Au- TiO_2 and 0.25%Au0.75Pd%-TiO_2 the degradation is 69.0%, 64.4% and 41.8% respectively which are all lower than the monometallic catalysts. In contrast, 64.5% degradation is obtained with unmodified TiO_2 (P25 Degussa) suggesting that the bimetallic catalysts do not contribute to that of the supported catalyst and can in fact lower it as presented on *Figure* 4.28. From the results it can be observed that the monometallic catalysts have the highest rate of adsorption of the phenol onto the surface of the catalyst over the first 20 min of the reaction. This would increase the availability of the phenol molecules on the surface for photocatalysis destruction (Takeda *et al*., 1995; Torimoto *et al*., 1996).These results confirm that the synergetic effect of Au-Pd alloy on titanium(IV) Oxide does not show enhanced activity toward phenol mineralization as it does in other reactions (Kaneko and Okura 2002). The rate of phenol photocatalytic degradation was determine after the first 20 min of the reaction assuming the Photocatalytic degradation of phenol follows the first order kinetics. Table 4.5 present the result obtained. The polymerization of phenol and formation of intermediates like catechol, pyrogallol and benzoquinone occurred immediately after the first 20 min of irradiation with UV light.

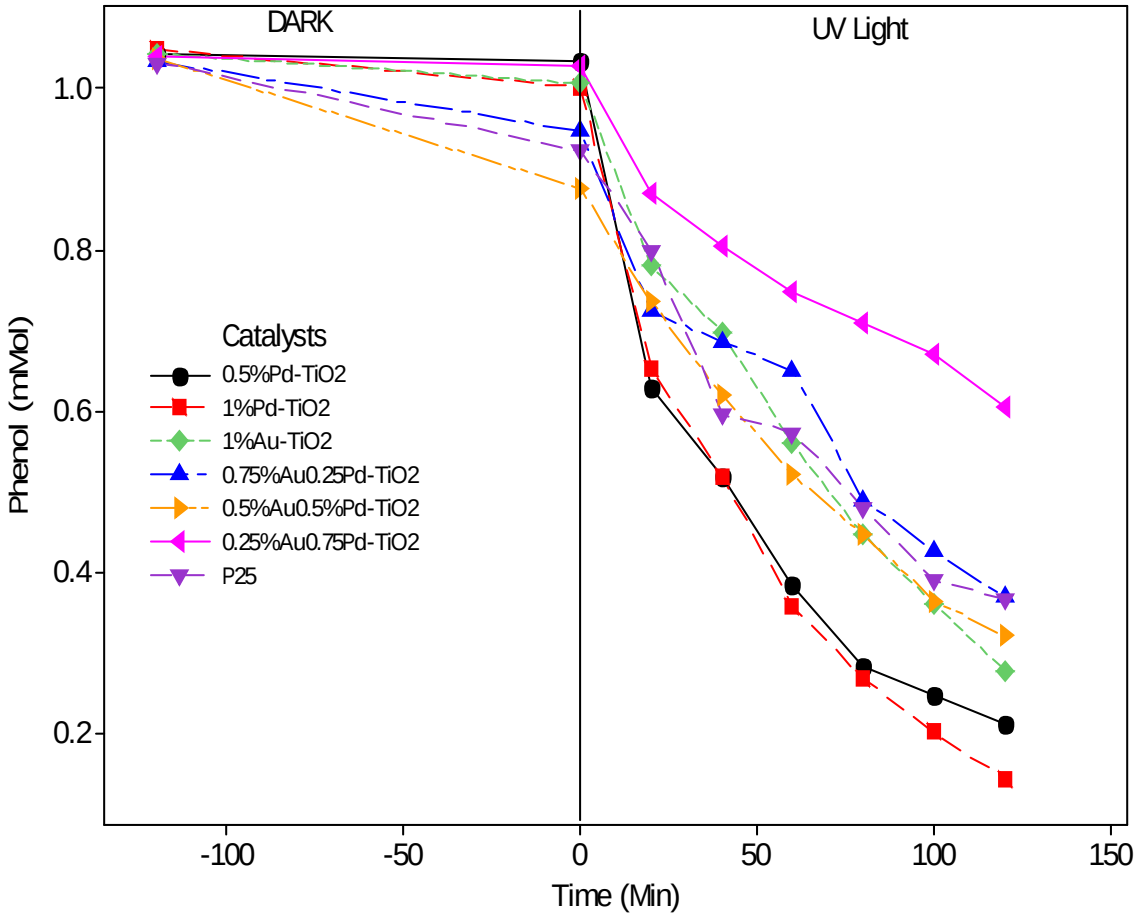


Figure 4.28: Photocatalytic degradation of phenol with oxygen as oxidant over P25 and Au-Pd/TiO_2 using the Slurry/suspension photoreactor with UV light

The brownish colours formed in the first 20 min of the reaction which slowly disappear confirm the presence of the polymeric phenol species and intermediates when analyzed with HPLC and GC-MS. The results of HPLC analysis indicated that the polymer was transformed to hydroxylated products that were the same as those intermediates produced in photocatalysis of phenol, and further oxidized via organic acids to CO_2 in the course of the photocatalytic degradation of phenol (Chun *et al*., 2000). The rate of the photocatalytic degradation of phenol was faster at the starting stage while there was a kind of a steady rate after 60 min of the reaction. This result was attributed to the changes of the amount of polymer produced. It is clear that the polymeric species from the phenol are constantly formed and then gradually disappeared as the reaction progresses. The extensive photocatalytic application of the 1.0wt%Pd-TiO_2 catalyst can be attributed to the particle size, surface area of 48.81m^2/g and the pore volume of 0.10cm^3/g which also indicates that the sample is a macro pores catalyst. Also it was found that BET surface areas of the P25 were slightly decreased after the impregnation with Pd and Au suggesting that the metals deposited in some of the pores of the TiO_2. The catalyst with higher percentage of gold deposition tends to exhibits low mineralization of phenol to CO_2 and water in the photocatalytic degradation of phenol. Due to this fact, the formation of phenol polymeric species on the catalyst are more favorable compare to the rate of mineralization (Su *et al.*, 2012).

4.3.7 **Phenol photocatalysis in O_2 with the batch mode in visible light**

The results of the metal analysis of the fresh and used catalyst using ICP-OES shows that the 0.5%Pd 0.5%Au-TiO_2 are more stable towards leaching in the photocatalytic conversion of phenol to water and CO_2 in UV light. Also the catalyst shows a remarkable ability to adsorb and destroy phenol thermally i.e. in the dark compared to the other catalyst as shown in *Table* 4.2 and *Figure* 4.28. Due to this the catalysts was used with visible light lamp at the wavelength of 555nm to assess the synergistic effect of the gold and palladium metals on the P25 support in improving the photo-response and the activity of the prepared catalysts. The experiment was done using similar condition as described earlier using the Slurry Batch reactor with oxygen as oxidant. *Figure* 4.29 represents the photocatalytic conversion of phenol using the Visible light with Oxygen at time t = 0 i.e., after the 2h equilibration in the dark. It was observed that 39% of phenol was converted to CO_2 and water using the 0.5%Pd 0.5%Au-TiO_2 in the visible light and 1%Pd-TiO_2, 0.75%Pd 0.25%Au-TiO_2, 0.5%Pd-TiO_2, 0.75%Au 0.25%Pd-TiO_2 and 1%Au-TiO_2 converted 22, 20, 25, 19 and 22% respectively which are higher than P25 which only converted 18% of the phenol in the visible light. These results show that the metals used in the modification of the titanium(IV) Oxide actually enhanced the photocatalytic activity of the catalyst both in the UV and Vis region. Comparing the amount of phenol converted using the visible light and the UV light as shown in the Bar Chart in *Figure* 4.30, it is concluded that the bimetallic photocatalyst i.e., the 0.5%Pd 0.5%Au-TiO2 are more stable to leaching and have an enhanced activity in the visible light region compare to the other catalysts. Meanwhile, the monometallic photocatalysts have enhanced reactivity with the UV light due to their ability to suppress the recombination of the photogenerated electron-hole pair in the reaction.

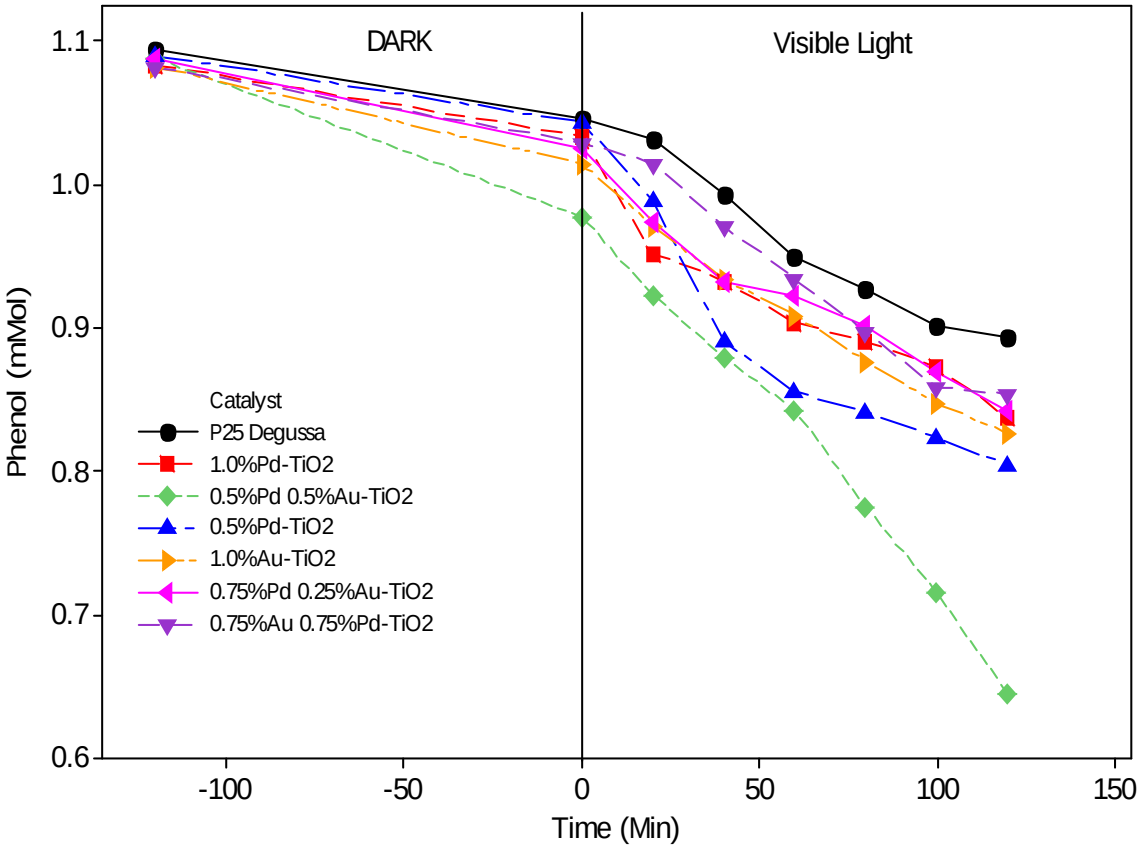


Figure 4.29: Photocatalytic conversion of phenol to CO_2 and H_2O using the Slurry batch reactor with oxygen in the visible light of 555nm wavelength

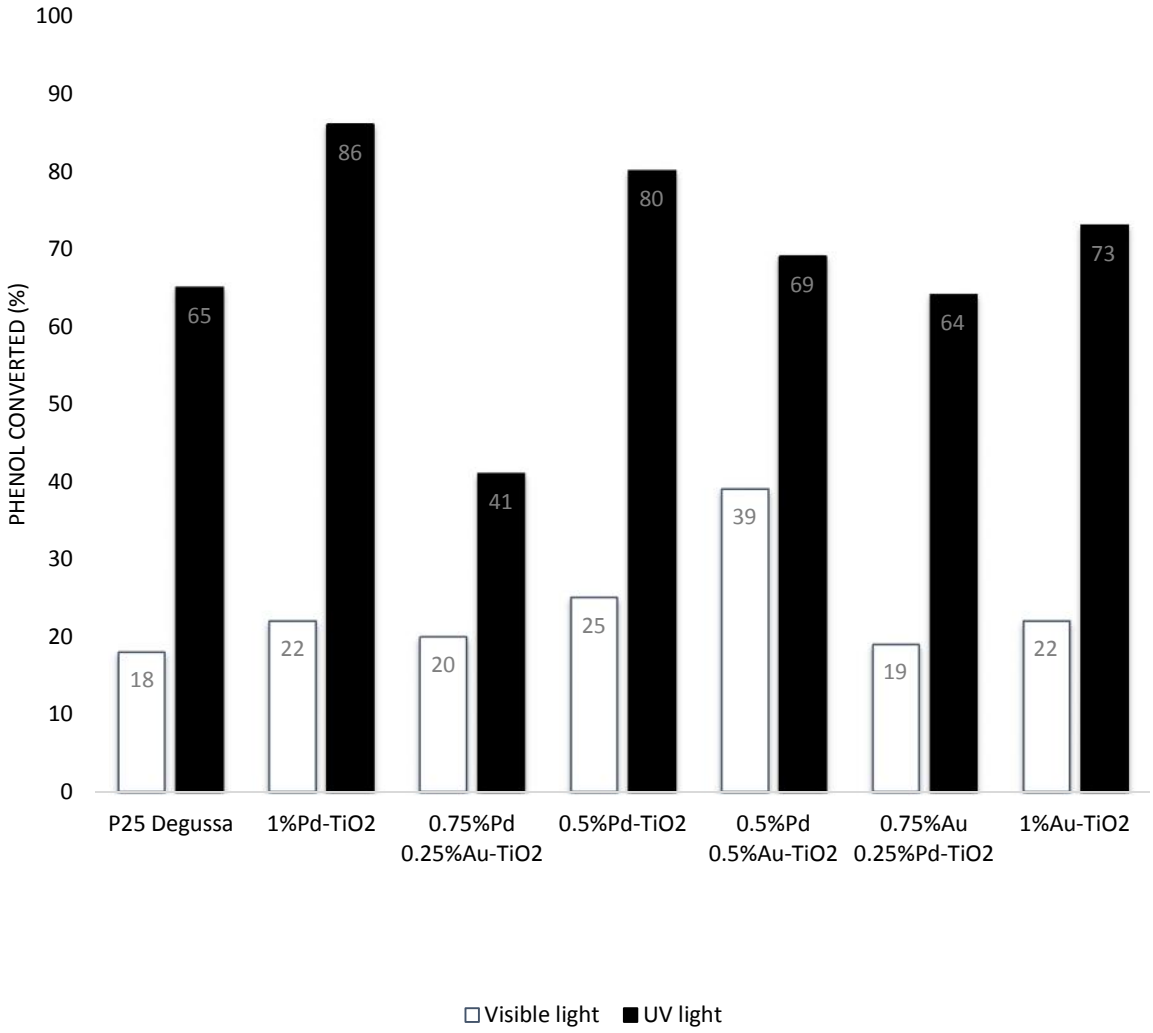


Figure 4.30: Comparison of phenol converted using the visible and ultra violet light source in oxygen with the slurry batch reactor

The stability of the 0.5%Pd 0.5%Au-TiO_2 catalyst towards leaching in aqueous solution during the photo oxidation reaction in both UV light and Visible light make the catalyst the most suitable catalyst, which led to the investigation of its thermal catalytic efficiency. The thermal catalytic efficiency of P25 was compared with 0.5%Pd 0.5%Au-TiO_2 in terms of the rate of the reaction and it was discovered that the rate at which 0.5%Pd 0.5%Au-TiO_2 thermally degraded phenol in the absence of light is 2.0 times higher than the P25 in the same condition. These implies that the 0.5%Pd 0.5%Au-TiO_2 can be used in a wastewater treatment plant that can be operated 24h non-stop using both photo catalysis and thermal catalysis simultaneously.

4.3.8 Reusability of 0.5wt%Pd-TiO_2 with O_2 using batch mode

After establishing that 0.5wt%Pd-TiO_2 has the highest efficiency in the photocatalytic mineralization of Phenol to CO_2, the same catalyst was used to determine the reusability of the catalyst in phenol photodegradation. The solutions resulting from the photocatalytic degradation of phenols were filtered, and the catalyst washed and dried. These dried catalyst samples were subsequently used again under the same experimental conditions. Clearly, there is a loss in activity which may be as a result of metal leaching hence the filtrate was subjected to ICP-OES analysis to assess the loss of Pd^{2+} ions to the solution as a result of dissolution of PdO. *Figure* 4.31 and *Table* 4.2 shows that the 0.5wt%Pd-TiO_2 catalyst loss 51.1% reactivity which is equivalent to 13.2% palladium metal loss after being reused for four times while some loss of reactivity could be attributed to leaching or poisoning of the catalyst surface with some of the intermediates. The ICP-OES results show that the estimated gold and palladium content on titanium(IV) Oxide are in good agreement with the expected theoretical values and within the a 2–5% deviation expected using this technique.

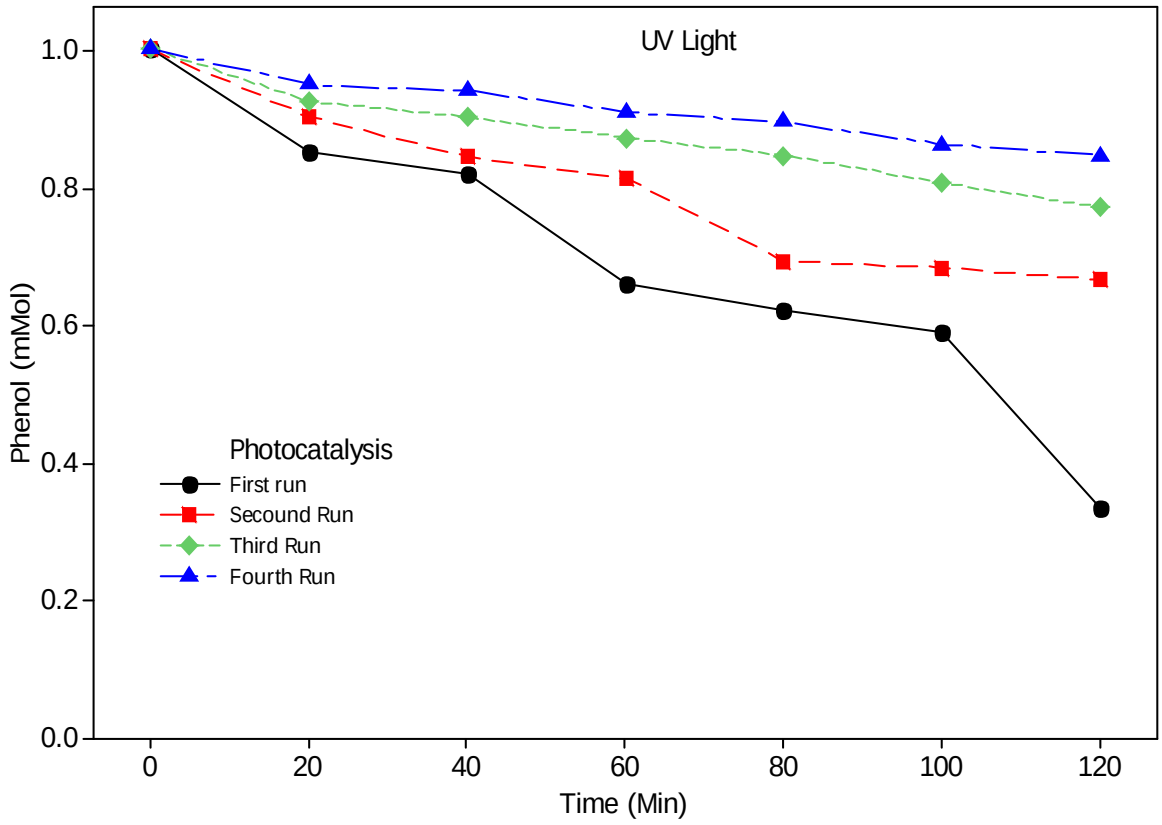


Figure 4.31: Reusability of 0.5wt%Pd-TiO_2 in phenol photocatalysis with oxygen using the Slurry/suspension batch mode

These results suggest a small degree of leaching of the gold metal compare to the palladium metals on the Trickle/Taylor system. Further tests were conducted using the fresh catalyst in the Trickle Bed mode with hydrogen peroxide as oxidant and another test was conducted using limited UV-light to confirm the formation of polymeric species on the surface of the catalyst during the reaction. After the test, the used catalyst where analyzed using the temperature program oxidation.

4.3.9 Photocatalysis of phenol in H_2O_2 with the batch mode

Figure 4.32 shows the phenol photocatalytic degradation results with hydrogen peroxide as oxidant at reaction pH 6.4 over Au-Pd/TiO_2 catalysts. In all cases the photocatalytic process was initiated after an initial equilibration period (120 min) during which relatively negligible amounts of phenol was chemisorbed on the catalyst surface, always lower than 3–4%. The final phenol conversion using Au-Pd/ TiO_2 catalyst is significantly higher than the conversion achieved when oxygen and air was used as oxidant agent. In a similar manner Tryba (2006), studied a similar reaction. The formation of hydroxyl radicals over the surface of the catalyst were detected and it was attributed to the decrease of the activity to the depletion of $^{\cdot}OH$ radicals' concentration. This behavior could be probably due to the inherent capacity of hydroxyl radicals to react with hydrogen peroxide and give rise to the formation of water and oxygen. This is in agreement with the results exhibited in Figure 4.32, where hydrogen peroxide conversions were 96.1% using the 0.5%Pd-TiO_2, 65.9%, 52.2% 40.3% and 33.3% using 1%Au-TiO_2, 0.25%Au0.75%Pd-TiO_2, 0.75%Au0.25%Pd-TiO_2 and 0.5%Au0.5%Pd-TiO_2 respectively, which did not correlate with the phenol conversion values obtained when oxygen and air were used. One of the major drawback in using TiO_2 as photocatalyst is the

photons wasting in the electron hole recombination which results in low quantum yield. Hence the prevention of electron hole recombination becomes very important. The prevention of electron hole recombination can be achieved by adding proper electron acceptors i.e. oxidant or deposition of the surface of titanium(IV) Oxide with transition metals. In these experiment gold and palladium were deposited on the surface of the titanium(IV) Oxide and compressed air, oxygen and hydrogen peroxide were used as oxidant to act as the electron acceptors in the photocatalytic degradation of phenol. The presence of some electron acceptors (oxidants), such as H_2O_2, Oxygen or air can serve as electron scavengers to prevent the recombination and enhance photodegradation efficiency. Besides the addition of molecular oxygen, the electron–hole recombination can be reduced by the addition of irreversible electron acceptors such as H_2O_2. The addition of these electron acceptors enhanced the degradation rate by several ways (i) preventing the electron–hole recombination by accepting the conduction band electron (ii) increasing the hydroxyl radical concentration (iii) generating other oxidizing species to accelerate the intermediate compound oxidation rate (Muruganandham and Swaminathan, 2006). The enhancement in degradation by the addition of H_2O_2 is due to its dual function which can act as an electron acceptor and it also increases the ·OH concentration as given by following reaction:

$$H_2O_2 + e_{CB}^- \rightarrow OH + OH^- \qquad 4.8$$

Furthermore, the enhanced degradation rate by H_2O_2 is probably due to direct photolysis by UV light. This generates the ·OH, which are likely to be dominant rate improving mechanism in the process. H_2O_2 has two hydrogen atoms bonded to oxygen atoms (H-O-O- H), thus it is more electropositive than O_2, suggesting that H_2O_2 is a better electron acceptor than oxygen (Chen and Liu, 2007).

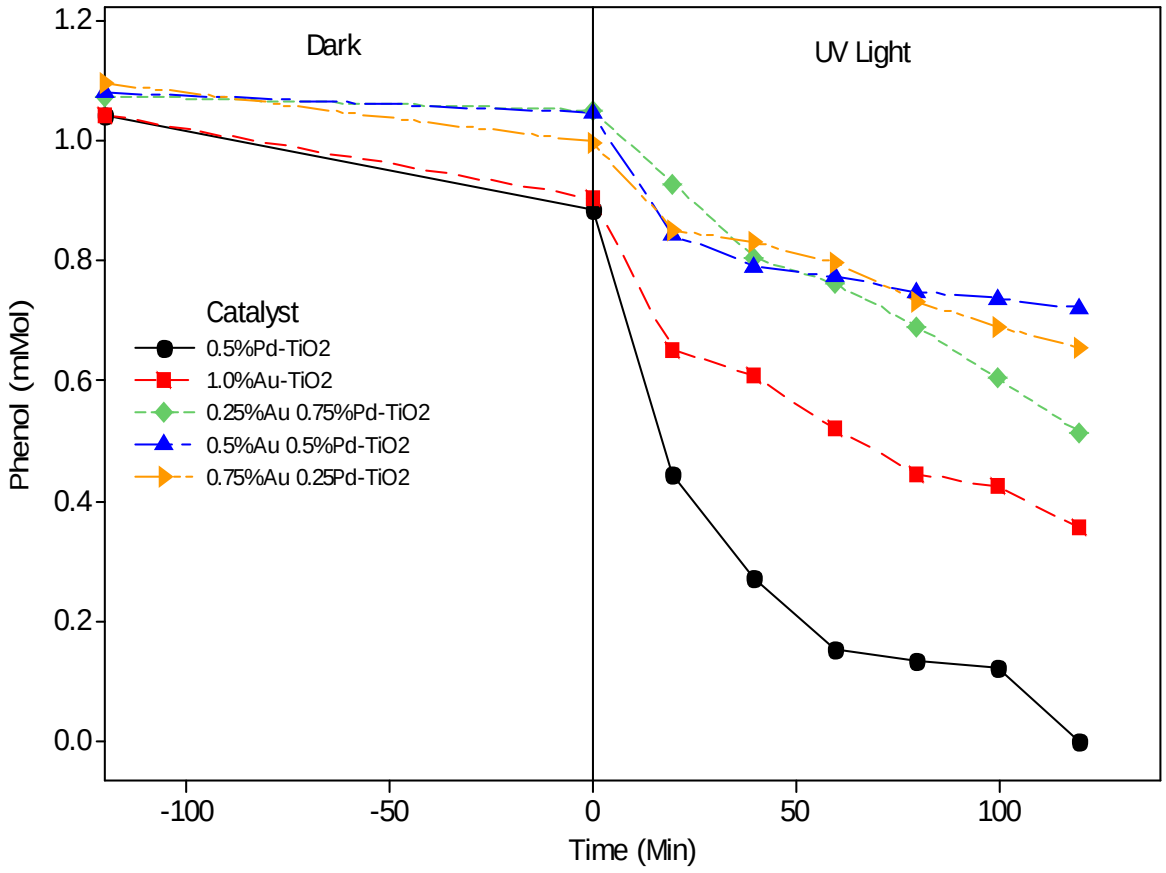


Figure 4.32: Photocatalytic degradation of phenol with hydrogen peroxide as oxidant over P25 and Au-Pd/TiO_2

The combination of H_2O_2 with TiO_2 under the UV illumination could greatly enhance the degradation of phenol compounds (Barakat *et al.*, 2005). However, extra addition of H_2O_2 which undoubtedly increased the cost of wastewater treatment process. These suggest that further study should be done using the Trickle bed and Taylor system with oxygen.

4.4 Quantum Efficiency of the Catalysts

From an energetic point of view, the photonic efficiency of a photo-induced process can be quantified in terms of its quantum yield (ϕ), i.e., the number of molecules which react according to this process divided by the number of photons absorbed by the system during the same time (Braun *et al.,* 1991). The determination of the quantum yield is an important tool used to compare the activity of different catalysts for the same reaction. The efficiency of semiconductors in promoting photocatalytic reactions is greatly determined by the extent of the major deactivation processes, which involves electron-hole pair recombination. These processes, which are characterized by a low kinetic barrier, are usually much faster than those of interfacial charge transfer and depend strongly on semiconductor material characteristics. The rate of charge carrier recombination can be reduced by trapping either the e_{CB}^- by a suitable surface adsorbed electron acceptor and/or the h_{VB}^+ by a suitable surface-adsorbed electron donor. Even electron transfer competes kinetically with the electron hole recombination processes (Kondarides 2010).

The quantum yield of a process may vary on a wide range according to the characteristics of the catalyst, the experimental conditions and especially the nature of the reactions under consideration. The photonic flux (Θ) is related to the radiant power of the lamp used in the

degradation experiments as well as the wavelength of radiation emission. However, in photocatalytic systems, the efficiency of a reaction is usually expressed in terms of its quantum yield (QY), which defined as the ratio between the number of molecules transformed per unit time and number of photons absorbed per unit time.

$$QY = \frac{Transformed\ Molecules/seconds}{Adsorbed\ Photons/second} \qquad 4.9$$

Thus, a completely efficient reaction will have a quantum yield of 1, while a process in which absorbed light is entirely dissipated as heat or energy gives a quantum yield of zero. In the present work, the lamp was used with the most important emission line at 350 nm, with a photon flux for this wavelength of 3.3477×10^{14} photons/cm^2/s. The quantum yields for the photocatalytic reactions of phenol with the different catalysts in different environment i.e. oxidant are compared.

4.4.1 **Quantum efficiency of Au-Pd/TiO_2 in air**

Shown in Table 4.4 is a summary of the initial reaction rates for the photocatalytic degradation of phenol using air as oxidant and quantum efficiency for the Au-Pd/TiO_2 in compressed air. The Initial reaction rate was determine from *Figure* 4.33 and the quantum efficiency were calculated as discussed in chapter three. It is clear that the maximum initial rate of reaction of 1.325×10^{-7}mol/s resulted to a quantum efficiency of 0.202. This value is low compared to quantum efficiency values obtained using oxygen and hydrogen peroxide.

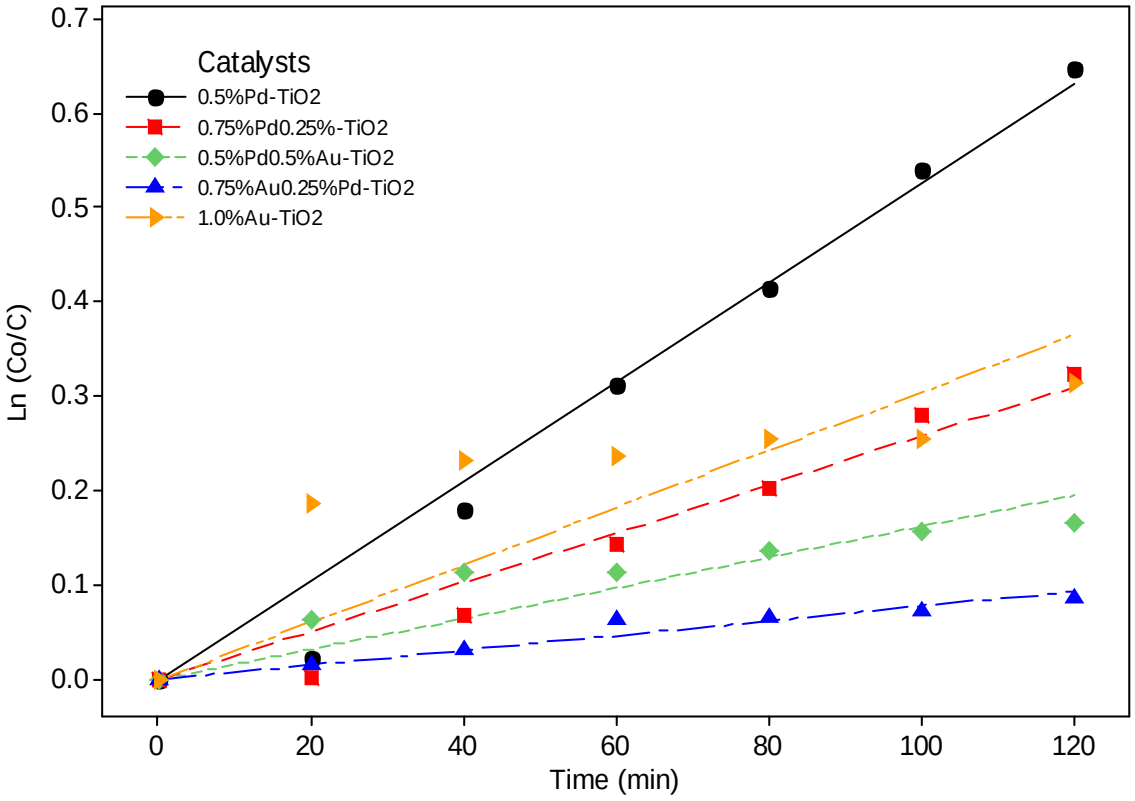


Figure 4.33: Photocatalytic degradation of phenol over Au-Pd/TiO_2 in air. The linear fit to the data represent first-order degradation kinetics

Table 4.4: Comparison of the photocatalytic rate of phenol degradation in air over Au-Pd/TiO_2 catalysts assuming first order kinetics and the corresponding quantum efficiency

Catalyst	Rate ($x10^{-7}$ s^{-1})	Quantum Efficiency
1%Au-TiO_2	1.325	0.202
0.75%Au.0.25%Pd-TiO_2	0.134	0.020
0.5%Au.0.5%Pd-TiO_2	0.522	0.079
0.25Au%.0.75Pd-TiO_2	0.034	0.00204
0.5%Pd-TiO_2	0.873	0.028

4.4.2 Quantum efficiency of Au-Pd/TiO_2 in oxygen

Shown in *Table* 4.5 is a summary of the initial reaction rates for the photocatalytic degradation of phenol and quantum efficiency for the Au-Pd/TiO_2 in oxygen. The Initial reaction rate was determined from *Figure* 4.34 and the quantum efficiency was calculated as discussed in Chapter Three. It is clear that the maximum initial rate of reaction of $3.385x10^{-7}$mol/s resulted to a quantum efficiency of 0.516 for 0.5%Pd-TiO_2.

4.4.3 Quantum efficiency of Au-Pd/TiO_2 in hydrogen peroxide

Shown in Table 4.6 is a summary of the initial reaction rates for the photocatalytic degradation of phenol and quantum efficiency for the Au-Pd/TiO_2 in hydrogen peroxide. The Initial reaction rate was determine from Figure 4.35 and the quantum efficiency were calculated as discussed in Chapter Three. It is clear that the maximum initial rate of reaction of $3.653x10^{-7}$mol/s resulted to a quantum efficiency of 0.557 for 0.5%Pd-TiO_2. This is the biggest quantum efficiency achieved for the Slurry/Suspension photoreactor in this work due to the dual role of hydrogen peroxide in the reaction as electron acceptor and as oxidant.

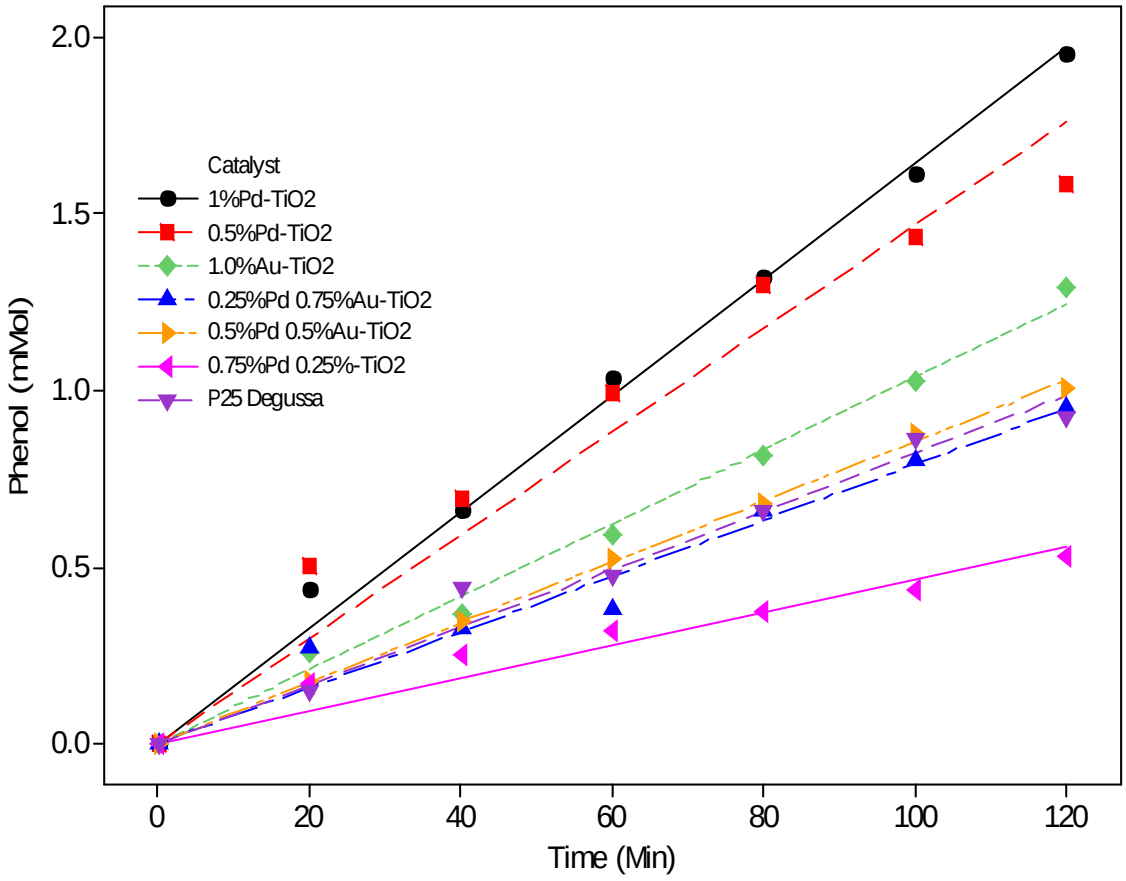


Figure 4.34: Photocatalytic degradation of phenol over Au-Pd/TiO_2 in oxygen. The linear fit to the data represent first-order degradation kinetics

Table 4.5: Comparison of the photocatalytic rate of phenol degradation in oxygen over Au-Pd/TiO_2 catalysts assuming first order kinetics and the corresponding quantum efficiency

Catalyst	Rate ($x10^{-7}$ s^{-1})	Quantum Efficiency
P25 Degussa	1.030	0.157
1.0%Au-TiO_2	1.887	0.288
0.75%Au.0.25%Pd-TiO_2	1.873	0.286
0.5%Au.0.5%Pd-TiO_2	1.173	0.180
0.25Au%.0.75Pd-TiO_2	1.337	0.204
0.5%Pd-TiO_2	3.385	0.516
1.0%Pd-TiO_2	2.916	0.445

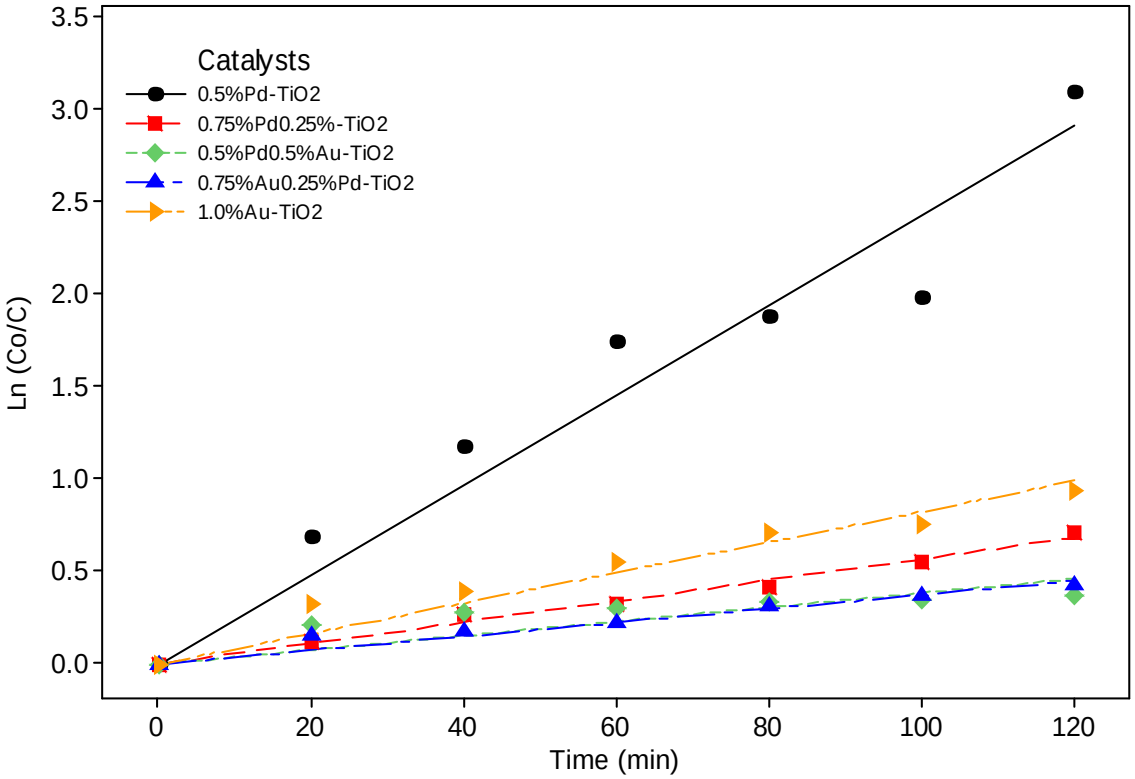


Figure 4.35: Photocatalytic degradation of phenol over Au-Pd/TiO_2 in hydrogen Peroxide. The linear fit to the data represent first-order degradation kinetics.

Table 4.6: Comparison of the photocatalytic rate of phenol degradation in hydrogen peroxide over Au-Pd/TiO_2 catalysts assuming first order kinetics and the corresponding quantum efficiency

Catalyst	Rate ($x10^{-7}$ s^{-1})	Quantum Efficiency
1%Au-TiO_2	2.113	0.322
0.75%Au.0.25%Pd-TiO_2	1.218	0.186
0.5%Au.0.5%Pd-TiO_2	1.685	0.257
0.25Au%.0.75Pd-TiO_2	1.017	0.155
0.5%Pd-TiO_2	3.653	0.557

4.5 Product Analysis and Reaction Mechanism

The HPLC and GCMS analysis performed during the photocatalytic reaction revealed that, irrespective of the catalyst and the oxidant used, the primary reaction intermediates are single-substituted hydroxyl derivates, indicating that HO· radicals are the key species involved in the oxidation process. Catechol and hydroquinone were detected as main intermediates, which is in agreement with the orientating properties of phenol's hydroxyl group. Photocatalytic oxidation of benzene-substituted substrates containing electron donor groups, such as phenol, generate ortho and para mono-hydroxyl derivatives as primary intermediates (Palmisano *et al.*, 2007). Trace concentrations of benzoquinone (in equilibrium with hydroquinone) were also detected. Thus, a simplified reaction mechanism is proposed in *Figure* 4.36. Typically catechol was observed to emerge within the first 20 min of the reaction there was also noticeable change in color of the reaction solution to light brown and the solution became colourless as the reaction proceeded. Thereafter, hydroquinone started to evolve. This observation is independent of the ratio of the metal and type of the metal deposited on the P25 Degussa. The photodegradation of phenol is noticeably faster over Au-Pd/TiO_2 than over the undoped P25 Degussa. It was note that 60% of the phenol molecules were decomposed within 20 min of the reaction using the mono-metallic Au-Pd/TiO_2, whereas only 45% could be oxidized when using P25 TiO_2 irrespective of the reaction oxidant. The photocatalytic decomposition of phenol in the presence of Au-Pd/TiO_2 photocatalysts is illustrated in *Figure* 4.36. Phenol can undergo a direct ring opening process or an indirect ring cleavage process, where the hydroxylated phenolic intermediates and its oxidized form, mainly hydroquinone, and p-benzoquinone, are generated by the nonselective attack of ·OH radicals (Zazo *et al.*, 2005).

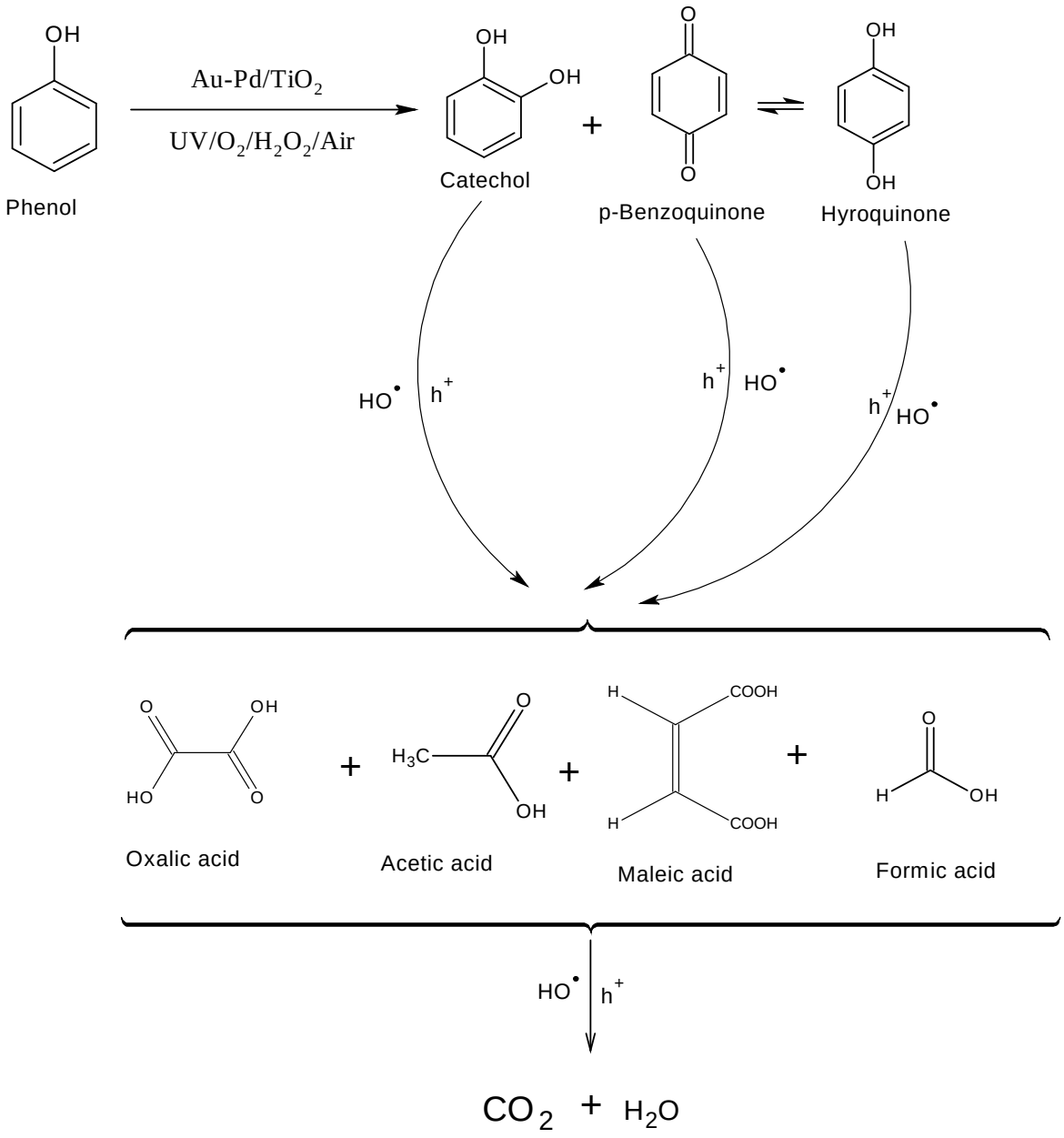


Figure 4.36: Simplified mechanism for phenol photocatalytic degradation.

All these intermediates can eventually be oxidized to CO_2 via various sub intermediates following the ring-opening processes (Mokrini *et al.*, 1997). Alternatively, photoinduced electron/hole pairs can also participate in the redox reaction described by

$$Benzoquinone + 2e^- + 2H^+ \xrightarrow{k_{BH}} hydroquinone + H_2O \quad 4.10$$

$$hydroquinone + 0.5O_2 \xrightarrow{k_{HB}} Benzoquinone + H_2O \quad 4.11$$

Eq. (4.10) and Eq. (4.11): where k_{BH} and k_{HB} are the rate constants for benzoquinone reduction and hydroquinone oxidation, respectively. It was reported by Su (2012), that in phenol photocatalytic decomposition, a minimum of seven oxygen molecules is required to fully oxidize a single phenol molecule and 28 electrons are necessary for this oxidation process. The optimum efficiency is only reached if all the photogenerated electrons participate in the oxidation of phenol and its intermediates. If, however, electrons are consumed by the benzoquinone reduction reaction Eq. (4.10), the overall efficiency decreases. Even worse, benzoquinone that has unintentionally been reduced to hydroquinone has to be oxidized again, which consumes two electrons more than required by the direct oxidation of benzoquinone. Thus, with each undesired benzoquinone reduction four electrons are wasted. If the kinetics of the benzoquinone reduction is faster than, for example, the oxygen reduction process, the consumption of photogenerated radicals by the redox couple B/H will probably dominate. In the worst case, the degradation efficiency will decrease severely and could even vanish. In the case of P25, photo-oxidized benzoquinone produced from phenol or hydroquinone is rapidly reduced to hydroquinone using the photogenerated electrons, which results in the observed accumulation of hydroquinone. This redox reaction

rapidly consumes both free electrons and oxygen in an ineffective manner, and consequently inhibits the overall photodecomposition efficiency. Conversely, the accumulation of benzoquinone observed in photodegradation experiments using metal decorated TiO_2 can be associated with the strongly depressed k_{BH}, which suggests that a lot less free electrons and oxygen molecules have been consumed in the redox reactions, thus resulting in an improvement of the overall photo-oxidation efficiency of phenol. Ring-opening of the aromatic intermediates leads to the formation of organic acids which were confirmed by the use GC-MS. As a result, the pH of the reacting solution decreases in the middle of the reaction, although the pH later increased slightly toward 100 min of the reaction which also signify the decomposition of the organic acids. The organic acids are intermediates and/or final oxidation products. Maleic, acetic, and formic acids were the earlier and more abundant products of the acid formation stage, oxalic acid was appearing at a lower rate.

4.5.1 Photocatalysis with P25 and 0.5%Pd-TiO_2 using trickle bed mode

The photo-response and photocatalytic efficiencies of the bimetallic (Au-Pd) and mono-metallic transition metals doped titanium(IV) Oxide using gold, palladium, iron, and copper where tested using phenol as a probe molecule in the presence of compressed air, oxygen and hydrogen peroxide as Oxidants with the Slurry/Suspension Batch mode. From the experiments conducted, it was observed that the 0.5%Pd-TiO_2 is the most photocatalytic active catalyst in the photocatalytic degradation of phenol in oxygen under the reaction conditions used as mentioned in the previous sections. In order to achieve the main aim of the research in developing a pilot wastewater treatment plant which worked in a continuous mode, the experiment was conducted using the 0.5%Pd-TiO_2 catalyst using the Trickle Bed system in continuous mode. In the Trickle bed system 1g of pelletized catalyst was used, the

oxidant used is oxygen with a flow rate of 15 Sccm (Standard Cubic Centimeters per Minute). The flow rate of the phenol solution from the reservoir is 0.083ml/min and the recycled phenol solution on the catalyst bed flows at 3ml/min. The detailed description of the experimental set up was explained in sectioned 3.5.8. More also the results of the experiments are presented in *Figure* 4.37, the results showed that the phenol conversion efficiency of 0.5%Pd-TiO_2 was 70.3% which remained stable in 48h. Similarly, in the trickle bed system when P25 was used with oxygen 71.9% conversion was obtained in 48h, but when P25 was used on the Trickle Bed reactor in the presence of hydrogen peroxide as the oxidant 99.5% conversion was obtained in 24h. The results from these experiments show that increasing the contact time between the phenol and the catalyst in the presence of sufficient oxidant promoted the photocatalytic degradation of phenol. These also indicate that the conversion of phenol to CO_2 and H_2O using the catalysts prepared is limited by Mass transfer and the availability of oxidant. Mass transfer limitation easily occurs in immobilized photocatalytic systems (Ollis *et al*., 1991; Ray and Beenackers, 1997). These results supported the fact that the rate of phenol mineralization using 0.5%Pd/TiO_2 photocatalyst was affected by the deposition of intermediates on the surface of the catalyst. These intermediates form a kind of polymeric hydrocarbons on the surface of the catalyst which tend to deactivate the catalyst by poisoning the catalyst active surface, also the active metals are slightly leached into the reacting solution. This was proven when P25 was used for the same reaction in the presence of insufficient supply of UV light. Only 67.2% conversion of phenol was obtained in 47 h which was attributed to the reduced rate of photocatalysis due to reduction in quantum yield (the number of molecules converted relative to the total number of photons incident on the reactor walls).

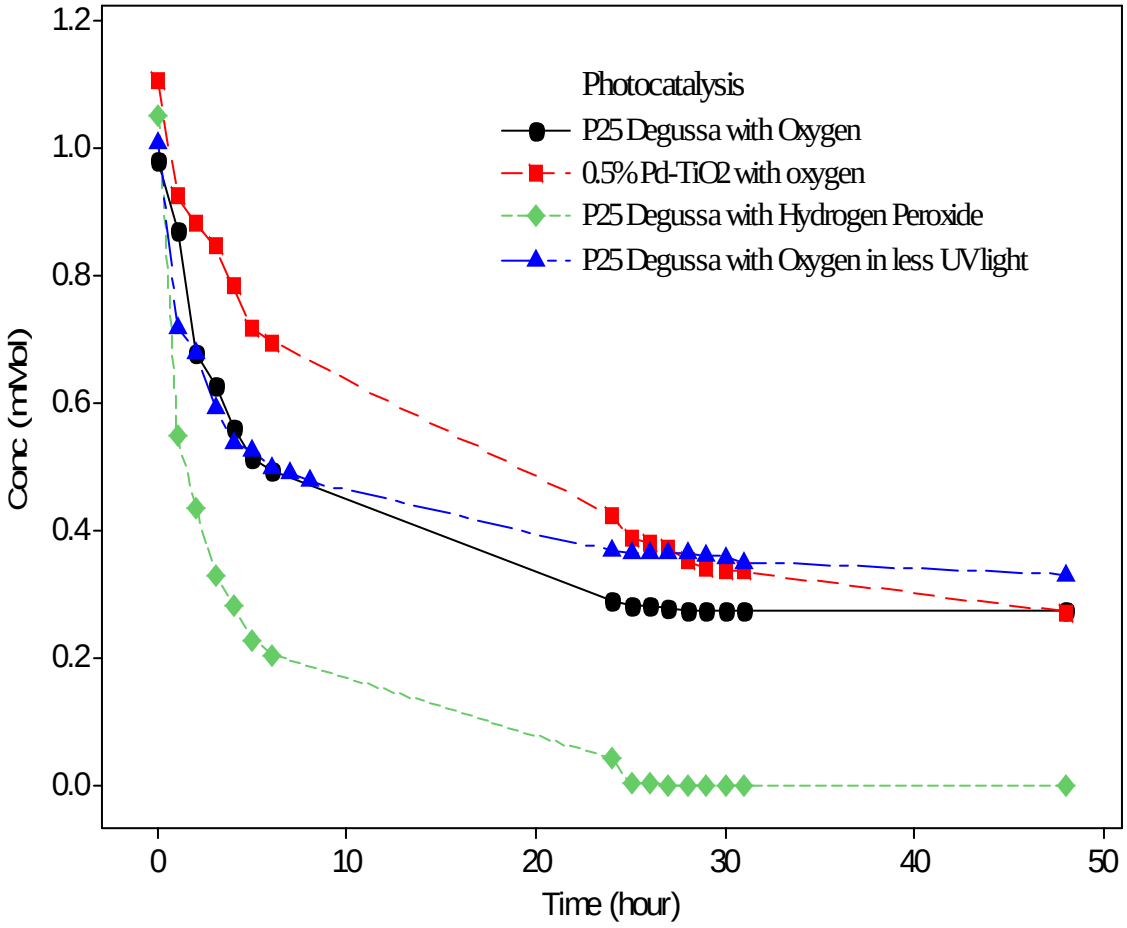


Figure 4.37 Phenol photocatalysis in oxygen and hydrogen peroxide with 0.5wt%Pd-TiO_2 and P25 using the Trickle bed mode

The used catalysts was subjected to Temperature Program Oxidation (TPO) and Diffuse Reflectance Infrared Fourier Transformed spectroscopy (DRIFTS) so that the amount of carbon deposited on the catalyst can be determine and the type of functional groups and hydrocarbons. The TPO result indicated that the carbons on the surface of the catalyst are not coke, which implies that the catalyst can easily be regenerated at a temperature range of 200-350°C.

4.5.2 TPO of the used catalyst after using on trickle bed system

The photocatalytic mineralization of phenol to CO_2 and H_2O involves the formation of some polymeric species and straight chain hydrocarbons as intermediates which tend to remain on the surface of the Catalysts as shown on *Figure* 4.38 and 4.39. From the results obtained in the TPO analysis some of the hydrocarbons tend to form a kind of carbonaceous compounds on the catalyst surface thereby deactivating the catalyst. The TPO analysis was used to quantify the carbon deposited on the catalyst during the photocatalytic degradation of phenol. The loss of catalyst activity due to the accumulation of hydrocarbon deposits from the polymeric species and the unmineralised intermediates makes it necessary for regeneration of the catalyst. The plot of CO_2 evolved during the TPO is shown on *Figure* 4.38. In order to optimize and properly design the regeneration of deactivated catalysts, knowledge of the coke burning kinetics is highly desirable (Sanchez *et al.*, 2009). From the pictures of the catalyst taken in the course of the photocatalytic oxidation of phenol as shown in Figure 4.39. It is evident from (B 1,2) that hydrogen peroxide is a good oxidant in photoxidation reaction by promoting the complete mineralization of time evolution Intermediates species that are form in the reaction. The P25 catalyst used in the reaction in the presence of hydrogen peroxide show a complete conversion of phenol to CO_2 and the catalyst retaining it color which proved

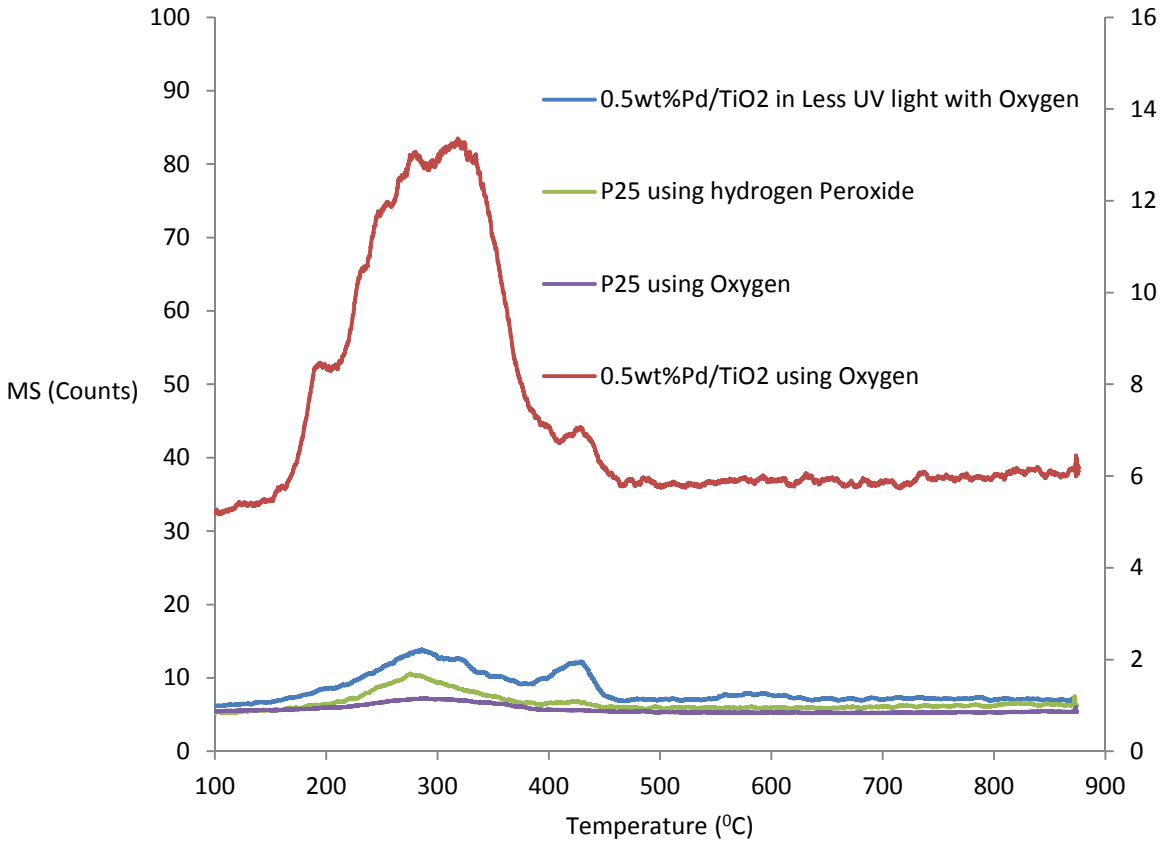


Figure 4.38: The plot of CO_2 evolved during the TPO using P25 and 0.5wt%Pd-TiO_2

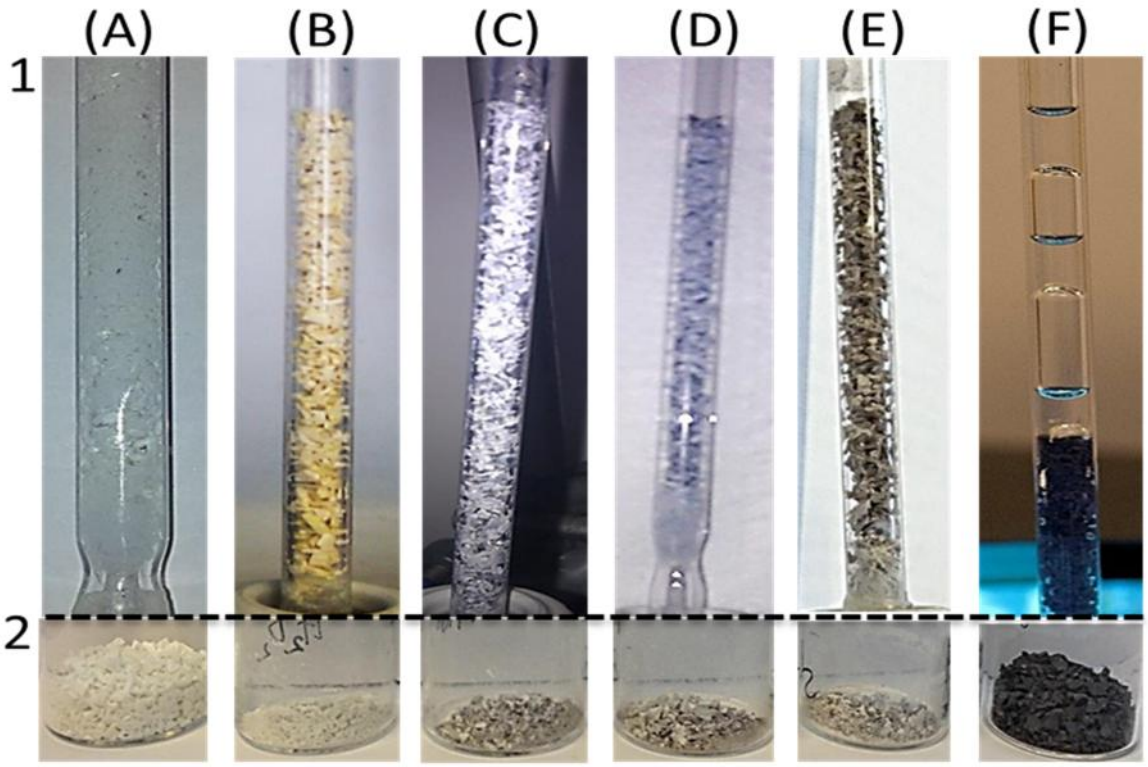


Figure 4.39: Picture of catalyst bed: (A 1) fresh P25. (B1) P25 in H_2O_2 with Trickle bed (C1) P25 in oxygen with Taylor flow (D1) P25 in oxygen and less UV light with Trickle bed (E1) P25 in oxygen and sufficient UV light with Trickle bed (F1) 0.5%Pd-TiO_2 in oxygen with Taylor flow. The Picture tags (2) are the same sample dried at 120°C overnight after the experiment

the presence of limited species deposited on the surface of the catalyst. On the other hand, the inhibition of TiO_2 arose as a consequence of surface modification of titania upon interaction with H_2O_2 (Pelizzetti *et al*., 1991). The result of the TPO analysis is also presented in Table 4.7 show the amount of hydrocarbons on the surface of the catalyst and the temperature at which the carbons are evolved as CO_2. This could be related to the yellow color of the catalyst observed at the end of the reaction, in contrast to initial white color, likely due to formation of surface peroxo complexes like $Ti(O)_2(OH)_2$ and $Ti(OOH)(OH)_3$, which are known to inhibit the photocatalytic activity (Marugan *et al.*, 2007; Chan *et al*., 2004; Xiao *et al*., 2003). When the same reaction was conducted with oxygen in limited UV light (D 1, 2) there is deposition of species on the surface of the catalyst which tend to deactivate the catalyst, these was confirmed when the TPO of the used catalyst where performed. Although the palladium based catalyst which is the most reactive in mineralization of phenol shows a great level of instability in the suspension mode which can be due to leaching or poising of the catalyst with hydrocarbons that are formed due to incomplete mineralization of the intermediates' formed in the course of the reaction. These also explain why the catalysts become deactivated after the fourth cycle in the photocatalysis of phenol as reported earlier. To overcome the leaching and deactivation of the photocatalysts, a new photoreactor was designed using the Taylor flow technique and also structural modification of the catalyst was also proposed using the microemulsion methods.

4.5.3 DRIFTS of the used and fresh P25 Degussa

To investigate the deactivation mechanism of the catalysts used, the DRIFT of the P25 and the used P25 in (a) Trickle bed reactor with less UV light, (b) Trickle bed reactor with hydrogen peroxide as oxidant and (c) Taylor flow reactor with oxygen as oxidant was done,

Table 4.7: The amount of carbons on the surface of the catalyst and the temperature at which the carbons are evolved as CO_2

Catalyst	Temperature (^{0}C)	Amount of Carbons (%)
P25 with Oxygen	285	33.6
P25 with H_2O_2	232	21.2
0.5wt%Pd-TiO_2 with Oxygen	300	47.9
0.5wt%Pd-TiO_2 with less UV light	314	78.1

after the photocatalytic degradation reaction of phenol with the catalyst, which was dried at 120°C overnight. The catalyst was used for the ex-situ DRIFT analysis to analyze the species deposited on the catalyst surface. Common to all spectra is a broad band located between 2500 and 3800 cm^{-1}, attributed to the stretching vibrations of hydrogen-bonded surface water molecules and hydroxyl groups (Brownson *et al*., 2005). This is confirmed by the presence of some weak bands around 1620 and 1685 cm^{-1} caused by bending vibration of coordinated water as well as from the Ti–OH group (Gao, *et al*., 2004; Jere and Patel, 1962). The results are compared with that of the fresh catalyst, as shown on *Figure* 4.40. The P25 catalyst used in the Trickle Bed reactor in less UV light shows peaks at (i) 1261.40cm^{-1} which is due to primary and secondary -OH Plane bending, from the intermediates of the phenol photo-oxidation, (ii) 1387.49cm^{-1} which is due to C-C bending caused by the deformation of CH_2 and CH_3. (iii) 1421.57cm^{-1} this is as a result of -C –O-H bending from the carboxylic acid and derivatives formed before the final mineralization of phenol to CO_2 also the peak is as a result of O-H in plane bending from phenol and (iv) 3687.80 cm^{-1} due to phenol OH stretching. The P25 catalyst used in the Trickle bed reactor with hydrogen peroxide shows only one distinct peak at 1421.57cm^{-1}. This is as a result of –C-O-H bending from the carboxylic acid and derivatives formed before the final mineralization of phenol to CO_2. The result of the P25 using the Taylor flow reactor in the presence of oxygen as oxidant shows all the peaks that correspond with the result obtained with the system in less UV light except for the peak at 3098.98cm^{-1} which is due to = C-H and =CH_2 stretching also from derivatives of the carboxylic acid formed. This is indicative of the presence of carboxylate species strongly bonded to the catalyst (Coates, 200; Dick *et al*., 2003).

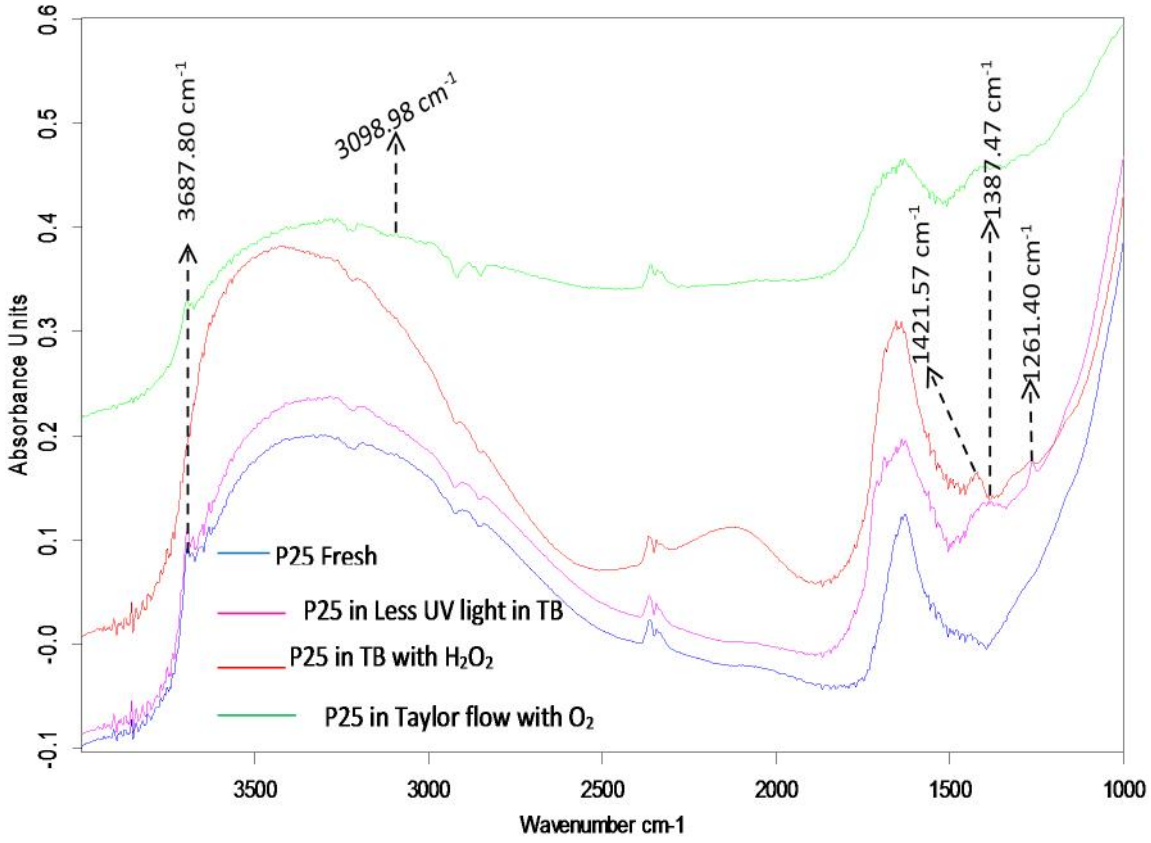


Figure 4.40: DRIFT of used P25 (Degussa)

4.5.4 **DRIFTS of the used and fresh 0.5%Pd-TiO_2**

The DRIFT spectrum of the 0.5%Pd-TiO_2 catalyst both fresh and used catalyst using the Taylor flow system are compared as shown in Figure 4.41 which revealed a typical pattern of phenol and carboxylic acid. (a) a peak at 1442.02cm^{-1} due to –C-O-H bending of -COOH from the carboxylic acid derivatives produced in the reactions, (c) a peak at 1339.78cm^{-1} due to OH deformation of -COOH, -C-OH bending of phenols and of tertiary alcohol; (d) a peak at 3575.34cm^{-1} ascribed to -OH stretching of free OH, because of the polymeric association of the –OH it is responsible for the shift of the frequency from 3500 to 3575.34cm^{-1}. The DRIFT result obtained support the mechanism of reaction postulated earlier and it also confirmed by the TPO result obtained. Phenol Photocatalysis with P25, 1%Au-TiO_2 and 0.5%Pd-TiO_2 using the Taylor flow mode To overcome the challenge of deactivation of the photocatalysts due to deposition of polymeric phenolic species formed on the surfaces of the catalyst due to unavailability of sufficient oxygen for the photocatalytic degradation of phenol using the Trickle bed system, a new photoreactor was designed using the Taylor flow technique. By using the Taylor flow system the photocatalytic efficiency of the monometallic palladium and gold on titanium(IV) Oxide catalyst was enhanced by reducing the mass transfer effect and increasing the availability of the oxygen required for the photodegradation of phenol. The rate of mineralization of phenol was enhanced through the availability of oxygen which supports the complete conversion of the intermediates formed during the photocatalytic conversion of phenol to CO_2 and water. These were achieved because the surface of the catalyst was not poisoned with the hydrocarbons which increased the reactivity life-time of the catalyst to 26h in case of the P25 in the continuous mode and 34h for 0.5wt%Pd-TiO_2 and for the 1wt%Au-TiO_2 the reaction rate was slow but consistent for 52h, Meanwhile for the 0.5%Pd 0.5%Au-TiO_2 converted 76% phenol and it retain its stability and

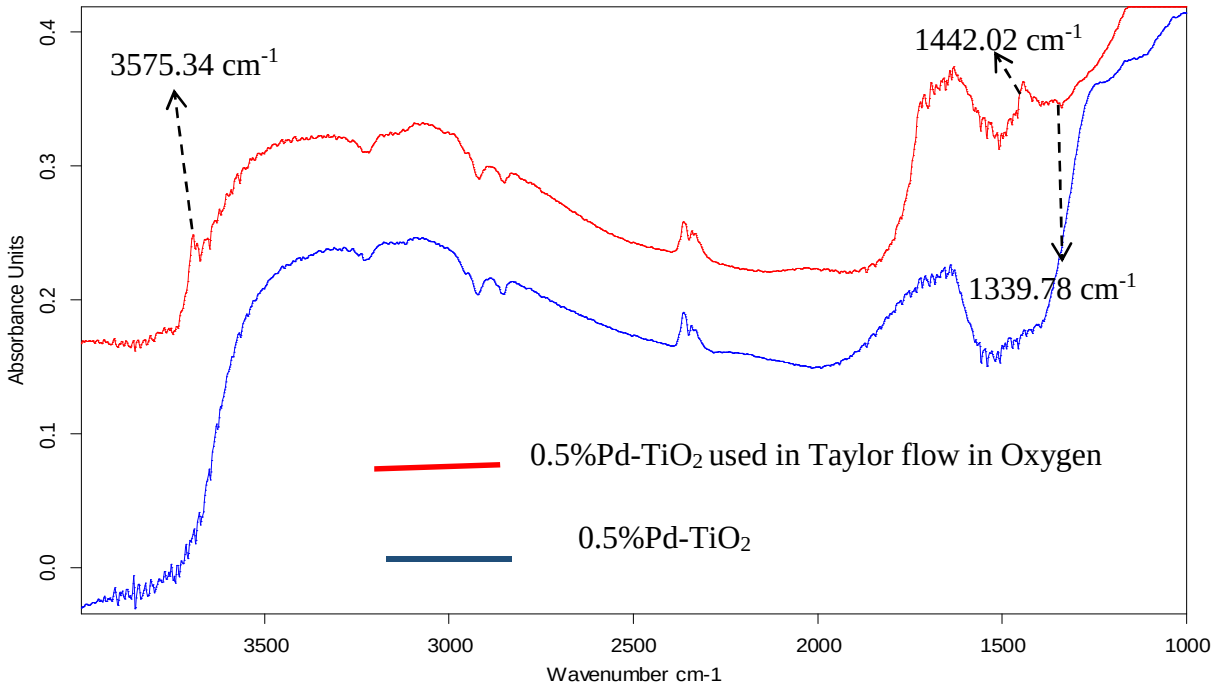


Figure 4.41: DRIFT of 0.5%Pd-TiO_2

activity for 52h due to its ability to withstand leaching in aqueous phase. More so the photoresponse of the 0.5%Pd 0.5%Au-TiO_2 in the visible light region make it a viable catalyst for industrial application in wastewater treatment as seen on *Figure* 4.42. It was evident from the experiment that reusability of the catalyst is strongly affected by the type of reactor and availability of oxygen controlled by gas-liquid ratio in Taylor flow for the reaction, seeing that the catalyst can remain active for 48h in the Taylor flow reactor. These results show that when there is sufficient supply of oxygen for the photocatalysis the deactivation of the catalyst by poisoning the surface is minimized. Au-Pd alloy formation on the surface helps to anchor Pd species and stop Pd leaching from TiO_2 surface. Leaching from the solid to the liquid phase is a general issue when using solids in heterogeneous catalysis. Particularly in the case of supported noble metals (Pt, Pd, Au, Ru, etc.) acting as active sites. It is necessary to establish that the observed catalytic activity is not due totally or partly to minimum traces of these metals becoming dissolved in the liquid phase. The occurrence of leaching is typically assessed by analyzing the liquid phase and the solid catalyst after several uses and by performing some catalytic tests in which the solid is filtered under the reaction conditions and the supernatant solution particles are surveyed for further conversion in the absence of solid (Primo *et al.,* 2011)

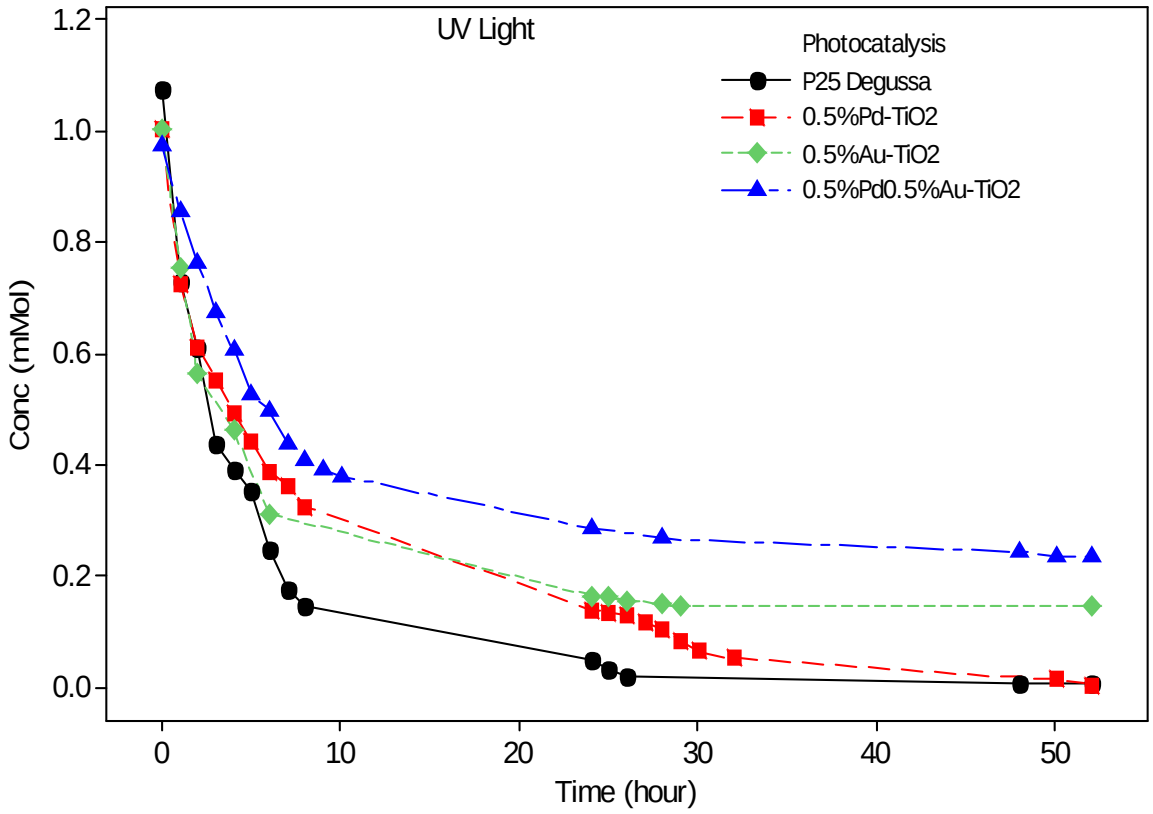


Figure 4.42: Phenol photocatalysis in oxygen with 0.5wt%Pd-TiO_2, 0.5wt%Pd 0.5wt%Au-TiO_2 and P25 using the Taylor flow mode

4.5.5 **Photocatalysis using 2%Pd@TiO_2 on Batch, Trickle bed and Taylor flow**

Addressing the leaching of the active metal (i.e. palladium) from the surface of the titanium(IV) Oxide support, a structural modification of the catalyst was done by using the microemulsion method in preparing the photocatalyst, this method aimed at placing the active metals within the catalyst core instead of depositing it on the surface as in the case of the sol immobilization method. The photocatalytic degradation of phenol was done varying the oxidants i.e. compressed air, oxygen and hydrogen peroxide and also using the different type of photoreactor used in the previous reaction. The photocatalytic degradation of phenol with 2%Pd@TiO_2 using (Slurry/Suspension batch mode, Trickle bed system and Taylor flow system) are shown in Figure 4.43 and Figure 4.44. With the Slurry/Suspension batch mode using oxygen as oxidant, there was a 24% conversion of phenol to CO_2 and water, but there was a 85% conversion with the Trickle bed system and 97% conversion with the Taylor flow system, the increase in the photodegradation rate of phenol compared to the value obtained with the Slurry/Suspension batch mode is ascribed to the structural modification made coupled with the increase in the metal loading from 1-2%, meanwhile the effect of the different type of photoreactor used also contributed to enhanced photocatalytic efficiency in the case of the Trickle bed and the Taylor flow system. On the other hand, few reports have revealed Ohtani *et al.*, (1997), the photocatalytic activity of amorphous TiO_2. So far, only few papers reported the negligible activity of amorphous TiO_2 by comparison with commercial crystalline TiO_2 catalysts, but no interpretation for such behavior was given (Tanaka *et al*., 1991).

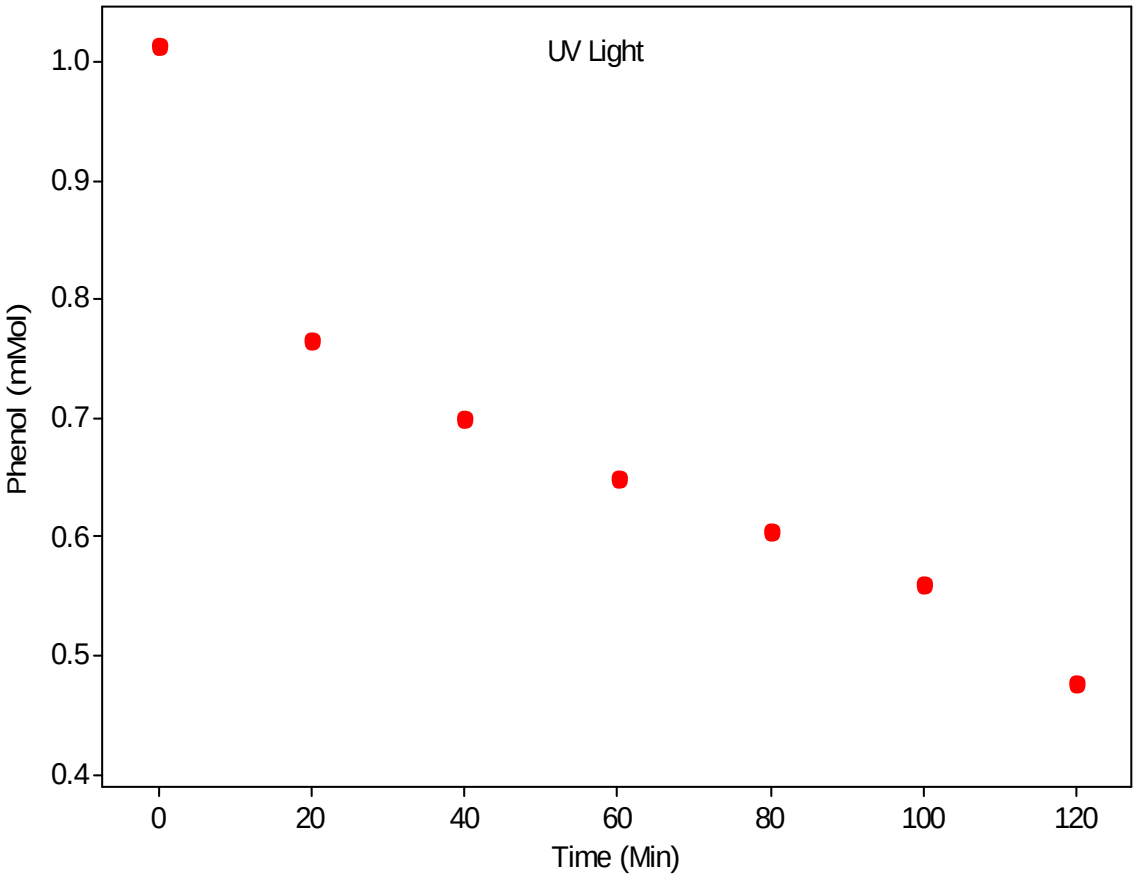


Figure 4.43: Photocatalytic degradation of phenol using 2%Pd@TiO_2 with the Slurry/suspension system in oxygen

The negligibly low activity of amorphous TiO_2 is attributable to the facilitated recombination of electron-hole traps on the surface and in the bulk of the particles. Although a few reports described the photocatalytic activity of less (or negligibly) crystallized TiO_2 particles, as amorphous TiO_2, prepared by hydrolytic precipitation from titanium (IV) alkoxides. From this study the remarkable photocatalytic activity of the 2%Pd@TiO_2 can be attributed to palladium, which has facilitate the electron transfer from the TiO_2 surface to the palladium present thereby reducing the recombination of the electron-hole pair. More also this significant change in the rate of phenol degradation is attributed to the impact of the Taylor flow system used, which increased the availability of the oxygen needed for the oxidation reaction. From the previous experiment conducted with the same catalyst in the Slurry/Suspension Mode it was noted that the reaction is affected by mass transfer effect. Using the Taylor flow system increased the mass transfer by enabling the complete mineralization of the phenol. The result on *Figure* 4.23 shows the effect of photolysis in the experiment that is the decomposition of the phenol molecule in the presence of UV light and oxidative species only. From the result obtained it is evident that more phenol is degraded with hydrogen peroxide compare to oxygen because the hydrogen peroxide is in liquid phase. Alternating the flow of the phenol solution with oxygen bubble increase the rate of the reaction, meanwhile, there was no significant difference in the reaction rate between the Trickle bed system and The Taylor system due to the fact that the both system actually increase the mass transfer thus enhance the availability of the oxygen required, but the Taylor flow system shows that the catalyst is more stable in the continuous mode and give 97% conversion of phenol to CO_2.

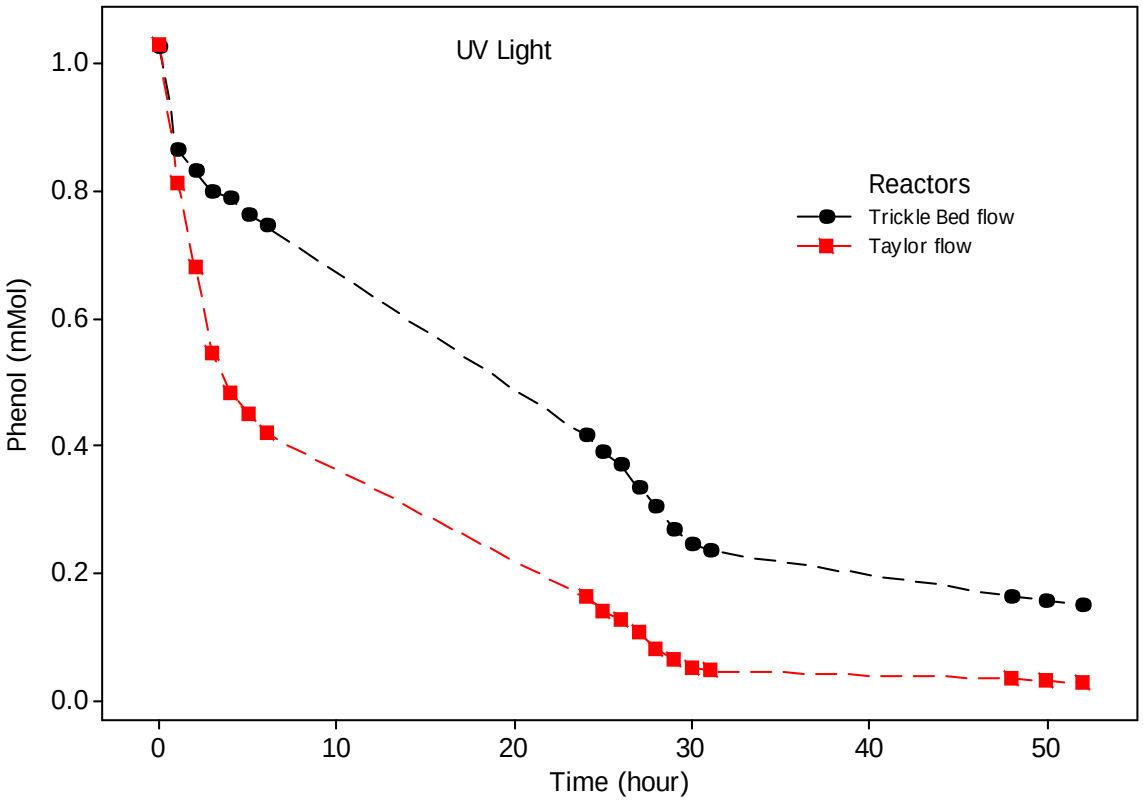


Figure 4.44: Phenol photocatalysis using 2%Pd@TiO_2 in oxygen using Trickle bed and Taylor flow system

On the other hand, comparing the result on Figure 4.45 and Figure 4.23, the results show that the rate of phenol degradation is increased with hydrogen peroxide as oxidant compare to oxygen, this is due to the fact that hydrogen peroxide inhibit electron-hole pair recombination thereby increasing the rate of the photocatalytic oxidation of phenol. Actually, the photocatalytic oxidation of phenol is extensively investigated and its degradation proceeded predominately via -OH radicals (Ilisz and La, 1999). Thus it suggest the Taylor flow system can enhance the reaction rate by increasing the production of -OH radical in the presence of oxygen on the surface of the palladium core shell on the titanium dioxide. Figure 4.45 show that the effect of hydrogen peroxide concentration on the photocatalytic degradation of phenol using the palladium core shell catalyst support the finding reported by Nam *et al* (2002), the result show that H_2O_2 is suitable for trapping electrons by preventing the recombination of electron (e^-) and photogenerated hole (h^+) pairs, also, the chances of formation of hydroxyl radical (-OH) on the surface of photocatalyst are also increased. However, in the presence of excess H_2O_2, the phenol degradation decreased due to the consumption of -OH radicals and the formation of proxyl Radicals (HO^{2-}) (Nam *et al*., 2002). Therefore, it can be observed that the degradation decreased due to the consumption of ^-OH radicals and formation of HO^{2-} radicals, which were significantly less reactive than $\cdot OH$ radicals. Thus, the addition of H_2O_2 with a suitable concentration could assist the photocatalytic reaction in enhancing the degradation by preventing the recombination of e^- and h^+. These results give essential and important information for the design and synthesis of highly active semiconductor photocatalyst using amorphous titanium(IV) Oxide and palladium which also resolved the issue of leaching in liquid phase photocatalytic reaction.

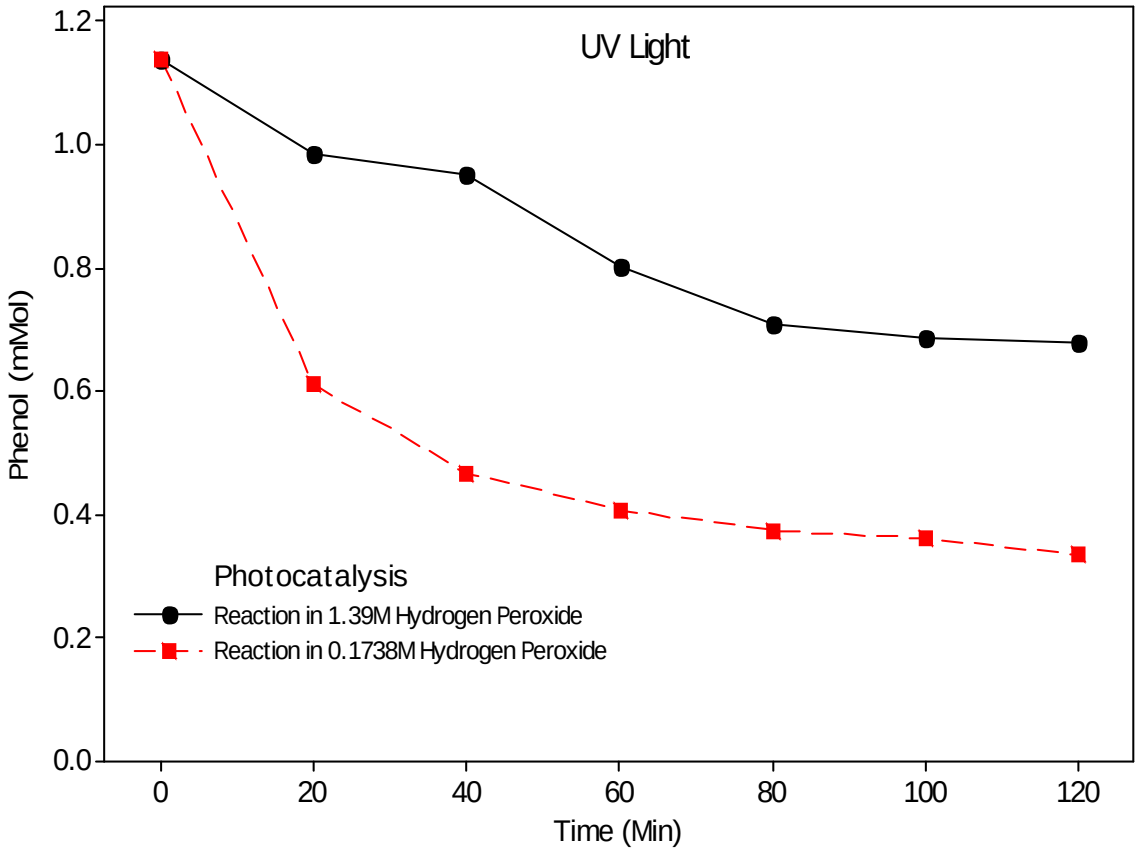


Figure 4.45: Effect of hydrogen peroxide concentration on phenol degradation using 2%Pd@TiO_2 catalyst

4.5.6 **Reusability of 2%Pd@TiO_2 in O_2 and H_2O_2 with batch mode**

The reusability efficiency of 2%Pd@TiO_2 catalyst on the Slurry/Suspension batch mode using oxygen and hydrogen peroxide as oxidant are shown on Figure 4.46 and *Figure* 4.47, after each run, it was observed that the color of the catalyst turned to black. The change in color of photocatalyst is due to the accumulation of intermediates on the 2%Pd@TiO_2 surface and this led to catalyst inhibition. The intermediates form are competing for the active side on the catalyst surface which leads to a gradual deactivation of the catalyst, also it was also discovered that the palladium used in the catalyst are leaching out which is a major problem in using palladium catalyst in liquid phase. Therefore, the competitive inhibition of the catalyst and leaching reduced the photocatalytic activity in the reuse catalyst. But using hydrogen peroxide showed that more phenol is converted to carbon dioxide due to the ability of the hydrogen peroxide to remove the intermediates that are bound on the surface of the catalyst. This was observed during the reaction, because the catalyst used with hydrogen peroxide are not black in colour but the catalyst used with oxygen are black in color. To confirm these claims, the Temperature Program Oxidation was done for the used catalyst to determine the amount and type of hydrocarbon deposited on the surface of the catalyst. It was found that light hydrocarbons are deposited on the catalyst and they are removed at 310°C. The result also showed that the catalyst can be regenerated when it is deactivated by competitive inhibition.

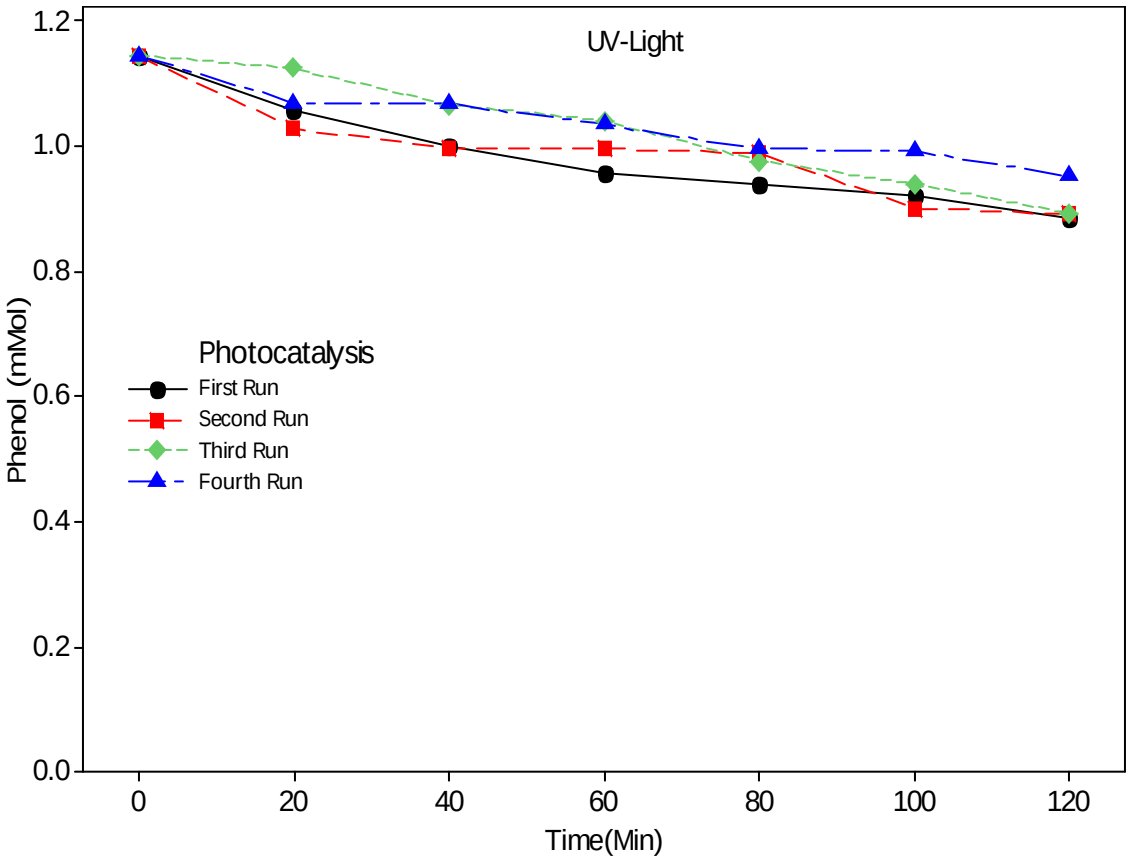


Figure 4.46: Reusability of 2%Pd@TiO_2 in photocatalysis of phenol in oxygen with Slurry/suspension batch mode

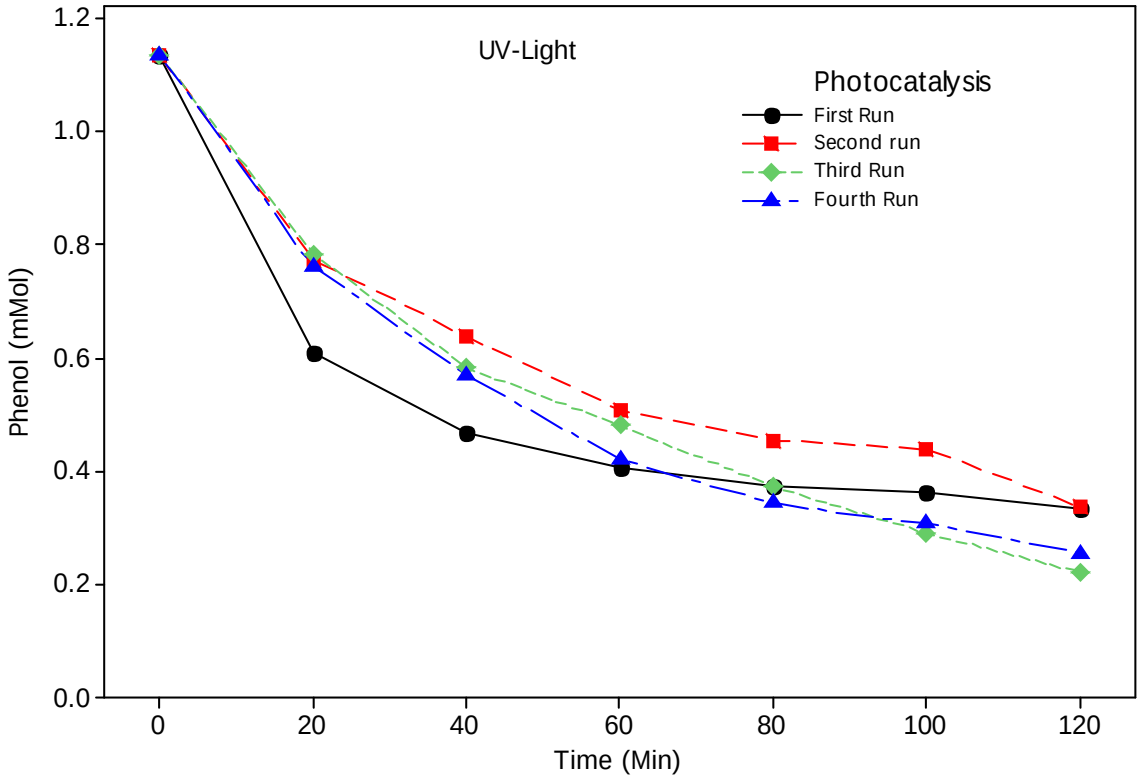


Figure 4.47: Reusability of 2%Pd@TiO_2 in photocatalysis of phenol in hydrogen peroxide with Slurry/suspension batch mode

4.5.7 **Thermocatalytic oxidation of phenol with P25 on the Taylor flow**

Thermocatalytic oxidation of phenol was carried out using the Taylor flow system as described in the previous Section 3.5.7, pelletized P25 Degussa was used, with oxygen flow rate of 15sccm, the phenol flow rate from the reservoir was at 0.083 ml/min and recycling rate of phenol over the catalyst at 3 ml/min. The main goals of these experiments were: (i) to assess the possibility of combining thermocatalysis (at the temperature range of 54±3°C) and photocatalytic destruction of phenol and (ii) depicts the oxidation/destruction of phenol as a function of maximum contact time (at 12h) and temperature (at 54±3°C) in the dark using P25 catalyst. These will give the viability of the wastewater treatment plant running for 24h continuously both in the presence of UV light and in the absence of UV light. From the results obtained, in the presence of P25 Degussa at 50°C and residence time of 8h, 22.4% phenol was destroyed. The plot of phenol destroyed with thermocatalytic oxidation in the presence of P25 TiO_2 as a function of time is given in *Figure* 4.48. Comparing the result obtained in the photocatalysis of phenol using the Taylor flow system with P25, 86.2% conversion of phenol was attained in 8h. By these it proved that combining photocatalysis and thermocatalysis at elevated temperatures (50±3°C) complete mineralization of phenol to CO_2 can be achieved in 16h. This conserved the time for attaining complete mineralization from 26±2h in the case of using only photocatalysis to 16h; thereby conserving energy from the UV light source.

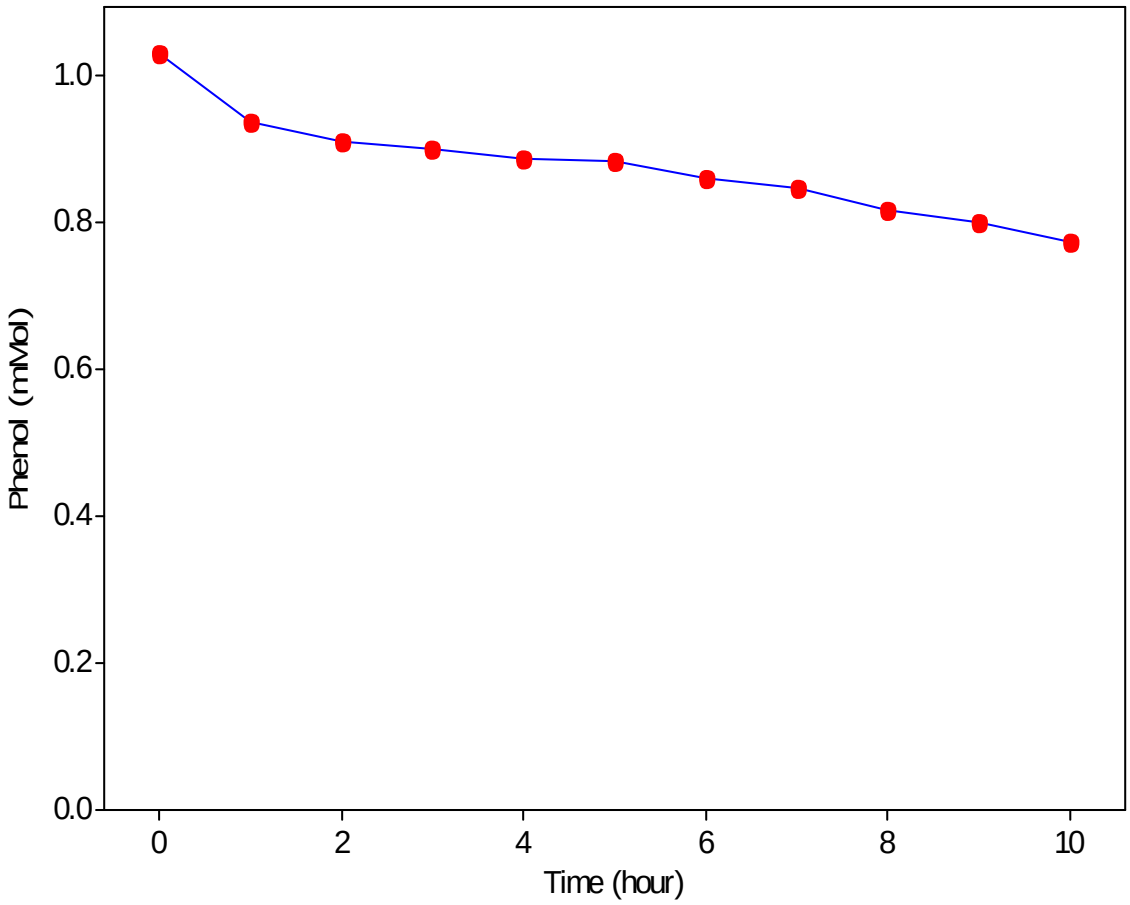


Figure 4.48: Thermocatalytic oxidation of phenol in the presence of P25 using the Taylor Flow system

CHAPTER FIVE

5.1 Summary, Conclusion and Recommendation

5.2 Summary and Conclusion

The application of photocatalysis for wastewater treatment and purification on an industrial scale can be assisted by the development of new photoreactor designs. A good photoreactor design should meet the following challenges: high ratio of the illuminated catalyst area to the volume of the reactor; uniform light distribution; fast overall removal rate; high quantum efficiency; high throughput; low power consumption; and easy scale-up capability. The complete mineralization of phenol into carbon dioxide and water via Photocatalysis is a major challenge for industry and academia. Due to the recent discoveries related to the ability of Au-Pd/TiO_2 in enhancing the photo-response and photocatalytic ability of titanium(IV) Oxide in the photoxidation of organic pollutant in wastewater, further work into the complete mineralization of phenol using the (i) Slurry/suspension Photoreactor, (ii) Trickle Bed continuous flow system and (iii) The Taylor flow Photoreactor with Au-Pd/TiO_2 was the central focused of this study and has been addressed in this PhD thesis. The research intends to develop a pilot waste water treatment plant which work with the principle of photocatalysis using both UV-Visible light source. Phenol is being used as probe molecule in aqueous solution. The plant was optimized for efficient wastewater treatment, which operates continually for 52h to obtain complete mineralization of phenol.

In addition, environmentally benign catalysis has been also focused on these studies. An area of heterogeneous catalysis including catalyst characterization, product analysis and validations, proposed reaction mechanisms and key reaction parameters for controlling

activity were briefly covered in this thesis. It is clear from the work outlined in the preceding chapters that the photocatalytic degradation of phenol was successfully carried out using heterogeneous Au and Pd based catalyst. In Chapter 4, a section was focused on the characterization of the Photocatalyst prepared. The formation of presence Au-Pd alloy in catalyst was confirmed by XRD, TEM/EDX, TPR and ICP-OES analysis, respectively and other techniques like BET, DRS, DRIFTS, and TPO were also used in the characterization of the catalyst. Preliminary experiments were done using the Slurry/Suspension batch mode using the transition metals doped TiO_2 to improve the photo-response and photocatalytic properties of the catalyst prepared, These was used as a guide to the reactor design and provide the comparison basis for the evaluation of the reactor in three simpler reactors including a Slurry/Suspension reactor, Trickle Bed reactor and Taylor flow continuous reactor. The Slurry/Suspension batch reactor was used to calculate rate of reactions in three types of Oxidant (i.e. compressed air, oxygen and hydrogen peroxide) and the quantum efficiencies of each catalyst prepared and also identifies the intermediates of phenol photocatalytic degradation by HPLC and GC/MS analysis and postulated the reaction mechanisms. Phenol is completely mineralized using the Taylor flow system with 0.5%Pd-TiO_2 and P25 in 12h and the catalysts remain stable for 52h without producing other stable intermediates products, whereas phenol photocatalytic degradation using the Slurry/suspension and Trickle Bed mode only shows partial mineralization which becomes a limitation of the heterogeneous photocatalytic degradation of phenol. Experimental results showed two orders of magnitude higher quantum efficiency and comparable overall rate constant with the 0.5%Pd-TiO_2 in oxygen with the Slurry reactor compared with the other bimetallic and their monometallic catalyst, which suggested that the palladium doped TiO_2 appropriately have potential in photocatalytic waste water treatment.

The presence of metal in metallic state especially Pd was identified to accelerate the photocatalytic decomposition of phenol subsequently increase the catalytic activity of palladium mono metallic catalyst. Synergistic effect of Au and Pd proof the enhancement of catalyst stability towards leaching compared to its photocatalytic activity when comparing to mono catalysts. Further the photoxidation of phenol with different Au/Pd metal ratio supported on TiO_2 in different oxidant was also studied to see effect of oxidant. This revealed that the addition of Pd to Au significantly enhance photo-response and stability toward deactivation towards leaching compare to the catalytic performance in the different oxidant by obtaining the same pattern in all reactions The effects of oxidant type, different metals dopant, and the phase transformation of TiO_2 (anatase and rutile) and the types of reactor design were investigated. The results showed that hydrogen peroxide is the best oxidant due to the dual role it is playing in the photocatalysis of phenol in generating the active radicals used in the oxidation reaction and also its ability to reduces recombination rate of the electron-hole pairs, but due to economic consideration oxygen was used to optimize the Taylor flow system, mass transfer effects could not be completely eliminated in the continuous mode due to the difference in phase between the oxygen and phenol solution.

The catalysts reusability was tested and it shows a good data when it does not change significantly in conversion during which 4 runs of the reaction was performed for the same catalyst. From this data, it is believed that the use of this catalyst is very useful because it can be reused many times in the photoreactor also when the TPO of the used catalyst was tested it shows that the carbons deposited on the catalyst surfaces can be regenerated at 350°C thus it is a good catalyst to be used in the wastewater treatment plant.

Using the Slurry/suspension mode a major problem was encountered with the process, the catalyst are leaching the active metals used in the modification of the TiO_2, addressing this challenge lead to structural modification of the catalyst by using the microemulsion methods to place the active metals within the core of the TiO_2 instead of the surface of the catalysts. The core shell 2%Pd@TiO_2 prepared was used both in the three types of reactors and in the different oxidants mentioned earlier.

The Taylor flow reactor was used to evaluate the rate of thermalcatalysis of phenol in the dark to test the viability of the wastewater treatment plant running for 24h by combining photocatalysis and thermal catalysis.

In a nut shell, this work produced a novel continuous flow micro photoreactor, which employed Taylor flow system designed to reduce the mass transfer limitation between oxygen gas and phenol solution, the reactor has the inherent advantages of a fixed-bed catalyst design to increase the reaction efficiencies over the Slurry batch reactor.

5.3 Recommendation for Future Work

Further investigations are possible for all fields explored in this thesis. Brief recommendation are shown below:

It was demonstrated in this study that supported Au-Pd nanoparticles catalysts were used to successfully oxidized phenol to CO_2 and water using hydrogen peroxide and oxygen as oxidant. However, it is important in the future study to utilize the effect of anions and cations on the same oxidant in the same reaction with the catalyst and it is possible to achieve by tuning the reaction conditions and morphology as well as characteristics of metal supported catalysts.

It has been proved in this study that Au-Pd supported catalysts are capable in oxidizing other aromatics compounds using oxygen. Therefore another step could be taken to further study the Au-Pd system for other aromatics products like pesticides.

The possible used of another characterization technique such as STEM could further help in identifying the nature of developed catalyst especially on Au-Pd supported systems, combination between STEM, XPS and XRD data might give a clear picture on any possible formation of alloy and also the average particle size of metal.

Concerning the kinetic aspect, the photodegradation by using TiO_2 or modified TiO_2 usually has the pseudo-first order kinetic based on the Langmuir-Hinshelwood law (LH). Hence, it is recommended that the substrate concentrations be varied and calculate the rate values in each concentration by plotting between 1/r and 1/c Then both the rate constant (k) and the adsorption equilibrium constant (K_{ad}) will be obtained (Sano *et al.,* 2008)

It has been proved in this study that the Taylor flow system is a good photo reactor for thermal catalysis of phenol, further study need to be done in simultaneous combination of photocatalysis and thermal catalysis which will also need some reactor modification.

In-depth research should be carried out to focus more on Taylor flow system by using other variables like phenol flow rate and oxygen flow rate and using the solar radiation.

REFERENCES

Adan, C., Coronado, J. M., Bellod, R., Soria, J., and Yamaoka, H. (2006). Photochemical and photocatalytic degradation of salicylic acid with hydrogen peroxide over TiO_2 SiO_2 fibres. *Applied Catalysis A: General, 303*(2), 199-206.

Adesina, A. (2004). Industrial exploitation of photocatalysis: progress, perspectives and prospects. *Catalysis Surveys from Asia, 8*(4), 265-273.

Ahmed, S., Rasul, M., Martens, W. N., Brown, R., and Hashib, M. (2010). Heterogeneous photocatalytic degradation of phenols in wastewater: A review on current status and developments. *Desalination, 261*(1-2), 3-18.

Al-Ekabi, H., and Serpone, N. (1988). Kinetics studies in heterogeneous photocatalysis. I. Photocatalytic degradation of chlorinated phenols in aerated aqueous solutions over titania supported on a glass matrix. *The Journal of Physical Chemistry, 92*(20), 5726-5731.

Al-Sayyed, G., D'Oliveira, J.-C., and Pichat, P. (1991). Semiconductor-sensitized photodegradation of 4-chlorophenol in water. *Journal of Photochemistry and Photobiology A: Chemistry, 58*(1), 99-114.

Arana, J., Martinez Nieto, J., Herrera Meli'an, J., Dona Rodriguez, J., Gonzalez Diaz, O., P'erez Pena, J., and M'endez, J. (2004). Photocatalytic degradation of formaldehyde containing wastewater from veterinarian laboratories. *Chemosphere, 55*(6), 893-904.

Armaroli, T., Becue, T., and Gautier, S. (2004). Diffuse reflection infrared spectroscopy (DRIFTS): Application to the in situ analysis of catalysts. *Oil and Gas Science and Technology, 59*(2), 215-237.

Asahi, R., Morikawa, T., Ohwaki, T., Aoki, K., and Taga, Y. (2001). Visible-light photocatalysis in nitrogen-doped titanium oxides. *Science, 293*(5528), 269-271.

Bansal, R. C., and Goyal, M. (2010). *Activated carbon adsorption.* New York: CRC press.

Barakat, M., Tseng, J., and Huang, C. (2005). Hydrogen peroxide-assisted photocatalytic oxidation of phenolic compounds. *Applied Catalysis B: Environmental, 59*(1-2), 99-104.

Basic Principle of Transmission Electron Microscope (2013). Retrieved December 4, 2013 from http://www.hk-phy.org/atomic_world/tem/tem02_e.html

Becker, D. L and Wilson, S. C (1978). The use of activated carbon for the treatment of pesticides and pesticidal wastes. *Carbon Adsorption Handbook*. Ann Arbor Science Publishers Inc, 5(1), 167-213.

Bernal, S., Botana, F., Calvino, J., Cauqui, M., Cifredo, G., Jobacho, A., and . Rodriguez-Izquierdo, J. (1993). Microstructural and chemical properties of ceria-supported rhodium catalysts reduced at 773 K. *The Journal of Physical Chemistry, 97*(16), 4118-4123.

Beydoun, D., Amal, R., Low, G., and McEvoy, S. (1999). Role of nanoparticles in photocatalysis. *Journal of Nanoparticle Research, 1*(4), 439-458.

Bideau, M., Claudel, B., Faure, L., and Kazouan, H. (1992). The photo-oxidation of propionic acid by oxygen in the presence of TiO_2 and dissolved copper ions. *Journal of Photochemistry and Photobiology A: Chemistry, 67*(3), 337-348.

Bloemer, M. J., Haus, J. W., and Ashley, P. R. (1990). Degenerate four-wave mixing in colloidal gold as a function of particle size. *JOSA B, 7*(5), 790-795.

Bowker, M. (1988). *The Basis and Application of Heterogeneous Catalysis.* (R. G. Compton, Ed.) Oxford Science Publications. England

Bradley, B. R., Daigger, G. T., Rubin, R., and Tchobanoglous, G. (2002). Evaluation of onsite wastewater treatment technologies using sustainable development criteria. *Clean Technologies and Environmental Policy, 4*(2), 87-99.

Braun, A. M., Maurette, M. T., and Oliveros, E. (1991). *Photochemical Technology*, Wiley, New York.

Brownson, J. R., Tejedor-Tejedor, M. I., and Anderson, M. A. (2005). Photoreactive anatase consolidation chracterized by FTIR spectroscopy. *Chemistry of Materials, 17*, 6304-6310.

Brunauer, S., Deming, L. S., Deming, W. E., and Teller, E. (1940). On a theory of the van der Waals adsorption of gases. *Journal of the American Chemical Society, 62*(7), 1723-1732.

Burns, A., Li, W., Baker, C., and Shah, S. I. (2001). Sol gel synthesis and characterization of neodymium-ion doped nanostructured titania thin films. *MRS Proceedings*, Cambridge University. (*703) V5-2.*

Carp, O., Huisman, C., and Reller, A. (2004). Photoinduced reactivity of titanium dioxide. *Progress In Solid State Chemistry, 32*(1), 33-177.

Cassano, A. E., and Alfano, O. M. (2000). Reaction engineering of suspended solid heterogeneous photocatalytic reactors. *Catalysis Today, 58*(2), 167-197.

Chan, C., Tao, S., Dawson, R., and Wong, P. K. (2004). Treatment of atrazine by integrating photocatalytic and biological processes. *Environmental Pollution, 131*(1), 45-54.

Chandrasekharan, N., and Kamat, P. V. (2000). Improving the photoelectrochemical performance of nanostructured TiO_2 films by adsorption of gold nanoparticles. *The Journal of Physical Chemistry B, 104*(46), 10851-10857.

Chatterjee, D., and Mahata, A. (2001). Photoassisted detoxification of organic pollutants on the surface modified TiO2 semiconductor particulate system. *Catalysis Communications, 2*(1), 1-3.

ChemBET-TPR/TPD Overview: Chemisorption Analyzer for Metal Area, TPR, TPO, TPD plus Metal BET surface Area. (2013). Retrieved June 30, 2013 from http://www.quantachrome.com/pdf_brochures/07118.pdf

Chen, S., and Liu, Y. (2007). Study on the photocatalytic degradation of glyphosate by TiO_2 photocatalyst. *Chemosphere, 67*(5), 1010-1017.

Chen, X., and Mao, S. S. (2007). Titanium dioxide nanomaterials: synthesis, properties, modifications, and applications. *Chemical Reviews, 107*(7), 2891-959.

Chin, S. S., Chiang, K., and Fane, A. G. (2006). The stability of polymeric membranes in a TiO_2 photocatalysis process. *Journal of Membrane Science, 275*(1), 202-211.

Chong, M. N., Jin, B., Chow, C. W., and Saint, C. (2010). Recent developments in photocatalytic water treatment technology: a review. *Water research, 44*(10), 2997-3027.

Chong, M. N., Jin, B., Zhu, H., Chow, C. W., and Saint, C. (2009). Application of {H--titanate} nanofibers for degradation of Congo Red in an annular slurry photoreactor. *Chemical Engineering Journal, 150*(1), 49-54.

Chorkendorff, I., and Niemantsverdriet, J. W. (2006). *Concepts of modern catalysis and kinetics.* Germany:Wiley-VcH.

Chun, H., Yizhong, W., and Hongxiao, T. (2000). Destruction of phenol aqueous solution by photocatalysis or direct photolysis. *Chemosphere, 41*(8), 1205-9.

Clarke, A. R., and Eberhardt, C. N. (2002). *Light Microscopy Techniques for Materials Science.* London: CRC Press.

Coates, J. (2000). *Interpretation of Infrared Spectra, A Practical Approach.* (R. Meyers, Ed.) John Wiley and Sons Ltd, Chichester.

Comninellis, C., Kapalka, A., Malato, S., Parsons, S. A., Poulios, I., and Mantzavinos, D. (2008). Advanced oxidation processes for water treatment: advances and trends for R&D. *Journal of Chemical Technology and Biotechnology, 83*(6), 769-776.

Cullity, B. (1978). *Elements of X-Ray Diffraction*. Massachusetts: Addison-Wesley Publishing Company, Inc:.

Cunningham, J., and Sedlak, P. (1994). Interrelationships between pollutant concentration, extent of adsorption, TiO_2-sensitized removal, photon flux and levels of electron or

hole trapping additives 1. aqueous monochlorophenol-TiO_2 P25 suspensions. *Journal of Photochemistry and Photobiology A: Chemistry*, *77*(2), 255-263.

Dagan, G., and Tomkiewicz, M. (1993). Titanium dioxide aerogels for photocatalytic decontamination of aquatic environments. *The Journal of Physical Chemistry*, *97*(49), 12651-12655.

Daneshvar, N., Salari, D., Niaei, A., and Khataee, A. (2006). Photocatalytic degradation of the herbicide erioglaucine in the presence of nanosized titanium dioxide: comparison and modeling of reaction kinetics. *Journal of Environmental Science and Health Part B*, *41*(8), 1273-1290.

Dick, D., Santos, J., and Ferranti, E. (2003). Chemical characterization and infrared spectroscopy of soil organic matter from two southern Brazilian soils. *Revista Brasileira de Ciencia do Solo*, *27*(1), 29-39.

Diebold, U. (2003). The surface science of titanium dioxide. *Surface Science Reports*, *48*(5-8), 53-229.

Dijkstra, M., Buwalda, H., De Jong, A., Michorius, A., Winkelman, J., and Beenackers, A. (2001). Experimental comparison of three reactor designs for photocatalytic water purification. *Chemical Engineering Science*, *56*(2), 547-555.

Dionysiou, D. D., Khodadoust, A. P., Kern, A. M., Suidan, M. T., Baudin, I., and Laine, J.-M. (2000). Continuous-mode photocatalytic degradation of chlorinated phenols and pesticides in water using a bench-scale TiO_2 rotating disk reactor. *Applied Catalysis B: Environmental*, *24*, 139-155.

Dobosz, A., and Sobczy'nski, A. (2003). The influence of silver additives on titania photoactivity in the photooxidation of phenol. *Water Research, 37*(7), 1489-1496.

Dutta, P. K., and Ray, A. K. (2004). Experimental investigation of Taylor vortex photocatalytic reactor for water purification. *Chemical engineering science, 59*(22), 5249-5259.

Egerton, R. F. (2005). *Physical principles of electron microscopy: an introduction to TEM, SEM, and AEM*. New York. Springer Science.

Erdei, L., Arecrachakul, N., and Vigneswaran, S. (2008). A combined photocatalytic slurry reactor--immersed membrane module system for advanced wastewater treatment. *Separation and Purification Technology, 62*(2), 382-388.

Esplugas, S., Gimenez, J., Contreras, S., Pascual, E., and Rodriguez, M. (2002). Comparison of different advanced oxidation processes for phenol degradation. *Water Research, 36*(4), 1034-1042.

Essam, T., Amin, M. A., El Tayeb, O., Mattiasson, B., and Guieysse, B. (2007). Sequential photochemical--biological degradation of chlorophenols. *Chemosphere, 66*(11), 2201-2209.

Farrauto, R., and Bartholomew, C. (1997). *Fundamentals of Industrial Catalytic Processes* (First ed.). London: *Black Academic and Professional* Chapmann and Hall.

FEI Tecnai G2 F20 TEM (2013). Retrieved March 18 2013, from http://www.fei.com/products/tem/tecnai/

Fornasiero, P., Kaspar, J., and Graziani, M. (1997). Redox Behavior of High-Surface-Area Rh-Loaded $Ce_{0.5}Zr_{0.5}O_2$ Mixed-Oxide. *Journal of Catalysis, 167*(2), 576-580.

Fujishima, A., Zhang, X., and Tryk, D. A. (2008). TiO_2 photocatalysis and related surface phenomena. *Surface Science Reports, 63*(12), 515-582.

Gao, Y., Masuda, Y., Seo, W. S., Ohta, H., and Koumoto, K. (2004). TiO_2 nanoparticles prepared using an aqueous peroxotitanate solution. *Ceramics International*. *30(7)*, 1365-1368.

Gaya, U. I., and Abdullah, A. H. (2008). Heterogeneous photocatalytic degradation of organic contaminants over titanium dioxide: A review of fundamentals, progress and problems. *Journal of Photochemistry and Photobiology C: Photochemistry Reviews, 9*(1), 1-12.

Gleckman, P., O'Gallagher, J., and Winston, R. (1989). Concentration of sunlight to solar-surface levels using non-imaging optics. *Nature, 339*(6221), 198-200.

Goldstein, J., Newbury, D. E., Joy, D. C., Lyman, C. E., Echlin, P., Lifshin, E., and Michael, J. R. (2003). *Scanning electron microscopy and X-ray microanalysis.* London: Springer Publisher.

Habibi, M. H., Hassanzadeh, A., and Mahdavi, S. (2005). The effect of operational parameters on the photocatalytic degradation of three textile azo dyes in aqueous TiO_2 suspensions. *Journal of Photochemistry and Photobiology A: Chemistry, 172*(1), 89-96.

Hadj Salah, N. B., and Boultif, A. (2004). Study of photocatalytic degradation of phenol. *Desalination, 166*, 347-354.

Halsey, G. (1948). Physical adsorption on non-uniform surfaces. *The Journal of Chemical Physics*, *16*(10), 931.

Hamill, C., Burch, R., Goguet, A., Rooney, D., Driss, H., Petrov, L., and Daous, M. (2014). Evaluation and Mechanistic Investigation of a AuPd alloy catalyst for the hydrocarbon selective catalytic reduction HC-SCR of NOx. *Applied Catalysis B: Environmental, 147*, 864-870.

Henderson, M. A. (2011). A surface science perspective on photocatalysis. *Surface Science Reports*, *66*(6), 185-297.

Hermann, J.-M. (2005). Heterogeneous photocatalysis: state of the art and present applications. *Topics in Catalysis, 34*(1-4), 49-65.

Herrmann, J. M. (1999). Heterogeneous photocatalysis: fundamentals and applications to the removal of various types of aqueous pollutants. *Catalysis today*, *53*(1), 115-129.

Higson, S. P. (2004). *Analytical Chemistry.* Oxford University Press.

Hoffmann, M. R., Martin, S. T., Choi, W., and Bahnemann, D. W. (1995). Environmental applications of semiconductor photocatalysis. *Chemical reviews*, *95*(1), 69-96.

Hong, S.-S., Ju, C.-S., Lim, C.-G., Ahn, B.-H., Lim, K.-T., and Lee, G.-D. (2001). A photocatalytic degradation of phenol over TiO_2 prepared by sol gel method. *Journal of Industrial and Engineering Chemistry*, *7*(2), 99-104.

Hossain, M., Raupp, G. B., Hay, S. O., Obee, T. N., and others. (1999). Three--dimensional developing flow model for photocatalytic monolith reactors. *AIChE Journal*, *45*(6), 1309-1321.

Hu, C., Tang, Y., Jiang, Z., Hao, Z., Tang, H., and Wong, P. K. (2003). Characterization and photocatalytic activity of noble-metal-supported surface TiO_2/SiO_2. *Applied Catalysis A: General, 253*(2), 389-396.

Huang, C.-R., and Shu, H.-Y. (1995). The reaction kinetics, decomposition pathways and intermediate formations of phenol in ozonation, UV/O_3 and UV/H_2O_2 processes. *Journal of Hazardous Materials, 41*(1), 47-64.

Hugul, M., Apak, R., and Demirci, S. (2000). Modeling the kinetics of UV/Hydrogen peroxide oxidation of some mono-, di-, and trichlorophenols. *Journal of Hazardous Materials, 77*(1), 193-208.

Hussain, S. T., and Siddiqa, A. (2011). Iron and chromium doped titanium dioxide nanotubes for the degradation of environmental and industrial pollutants. *International Journal of Environmental Science Technology., 8*(2), 351-362.

Ilisz, A., and La, Z. (1999). Investigation of the photodecomposition of phenol in near UV irradiated aqueous TiO_2 suspensions . I : Effect of charge-trapping species on the degradation kinetics. *Applied Catalysis A: General, 180*, 25-33.

Ismail, A. A., Bahnemann, D. W., Bannat, I., and Wark, M. (2009). Gold nanoparticles on mesoporous interparticle networks of titanium dioxide nanocrystals for enhanced photonic efficiencies. *The Journal of Physical Chemistry C, 113*(17), 7429-7435.

Jackson, S. D., and Hargreaves, J. S. (2009). *Metal oxide catalysis*. Weinheim: Wiley-VCH

Jang, J. S., Choi, S. H., Kim, H. G., and Lee, J. S. (2008). Location and state of Pt in platinized CdS/TiO_2 photocatalysts for hydrogen production from water under visible light. *The Journal of Physical Chemistry C, 112*(44), 17200-17205.

Jentoft, F. C. (2009). Ultraviolet-Visible-Near Infrared Spectroscopy in Catalysis: Theory, Experiment, Analysis, and Application Under Reaction Conditions. *Advances in catalysis, 52,* 129-211.

Jere, G. V., and Patel, C. C. (1962). Infrared absorption studies on peroxy titanium sulphate. *Canadian Journal of Chemistry 40(8),* 1576-1578.

Kamat, P. V., and Meisel, D. (2002). Nanoparticles in advanced oxidation processes. *Current Opinion in Colloid and Interface Science, 7*(5), 282-287.

Kaneko, M., and Okura, I. (2002). *Photocatalysis: science and technology*. Tokyo: Springer.

Kar, R., Gupta, O., Mandol, K., and Bhattacharjee, S. (2013). Performance Study on Photocatalysis of Phenol Solution in a UV Irradiated Reactor. *Journal of Chemical Engineering and Process Technology, 4*(143), 1-7.

Karvinen, S., and Lamminmaki, R.-J. (2003). Preparation and characterization of mesoporous visible--light--active anatase. *Solid State Sciences, 5*(8), 1159-1166.

Kato, S., Hirano, Y., Iwata, M., Sano, T., Takeuchi, K., and Matsuzawa, S. (2005). Photocatalytic degradation of gaseous sulfur compounds by silver-deposited titanium dioxide. *Applied Catalysis B: Environmental, 57*(2), 109-115.

Khezrianjoo, S., and Revanasiddappa, H. (2012). Langmuir-Hinshelwood kinetic expression for the photocatalytic degradation of Metanil Yellow aqueous solutions by ZnO catalyst. *Chemical Sciences Journal, 85*, 1-8.

Khlebtsov, N. G., Bogatyrjov, V. A., Dykman, L. A., and Melnikov, A. G. (1996). Spectral properties of coloidal gold and its conjugates with biospecific macromolecules.

Proceedings for International Society for Optics and Photonics *BiOS Europe'95*, (pp. 35-45).

Khoshhesab, Z. M. (2012). *Reflectance IR Spectroscopy, Infrared Spectroscopy - Materials Science, Engineering and Technology,*. (T. Theophile, Ed.) InTech.

Kim, J., Choi, W., and Park, H. (2010). Effects of TiO_2 surface fluorination on photocatalytic degradation of methylene blue and humic acid. *Research on Chemical Intermediates, 36*(2), 127-140.

Kiselev, A. (1968). Adsorption properties of hydrophobic surfaces. *Journal of Colloid and Interface Science, 28*(3), 430-442.

Kolen'ko, Y. V., Kovnir, K. A., Gavrilov, A. I., Garshev, A. V., Frantti, J., Lebedev, O. I., and Yoshimura, M. (2006). Hydrothermal synthesis and characterization of nanorods of various titanates and titanium dioxide. *The Journal of Physical Chemistry B, 110*(9), 4030-4038.

Kondarides, D. I. (2010). *Photocatalysis in Catalysis.* (G. Centi, Ed.) UNESCO, EOLSS Oxford UK. Pp 15-30.

Kormann, C., Bahnemann, D. W., and Hoffmann, M. R. (1988). Preparation and characterization of quantum--size titanium dioxide. *The Journal of Physical Chemistry, 92*(18), 5196-5201.

Korosi, L., Papp, S., Bert'oti, I., and D'ek'any, I. (2007). Surface and bulk composition, structure, and photocatalytic activity of phosphate-modified TiO2. *Chemistry of Materials, 19*(19), 4811-4819.

Kowalska, E., Mahaney, O. O., Abe, R., and Ohtani, B. (2010). Visible-light-induced photocatalysis through surface plasmon excitation of gold on titania surfaces. *Physical Chemistry Chemical Physics, 12*(10), 2344-2355.

Kratschmer, W., Rathousky, J., and Zukal, A. (1999). Adsorption of krypton at 77K on fullerene C60, graphitized carbon black and diamond. *Carbon, 37*(2), 301-305.

Kubelka, P., and Munk, F. (1931). An article on optics of paint layers. *Z. Tech. Phys, 12*, 593-601.

Kutty, T., and Ahuja, S. (1995). Retarding effect of surface hydroxylation on titanium (IV) oxide photocatalyst in the degradation of phenol. *Materials Research Bulletin, 30*(2), 233-241.

Laoufi, N., Tassalit, D., and Bentahar, F. (2008). The degradation of phenol in water solution by TiO2 photocatalysis in a helical reactor. *Global NEST Journal, 10*(3), 404-418.

Lapena, L., Cerezo, M., and Garcia-Augustin, P. (1995). Possible reuse of treated municipal wastewater for Citrus spp. plant irrigation. *Bulletin of Environmental Contamination and Toxicology, 55*(5), 697-703.

Legrini, O., Oliveros, E., and Braun, A. (1993). Photochemical processes for water treatment. *Chemical Reviews, 93*(2), 671-698.

Leofanti, G., Tozzola, G., Padovan, M., Petrini, G., Bordiga, S., and Zecchina, A. (1997). Catalyst characterization: characterization techniques. *Catalysis Today, 34*(3-4), 307-327.

Leytner, S., and Hupp, J. T. (2000). Evaluation of the energetics of electron trap states at the nanocrystalline titanium dioxide/aqueous solution interface via time-resolved photoacoustic spectroscopy. *Chemical Physics Letters, 330*(3), 231-236.

Lide, D. E. (1993). *CRC Handbook of Chemistry and Physics.* (73 ed.). New York: CRC Press.

Lifka, J., Ondruschka, B., and Hofmann, J. (2003). The use of ultrasound for the degradation of pollutants in water: aquasonolysis-a review. *Engineering in Life Sciences, 3*(6), 253-262.

Lin, W., Herzing, A., Kiely, C., and Wachs, I. (2008). Probing metal--support interactions under oxidizing and reducing conditions: in situ Raman and infrared spectroscopic and scanning transmission electron microscopic-X-ray energy-dispersive spectroscopic investigation of supported platinum catalysts. *The Journal of Physical Chemistry C, 112*(15), 5942-5951.

Linsebigler, A. L., Lu, G., and Yates, J. T. (1995). Photocatalysis on TiO_2 Surfaces: Principles, Mechanisms, and Selected Results. *Chemical Reviews, 95*, 735-758.

Litter, M. I. (1999). Heterogeneous photocatalysis: transition metal ions in photocatalytic systems. *Applied Catalysis B: Environmental, 23*(2), 89-114.

Liu, L., Chen, F., Yang, F., Chen, Y., and Crittenden, J. (2012). Photocatalytic degradation of 2, 4-dichlorophenol using nanoscale Fe/TiO_2. *Chemical Engineering Journal, 181*, 189-195.

Loganathan, K., Bommusamy, P., Muthaiahpillai, P., and Velayutham, M. (2011). The Syntheses, Characterizations, and Photocatalytic Activities of Silver, Platinum, and

Gold Doped TiO 2 Nanoparticles. *Environmental Engineering Research, 16*(2), 81-90.

Maicu, M., Hidalgo, M., Col'on, G., and Nav'io, J. (2011,). Comparative study of the photodeposition of Pt, Au and Pd on pre-sulphated TiO_2 for the photocatalytic decomposition of phenol. *Journal of Photochemistry and Photobiology A: Chemistry, 217*(2-3), 275-283.

Malato, S., Fernandez-Ibanez, P., Maldonado, M. I., Blanco, J., and Gernjak, W. (2009). Decontamination and disinfection of water by solar photocatalysis: Recent overview and trends. *Catalysis Today, 147*(1), 1-59.

Mangrulkar, P. A., Kamble, S. P., Joshi, M. M., Meshram, J. S., Labhsetwar, N. K., and Rayalu, S. S. (2011). Photocatalytic degradation of phenolics by N-doped mesoporous titania under solar radiation. *International Journal of Photoenergy, 2012*.

Marugan, J., Aguado, J., Gernjak, W., and Malato, S. (2007). Solar photocatalytic degradation of dichloroacetic acid with silica--supported titania at pilot--plant scale. *Catalysis Today, 129*(1), 59-68.

Matatov-meytal, Y. I., and Sheintuch, M. (1998). Catalytic Abatement of Water Pollutants. *Industrial and Engineering Chemistry Research, 5885*(97), 309-326.

Matsumoto, Y. (1996). Energy positions of oxide semiconductors and photocatalysis with iron complex oxides. *Journal of Solid State Chemistry, 126*(2), 227-234.

Matthews, R. W. (1990). Purification of water with near-UV illuminated suspensions of titanium dioxide. *Water Research, 24*(5), 653-660.

Mccullagh, C. A. (2011). Photocatalytic reactors for environmental remediation: a review. *Journal of Chemical Technology and Biotechnology, 86*(8), 1002-1017.

Mehrotra, K., Yablonsky, G. S., and Ray, A. K. (2003). Kinetic studies of photocatalytic degradation in a TiO_2 slurry system: Distinguishing working regimes and determining rate dependences. *Industrial and Engineering Chemistry Research, 42*(11), 2273-2281.

Mehrvar, M., Anderson, W. A., and Moo-Young, M. (2002). Preliminary analysis of a tellerette packed-bed photocatalytic reactor. *Advances in Environmental Research, 6*(4), 411-418.

Meli'an, E. P., Diaz, O. G., Rodriguez, J., Col'on, G., Navio, J., Macias, M., and Pena, J. P. (2012). Effect of deposition of silver on structural characteristics and photoactivity of TiO_2-based photocatalysts. *Applied Catalysis B: Environmental, 127*, 112-120.

Micromeritics Instrument Corporation, AutoChem 2910 Operator's Manual. (1999). Pp 30-55

Mills, A., Davies, R. H., and Worsley, D. (1993). Water purification by semiconductor photocatalysis. *Chemical Society Reviews, 22*(6), 417-425.

Mogyorosi, K., Farkas, A., Dekany, I., Ilisz, I., and Dombi, A. (2002). TiO_2-based photocatalytic degradation of 2-chlorophenol adsorbed on hydrophobic clay. *Environmental science and technology, 36*(16), 3618-3624.

Mohseni, M. (2005). Gas phase trichloroethylene (TCE) photooxidation and byproduct formation: photolysis vs. titania/silica based photocatalysis. *Chemosphere, 59*(3), 335-342.

Mokrini, A., Ousse, D., and Esplugas, S. (1997). Oxidation of aromatic compounds with UV radiation/ozoneihydrogen peroxide. *Water Science and Technology, 35*(4), 95-102.

Mrowetz, M., and Selli, E. (2006). Photocatalytic degradation of formic and benzoic acids and hydrogen peroxide evolution in TiO_2 and ZnO water suspensions. *Journal of photochemistry and photobiology A: Chemistry, 180*(1), 15-22.

Muruganandham, M., and Swaminathan, M. (2006). Photocatalytic decolourisation and degradation of Reactive Orange 4 by TiO_2/ UV process. *Dyes and pigments, 68*(2), 133-142.

Nam, W., Kim, J., and Han, G. (2002). Photocatalytic oxidation of methyl orange in a three phase fluidized bed reactor. *Chemosphere, 47*(9), 1019-1024.

Ni, M., Leung, M. K., Leung, D. Y., and Sumathy, K. (2007). A review and recent developments in photocatalytic water-splitting using TiO_2 for hydrogen production. *Renewable and Sustainable Energy Reviews, 11*(3), 401-425.

Nickheslat, A., Amin, M. M., Izanloo, H., Fatehizadeh, A., and Mousavi, S. M. (2013). Phenol photocatalytic degradation by advanced oxidation process under ultraviolet radiation using titanium dioxide. *Journal of Environmental and Public Health*, 815310.

Niemantsverdriet, J. W. (2007). *Spectroscopy in catalysis An Introduction.* Germany: Wiley-VCH

Nosaka, Y., and Fox, M. A. (1988). Kinetics for electron transfer from laser-pulse irradiated colloidal semiconductors to adsorbed methylviologen: dependence of the quantum yield on incident pulse width. *The Journal of Physical Chemistry, 92*(7), 1893-1897.

Nozik, A. J., and Memming, R. (1996). Physical chemistry of semiconductor-liquid interfaces. *The Journal of Physical Chemistry, 100*(31), 13061-13078.

Ochuma, I. J., Fishwick, R. P., Wood, J., and Winterbottom, J. M. (2007). Optimisation of degradation conditions of 1, 8-diazabicyclo [5.4. 0] undec-7-ene in water and reaction kinetics analysis using a cocurrent downflow contactor photocatalytic reactor. *Applied Catalysis B: Environmental, 73*(3), 259-268.

Ohde, H., Wai, C. M., Kim, H., Kim, J., and Ohde, M. (2002). Hydrogenation of olefins in supercritical CO_2 catalyzed by palladium nanoparticles in a water-in-CO_2 microemulsion. *Journal of the American Chemical Society, 124*(17), 4540-1.

Ohtani, B., Ogawa, Y., and Nishimoto, S.-i. (1997). Photocatalytic activity of amorphous-anatase mixture of titanium(IV) Oxide particles suspended in aqueous solutions. *The Journal of Physical Chemistry B, 101*(19), 3746-3752.

Ollis, D. F., Pelizzetti, E., and Serpone, N. (1991). Photocatalyzed Destruction of water contaminants. *Enviromental Science Technology, 25*(9), 1522-1529.

Ollis, D. P. (1989). *Photocatalysis: Fundamentals and applications;*. Wiley: New York.

Ozkaya, B. (2006). Adsorption and desorption of phenol on activated carbon and a comparison of isotherm models. *Journal of Hazardous Materials, 129*(1), 158-163.

Palmisano, G., Addamo, M., Augugliaro, V., Caronna, T., Di Paola, A., Lopez, E. G., and Schiavello, M. (2007). Selectivity of hydroxyl radical in the partial oxidation of aromatic compounds in heterogeneous photocatalysis. *Catalysis today, 122*(1), 118-127.

Panayotov, D., and Yates Jr, J. (2003). Electron exchange on TiO_2-SiO_2 photocatalysts during Oxygen and organic molecule adsorption--the role of adsorbate electrophilicity. *Chemical Physics Letters, 381*(1), 154-162.

Parida, K., and Parija, S. (2006). Photocatalytic degradation of phenol under solar radiation using microwave irradiated zinc oxide. *Solar Energy, 80*(8), 1048-1054.

Park, H., and Choi, W. (2004). Effects of TiO_2 Surface Fluorination on Photocatalytic reactions and Photoelectrochemical behaviors. *Journal of Physical Chemistry B, 108*(13), 4086-4093.

Park, H., Park, Y., Kim, W., and Choi, W. (2013). Surface modification of TiO_2 photocatalyst for environmental applications. *Journal of Photochemistry and Photobiology C: Photochemistry Reviews, 15*, 1-20.

Peill, N. J., and Hoffmann, M. R. (1995). Development and optimization of a TiO_2-coated fiber-optic cable reactor: photocatalytic degradation of 4-chlorophenol. *Environmental Science and Technology, 29*(12), 2974-2981.

Pelizzetti, E., Carlin, V., Minero, C., and Gratzel, M. (1991). Enhancement of the rate of photocatalytic degradation on TiO_2 of 2-chlorophenol, 2, 7-dichlorodibenzodioxin and atrazine by inorganic oxidizing species. *New journal of chemistry, 15*(5), 351-359.

Perrichon, V., Retailleau, L., Bazin, P., Daturi, M., and Lavalley, J. (2004). Metal dispersion of CeO_2-ZrO_2 supported platinum catalysts measured by H_2 or CO chemisorption. *Applied Catalysis A: General, 260*(1), 1-8.

Petrovic, M., Radjenovic, J., and Barcelo, D. (2011). ADVANCED OXIDATION PROCESSES (AOPs) APPLIED FOR WASTEWATER AND DRINKING WATER TREATMENT. ELIMINATION OF PHARMACEUTICALS. *The Holistic Approach to Environment, 1*(2), 63-74.

Porter, J. F., Li, Y.-G., and Chan, C. K. (1999). The effect of calcination on the microstructural characteristics and photoreactivity of Degussa P25 TiO_2. *Journal of Materials Science, 34*(7), 1523-1531.

Primo, A., Corma, A., and Garc'ia, H. (2011). Titania supported gold nanoparticles as photocatalyst. *Physical Chemistry Chemical Physics, 13*(3), 886-910.

Quanta Scanning Electron Microscope FEI Quanta 650. (2013). Retrieved March, 16 2013, from http://www.fei.com/products/sem/inspect/

Rahman, M. A., and Muneer, M. (2005). Photocatalysed degradation of two selected pesticide derivatives, dichlorvos and phosphamidon, in aqueous suspensions of titanium dioxide. *Desalination, 181*(1), 161-172.

Rahmani, A., Samadi, M., and Enayati Moafagh, A. (2008). Investigation of photocatalytic degradation of phenol by UV/TiO_2 process in aquatic solutions. *Journal of Research in Health Sciences, 8*(2), 55-60.

Raj, K. J., Ramaswamy, A., and Viswanathan, B. (2009). Surface area, pore size, and particle size engineering of titania with seeding technique and phosphate modification. *The Journal of Physical Chemistry C, 113*(31), 13750-13757.

Ray, A. K., and Beenackers, A. A. (1997). Novel swirl flow reactor for kinetic studies of semiconductor photocatalysis. *AIChE journal, 43*(10), 2571-2578.

Reimer, L. (1998). *Scanning electron microscopy : physics of image formation and microanalysis.* New York: Springer.

Rengaraj, S., and Li, X. (2006). Enhanced photocatalytic activity of TiO_2 by doping with Ag for degradation of 2, 4, 6-trichlorophenol in aqueous suspension. *Journal of Molecular Catalysis A: Chemical, 243*(1), 60-67.

Richardson, S. D. (2008). Environmental mass spectrometry: emerging contaminants and current issues. *Analytical chemistry, 80*(12), 4373-4402.

Rincon, A.-G., and Pulgarin, C. (2005). Use of coaxial photocatalytic reactor (CAPHORE) in the TiO_2 photo-assisted treatment of mixed E. coli and Bacillus sp. and bacterial community present in wastewater. *Catalysis Today, 101*(3), 331-344.

Robert, D., and Malato, S. (2002). Solar photocatalysis: a clean process for water detoxification. *Science of the Total Environment, 291*(1), 85-97.

Rycenga, M., Cobley, C. M., Zeng, J., Li, W., Moran, C. H., Zhang, Q., and Xia, Y. (2011). Controlling the synthesis and assembly of silver nanostructures for plasmonic applications. *Chemical Reviews, 111*(6), 3669-3712.

Safarzadeh-Amiri, A. (2001). O_3/H_2O_2 treatment of methyl-tert-butyl ether (MTBE) in contaminated waters. *Water Research, 35*(15), 3706-3714.

Salasc, S., Perrichon, V., Primet, M., and Mouaddib-Moral, N. (2002). Titration by oxygen of the spill-over hydrogen adsorbed on ceria--zirconia supported palladium--rhodium catalysts. *Journal of Catalysis, 206*(1), 82-90.

Samantaray, S. K., Mohapatra, P., and Parida, K. (2003). Physico-chemical characterisation and photocatalytic activity of nanosized SO_4/TiO_2 towards degradation of 4-nitrophenol. *Journal of Molecular Catalysis A: Chemical, 198*(1), 277-287.

San, N., Hatipoglu, A., Kocct"urk, G., and CCinar, Z. (2001). Prediction of primary intermediates and the photodegradation kinetics of 3-aminophenol in aqueous TiO_2 suspensions. *Journal of Photochemistry and Photobiology A: Chemistry, 139*(2), 225-232.

Sanchez, B., Gross, M. S., Costa, B. D., and Querini, C. A. (2009). Coke analysis by temperature-programmed oxidation: Morphology characterization. *Applied Catalysis A: General, 364*(1-2), 35-41.

Sanchez-Dominguez, M., Boutonnet, M., and Solans, C. (2009). A novel approach to metal and metal oxide nanoparticle synthesis: the oil-in-water microemulsion reaction method. *Journal of Nanoparticles Research, 11*, 1823–1829.

Sano, T., Puzenat, E., Guillard, C., Geantet, C., and Matsuzawa, S. (2008). Degradation of C2H2 with modified-TiO2 photocatalysts under visible light irradiation. *Journal of Molecular Catalysis A: Chemical, 284*(1), 127-133.

Saquib, M., and Muneer, M. (2003). TiO_2-mediated photocatalytic degradation of a triphenylmethane dye (gentian violet), in aqueous suspensions. *Dyes and Pigments, 56*(1), 37-49.

Saravanan, P., Pakshirajan, K., and Saha, P. (2009). Degradation of phenol by TiO_2 based heterogeneousphotocatalysts in presence of sunlight. *Journal of Hydro-environment Research, 3*(1), 45-50.

Satterfield, C. N. (1980). *Heterogeneous catalysis in practice.* New York: McGraw Hill Company.

Sauer, T., Cesconeto Neto, G., Jose, H., and Moreira, R. (2002). Kinetics of photocatalytic degradation of reactive dyes in a TiO2 slurry reactor. *Journal of Photochemistry and Photobiology A: Chemistry, 149*(1), 147-154.

Schematic of TGA/DSCI. (2012). Retrieved October, 26 2013 from http://uk.mt.com/gb/en/home/products/Laboratory_Analytics_Browse/TA_Family_Browse/TGA.html

Sclafani, A. P., and Schiavello, M. (1992). Photoreduction of Dinitrogen and photooxidation of Phenol and Nitrophenol isomers as examples of heterogeneous photocatalytic reactions. *Research on Chemical Intermediates, 18,* 211-226.

Sczechowski, J. G., Koval, C. A., and Noble, R. D. (1995). A Taylor vortex reactor for heterogeneous photocatalysis. *Chemical Engineering Science, 50*(20), 3163-3173.

Serpone, N., and Salinaro, A. (1999). Terminology, relative photonic efficiencies and quantum yields in heterogeneous photocatalysis. Part I: Suggested protocol. *Pure and applied chemistry, 71*(2), 303-320.

Shifu, C., and Gengyu, C. (2005). Photocatalytic degradation of organophosphorus pesticides using floating photocatalyst TiO_2-SiO_2/beads by sunlight. *Solar Energy, 79*(1), 1-9.

Sing, K., Everett, D., Haul, R., Moscou, L., Pierotti, R., Rouquerol, J., and Siemieniewska, T. (1985). International Union Of Pure Commission On Colloid And Surface Chemistry Including Catalysis : Reporting Physisorption Data For Gas / Solid

Systems with Special Reference to the Determination of Surface Area and Porosity. *Pure and Applied Chemistry*, *57*(4), 603-619.

Singh, H. K., Saquib, M., Haque, M. M., Muneer, M., and Bahnemann, D. W. (2007). Titanium dioxide mediated photocatalysed degradation of phenoxyacetic acid and 2, 4, 5--trichlorophenoxyacetic acid, in aqueous suspensions. *Journal of Molecular Catalysis A: Chemical, 264*(1), 66-72.

Skoog, D. A., Holler, F. J., and Nieman, T. A. (1998). *Principles of instrumental analysis.* Saunders College Publication. Philadelphia,

Sobczynski, A., Duczmal, L., and Zmudzinski, W. (2004). Phenol destruction by photocatalysis on TiO_2: an attempt to solve the reaction mechanism. *Journal of molecular catalysis A: chemical, 213*(2), 225-230.

Sonawane, R., and Dongare, M. (2006). Sol-gel synthesis of Au/TiO_2 thin films for photocatalytic degradation of phenol in sunlight. *Journal of Molecular Catalysis A: Chemical, 243*(1), 68-76.

Song, K. C., and Pratsinis, S. E. (2000). The effect of alcohol solvents on the porosity and phase composition of titania. *Journal of Colloid and Interface Science, 231*(2), 289-298.

Su, R., Tiruvalam, R., He, Q., Dimitratos, N., Kesavan, L., Hammond, C., and Besenbacher, F. (2012). Promotion of Phenol Photodecomposition over TiO_2 Using Au, Pd and Au-Pd Nanoparticles. *ACS nano*, *6*(7), 6284-6292.

Suarez, S., Carballa, M., Omil, F., and Lema, J. M. (2008). How are pharmaceutical and personal care products (PPCPs) removed from urban wastewaters. *Reviews in Environmental Science and Biotechnology, 7*(2), 125-138.

Subramanian, V., Pangarkar, V., and Beenackers, A. M. (2000). Photocatalytic degradation of para--hydroxybenzoic acid: Relationship between substrate adsorption and photocatalytic degradation. *Clean Products and Processes, 2*(3), 149-156.

Subramanian, V., Wolf, E. E., and Kamat, P. V. (2004). Catalysis with TiO_2/gold nanocomposites. Effect of metal particle size on the Fermi level equilibration. *Journal of the American Chemical Society, 126*(15), 4943-4950.

Subramanian, V., Wolf, E., and Kamat, P. V. (2001). Semiconductor-metal composite nanostructures. To what extent do metal nanoparticles improve the photocatalytic activity of TiO_2 films? *The Journal of Physical Chemistry B, 105*(46), 11439-11446.

Sun, J., Wang, X., Sun, J., Sun, R., Sun, S., and Qiao, L. (2006). Photocatalytic degradation and kinetics of Orange G using nano-sized Sn(IV)/TiO_2/AC photocatalyst. *Journal of molecular catalysis A: Chemical, 260*(1), 241-246.

Takeda, N., Torimoto, T., Sampath, S., Kuwabata, S., and Yoneyama, H. (1995). Effect of inert supports for titanium dioxide loading on enhancement of photodecomposition rate of gaseous propionaldehyde. *The Journal of Physical Chemistry, 99*(24), 9986-9991.

Tanaka, K., Capule, M. F., and Hisanaga, T. (1991). Effect of crystallinity of TiO_2 on its photocatalytic action. *Chemical Physics Letters, 187*(1), 73-76.

Torimoto, T., Ito, S., Kuwabata, S., and Yoneyama, H. (1996). Effects of adsorbents used as supports for titanium dioxide loading on photocatalytic degradation of propyzamide. *Environmental science and technology, 30*(4), 1275-1281.

Toxicological profile for phenol. Updated version. (1998). Agency for Toxic Substances and Disease Registry. Retrieved November 16, 2013 from http://www.atsdr.cdc.gov/toxprofiles/tp115-p.pdf.

Tryba, B., Morawski, A. W., Inagaki, M., and Toyoda, M. (2006). The kinetics of phenol decomposition under UV irradiation with and without H_2O_2 on TiO_2, Fe-TiO_2 and Fe-C-TiO2 photocatalysts. *Applied catalysis. B, Environmental, 63*(3-4), 215-221.

Venkatadri, R., and Peters, R. W. (1993). Chemical oxidation technologies: ultraviolet light/hydrogen peroxide, Fenton's reagent, and titanium dioxide assisted photocatalysis. *Hazardous Waste and Hazardous Materials, 10*(2), 107-149.

Viessman Jr., W., and Hammer, M. (1998). *Water Supply and Pollution Control* (sixth ed. ed.). Addison Wesley Longman Inc, California .

Vincent, G., Marquaire, P.-M., and Zahraa, O. (2008). Abatement of volatile organic compounds using an annular photocatalytic reactor: Study of gaseous acetone. *Journal of Photochemistry and Photobiology A: Chemistry, 197*(2), 177-189.

Vinodgopal, K., Wynkoop, D. E., and Kamat, P. V. (1996). Environmental photochemistry on semiconductor surfaces: photosensitized degradation of a textile azo dye, acid orange 7, on TiO_2 particles using visible light. *Environmental Science and Technology, 30*(5), 1660-1666.

Wan, Y. H., Wang, X. D., and Zhang, X. J. (1997). Treatment of high concentration phenolic waste water by liquid membrane with N_50_3 as mobile carrier. *Journal of Membrane Science, 135*(2), 263-270.

Wang, K.-H., Hsieh, Y.-H., Chou, M.-Y., and Chang, C.-Y. (1999). Photocatalytic degradation of 2-chloro and 2--nitrophenol by titanium dioxide suspensions in aqueous solution. *Applied Catalysis B: Environmental, 21*(1), 1-8.

Wanke, S. E., and Flynn, P. C. (1975). The sintering of supported metal catalysts. *Catalysis Reviews, 12*(1), 93-135.

Weckhuysen, B. M. (2004). *In-situ spectroscopy of catalysts.* Califonia: American Scientific Publishers.

Weckhuysen, B. M., and Schoonheydt, R. A. (1999). Recent progress in diffuse reflectance spectroscopy of supported metal oxide catalysts. *Catalysis Today, 49*(4), 441-451.

Weckhuysen, B. M., Van Der Voort, P., and Catana, G. (2000). *Spectroscopy of transition metal ions on surfaces.* Belgium: Leuven University Press.

Wen-Yu, W., and Ku, Y. (2007). Effect of solution pH on the adsorption and photocatalytic reaction behaviors of dyes using TiO2 and Nafion-coated TiO_2. *Colloids and Surfaces A: Physicochemical and Engineering Aspects, 302*(1), 261-268.

Wijngaarden, R., Kronberg, A., and Westerterp, K. (1998). *Industrial Catalysis: Optimizing Catalysts and Processes.* New York:Wiley Pp 1-17.

Wintgens, T., Salehi, F., Hochestrat, R., and Melin, T. (2008). Emerging contaminants and treatment options in water recycling for indirect potable use. *Water Science and Technology, 57*(1), 99-108.

Xiao, F., Tsuru, K., Hayakawa, S., and Osaka, A. (2003). In vitro apatite deposition on titania film derived from chemical treatment of Ti substrates with an oxysulfate solution containing hydrogen peroxide at low temperature. *Thin Solid Films, 441*(1), 271-276.

Yang L, L. G. (2000). Effects of surface resonance state on the plasmon resonance absorption of Ag nanoparticles embedded in partially oxidized amorphous Si matrix. *Applied Physics Letters., 76*, 1537-1539.

Yang, L., and Liu, Z. (2007). Study on light intensity in the process of photocatalytic degradation of indoor gaseous formaldehyde for saving energy. *Energy Conversion and management, 48*(3), 882-889.

Yu, H., Quan, X., Chen, S., and Zhao, H. (2007). TiO_2-multiwalled carbon nanotube heterojunction arrays and their charge separation capability. *The Journal of Physical Chemistry C, 111*(35), 12987-12991.

Yu, H., Wang, X., Sun, H., and Huo, M. (2010). Photocatalytic degradation of malathion in aqueous solution using an Au-Pd-TiO_2 nanotube film. *Journal of hazardous Materials, 184*(1-3), 753-8.

Yu, J., Zhao, X., and Zhao, Q. (2000). Effect of surface structure on photocatalytic activity of TiO_2 thin films prepared by sol-gel method. *Thin solid films, 379*(1), 7-14.

Yu, X., Wang, Y., Meng, X., and Yang, J. (2013). Preparation and characterization of Pd/N codoped TiO_2 photocatalysts with high visible light photocatalytic activity. *Chinese Journal of Catalysis, 34*(7), 1418-1428.

Yu, Y., Yu, J. C., Chan, C.-Y., Che, Y.-K., Zhao, J.-C., Ding, L., and Wong, P.-K. (2005). Enhancement of adsorption and photocatalytic activity of TiO_2 by using carbon nanotubes for the treatment of azo dye. *Applied Catalysis B: Environmental, 61*(1), 1-11.

Zazo, J., Casas, J., Mohedano, A., Gilarranz, M., and Rodriguez, J. (2005). Chemical pathway and kinetics of phenol oxidation by Fenton's reagent. *Environmental Science and Technology, 39*(23), 9295-9302.

Zhang, D., Qiu, R., Song, L., Eric, B., Mo, Y., and Huang, X. (2009). Role of oxygen active species in the photocatalytic degradation of phenol using polymer sensitized TiO_2 under visible light irradiation. *Journal of Hazardous Materials, 163*(2-3), 843-7.

Zhang, W., Qiao, X., and Chen, J. (2007). Synthesis of silver nanoparticles-Effects of concerned parameters in water/oil microemulsion. *Material Science and Engineering. B, 142*, 1–15.